# Interactions between humic acid and hematite

## and their effects on metal ion speciation

Ronald Vermeer

Promotor:        dr. W.H. van Riemsdijk
hoogleraar in de bodemscheikunde en chemische
grond en gewasanalyse

Co-promotor:    dr. ir. L.K. Koopal
universitair hoofddocent bij de vakgroep
Fysische en Kolloïdchemie

A.W.P. Vermeer

# Interactions between humic acid and hematite

## and their effects on metal ion speciation

# Stellingen

## (1)

De enorme verschillen in dimensie van het humuszuur die worden verkregen als de theorie van de Wit wordt vergeleken met de laagdikten uit dit proefschrift zijn niet tegenstrijdig.

Dit proefschrift (hst 4 en 5)
De Wit, J.C.M.; Van Riemsdijk, W.H.; Koopal, L.K.; Environ. Sci. Technol. 27, 10, 1993

## (2)

Bij de adsorptie van humuszuur aan de minerale fase in de bodem is het inzichtelijker om de adsorptie te beschrijven vanuit het humuszuur (polyelectroliet adsorptie) dan vanuit het oppervlak (Langmuir).

Dit proefschrift (hst 5)

## (3)

Adsorberen is nivelleren.

Dit proefschrift (hst 7)

## (4)

De specifieke eigenschappen van de verschillende humeuze verbindingen in een natuurlijke situatie worden veeleer bepaald door andere eigenschappen dan de protonaffiniteitsverdeling.

Dit proefschrift, n.a.v. stelling 6, "Proton & metal ion binding to humic substances", Han de Wit
(De protonaffiniteitsverdelingen van verschillende humeuze verbindingen zijn sterk vergelijkbaar)

## (5)

Het spreken over humuszuur als goed gedefinieerd modelsysteem is een contradictio in terminis.

## (6)

De voorloper van CD MUSIC zou logischerwijs LP MUSIC hebben moeten heten omdat de lokale potentiaal werd beschreven (local potential).

Hiemstra, T.; Van Riemsdijk, W.H.; Bolt, G.H.; J. Colloid Interface Sci. 133, 1, 1989

## (7)

Het implementeren van de PBC analyse in het CD MUSIC model is een verbetering voor het beschrijven van een kristalstructuur afhankelijke ion adsorptie.

## (8)

Zowel het magnetisch veld van de aarde, als de adsorptie van zwak geladen polyelectrolieten aan een tegengesteld zwak geladen oppervlak kan men beschrijven als een self constructing systeem.

Dr. James Jackson; The Royal Institute Christmas Lectures - Planet Earth, an explorers guide

(9)

Om de kwaliteit van het onderwijs te handhaven is vernieuwing essentieel.

(10)

Net zoals experimentele onderzoekers hun experimenten toetsen aan theoretische modellen, zo zouden theoretische onderzoekers hun modellen moeten toetsen met experimenten.

(11)

Voor het integreren van een apparaat binnen een onderzoeksgroep is een duidelijke handleiding evenals een gekwalificeerde beheerder noodzakelijk.

(12)

Op grond van de eerste en tweede hoofdwet van de thermodynamica is het voeren van een actief milieubeleid dweilen met de kraan open.

(n.a.v. het afscheidscollege van Hans Lyklema)

(13)

Om het fileprobleem op te lossen zou men meer vooruit moeten kijken.

(Korps Landelijke Politiediensten)

(14)

Individualisering is de ondergang van een samenleving.

(15)

Gezien de specifieke eigenschappen van de verschillende tandpasta's zou het leiden tot een betere mondhygiëne indien regelmatig wordt gepoetst met een andere tandpasta.

(16)

Wetenschap leidt hedentendagen tot een nomadenbestaan.

(17)

Meten is weten; maar zonder te interpreteren kunnen we er niets van leren.

(18)

De belangrijkste tijdschalen waarbinnen experimenteel onderzoek kan plaatsvinden zijn afhankelijk van de resolutie van het experiment en de halfwaarde tijd van een AIO/ student.

(19)

Het aannemen van werknemers op tijdelijke contracten is kapitaalvernietiging.

**Stellingen**

behorende bij het proefschrift "Interactions between humic acid and hematite and their effects on metal ion speciation" van Ronald Vermeer, Landbouwuniversiteit Wageningen, 25 november 1996.

'De wind, die eigenlijk alleen zo nu en dan maar eens komt neergestreken, voortdurend komende van en onderweg naar elders, maar nooit constant op één plaats bezig, draagt vlaagsgewijs nu eens verkwikkende, dan weer onverkwikkende geuren aan, en soms een wolk vlinders of libellen, maar ook wel soms een zwerm vogels, - en is hij weer voorbij, dan blijft nog geruime tijd alles in de tuin, wat maar bewegen kan en door hem is aangeraakt, in beweging.'

'Niets bestaat dat niet iets anders aanraakt.'

Uit: Jeroen Brouwers, Bezonken rood.

# CONTENTS

Chapter 1

# Interactions between humic acid and hematite

# and their effects on metal ion speciation

## Introduction

Over the last decades soil pollution has been recognised as a major topic of concern. Every now and then, pollution of the natural environment with for example heavy metal ions, benzene derivatives, phosphates, fertilisers, herbicides and pesticides has been reported and throughout the Netherlands numerous polluted sites have been located. The most notorious examples in The Netherlands are the severe soil pollution under a newly built residential area in Lekkerkerk 1980 and the cadmium and zinc pollution in the Kempen area (1,2). Many of the polluted locations are considered to be so heavily polluted that treatment seems inevitable. The cost associated with the recovery of the environment are high and have been an issue of political debate. Recently the tendency can be observed that the politics and the society in general are not prepared to come up with all these expenses. Consequently not all polluted sites can be treated and choices have to be made regarding the sites that have to be recovered. These choices can only be well considered and justified if we are able to compare the risks associated with the different polluted sites. To make a sound risk assessment, knowledge of the bio-availability of the pollutants under the different circumstances has to be obtained.

The uptake of contaminants by living organisms mostly occurs by exposure to dissolved species. Plants are exposed to pollutants in the soil by their roots and animals mainly by drinking contaminated water (including contaminants bound to the dissolved soil components) or indirectly by eating contaminated plants or animals. Thus the concentration of the contaminants in the aqueous phase is of prime importance. These aqueous concentrations are affected by soil factors such as pH, the mineral, clay, and organic matter content and the content of the toxic species. Further it is well known that the soil can immobilise toxic chemicals by precipitation, adsorption or (bio)transformation and that the soil acts as a sort of buffer. The buffer capacity of the natural environment strongly influences the impact of toxic chemicals. Buffering in this sense is described as storage of the chemicals without a direct effect of these chemicals on the toxicity experienced at the contaminated site. Exceedance of this capacity may be harmful to the ecosystem because it implies an increased transport and an increased bio-availability of the toxic chemicals.

It has been generally recognised that not the overall concentration of a pollutant controls the toxicity of the contaminated site, but that the concentration of the different speciation forms of a pollutant and the bio-availability of each of the different species have to be considered. As examples of these effects we can mention the precipitation of cadmium hydroxide complexes or the adsorption of cadmium to the soil matrix. These processes are reflected in greenhouse experiments that showed that the uptake of cadmium by plants did not correlate with the total cadmium concentration but rather with the assessable cadmium concentration (3).

Besides the local interactions between contaminants and the soil components the transport of the dissolved species due to the soil water dynamics is an important factor when studying the risks associated with contaminated sites. Contaminants can be transported by the ground water. The species bound to the soil components that are soluble and transportable by the aqueous phase are considered as mobile. Species bound to the non-dissolvable or settled particles and the material bound to these particles belong to the immobile soil fraction. The transport of contaminants that bind strongly to the mobile soil components may be enhanced in the environment, this phenomenon is known as colloid facilitated transport. Binding of contaminants to the different soil components has often been recognised as a process which controls the bio-availability of the contaminants and affects the risks associated with the contamination (4-7). For example hydrophobic herbicides as Atrazine or pesticides as Tefluthrin may be captured in the hydrophobic cavities of the humic substances (8) and thus the transport of these hydrophobic molecules is related to that of the organic matter. Murphy et al. (5) pointed out that, due to the partly hydrophobic structure of the humic material, adsorption of other hydrophobic organic compounds to the soil matrix was increased. Humic acids are generally more hydrophobic than the fulvic acids, thus the speciation of hydrophobic pollutants may be related to that of the humic acid fraction. Adsorption of the humic acids will thus also immobilise the hydrophobic pollutants. Further it has been shown that metal ions form complexes, mainly with the functional groups of humic substances (9-11), and that the adsorbed humic matter plays an important role (5,12) in contaminant binding to mineral particles. Therefore the speciation of the different soil components seems to be of critical importance for a better understanding of the speciation of contaminants. Here we will focus on the metal ion speciation and in particular that of cadmium ions.

A schematic diagram of the most significant speciation forms of metal ions is given in Figure 1. The metal ions can be dissolved in the aqueous phase (the inner circle), where the speciation depends on the environmental conditions (13) (e.g. pH and concentration of indifferent electrolyte) and on the concentration of anions (e.g. $Cl^-$ or $SO_4^{2-}$) and other cations (e.g. $Ca^{2+}$). The metal ions can also be bound to living organisms and non-living components. As an example the binding of cadmium to bacterial cell walls (14,15) and the speciation of these cells in general (16) is mentioned. Contaminant binding to the non-living components can be separated into two classes; binding to the particulate matter, which makes the bound metal ions immobile, and binding to the dissolved soil components. Important dissolved components are humic substances (the organic fraction) and small oxide and clay colloids (the inorganic fraction). Interactions between both dissolved soil fractions may influence the speciation of these components. As examples we mention that due to the

interactions between hematite particles and humic acid complexes of these components may settle or even that settled particles may be dispersed due to the adsorption of humics (17,18). Whatever process is dominating depends on the environmental conditions. Within this thesis we will focus on the meal ion binding to the inorganic and especially to the organic fraction and study the effect on the metal ion binding due to interactions between the two fractions.
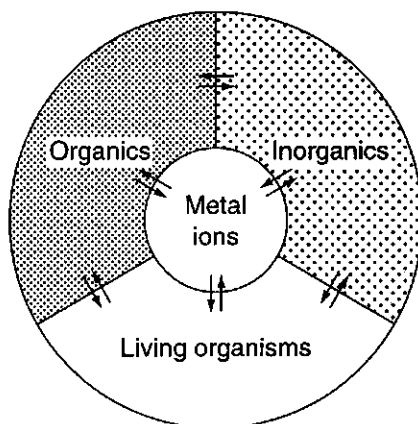


**Figure 1:** The distribution of metal ions in the natural environment.

Humic substances are generally seen as important soil and fresh water components (19). They are generally recognised as the component that is often responsible for the binding of the major part of the available metal ions, therefore the metal ion adsorption onto humics has been studied extensively over the last decades. Humic substances can be dissolved or bound to the other soil components. Naturally, the adsorption of humic matter onto the mineral particles may influence the speciation and the mobility of these dissolved entities and may also influence the binding of metal ions to these components.

To approximate the metal ion binding to the entire soil, the composition of the soil has to be studied, the different components have to be characterised, proton and metal ion binding to the different components should be measured, and the effects of the interactions between the different soil components have to be investigated. Once this is achieved we may be able to predict the speciation of the contaminating metal ions in polluted soils and make a statement about the risks associated with the contaminated sites.

**Humic substances in the environment**

When we are interested in the dissolved components of the natural environment, we can not restrict our study to the aqueous phase, since the dissolved species can be found in all type of ecosystems. The diagram in Figure 2 shows the different flowpaths of the dissolved humic substances in the natural environment. Soil and Peat humic substances

found in the different terrestrial systems may leach into the groundwater and can be transported until they settle in one of the sediments. The composition of the different ecosystems is mainly controlled by a net balance of formation, degradation, and transfer of the humics (20-22). The contribution of the latter to this balance is relatively small, although it can not be neglected (9,23,24).
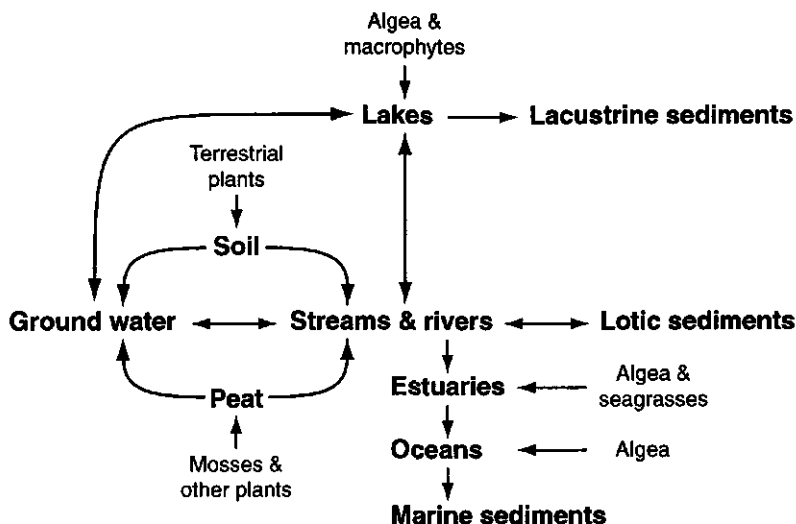


**Figure 2:** Diagram of the possible environmental flowpaths of humic substances (23).

In general Humic substances are described as a mixture of naturally occurring, polydisperse, heterogeneous polyelectrolytes (20-22) that can be divided into three fractions; fulvic acid, humic acid and humin. These fractions are differentiated on the basis of their solubility at different pH (23). Humic acids remain in solution at pH 2 and higher, fulvics even at lower pH and humin is not soluble under alkaline or acid conditions. Humic substances are predominantly negatively charged due to the abundance of carboxylic and phenolic type of groups. Due to the hydration of the charged groups and the electrostatic repulsion between the charges the dissolved humic substances can be described by an extended conformation (25,26) that adjusts itself due to changes in the environmental conditions, resulting in a reduction or increase of the electrostatic repulsion and a more tightly or respectively loosely coiled configuration.

A comprehensive review of the different analytical techniques that can be used to characterise the humic substances can be found in reference (21). A first method to differentiate between the humics in the different ecosystems is based on the elemental content (Table I). Comparison of Figure 2 with Table I shows that the differences in input of the humic matter are connected to the differences in composition. A convenient method to study the relation between the elemental content and the origin of the humic material is based on the graphical method developed by Van Krevelen (27). Van Krevelen used diagrams in which the atomic hydrogen to carbon ratio was plotted as a function of the atomic oxygen to carbon ratio. These diagrams have been used frequently to illustrate compositional differences (28) between fulvic acid, humic acid

and humin, and also to show variations in humic substances as a function of their origin (29): fresh water, marine water, soil or peat. Other useful analytical techniques are for example Fluorescence spectroscopy, UV-Visual spectrophotometry, Infra Red spectroscopy, NMR and potentiometric titrations. Based on these techniques a sample of a specific humic substance can be characterised and classified as one of the above mentioned possibilities. To study the interactions of a certain humic acid sample with other species present in the system one should know which soil type or ecosystem it may represent.

**Table I:** Mean elemental compositions of different humic substances from different origin expressed as weight percentage. Adapted from Rice et al. (29) (All values are on an ash free basis).

| Element | Humic acid | | | | Fulvic acid | | | |
|---------|------|----------------|--------|------|------|----------------|--------|------|
|         | Soil | Fresh-water | Marine | Peat | Soil | Fresh-water | Marine | Peat |
| C | 55.4 | 51.2 | 56.3 | 57.1 | 45.3 | 46.7 | 45.0 | 54.2 |
| H | 4.8 | 4.7 | 5.8 | 5.0 | 5.0 | 4.2 | 5.9 | 5.3 |
| N | 3.6 | 2.6 | 3.8 | 2.8 | 2.6 | 2.3 | 4.1 | 2.0 |
| S | 0.8 | 1.9 | 3.1 | 0.4 | 1.3 | 1.2 | 2.1 | 0.8 |
| O | 36.0 | 40.4 | 31.7 | 35.2 | 46.2 | 45.9 | 45.1 | 37.8 |

## Polyelectrolyte properties of humic acids

Unfortunately a unified structure of humic acid (macro)molecules does not exist. Therefore the structure and the geometry of the molecules always has to be approximated. To study the adsorption of these natural polyelectrolytes and the conformation of the adsorbed molecules and that of the molecules in solution a model would be appropriate. Several models have been proposed to describe the humics (27). The most frequently cited structures are those described by Ghosh and Schnitzer (26) and Cameron et al. (25). More recently computational analytical chemistry has been used to calculate a three dimensional structure of humic substances (30). These calculations resulted in a more or less spherical structure with a significant amount of space within the boundary of the humic acid entities.

Based on the structural features of humic substances, humic acids molecules are often described as fairly flexible polyelectrolytes (25,26,31-33). Chen and Schnitzer (31) mentioned that fulvic and humic acids behave like flexible, linear, synthetic polyelectrolytes, and concluded that the humics are not exclusively composed of condensed rings, but that there must be numerous linkages about which relatively free rotation occurs. Ghosh and Schnitzer (26) showed that humic acids can be described as flexible linear colloids under the conditions that normally prevail in natural soils. Cameron et al. (25) visualised the humic acid molecules in solution as a series of charged, occasionally branched strands. They concluded that the strands coil and wind randomly with respect to both space and time so that the mean distribution of molecular mass is spherical and Gaussian about the centre. Branching results in an increased coil density within the molecule giving rise to more compact spheres compared with a linear

molecule of equivalent weight. They described the humic acid molecules as a structure that is perfused with solvent molecules which are able to exchange with bulk solvent molecules. Summers and Roberts (33) studied the effect of preferential adsorption of polydisperse humic acid samples on the measured adsorption isotherms and reported that previously developed concepts for well defined synthetic polymers (34-37) were also applicable to macromolecules of natural origin whose chemical composition was less well defined.

Throughout this study the properties of simple polyelectrolytes will be compared with the properties of humic substances. It has to be emphasised that the humics are not described as simple polyelectrolytes, only the properties of both components are shown to be similar. Naturally the degree of branching affects these similarities, but this was shown to be a second order effect.

## Proton and metal ion binding to the different soil components

Studying metal ion binding the soil heterogeneity is of great importance. Soil usually consist of a mixture of organic and inorganic constituents. The inorganic fraction may contain silica ($SiO2$), metal(hydr)oxides of iron, aluminium, and manganese, clay minerals, and calcium carbonates. Clay minerals exhibit a "constant" negative charge on their plates and a variable charge on the edges, whereas the metal oxides and the organic fraction have a pH dependent charge. For metal oxides this variable charge depends on the pK of the surface sites, for humic substances a range of surface groups (carboxylic and phenolic type of groups) with different pK values can be observed. The distribution of these pK values is an important factor in metal ion binding. As was reported by Kinniburgh et al. (38) cadmium ions were mostly bound to the carboxylic groups, whereas the phenolic type of groups also contributed significantly in copper and lead binding.

A well suited method to measure proton and metal ion binding to the different soil components is based on potentiometric titrations. The proton adsorption isotherms have been studied extensively for systems consisting of only one soil component. Simply by taking the first derivative of the measured proton titrations of the humic substances, insight into the pK distribution of the different groups can be obtained (39,40).

Proton and metal ion binding to humic substances have been discussed extensively in literature (41-43) and several models have been proposed. The different approaches have led to two major types of modelling, the discrete ligand approach (44-51) and the continuous distribution approach (38,52-57). Within the discrete approach the observed behaviour is described by assuming the presence of a certain number of different types of groups. Each type of groups has a certain affinity and a certain number of equivalents per gram of material. The continuous approach assumes a continuous distribution of pK values that can be described by an analytical expression or site binding isotherm. The latter approach is assumed to be more realistic since humic substances are thought to contain a spectrum of different groups.

From a series of proton adsorption isotherms only apparent affinities can be determined due to the electrostatic interactions. To "remove" the electrostatic

interaction, a model is required that accounts for the salt effect on the proton adsorption (52,58). With such an electrostatic model and under the assumption of random heterogeneity, the isotherms measured at different salt concentrations can be recalculated. When the electrostatic model is adequate the recalculated isotherms should merge into a "Master Curve", which reflects the chemical heterogeneity of the material studied. Its derivative can be used as a fingerprint describing the intrinsic affinities which in turn are related to the chemical composition (39,40,52). Within the proposed electrostatic model the polyelectrolyte character of the humic substances, as described above, is not yet incorporated successfully. A first attempt to incorporate the polyelectrolyte properties into this model (59) made use of a simple form of the description of humic substances as a Donnan gel, as was originally proposed by Marinsky and co-workers (43,60). A disadvantage of the followed approach was that the humic acid entities were modelled as very small and compact domains with a low water content, which is not expected on the basis of the polyelectrolyte character. Tanford (61) in his treatment of random coiled polymers has shown that the molecule itself occupies only a very small fraction of the volume that it pervades.

Once the Master Curve is found and an impression is obtained about the intrinsic affinity distribution one can look for a way to model the proton and metal ion binding. The site binding model which describes the proton and metal ion adsorption within a multicomponent system most accurate is the Non Ideal Competitive Adsorption model (NICA) (53). The monocomponent equivalent of this site binding model is the well known Langmuir Freundlich model.

Next to the interactions with the humic substances the binding of both proton and metal ions to the mineral surface has been investigated thoroughly. The soil particles studied most frequently are mineral oxides, especially iron oxides (62-68), and clays (69,70).

The model that describes the ion binding to the oxide surface most accurate is the Charge Distribution MUltiple SIte Complexation model (71) (CD MUSIC) applied by Venema et al. (63), for the adsorption of cadmium on goethite. The model concept is based on the Pauling concept of charge distribution (72). As described in the one-pK model that was introduced by Van Riemsdijk et al. (73) and later reviewed by Koopal (74) the charge of an adsorbing ion is distributed over all its ligands both on the surface and solution side. The patchwise heterogeneity of the oxide particles can be taken into account by considering the structure of the most important crystal planes.

Overall it may be concluded that the proton and metal ion binding to the single components has been evaluated thoroughly.

## Interactions between the different soil components

A second aspect of interest concerning the speciation within a natural system is the interaction between the different soil components. Several authors studied the adsorption of humic substances onto mineral particles. Adsorption isotherms of humic acid on iron oxides (6,75-77), alumina (78-80) and manganese (81) were reported as well as the adsorption onto clays (8,82,83). It is commonly observed that the adsorption increases with decreasing pH and in most studies the adsorption was found to increase

7

with increasing salt concentration. The effect of these interactions on the speciation of the different components and complexes depends strongly on the conditions and more specifically on the conformation of the adsorbed humic acid (18). The relation between humic acid and mineral particles was also reported by McKnight et al. (6) who investigated the association of humic substances with colloidal particles in a mountain stream. A clear correlation between the deposited oxide and the organic carbon content was observed. It was mentioned that the iron oxide particles precipitated preferentially compared to other oxides.

Further it has been shown that adsorbed humic material played an important role in metal ion binding to mineral particles. The importance of adsorbed humic substances was also reported by Beckett et al. (84) who showed that the electrophoretic mobility of goethite particles was reduced from a positive to a negative value even with the adsorption of very low concentrations of natural organic matter (about 10 mg $l^{-1}g^{-1}$ hematite). The negative particle charge was developed due to the charges associated with the adsorbed polyelectrolyte segments extending into the solution. Comparable results were mentioned by other authors (85-87). These results suggest that the humic acid molecules do not adsorb in a flat conformation as was proposed by Gu et al. (75), but form a relatively thick layer of which the conformation adjusts to the local conditions (17,18). The latter description seems to be in correspondence with the polyelectrolyte adsorption theories (88,89) indicating that these theories can be used to describe the polyelectrolyte character of the humic substances.


## Proton and metal ion binding to natural soil and fresh water systems

The adsorption of protons and metal ions by a natural system is complex and cannot be predicted straightforward from studies characterising the single components. Several studies have been reported describing metal ion adsorption to mixtures. Hiraide (90) described the binding of copper and iron ions; copper was found to be bound mainly by the dissolved humics, whereas the iron ions formed complexes mainly with the colloidal particles. McLaren et al. (91) and Bibak (92) mentioned that metal ion adsorption characteristics of complete soils are controlled to a large extent by their organic matter and oxides content, whereas clay minerals are unlikely to have a significant influence on the sorption of metal ions. Numerous studies indicated that the adsorption of metal ions onto oxides was increased due to the interaction with humic substances (12,19,93-97). However, these studies did not take into account the charge associated with the humics. Only a few studies discussed the additivity of the different components (92,96). The calculated additive adsorption capacities of the entire soil, as reported by Bibak, were about half of the measured values. These studies indicate that models based on the surface chemistry of uncovered oxides or dissolved humic substances may not be directly applicable to natural systems. The binding characteristics will be modified due to mutual interaction between the different components. Considering the effects of specific interactions on the surfaces charge, we tend to ascribe the difference between the actual and the non-interacting adsorbed amount to both components.

## Outline of this thesis

The aim of the present study is to investigate the effects of the interactions between two important soil components, mineral oxides and humic substances, on the proton and metal ion binding. A qualitative model will be developed with which the metal ion binding to a complicated system can be estimated, based on laboratory experiments with the single components of this model soil. The model soil used in this study consists of a well-characterised iron oxide (Breeuwsma hematite) and a purified commercial humic acid. Both components are characterised by a variable charge and it will be shown that the adsorption process affects the degree of dissociation of the individual components.

Throughout this thesis we will model the humic acid molecules as polyelectrolytes and we will show that this approach is useful to gain insight into the binding characteristics in a mixed system.

In the first part of this thesis we will introduce the polyelectrolyte adsorption theory and describe the Self Consistent Field theory used to model the system. The single components will be characterised and classified based on different analytical techniques and proton and metal ion titrations (A detailed description of the titration set-up and the procedure used for the data treatment is given in appendix I.). Further the adsorption of humic acid onto the hematite particles will be described (chapter 5 and 6) and finally the proton and metal ion binding to a mixed system will be discussed, based on the single component characteristics (chapter 7 and 8). The content of the different chapters is given below.

In chapter 2 the Self Consistent Field (SCF) theory of Scheutjens and Fleer (*98*) will be extended to describe an oxide surface with a variable charge. This theory is used to gain insight into the mechanisms regulating the degree of dissociation of both components due to the adsorption of a weak polyelectrolyte onto an oxide surface. Although we are aware of the fact that this model is not appropriate for a quantitative description, since the number of parameters is too large, we will show that this model is very useful to gain insight into the adsorption. It will be shown that due to the specific adsorption, extra charges are induced to the surface and the polyelectrolyte molecules. The mutual interaction is dominated by the component with the highest charge density, as a function of pH, and this component induces extra charge on the other species.

In chapter 3, the properties of a purified Aldich humic acid are compared with those of several more accepted, naturally occurring humic substances. To this aim, PAHA will be characterised by Elemental analysis, Fluorescence, UV and FT-IR spectroscopy, CPMAS $^1$H and $^{13}$C NMR, Viscosity measurements, Gel Permeation Chromatography and Ellipsometry. It will be shown that PAHA can be used as an analogue for natural humic substances and is classified as a soil humic acid.

The volume and molecular weight distribution of PAHA will be determined in chapter 4 using viscosity measurements in combination with gel permeation chromatography and dynamic light scattering experiments. The determined volumes correspond to the

Donnan volumes which are used to "remove" the electrostatic interaction in the calculation of the Master Curve. At moderate and high salt concentrations ( $\geq 10^{-2}$ M) the Donnan model in combination with the measured volumes, described the proton and metal ion binding very well. At very low salt concentrations ($10^{-3}$ M) the measured volume in combination with the Donnan model was not suitable and the extension of the double layer thickness had to be considered. It will be shown that the Donnan volumes as determined by Benedetti (59) are too small and lead to unrealistic small radii of the humic acid molecules. The proposed approach leads to larger radii and reflects the polyelectrolyte properties of the humic acid molecules very well. The Master Curve as determined with the measured Donnan volumes will be presented and discussed. Finally the proton and metal ion binding characteristics of the commercial humic acid will be compared with a natural peat sample.

Chapter 5 deals with the adsorption of humic acid onto the hematite particles. The effects of changes in the environmental conditions (pH, salt concentration and the presence of divalent ions) on the magnitude of the adsorption will be discussed. A description based on general polyelectrolyte adsorption characteristics (88,89) will be used to explain the level of the different adsorption plateaux and the layer thicknesses, as determined with dynamic light scattering. Finally, the observed trends will be compared with SCF calculations, which gives insight into the importance of the different interaction mechanisms.

Based on experiments with a mixture of a fulvic acid and a humic acid the occurrence of adsorption fractionation will be investigated and the fractionation effect on the shape of the adsorption isotherm will be discussed in chapter 6. It will be shown that the larger molecular weight fraction adsorbs preferentially. The experiments will be complemented with SCF calculations and it will be shown that adsorption fractionation results in the commonly observed adsorption/ desorption hysteresis.

In chapter 7 the proton adsorption onto a humic acid/ hematite mixture will be investigated and compared in detail with the proton adsorption to the single components. It will be shown that two opposite processes determine the extent of the proton adsorption. Due to the adsorption, sites on the humic acid are lost for further proton binding. On the other hand, extra protons are adsorbed onto the hematite surface. Due to the negative charge associated with the adsorbed polyelectrolyte the electrostatic potential in the vicinity of the surface will be less positive or even negative resulting in an increased proton adsorption to the oxide.

Chapter 8 deals with the metal ion adsorption onto the PAHA/ hematite complex. The metal ion adsorption to the complex will be explained based on the methods discussed in chapter 7, combined with the metal ion binding characteristics of the single components.

# References

(1) Klitsie, C.G.M. Cadmiumproblematiek in de Kempen In *PHLO-course 'Soil protection and soil pollution'*; Ministry of Agriculture and Fisheries: 1988;

(2) Boekhold, A.E.; Van der Zee, S.E.A.T.M.; De Haan, F.A.M. Spatial Patterns of Cadmium Contents Related to Soil Heterogeneity. *Water,Air,Soil Pollut.* **1991**, *57/58*, 479 -488.

(3) Steperek, P. Ph. D. dissertation, Georg-August Universität, Göttingen, Germany. Die Cd-aufnahme von Pflanzen aus verschiedenen Böden und Bindungsformen und ihre Prognose durch chemische Extractionsverfahren.

(4) Takács, M. Cu(II) and Pb(II) Complexation by Humic and Fulvic Acids: Conditional Stability Constants and their Correlation with Humus Quality. Humic Subst. Global Environ. Implic. Hum. Health, Proc. Int. Meet. Int. Humic Subst. Soc., 6th. Senesi N and Miano TM. Amsterdam. Elsevier. 1994 475-480.

(5) Murphy, E.M.; Zachara, J.M.; Smith, S.C.; Philips, J.L.; Wietsma, T.W. Interaction of hydrophobic organic compounds with mineral-bound humic substances. *Environ.Sci.Technol.* **1994**, *28(7)*, 1291 - 1299.

(6) McKnight, D.M.; Wershaw, R.L.; Bencala, K.E.; Zellweger, G.W.; Feder, G.L. Humic substances and trace metals associated with Fe and Al oxides deposited in an acidic mountain stream. *Sci.Total Environ.* **1992**, *117/118*, 485 -498.

(7) Town, R.M.; Powell, H.K.J. Ion-selective electrode potentiometric studies on the complexation of copper(II) by soil-derived humic and fulvic acids. *Anal.Chim.Acta* **1993**, *279*, 221 -233.

(8) Zhou, J.L.; Rowland, S.J.; Braven, J.; Mantoura, R.F.C.; Harland, B.J. Tefluthrin sorption to mineral particles: role of particle organic coatings. *Int.J.Env.Anal.Chem.* **1995**, *58*, 275 -285.

(9) Buffle, J. Natural organic matter and metal-organic interactions in aquatic systems In *Metal ions in biological systems*; Sigel, H. Ed.; Marcel Dekker: New York, 1984; 165-221.

(10) Ephraim, J.H.; Marinsky, J.A.; Cramer, S.J. Complex-forming properties of natural organic acids. *Talanta* **1989**, *36(4)*, 437 -444.

(11) Sposito, G. Sorption of trace metals by humic materials in soils and natural waters. *CRC Crit.Rev.Environ.Control* **1986**, *16(2)*, 193 -229.

(12) Tipping, E.; Griffith, J.R.; Hilton, J. The Effect of Adsorbed Humic Substances on the Uptake of Copper(II) by Goethite. *Croat.Chem.Acta* **1983**, *56(4)*, 613 -621.

(13) Boekhold, A.E.; Temminghoff, E.; Van der Zee, S.E.A.T.M. Influence of electrolyte composition and soil pH on Cd sorption by a sandy soil. *J.Soil Sci.* **1993**, *44*, 85 -96.

(14) Plette, A.C.C.; Van Riemsdijk, W.H.; Benedetti, M.F. Competitive Binding of Protons, Calcium, Cadmium and Zinc to Isolated Cell Walls of a Gram-positive Soil Bacterium. *Environ.Sci.Technol.* **1996**, *30(6)*, 1902 -1910.

(15) Plette, A.C.C.; Haanstra, L.; Van Beelen, P.; Van Riemsdijk, W.H. Sorption of metal ions by intact cells. *in preparation* **1996**,

(16) Rijnaarts, H.H.M.; Norde, W.; Bouwer, E.J.; Zehnder, A.J.B.; Lyklema, J. Bacterial adhesion under static and dynamic conditions. *Appl. Environ. Microbiol.* **1995**, *59*, 3255 -3265.

(17) Amirbahman, A.; Olson, T.M. Transport of Humic Matter-Coated Hematite in Packed Beds. *Environ.Sci.Technol.* **1993**, *27(13)*, 2807 -2813.

(18) Amirbahman, A.; Olson, T.M. The role of surface conformations in the deposition kinetics of humic matter-coated colloids in porous media. *Colloids Surf.A* **1995**, *95*, 249 -259.

(19) Ephraim, J.H.; Allard, B. Influence of humic substances on the uptake of metal ions by naturally occurring materials. *Ion Exch.Solvent Extr.* **1993**, *11*, 335 -367.

(20) Stevenson, F.J. *Humus Chemistry. Genesis, Composition, Reactions*; Wiley Interscience: New York, 1982.

(21) Hayes, M.H.B.; MacCarthy, P.; Malcolm, R.L.; Swift, R.S. *Humic Substances II: In search of structure*; Wiley Interscience: New York, 1989.

(22) Schnitzer, M.; Khan, S.U. *Humic substances in the environment*; Marcel Decker Inc. New York, 1972.

(23) Aiken, G.R.; McKnight, D.M.; Wershaw, R.L.; MacCarthy, P. *Humic Substances in Soil, Sediment, and Water*; Wiley Interscience: New York, 1985.

(24) Buffle, J. *Complexation Reactions in Aquatic Systems: An Analytical Approach*; Ellis Horwood Limited: Chichester, 1988.

(25) Cameron, R.S.; Thornton, B.K.; Swift, R.S.; Posner, A.M. Molecular weight and shape of humic acid from sedimentation and diffusion measurements on fractionated extracts. *J.Soil Sci.* **1972**, *23(4)*, 394 -408.

(26) Ghosh, K.; Schnitzer, M. Macromolecular structures of humic substances. *Soil Sci.* **1980**, *129(5)*, 266 -276.

(27) Van Krevelen, D.W. Graphical-statistical method for the study of structure and reaction processes of coal. *Fuel* **1961**, *29*, 269 -284.

(28) Visser, S.A. Application of Van Krevelen's Graphical-Statistical Method for the Study of Aquatic Humic Material. *Environ.Sci.Technol.* **1983**, *17(7)*, 412 -417.

(29) Rice, J.A.; MacCarthy, P. Statistical evaluation of the elemental composition of humic substances. *Org.Geochem.* **1991**, *17(5)*, 635 -648.

(30) Schulten, H.R. The three-dimensional structure of humic substances and soil organic matter studied by computational chemistry. *Fresenius Anal.Chem.* **1995**, *351*, 62 -73.

(31) Chen, Y.; Schnitzer, M. Viscosity Measurements on Soil Humic Substances. *Soil Sci.Soc.Am.J.* **1976**, *40*, 866 -872.

(32) Cornel, P.K.; Summers, R.S.; Roberts, P.V. Diffusion of Humic Acid in Dilute Aqueous Solution. *J.Colloid Interface Sci.* **1986**, *110(1)*, 149 -165.

(33) Summers, R.S.; Roberts, P.V. Activated Carbon Adsorption of Humic Substances. *J.Colloid Interface Sci.* **1988**, *122(2)*, 367 -381.

(34) Cohen Stuart, M.A.; Fleer, G.J.; Bijsterbosch, B.H. The Adsorption of Poly(vinyl pyrrolidone) onto Silica. I. Adsorbed Amount. *J.Colloid Interface Sci.* **1982**, *90(2)*, 310 -320.

(35) Koopal, L.K. The Effect of Polydispersity on the Adsorption Isotherm. *J.Colloid Interface Sci.* **1981**, *83(1)*, 116 -129.

(36) Cohen Stuart, M.A.; Scheutjens, J.M.H.M.; Fleer, G.J. Polydispersity Effects and the Interpretation of Polymer Adsorption Isotherms. *J.Polym.Sci.Polym.Phys.Ed.* **1980**, *18*, 559 -573.

(37) Hlady, V.; Lyklema, J.; Fleer, G.J. Effect of Polydispersity on the Adsorption of Dextran on Silver Iodide. *J.Colloid Interface Sci.* **1982**, *87(2)*, 395 -406.

(38) Kinniburgh, D.G.; Milne, C.J.; Benedetti, M.F.; Pinheiro, J.P.; Filius, J.; Koopal, L.K.; Van Riemsdijk, W.H. Metal Ion Binding by Humic Acid: Application of the NICA-Donnan Model. *Environ.Sci.Technol.* **1996**, *30(5)*, 1687 -1698.

(39) Nederlof, M.M.; Van Riemsdijk, W.H.; Koopal, L.K. Determination of Adsorption Affinity Distributions: A General Framework for Methods Related to Local Isotherm Approximations. *J.Colloid Interface Sci.* **1990**, *135(2)*, 410 -425.

(40) Nederlof, M.M.; Van Riemsdijk, W.H.; Koopal, L.K. Heterogeneity Analysis for Binding Data Using an Adapted Smoothing Spline Technique. *Environ.Sci.Technol.* **1994**, *28(6)*, 1037 -1047.

(41) Benedetti, M.F.; Milne, C.J.; Kinniburgh, D.G.; Van Riemsdijk, W.H.; Koopal, L.K. Metal Ion Binding to Humic Substances: Application of the Non-Ideal Competitive Adsorption Model. *Environ.Sci.Technol.* **1995**, *29(2)*, 446 -456.

(42) Milne, C.J.; Kinniburgh, D.G.; De Wit, J.C.M.; Van Riemsdijk, W.H.; Koopal, L.K. Analysis of Metal-Ion Binding by Peat Humic Acid Using a Simple Electrostatic Model. *J.Colloid Interface Sci.* **1995**, *175*, 448 -460.

(43) Ephraim, J.H.; Alegret, S.; Mathuthu, A.; Bicking, M.; Malcolm, R.L.; Marinsky, J.A. A United Physicochemical Description of the Protonation and Metal Ion Complexation Equilibria of Natural Organic Acids (Humic and Fulvic Acids). 2. Influence of Polyelectrolyte Properties and Functional Group Heterogeneity on the Protonation Equilibria of Fulvic Acid. *Environ.Sci.Technol.* **1986**, *20(4)*, 354 -366.

(44) Tipping, E.; Hurley, M.A. A unifying model of cation binding by humic substances. *Geochim.Cosmochim.Acta* **1992**, *56(10)*, 3627 -3641.

(45) Dzombak, D.A.; Fish, W.; Morel, F.M.M. Metal-Humate Interactions. 1. Discrete Ligand and Continuous Distribution Models. *Environ.Sci.Technol.* **1986**, *20(7)*, 669 -675.

(46) Paxéus, N.; Wedborg, M. Acid-base properties of aquatic fulvic acid. *Anal.Chim.Acta* **1985**, *169*, 87 -98.

(47) Bartschat, B.M.; Cabaniss, S.E.; Morel, F.M.M. Oligoelectrolyte Model for Cation Binding by Humic Substances. *Environ.Sci.Technol.* **1992**, *26(2)*, 284 -294.

(48) Westall, J.C.; Jones, J.D.; Turner, G.D.; Zachara, J.M. Models for Association of Metal Ions with Heterogeneous Environmental Sorbents. 1. Complexation of Co(II) by Leonardite Humic Acid as a Function of pH and NaClO$_4$ Concentration. *Environ.Sci.Technol.* **1995**, *29(4)*, 951 -959.

(49) Marinsky, J.A.; Reddy, M.M.; Ephraim, J.H.; Mathuthu, A.S. Computational scheme for the prediction of metal ion binding by a soil fulvic acid. *Anal.Chim.Acta* **1995**, *302*, 309 -322.

(50) Gregor, J.E.; Powell, H.K.J. Protonation reactions of fulvic acids. *J.Soil Sci.* **1988**, *39*, 243 -252.

(51) Ephraim, J.H.; Pettersson, C.; Nordén, M.; Allard, B. Potentiometric Titrations of Humic Substances: Do Ionic Strength effects Depend on the Molecular Weight? *Environ.Sci.Technol.* **1995**, *29(3)*, 622 - 628.

(52) De Wit, J.C.M.; Van Riemsdijk, W.H.; Koopal, L.K. Proton Binding to Humic Substances. 2. Chemical Heterogeneity and Adsorption Models. *Environ.Sci.Technol.* **1993**, *27*, 2015 -2022.

(53) Koopal, L.K.; Van Riemsdijk, W.H.; De Wit, J.C.M.; Benedetti, M.F. Analytical Isotherm Equations for Multicomponent Adsorption to Heterogeneous Surfaces. *J.Colloid Interface Sci.* **1994**, *166*, 51 -60.

(54) Perdue, E.M.; Reuter, J.H.; Parrish, R.S. A statistical model of proton binding by humus. *Geochim.Cosmochim.Acta* **1984**, *48*, 1257 -1263.

(55) Fukushima, M.; Tanaka, S.; Hasebe, K.; Taga, M.; Nakamura, H. Interpretation of the acid-base equilibrium of humic acid by a continuous pK distribution and electrostatic model. *Anal.Chim.Acta* **1995**, *302*, 365 -373.

(56) Dobbs, J.C.; Susetyo, W.; Carreira, L.A.; Azarraga, L.V. Competitive binding of protons and metal ions in humic substances by lanthanide ion probe spectroscopy. *Anal. Chem.* **1989**, *61*, 1519 -1524.

(57) Manunza, B.; Deiana, S.; Maddau, V.; Gessa, C.; Seeber, R. Stability constants of metal humate complexes: titration data analyzed by bimodal Gaussian distribution. *Soil Sci.Soc.Am.J.* **1995**, *59*, 1570 -1574.

(58) De Wit, J.C.M.; Van Riemsdijk, W.H.; Koopal, L.K. Proton Binding to Humic Substances. 1. Electrostatic Effects. *Environ.Sci.Technol.* **1993**, *27(10)*, 2005 -2014.

(59) Benedetti, M.F.; Van Riemsdijk, W.H.; Koopal, L.K. Humic substances considered as a heterogeneous Donnan gel phase. *Environ.Sci.Technol.* **1996**, *30(6)*, 1805 -1813.

(60) Marinsky, J.A.; Reddy, M.M. Proton and metal ion binding to natural organic polyelectrolytes-II. Preliminary investigations with a peat and a humic acid. *Org.Geochem.* **1984**, *7(3/4)*, 215 -221.

(61) Tanford, C. *Physical chemistry of macromolecules*; Wiley Interscience: New York, 1967.

(62) Fokkink, L.G.J.; De Keizer, A.; Lyklema, J. Specific Ion Adsorption on Oxides: Surface Charge Adjustment and Proton Stoichiometry. *J.Colloid Interface Sci.* **1987**, *118*, 454 -462.

(63) Venema, P.; Hiemstra, T.; Van Riemsdijk, W.H. Multiple site modelling of cadmium adsorption on goethite using an extended data set. *J.Colloid Interface Sci.* **1996**, , submitted

(64) Djafer, M.; Lamy, I.; Terce, M. Interaction of metallic cations with the hydrous goethite surface. *Prog. Colloid Polym. Sci.* **1989**, *79*, 150 -154.

(65) Johnson, B.B. Effect of pH, Temperature, and Concentration on the Adsorption of Cadmium on Goethite. *Environ.Sci.Technol.* **1990**, *24(1)*, 112 -118.

(66) Gutzman, D.W.; Langford, C.H. Multicomponent kinetic analysis of trace metal binding sites on iron hydrous oxide colloids. *Water Poll.Res.J.Canada* **1988**, *23(3)*, 379 -387.

(67) Breeuwsma, A.; Lyklema, J. Physical and chemical adsorption of ions in the electric double layer in hematite (a-$Fe_2O_3$). *J.Colloid Interface Sci.* **1973**, *43*, 437 -448.

(68) Benjamin, M.M.; Leckie, J.O. Multiple-Site Adsorption of Cd, Cu, Zn, and Pb on Amorphous Iron Oxyhydroxide. *J.Colloid Interface Sci.* **1981**, *79(1)*, 209 -221.

(69) Hirsch, D.; Nir, S.; Banin, A. Prediction of Cadmium Complexation in Solution and Adsorption to Montmorillonite. *Soil Sci.Soc.Am.J.* **1989**, *53*, 716 -721.

(70) Pohlmeier, A. The kinetic spectrum method applied to the ion exchange of Cd(II) at Mg(II)-montmorillonite. *Prog. Colloid Polym. Sci.* **1994**, *95*, 113 -118.

(71) Hiemstra, T.; Van Riemsdijk, W.H.; Bolt, G.H. Multisite Proton Adsorption Modelling at the Solid/Solution Interface of (Hydr)oxides: A New Approach I. Model Description and Evaluation of Intrinsic Reaction Constants. *J.Colloid Interface Sci.* **1996**, *133(1)*, 91 -104.

(72) Pauling, L. The Principles Determining the Structure of Complex Ionic Crystals. *J. Amer. Chem. Soc.* **1929**, *51*, 1010 -1026.

(73) Van Riemsdijk, W.H.; Bolt, G.H.; Koopal, L.K.; Blaakmeer, J. Electrolyte Adsorption on Heterogeneous Surfaces: Adsorption Models. *J.Colloid Interface Sci.* **1986**, *109(1)*, 219 -228.

(74) Koopal, L.K. Ion adsorption on mineral oxide surfaces In *Adsorption on new and modified inorganic sorbents*; Dabrowski, A.; Tertykh, V.A. Eds.; Elsevier: Amsterdam, 1996; 757-796.

(75) Gu, B.; Schmitt, J.; Chen, Z.; Liang, L.; McCarthy, J.F. Adsorption and Desorption of Natural Organic Matter on Iron Oxide: Mechanisms and Models. *Environ.Sci.Technol.* **1994**, *28(1)*, 38 -46.

(76) McD.Day, G.; Hart, B.T.; McKelvie, I.D.; Beckett, R. Adsorption of natural organic matter onto goethite. *Colloids Surf.A* **1994**, *89*, 1 -13.

(77) Tipping, E. The adsorption of aquatic humic substances by iron oxides. *Geochim.Cosmochim.Acta* **1981**, *45*, 191 -199.

(78) Davis, J.A.; Gloor, R. Adsorption of Dissolved Organics in Lake Water by Aluminum Oxide. Effect of Molecular Weight. *Environ.Sci.Technol.* **1981**, *15(10)*, 1223 -1229.

(79) Zhou, J.L.; Rowland, S.J.; Fauzi, R.; Mantoura, R.F.C.; Braven, J. The formation of humic coatings on mineral particles under simulated estuarine conditions - A mechanistic study. *Water Res.* **1994**, *28(3)*, 571 -579.

(80) Wais Mossa, M.T.; Mazet, M. Influence des sels mineraux sur l'adsorption des acides humiques sur flocs d'hydroxydes de fer preformes. *Env.Technol.* **1991**, *12*, 725 -730.

(81) Waite, T.D.; Wrigley, I.C.; Szymczak, R. Photoassisted Dissolution of a Colloidal Manganese Oxide in the presence of Fulvic Acid. *Environ.Sci.Technol.* **1988**, *22(7)*, 778 -785.

(82) Tombácz, E.; Gilde, M.; Abrahám, I.; Szántó, F. Effect of sodium chloride on interactions of fulvic acid and fulvate with montmorillonite. *Appl.Clay Sci.* **1990**, *5*, 101 -112.

(83) Makoto, K. Adsorption of humic acid on Ca-montmorillonite. *Soil Sci.Plant Nutr.(Tokyo)* **1995**, *41(2)*, 215 -223.

(84) Beckett, R.; Le, N.P. The Role of Organic Matter and Ionic Composition in Determining the Surface Charge of Suspended Particles in Natural Waters. *Colloids Surf.* **1990**, *44*, 35 -49.

(85) Tipping, E.; Cooke, D. The effects of adsorbed humic substances on the surface charge of goethite in freshwaters. *Geochim.Cosmochim.Acta* **1982**, *46*, 75 -80.

(86) Davis, J.A. Adsorption of natural dissolved organic matter at the oxide/water interface. *Geochim.Cosmochim.Acta* **1982**, *46*, 2381 -2393.

(87) Morris, G.; Newcombe, G. Granual Activated Carbon: The Variation of Surface Properties with the Adsorption of Humic Substances. *J.Colloid Interface Sci.* **1993**, *159*, 413 -420.

(88) Cohen Stuart, M.A.; Fleer, G.J.; Lyklema, J.; Norde, W.; Scheutjens, J.M.H.M. Adsorption of Ions, Polyelectrolytes and Proteins. *Adv.Colloid Interface Sci.* **1991**, *34*, 477 -535.

(89) Cohen Stuart, M.A. Polyelectrolyte adsorption. *J.Phys.France* **1988**, *49*, 1001 -1008.

(90) Hiraide, M. Heavy Metals Complexed with Humic Substances in Fresh Water. *Anal.Sci.* **1992**, *8*, 453 -459.

(91) McLaren, R.G.; Lawson, D.M.; Swift, R.S. Sorption and desorption of cobalt by soils and soil components. *J.Soil Sci.* **1986**, *37*, 413 -426.

(92) Bibak, A. Cobalt, Copper, and Manganese adsorption by aluminium and iron oxides and humic acid. *Commun.Soil Sci.Plant Anal.* **1994**, *25(19&20)*, 3229 -3239.

(93) Taylor, M.D.; Theng, B.K.G. Sorption of Cadmium by complexes of Kaolinite with humic acid. *Commun.Soil Sci.Plant Anal.* **1995**, *26(5&6)*, 765 -776.

(94) Davis, A.P.; Bhatnagar, V. Adsorption of Cadmium and humic acid onto hematite. *Chemosphere* **1995**, *30(2)*, 243 -256.

(95) Laxen, D.P.H. Trace metal adsorption/coprecipitation on hydrous ferric oxide under realistic conditions. *Water Res.* **1985**, *19(10)*, 1229 -1236.

(96) Robertson, A.P.; Leckie, J.O. Humic Acid/Goethite Interactions and their Effect on Copper Binding. Humic Subst. Global Environ. Implic. Hum. Health, Proc. Int. Meet. Int. Humic Subst. Soc., 6th. Senesi N and Miano TM. Amsterdam. Elsevier. 1994 487-492.

(97) Ho, C.H.; Miller, N.H. Effect of Humic Acid on Uranium Uptake by Hematite Particles. *J.Colloid Interface Sci.* **1985**, *106(2)*, 281 -288.

(98) Fleer, G.J.; Cohen Stuart, M.A.; Scheutjens, J.M.H.M.; Cosgrove, T.; Vincent, B. *Polymers at Interfaces*; Chapman & Hall: London, 1993.

Chapter 2

# Adsorption of weak polyelectrolytes on a surface

# with a variable charge,

## Self-Consistent-Field calculations

## Abstract

A theoretical model for the adsorption of weak flexible polyelectrolytes onto a surface with a variable charge is developed. The model is an extension of the self-consistent field theory for chain molecules. The electrostatic double layer is described using a multi-Stern-layer model and the degree of dissociation of the chargeable polyelectrolyte segments is allowed to vary with the distance from the surface. Results for the decay of the electrostatic potential as a function of the distance to the surface and the volume fraction profiles of the polyelectrolyte molecules are calculated numerically as a function of pH, ionic strength and segment-solvent/ segment-surface interaction parameters. Based on these quantities the adsorbed amount, the charge associated with the surface and the adsorbed polyelectrolyte are calculated. The importance of different interaction mechanisms; pure electrosorption, specific binding and hydrophobic binding is evaluated. Both the surface and the adsorbed polyelectrolyte are able to titrate each other. Depending on the conditions the charge associated with the adsorbed polyelectrolyte molecules compensates or even overcompensates the surface charge. The component that dominates the decay of the electrostatic potential determines to a large extent the degree of dissociation of the other component. Due to these differences in the degree of dissociation of both components the fraction of train segments increases with increasing pH, decreasing salt concentration and increasing adsorption energy.

## Introduction

The adsorption of strong polyelectrolytes onto a surface with an opposite, constant charge has been discussed extensively in the literature, both experiments (1-5) and calculations (5-7) have been reported. It was discussed that the adsorbed amount often compensates, or even slightly overcompensates, the surface charge and that mostly the adsorption increases with increasing ionic strength (6). A decreased adsorption with increasing ionic strength was considered by Muthukumar (8). This effect can be expected when the adsorption is mainly driven by electrostatic attraction, under these circumstances salt screens not only the lateral repulsion but also the segment-surface attraction. Thus the effect of the ionic strength on the adsorption is determined by a subtle balance between coulombic and specific forces. For strong polyelectrolytes and surfaces with a fixed charge Van der Steeg et al. (9) introduced the following classification. When the electrostatic attraction between both components dominates the adsorption process, the adsorption is called screening-reduced. In situations where the segments also have a specific (short-range, non-electrostatic) interaction with the surface, the force balance is changed. Now the majority of the cases are described as screening-enhanced, where the adsorption increases with increasing ionic strength.

The adsorption of weak polyelectrolytes on surfaces with fixed charges is more complicated. The charge density of the polyelectrolytes is influenced by the local conditions (pH and salt concentration) and may even increase or decrease upon adsorption. Theories of weak polyelectrolyte adsorption have been developed by Van der Schee and Lyklema (10) who extended the theory of Roe (11) by incorporating electrostatic interactions in the lattice-based models for polymer adsorption, Evers et al. (12) and Böhmer et al. (13). The latter theories are an extension of the Self-Consistent-Field (SCF) theory of Scheutjens and Fleer (14-16). Böhmer et al. (13,17) presented a rigorous lattice model for the adsorption of weak polyelectrolytes, and confirmed their theoretical predictions by experiments (17). It was mentioned that the adsorption occurred in the screening enhanced regime and that the adsorbed layer became more extended with increasing ionic strength. A maximum in the adsorbed amount was found as a function of pH, at 1-1.5 units below the pK of the chargeable segments of the polyelectrolyte. This phenomenon can be explained by an increasing attraction between surface and polyelectrolyte with increasing polyelectrolyte charge, which is followed by an increased lateral repulsion that builds up when the polyelectrolyte charge increases further. Later it was shown by Israëls et al. (18) that the incorporation of the degree of dissociation ($\alpha$) of the polyelectrolytes, within the Böhmer approach, was not entirely correct. Israëls et al. showed that $\alpha$ should be incorporated into the effective weighting factor and not into the electrostatic potential term as described by Böhmer et al. Fortunately the conclusions drawn from the calculations presented by Böhmer et al., are not affected by this aspect and are still valid.

Although the extension of the theory to weak polyelectrolytes has been a major improvement, a further extension of the polyelectrolyte adsorption theory is desirable. In a variety of applied fields the surface upon which the polyelectrolytes adsorb can not be described by groups with a constant charge, but is composed of weak surface groups. As examples we can give mineral oxides, edge faces of clay minerals or

microcrystalline cellulose. Due to this, the adsorbed amount will be a function of the charge density of both components, and the charge density of the surface and the adsorbed polyelectrolyte will depend on the adsorbed amount. Regarding these mutual influences the theoretical description of weak polyelectrolytes in contact with a surface with a variable charge requires a most delicate description.

Such a description is of relevance for many industrial processes such as food technology, pharmacy, paper industry (5), paint production, production of television screens, collection of metals in mining industry (19), and the adsorption of natural polyelectrolytes onto activated carbon in drinking water treatment (20,21). Regarding the widespread use of these systems, a better understanding of the processes, controlling the adsorption, is required.

Early models of polyelectrolyte adsorption (12,13) showed that the charge density of the weak polyelectrolyte molecules was influenced due to the accumulation of these molecules at a surface. Within this study we will show that the charge density of the surface also adjusts to the changing local conditions. Both the surface and the adsorbed polyelectrolytes will titrate each other. Several interaction mechanisms will be discussed to obtain a better insight into such a complicated variable charge systems.

In the theoretical section the SCF theory is briefly summarised, the incorporation of the weak surface charges is carried out, and an evaluation of the potential profile is given. We will discuss the charge density of both components due to the interaction as a function of the conditions. The effects of specific adsorption and hydrophobicity of the polyelectrolyte on the surface charge density will be described. These aspects will be shown to be of great importance for the adsorbed amount, the decay of the potential profile and the conformation of the adsorbed layer.

## Theory

### Model and system definition

The SCF theory is a lattice based model. The lattice serves as discrete sites onto which polymer units, ions and solvent can take positions. It consists of M parallel layers of thickness d. The layers are numbered from $z = 1$ to $z = M$. Each layer contains L lattice sites. An impenetrable wall is placed at $z = 0$, representing the surface. At the other boundary at $z = M + 1$, reflecting conditions are assumed. Each lattice site has a number of neighbouring sites of which a fraction $\lambda_0$ is found in the same layer and a fraction $\lambda_1$ in each of the adjacent layers. A molecule of type i has a volume fraction of $\rho_i(z)$ in layer z and $\Phi_i$ in the bulk. The lattice sites in each layer are indistinguishable so that a mean-field approximation should be applied. Then only inhomogeneities perpendicular to the surface can be considered.

The surface with surface sites of type S is composed of one type of group, which is assumed to be hydrophilic. This group has a variable charge and can be titrated from +0.5 to -0.5 (Equation (2.1)), according to the one pK model of Van Riemsdijk et al. (22) that was later reviewed by Koopal (23)).

17

$$SH^{\frac{1}{2}+} \overset{K_s}{\rightleftarrows} S^{\frac{1}{2}-} + H^+ \tag{2.1}$$

The intrinsic equilibrium constant of this acid-base reaction is denoted as $K_s$. The pristine point of zero charge (p.p.z.c.) is at $pH = pK_s$. A polyelectrolyte molecule i is considered as a chain of $N_i$ segments numbered $s = 1,...,N_i$. We will consider chains composed of two type of segments; U and C, where U stands for an uncharged segment and C for an acid segment with a variable charge. The C segment is titrated according to equation (2.2).

$$CH \overset{K_c}{\rightleftarrows} C^- + H^+ \tag{2.2}$$

The equilibrium constant of the acid base reaction of the polyelectrolyte segment C is denoted as $K_c$. The other components in the system are water (W), monovalent indifferent salt ions (for sake of convenience denoted as $Na^+$ and $Cl^-$) and protons and hydroxyl ions ($H^+$ and $OH^-$). Except for the $H^+$ and $OH^-$ ions all components and the polymer segments are equally sized. The protons and hydroxyl ions are point charges and are used to define the pH of the system.

Each segment type x ($x = U, C, Na^+, Cl^-, W, S$ (note that in the group of segment types x, $H^+$ and $OH^-$ are not included)) experiences a potential energy $u_x(z)$ at a distance z·d from the surface. The potential $u_x(z)$ is normalised with respect to the bulk solution. Thus $u_x(\infty) = 0$. This segment potential is composed of an excluded volume contribution and nearest neighbour and electrostatic contributions. The excluded volume potential is linked to the boundary condition, $\Sigma \rho_i(z) = 1$. Flory-Huggins (24) $\chi$ parameters are used to quantify nearest neighbour segment-segment interactions. The electrostatic interactions are incorporated using the multi-Stern-layer model (12,13). The so-called two state approach (18,25) is used to describe the acid-base equilibrium of the weak polyelectrolyte and the surface. With a mean-field approximation the weighted probability $G_i(z,s)$ of finding a segment s of component i in a layer z is calculated using a Boltzmann equation (2.3). If segment s of molecule i is of type x: $G_i(z,s) = G_x(z)$ and

$$G_x(z) = \exp(-u_x(z)/kT) \tag{2.3}$$

where kT is the thermal energy. (Obviously the concentration of S segments in the bulk equals zero. Still the weighting factor can be defined with respect to the bulk by defining a virtual reference potential for the S segments.)

To evaluate the statistical weight of all possible conformations a first order Markov approach is used. On the basis of these weights equilibrium volume fractions $\rho_i(z)$ ($\Phi_i$ for bulk values) are calculated for all components in the system. The volume fraction of a specific component both depends on and determines the potential energy. A consistent equilibrium solution has to be determined numerically. Once $\rho_i(z)$ and $u_x(z)$ are determined other thermodynamic properties of the system can be derived.

## Segment density distribution

The distribution of molecules, as a function of the distance from the surface, depends on the potential profile under the specified circumstances. A segment of type x in layer z in internal state $\beta$, ($\beta$ = 0, 1) indicating the charge situation, is subjected to a potential field, $u_{x,\beta}(z)$, as described in equation (2.4).

$$u_{x,\beta}(z) = u'(z) + kT \sum_y \chi_{x,y}\left(\langle \rho_y(z) \rangle - \Phi_y\right) + \upsilon_{x,\beta} e \psi(z) \tag{2.4}$$

For the chargeable polymer units $\upsilon_{c,0} = 0$ or $\upsilon_{c,1} = -1$, for the surface $\upsilon_{s,0} = 1/2$ or $\upsilon_{s,1} = -1/2$, $\upsilon_{Na} = 1$, $\upsilon_{Cl} = -1$, $\upsilon_U = 0$ and $\upsilon_W = 0$. Equation (2.4) can be divided into three independent parts. The first term, u'(z), ensures, as told above, that all layers remain completely filled; it keeps the sum of the volume fractions of all molecules in layer z equal to unity. The second term presents the nearest neighbour segment-segment interactions, quantified by the Flory-Huggins $\chi_{x,y}$-parameters. The $\chi_{x,y}$-parameter models the hydrophilic and hydrophobic interactions in the system. The sum over y includes the surface S and thus the interaction with the surface is included. The third term describes the electrostatic interactions. These interactions are proportional to the valence of segment type x in state $\beta$ and the electrostatic potential in layer z, $\psi(z)$. The contact fraction, $\langle \rho_x(z) \rangle$, of a site in layer z with segment x is expressed as:

$$\langle \rho_x(z) \rangle = \lambda_1 \, \rho_x(z-1) + \lambda_0 \, \rho_x(z) + \lambda_1 \, \rho_x(z+1) \tag{2.5}$$

The acid base equilibrium is modelled in the SCF theory following a two state approach suggested by (25) and introduced in the present model by Israëls et al. (18). An important parameter is the weighting factor $G_x(z)$. This parameter is defined as the statistical weight of finding a segment of type x irrespective in which internal charge state the segments is. For a two state model $G_x(z)$ is given by equation (2.6).

$$G_x(z) = \sum_{\beta=0,1} \alpha_{x,\beta}{}^b G_{x,\beta}(z) \tag{2.6}$$

where $\alpha_{x,\beta}{}^b$ is the probability of finding a unit of type x in state $\beta$ in the bulk (indicated by the superscript b)

$$\alpha_{x,1}{}^b = \frac{K_x}{K_x + \Phi_{H^+}} = 1 - \alpha_{x,0}{}^b \tag{2.7}$$

By definition the degree of dissociation $\alpha_x$ of the segment types U and W equals 0 and that of the segment types $Na^+$ and $Cl^-$ equals 1.

If $G_x(z)$ and the bulk volume fractions, $\Phi_x$, are known, the volume fractions of the molecules, composed of a single segment can easily be calculated. If molecule i is of type x:

$$\rho_x(z) = \Phi_x \ G_x(z) \tag{2.8}$$

To model a polyelectrolyte chain, we should at least consider that the different segments are connected to each other. A segment s of a chain can only be located in layer z if segment s-1 is located in one of the layers z-1, z or z+1. The end-segment distribution of a chain of s segments can be expressed in that of a chain with s-1 segments by use of a recurrence relation (Equation (2.9)), with a starting condition as expressed in Equation (2.10).

$$G_i(z, s|1) = G_i(z, s) \ \langle G_i(z, s-1|1) \rangle \tag{2.9}$$

$$G_i(z, 1|1) = G_i(z, 1) \tag{2.10}$$

The equations (2.11) and (2.12) can be used for the end-segment distribution of the polyelectrolyte chain, starting from segment N.

$$G_i(z, s|N) = G_i(z, s) \ \langle G_i(z, s+1|N) \rangle \tag{2.11}$$

$$G_i(z, N|N) = G_i(z, N) \tag{2.12}$$

To obtain the volume fraction $\rho_i(z,s)$, both end-point distributions are required. The product of both functions and a normalisation constant $(C_i)$, divided by the segment weighting factor of segment s (to avoid double counting of this segment), gives the volume fraction of segment s of molecule i.

$$\rho_i(z,s) = C_i \ \frac{G_i(z, s|1) \ G_i(z, s|N)}{G_i(z, s)} \tag{2.13}$$

The normalisation constant $C_i$ depends on the bulk volume fraction and the chain length of molecule i.

$$C_i = \Phi_i \ / \ N_i \tag{2.14}$$

Finally the total volume fraction profile of segment x can be calculated by a summation over all molecules i and over all segments s.

$$\rho_x(z) = \sum_i \sum_{s=1}^{N_i} \rho_i(z,s) \ \delta_{i,x}^s \tag{2.15}$$

where $\delta_{i,x}^s$ is a Kroniker delta function, which equals 1 if segment s of molecule i is of type x and 0 otherwise.

*"Surface" charge*

Once the segment density distributions and the weighting factors are known, the degree of dissociation, of segment x in layer z as a function of the local conditions, can be calculated:

$$\alpha_{x,\beta}(z) = \frac{\alpha_{x,\beta}^b \; G_{x,\beta}(z)}{G_x(z)} \tag{2.16}$$

Equation (2.7) can be rewritten, now $\alpha(z)$ depends on the local proton concentration, that can be expressed as a Boltzmann factor of the local electrostatic potential.

$$\alpha_{x,1}(z) = \frac{K_x}{K_x + \Phi_{H^+} \; e^{-\Psi(z)/kT}} = 1 - \alpha_{x,0}(z) \tag{2.17}$$

For the sites in the surface it has to be taken into account that $\rho_s(0)$ equals 1 and that the average weighting factor is defined with respect to the bulk, where $\alpha_{s,\beta}{}^b$, is the virtual degree of dissociation in the reference state ($\psi=0$).

By combination with the local segment density, the excess charge per unit area $(d^2)$ of the polyelectrolyte chains can be calculated. In the following we will discuss both the overall charge per unit area per layer as well as the charge per unit area per type of molecule per layer. The former can be calculated by equation (2.18) the latter by equation (2.19):

$$\sigma(z) = \sum_x \sum_\beta \upsilon_{x,\beta} \; e \; \alpha_{x,\beta}(z) \; \rho_x(z) \, / \, d^2 \tag{2.18}$$

$$\sigma_i(z) = \sum_{s=1}^{N_i} \sum_x \sum_\beta \frac{\upsilon_{x,\beta} \; e \; \alpha_{x,\beta}(z) \; \rho_i(z,s)}{d^2} \, \delta_{i,x}^s \tag{2.19}$$

The excess charge per unit area, $q^{exc}$, associated with the adsorbed polyelectrolyte molecules of type i compared to that of the molecules in the bulk, is calculated by Eq. (2.20).

$$q_{i,ads}^{exc} = \sum_z \sum_{s=1}^{N_i} \sum_x \sum_\beta \upsilon_{x,\beta} \; e \; \left( \alpha_{x,\beta}(z) \, \rho_i(z,s) - \alpha_{x,\beta}^b \; \Phi_i^b \right) \delta_{i,x}^s \tag{2.20}$$

*Electrostatic potential*

The relation between the surface charge and the electrostatic potential of the surface has been described by several authors (*26-28*) and can be formally described as a condensor with plate charge $\sigma_0$ and potential drop $\psi_0$. According to the constant-capacitance model the correlation between the surface charge of an uncovered particle and the surface potential is given by Eq. (2.21), where C is a constant capacitance,

which is a measure for the properties of the dielectricum in the condensor, according to Eq. (2.22).

$$\sigma_0 = \psi_0 * C \tag{2.21}$$

$$C = \frac{\varepsilon_0 \varepsilon_r}{d} = \frac{\varepsilon}{d} \tag{2.22}$$

Within the SCF theory the charge and potential decay can be described as a series of parallel condensors , each with its own charge and capacitance. The charge density in each layer is calculated following Equation (2.18). All charges are thought to be located halfway in-between two successive layers, in-between these charge-planes no electrostatic charge is allowed, fully in the spirit of both the lattice and the condensor model. This model is usually called the multi-Stern- layer model (12,13).

Within the presented calculations all dielectric permittivities were set to be equal, thus the electrostatic potential difference between two successive charge planes varies linearly with distance. The electrostatic field strength (Equation (2.23)) at a distance z from the surface,

$$E(z) = \frac{1}{\varepsilon} \sum_{z=0}^{z} \sigma(z') \tag{2.23}$$

and hence the electrostatic potential (Equation (2.24)) between two successive layers depends on the total charge in-between these planes.

$$\psi(z) - \psi(z+1) = \int_{z'=(z-\frac{1}{2})d}^{(z+\frac{1}{2})d} E(x)dx = \frac{d}{\varepsilon} \sum_{z'=0}^{z} \sigma(z') \tag{2.24}$$

*Calculation of the bulk properties of the polyelectrolyte*

Following the approach described above it is not possible to calculate the bulk properties of the polyelectrolyte molecules accurately. In the bulk the electrostatic potential is relaxed (equal to 0) and all polyelectrolyte segments are indistinguishable; irrespective of the position of the segment along the chain each segment feels $\psi = 0$. Only the trivial titration result is obtained. The polyelectrolyte molecules in the vicinity of the surface are, however, subjected to the developed potential field. To overcome this aspect of the planar SCF lattice theory a second type of calculations is introduced to calculate the spatial degree of dissociation of the polyelectrolyte molecules in the bulk as a function of pH, salt concentration and bulk concentration. We will calculate the properties of the polyelectrolyte by placing these in a lattice with a spherical geometry. The structure of non-planar lattice symmetries were first used by Leermakers and Scheutjens (29) for the calculation of surfactant micelle. The differences between a curved and a planar lattice are that the volume of the lattice layer and consequently the number of lattice sites in a layer increase on moving away from the centre. Further the number of neighbouring sites $\lambda_i$ in each of the adjacent layers has to be treated

separately, $\lambda_{-1}$ and $\lambda_{+1}$, and are layer dependent. A further discussion on the theory of SCF calculations with a curved lattice are described by Barneveld et al. (30). Within our calculations a spherical lattice was applied.

The charge/ pH curves are obtained by studying one polyelectrolyte molecule grafted with one segment at the centre of this spherical lattice; i.e. at $z = 0$. Calculations were performed following the procedures described by Wijmans and Zhulina (31) and Israëls et al. (18) for a grafted polymer brush. We choose to restrict the middle segment of the polyelectrolyte molecule. All other segments are allowed to distribute according to all possible and allowed conformations and interactions. Following this procedure a potential profile develops from the centre of the lattice decaying into the bulk. This potential profile then generates a spatial distribution of the degree of dissociation for the polymer units.

Usually the polyelectrolyte molecules are not isolated. Within most calculations presented in this paper, significant bulk concentrations were present. To model the influence of the polyelectrolyte concentration on the titration of the polyelectrolyte, other polyelectrolyte chains were included in the system. These extra molecules have similar properties as those of the grafted one, but are of course fully free to translate through the system.

*Choice of parameters*

The calculations were performed using a lattice of simple cubic symmetry with a characteristic size d of 0.311 nm. The cell size corresponds with a water density of 55.2 mol $l^{-1}$. Regarding this lattice type, each lattice site has 6 neighbouring sites of which a fraction $\lambda_0 = 4/6$ is found in the same layer and a fraction $\lambda_1 = 1/6$ in each of the adjacent layers. Throughout our study, the number of lattice layers M equals 100. This number was chosen to assure that all concentration and potential profiles were relaxed in the bulk of the system. All segments (U, C, Na$^+$, Cl$^-$, W and S) have a relative dielectric permittivity $\varepsilon_r$ of 80.

A surface with a variable charge was introduced within the calculations. The surface was composed of segments S with a pK of 8, i.e. a p.p.z.c. of 8. For the present choice of the lattice cell this results in a maximal charge density of 10.4 charged sites nm$^{-2}$. The surface charge density is usually given in C m$^{-2}$; the multiplication factor to convert unit charges per cell to C m$^{-2}$ is 1.66 (e d$^{-2}$). The polyelectrolyte molecules were composed of segments U and C in the ratio 2:1, $(H_2C_1)_{50}$, where segment C has a pK of 4. The number of segments of the polyelectrolyte molecules presented in this paper was 150, but the trends were the same for longer molecules. The concentrations of all components are given as volume fractions. The volume fraction $\rho$ can be converted to a molarity c through $\rho = cV_m$ where $V_m = N_A V_{cell}$ is the molar volume (l mol$^{-1}$) and $N_A$ the number of Avogadro. $V_{cell}$ follows from the lattice spacing d and the lattice type, for the present choice of parameters $V_m = 0.0181$ l. For the non-electrostatic nearest neighbour segment-segment interactions, Flory-Huggins (24) $\chi$ parameters are used. By definition $\chi = 0$ for molecules of the same kind and $\chi_{x,y} = \chi_{y,x}$. A $\chi$ of 0.5 indicates a $\theta$ solvent. Unless otherwise indicated, all Flory-Huggins parameters were taken to be zero. The fact that the $\chi_{x,y}$ parameters that involve the salt ions are all zero, indicates that the salt is indifferent. In some cases different non-electrostatic interactions are modelled in this

study to account for a specific interaction energy between segment x and the surface S ($\chi_{x,s}$), and for hydrophobic interactions. In the case that all other $\chi$ parameters are zero the relation between the adsorption energy ($u_A$) and $\chi_{x,s}$ is $u_A = \lambda_1 \chi_{x,s}$, since only a fraction $\lambda_1$ of an adsorbed segment is in contact with the surface. In the major part of this paper we will only describe the effects due to specific adsorption of polyelectrolyte molecules. In the last section we will shortly discuss the effects due to hydrophobic interactions ($\chi_{U,W} = \chi_{C,W} > 0.5$).

## Results and discussion

We start our survey by examining the properties of the single components; the bare surface and pure polyelectrolyte.

The surface charge curves as a function of pH at different salt concentrations are shown in Figure 1a. It is observed that the surface charge increases with increasing ionic strength. The accumulation of (mainly) counterions close to the surface screens the surface charge and consequently the double layer thickness and the electrostatic potential profile will be compressed as is commonly observed for oxide surfaces (32,33). As an example of this salt effect the potential-distance curves at pH 3 and 9 for different ionic strengths are sketched in Figure 1b. These curves can be described by the classical Gouy-Chapman double layer theory. According to the one pK model (22,33) in an indifferent electrolyte the overall surface charge at a pH value equal to the pK of the surface groups will be zero and consequently the potential-distance curve will be constant and zero. As a result the electrostatic effects have disappeared and the surface charge/ pH curves at different salt concentration merge through a common intersection point, the so-called point of zero charge (p.z.c.).



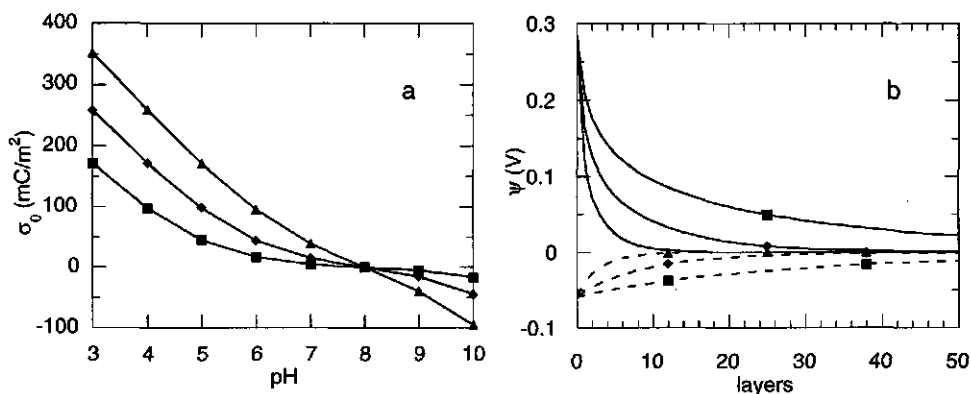**Figure 1: a:** Calculated surface charge as a function of pH for different salt concentrations: ■ = $10^{-3}$ M; ♦ = $10^{-2}$ M; ▲ = $10^{-1}$ M and **b:** the corresponding potential profiles for pH 3 (solid lines) and 9 (broken lines). Layer z = 0 corresponds to the surface segments. The pK of surface segment S equals 8 and S is titrated from +0.5 to -0.5.

In Figure 2a and 2b the surface charge/ pH curves of the polyelectrolyte are shown for respectively different salt concentrations and different polyelectrolyte concentrations. The bulk polyelectrolyte concentration within the calculations presented in Figure 2a was zero. It is observed that with decreasing ionic strength the chargeable polyelectrolyte segments are more difficult to dissociate due to the increasing electrostatic potential close to the polyelectrolyte sites. Salt ions screen the chargeable polyelectrolyte segments. The volume fraction profiles at the different salt concentrations (not shown) indicate that the molecular size is decreased by about a factor 2 with increasing salt concentration ($10^{-3}$ to $10^{-1}$ M). As can be observed in Figure 2b, the electrostatic effects also disappear at high polyelectrolyte concentration. At a bulk concentration of $\Phi = 0.1$, the chargeable polyelectrolyte segments dissociate according to their pK value. The $R_{rms}$ of the molecule is decreased with increasing bulk concentration.
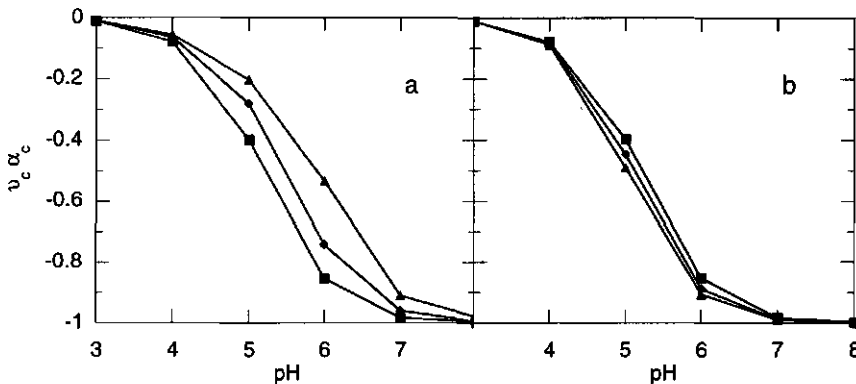


**Figure 2**: Degree of dissociation of the polyelectrolyte in the bulk solution as a function of pH for **a:** different salt concentrations (at $\Phi_i = 0$ (i = polyelectrolyte)): ■ = $10^{-1}$ M; ♦ = $10^{-2}$ M; ▲ = $10^{-3}$ M and **b:** different polyelectrolyte bulk volume fractions ($c_{salt} = 10^{-1}$ M): ■ $\Phi_i = 10^{-3}$; ♦ $\Phi_i = 10^{-2}$; ▲ $\Phi_i = 10^{-1}$. The middle segment of a molecule with a chain length of 151 is restricted within the centre of a spherical lattice. The polyelectrolyte molecules in the bulk are composed of 150 segments, missing the anchor molecule. The pK of the chargeable polyelectrolyte segment C equals 5 and C is titrated from 0 to -1.

*Adsorption characteristics*

The next step in the evaluation of the charge characteristics of the mixed system is the calculation of the adsorbed amount. For all further calculations the total amount of polyelectrolyte in the system equals 2 equivalent monolayers. This amount is sufficient to assure that under all conditions the bulk solution contained sufficient polyelectrolyte after adsorption, it reflects a point on the plateau of the adsorption isotherm. Especially the mechanisms underlying the adsorption are of importance to gain understanding of the mixed system. Comparison of the charge/ pH curves given in Figure 1a and 2a learns us that below the p.z.c. of the surface the two components are oppositely charged, although the polyelectrolyte charge in the bulk at a pH lower than pH 3 is negligible. Above pH 8 (p.z.c.) both components are negatively charged.

Many different interactions can be proposed, for the present system. As explained in the parameter section we will discuss pure electrostatic interaction, electrostatic plus specific or "chemical" interaction and finally we will briefly discuss effects due to hydrophobicity of the polyelectrolyte interactions.

The general shape of the adsorption isotherms given in Figure 3 show a maximum in the adsorbed amount around 1-1.5 pH unit below the pK of the polyelectrolyte segments. The pH shift of this maximum increases slightly with increasing adsorption energy. The occurrence of this maximum was already described by Böhmer et al. (*13*) and Evers et al. (*12*). They explained the observed maximum as arising due to the adjustment of the polyelectrolyte charge in the first layer such that the surface charge could be neutralised, even if the pH in the bulk of the system is several pH units below the pK of the polyelectrolyte segments. At much lower pH values the charge on the polyelectrolyte will be decreased and charge compensation can no longer be accomplished by the polyelectrolyte adsorption and ion adsorption takes over. It may be clear that these interactions are even more complicated for systems composed of both a surface with a variable charge and weak polyelectrolyte molecules. As will be shown in a later paragraph the mutual charge adjustment is also observed in these complicated systems.
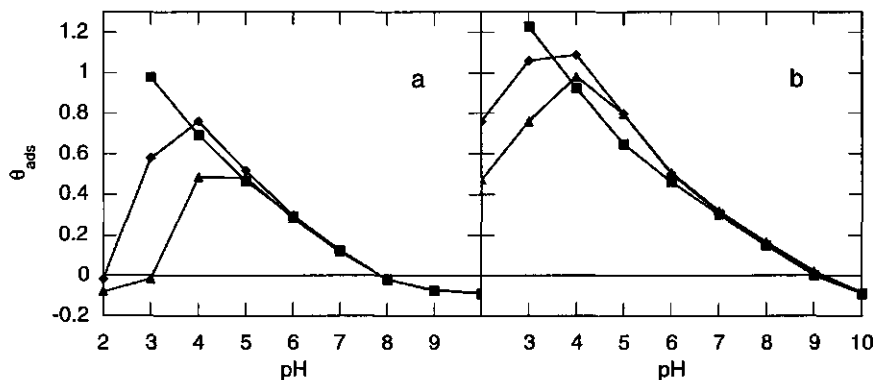


**Figure 3:** Adsorbed amount of a (weak) polyelectrolyte as a function of pH for three salt concentrations onto a surface with a variable charge: ■ = $10^{-3}$ M; ◆ = $10^{-2}$ M; ▲ = $10^{-1}$ M. The Flory-Huggins interaction parameter, $\chi_{s,c}$, between surface S and polyelectrolyte segment C is a: 0 and b: -15. All other interaction parameters are zero. The chain length of the polyelectrolyte is 150 and the amount of polyelectrolyte equals 2 equivalent monolayers.

Figure 3a and 3b present the excess adsorbed amount of polyelectrolyte as a function of pH. The adsorbed amount is expressed in equivalent monolayers. Figure 3a reflects a situation where the interaction mechanism was pure electrostatic attraction ($\chi_{s,c} = 0$, $\chi_{s,u} = 0$). At low pH values (< pH4) the effect of the indifferent electrolyte concentration is screening reduced. The adsorbed amount decreases with increasing ionic strength; the salt ions screen the surface charge/ polyelectrolyte charge attraction. At a salt concentration of 0.1 M the electrostatic attraction vanishes due to the screening effect and a depletion layer arises. At 0.001 M salt the electrostatic attraction between

polymer and surface is still significant at pH 3. This salt effect changes gradually with increasing pH and shows a weak screening enhanced regime between pH 4.5 and 6. The adsorption is increased with increasing ionic strength due to the screening of the lateral repulsion within the adsorbed polyelectrolyte layer. Beyond pH 6 the salt effects becomes very small. At the p.z.c. of the surface no adsorption is observed because the attraction for the surface has vanished.

Besides electrostatic attraction we have introduced specific attraction. Figure 3b presents the adsorption isotherms of a polyelectrolyte of which the chargeable segments also have a specific attraction for the surface ($\chi_{s,c} = -15$, $\chi_{s,u} = 0$). Due to this specific adsorption energy, adsorption occurs upto one pH unit above the p.z.c. of the surface. The screening enhanced regime is now significant from about pH = 4 to pH = 7. At pH values below pH = 4 the screening reduced regime starts. The effect diminished compared to the pure electrostatic situation. Due to the non-electrostatic interaction even at pH 2 and below a significant adsorption is observed. Calculations for other $\chi_{s,c}$ values show that these effects occurred gradually with increasing adsorption energy.

The amount of adsorbed polyelectrolyte can also be described with the polymer density as a function of the distance from the surface. In Figure 4 these volume fraction profiles are shown for different pH values, ionic strengths and adsorption energies. The distance from the surface is expressed in lattice layers.
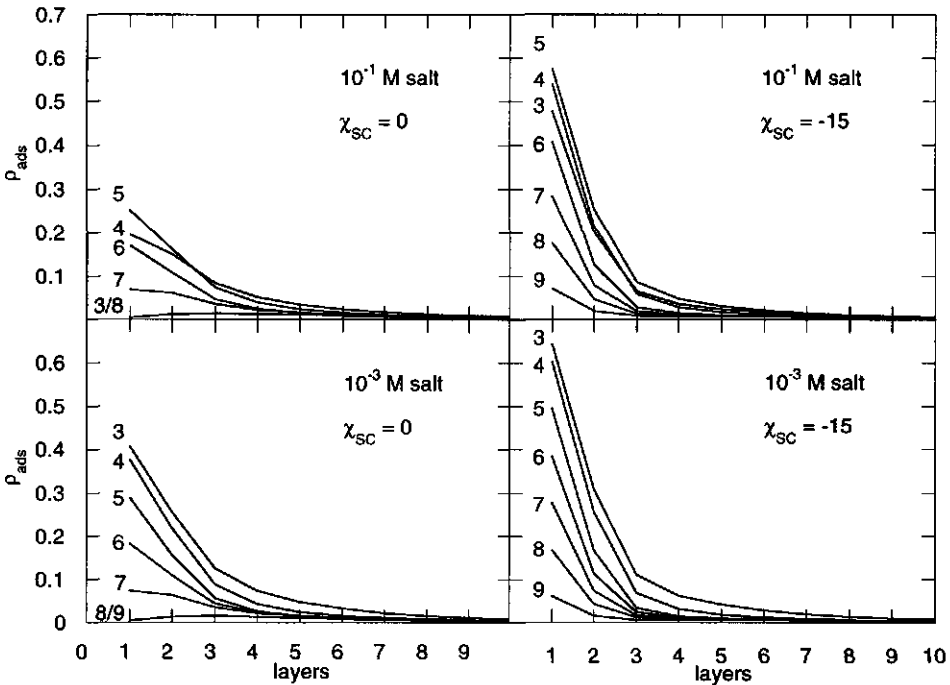


**Figure 4:** Volume fraction profiles of the adsorbed polyelectrolyte for different pH values as indicated, two ionic strengths $10^{-3}$ M and $10^{-1}$ M and two values for the interaction parameter $\chi_{s,c} = 0$ and $\chi_{s,c} = -15$. Layer z = 1 corresponds to the boundary between surface and solution. All other parameters as in Figure 3.

Based on these volume fraction profiles some important observations can be made regarding the conformation of the adsorbed polyelectrolyte molecules. If the adsorption is purely electrostatic, the polyelectrolyte layer protrudes further into the solution with increasing ionic strength. At 0.1 M the adsorption layer at pH values deviating from the pK of the polyelectrolyte segments decreases only slightly in the first layers as a function of z. This effect is reflected in the crossing of some of the potential profiles in Figure 4 (0.1 M salt). With decreasing ionic strength ($10^{-3}$ M) electrostatic attraction is more profound and consequently the volume fraction in the first layer increases resulting in a more compact layer. At pH values lower than pH 5 the degree of dissociation of the polyelectrolyte segments extending beyond layer 1 is relatively low and loops and long tails are favourable. At higher pH values the electrostatic attraction decreases due to the low surface charge and the lateral repulsion between the adsorbed polyelectrolyte segments increases. Due to this repulsion some of the charged polyelectrolyte segments are expelled from the surface. It is well known that just above the critical adsorption energy (in the absence of coulombic attraction) relatively thick layers are developed due to the few contacts per molecule. Under these circumstances the loss of entropy is just compensated by the adsorption energy.

An increasing adsorption energy results in a higher adsorption and a more compact adsorbed polyelectrolyte layers. The relative volume fraction of polyelectrolyte segments in the first layer is increased with increasing pH. At pH values higher than the pK of the surface groups depletion effects are observed. Thus it has to be concluded that the adsorbed amount and the conformation of the molecules depend on a delicate equilibrium between pH, ionic strength and adsorption energy.

### Electrostatic potential profiles

As discussed by Böhmer et al. (13) and Evers et al. (12) adjustment of the polyelectrolyte charge in the first layer such that the surface charge could be neutralised, determined to a large extend the adsorbed amount. In their calculations the surface charge was taken to be constant. In our calculations both the surface and the polyelectrolytes have units with a variable charge. In order to study the charge associated with the separate components in the mixed system and to investigate whether or not charge compensation is a limiting factor controlling the adsorption the degree of dissociation of the chargeable segments as a function of z has been calculated. The degree of dissociation of segment x in layer z depends on the electrostatic potential in this layer (Eq. (2.17)). The electrostatic potential decay as a function of z for different pH values, ionic strength and adsorption energy is shown in Figure 5. If we compare these potential profiles with those of the bare surface (Figure 1b) it is observed that, especially at the lowest salt concentration, the profiles are collapsed. Due to the screening of the oppositely charged polyelectrolyte the potential is relaxed to the bulk potential within about 10 layers. Only a small salt effect can be observed indicating that compensation of the surface charge within the first layers is significant (see Eqs. ((2.23)) and ((2.24))). At low pH (pH 3 and 4 (0.1 M salt) and pH 3 (0.001 M salt)) the potential decay is more extended. This is due to the low adsorbed amount at these pH values (Figure 3a); the charge associated with the adsorbed molecules is not sufficient to compensate the surface charge. However, even at these

low pH values the small amount of adsorbed polyelectrolyte screens the surface effectively and consequently the potential decay can not be described by the classical Gouy-Chapman double layer theory. According to this familiar limiting law, in a flat diffuse layer the potential drops exponentially with distance. If we compare the potential decay of the bare surface with that of the surface with an adsorbed amount of polyelectrolyte we find that even at low surface coverage the charge associated with the adsorbed polyelectrolyte is significant. The introduction of an extra adsorption energy results for pH > 4 in a super equivalent adsorption. The overall polyelectrolyte charge exceeds the surface charge and consequently the excess of negatively charged polyelectrolyte segments, accumulated close to the surface, cause an overall negative charge of the complex. Due to this accumulation a negative electrostatic potential is developed in the layers close to the surface (Figure 5).
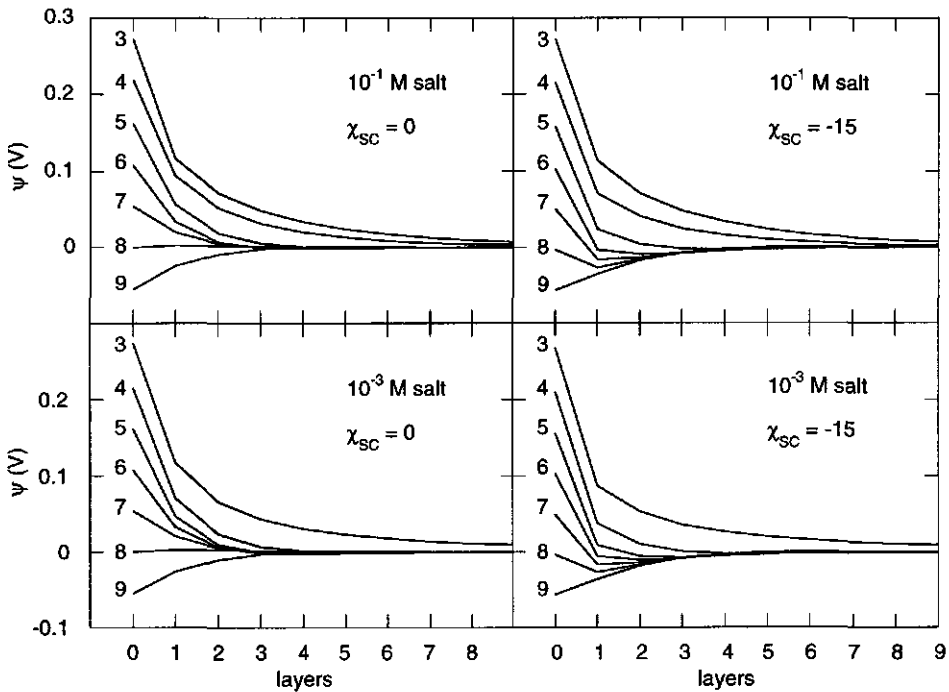


**Figure 5:** Potential-distance profiles developed from the surface in contact with the adsorbed polyelectrolyte for different pH values as indicated, two ionic strengths $10^{-3}$ M and $10^{-1}$ M and two values for the interaction parameter $\chi_{s,c} = 0$ and $\chi_{s,c} = -15$. Layer $z = 0$ corresponds to the surface potential. All other parameters as in Figure 3.

*Surface charge compensation*

The potential profiles shown in Figure 5 indicated that the compensation of the surface charge may be an important aspect controlling the adsorbed amount. Both the surface charge (Eq. (2.21)) and the excess polyelectrolyte charge (Eq. (2.20)) are calculated for comparison. The excess polyelectrolyte charge equals the extra charge that is

associated with the molecules in the vicinity of the surface. Figure 6 shows both charge densities as a function of pH for different ionic strengths and specific adsorption energies. Note that the surface charge is multiplied by a factor -1 to obtain a more convenient comparison with the polyelectrolyte charge.
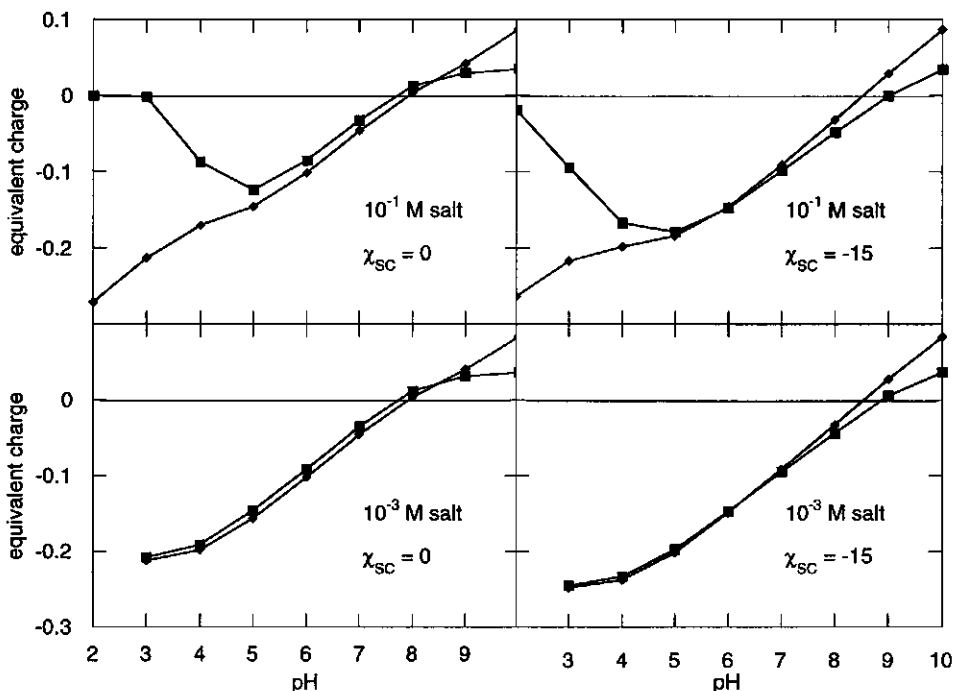


**Figure 6:** The negative surface charge/ pH curve (♦) and the excess polyelectrolyte charge (■) reflecting the charge (over)compensation as a function of the ionic strength ($10^3$ M and $10^{-1}$ M) and the specific adsorption energy ($\chi_{s,c} = 0$ and $\chi_{s,c} = -15$). All other parameters as in Figure 3.

With decreasing salt concentration and pure electrostatic attraction the polyelectrolyte charge is increased especially at lower pH values. This effect can be ascribed to the decreased screening of the surface groups. At 0.1 M salt the degree of dissociation of the polyelectrolyte groups is only slightly influenced by the surface charge. Whereas the surface charge is compensated by the polyelectrolyte for most pH values at 0.001 M salt. The apparent positive charge subscribed to the polyelectrolyte at pH values above the p.z.c. of the surface reflect the depletion layer which was already shown in Figure 3. The surface charge/ pH curves at different salt concentrations merge through the common intersection point (p.z.c.) as was observed for the bare surface. Both the surface charge/ pH curve and that of the polyelectrolyte are affected due to the introduction of a specific adsorption energy. The common intersection point of the surface charge/ pH curves is shifted to a higher pH value and the adsorbed polyelectrolyte charge is increased over the entire pH range. Compared to the pure electrostatic case the charge associated with the adsorbed molecules overcompensates the surface charge at pH values above the pK of the chargeable

polyelectrolyte segments even if it is taken into account that the surface charge was increased.

## Charge adjustment and specific adsorption

In Figure 7 and Figure 8, the "new" effect of charge adjustment of the single components is shown for different values of the specific adsorption energy.
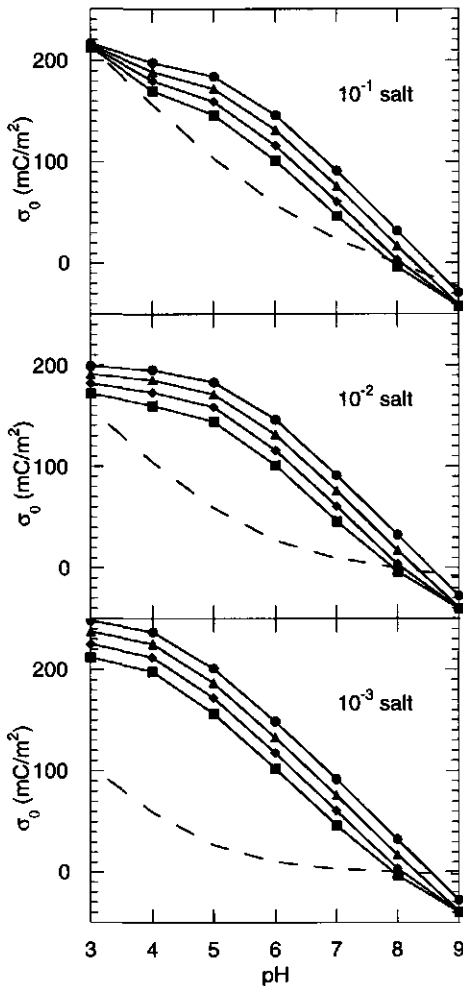
**Figure 7:** Surface charge as a function of pH of the bare surface (broken line) and for the surface in contact with adsorbed polyelectrolyte for different interaction parameters: ■ $\chi_{s,c} = 0$; ♦ $\chi_{s,c} = -5$; ▲ $\chi_{s,c} = -10$ and ● $\chi_{s,c} = -15$ and three salt concentrations $10^{-3}$ M; $10^{-2}$ M and $10^{-1}$ M.
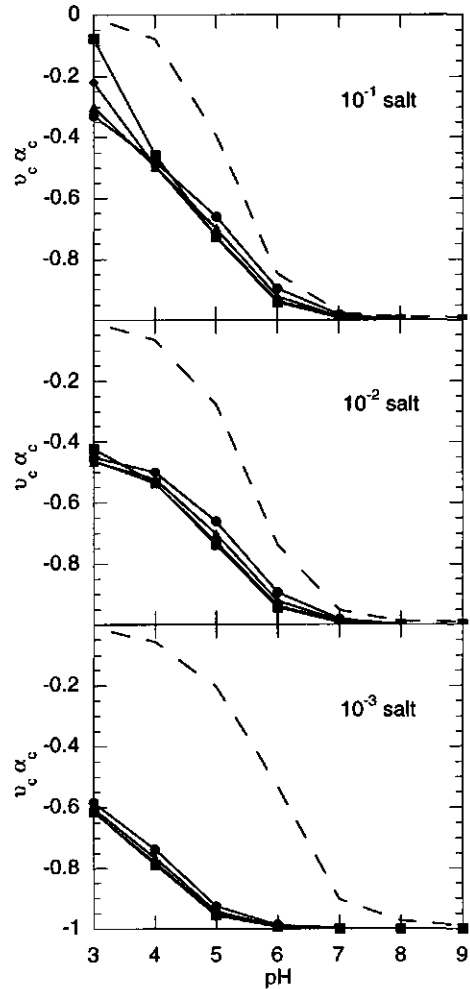
**Figure 8:** Degree of dissociation as a function of pH of the polyelectrolyte in the bulk solution (broken line) and for the polyelectrolyte adsorbed onto the surface for different interaction parameters: ■ $\chi_{s,c} = 0$; ♦ $\chi_{s,c} = -5$; ▲ $\chi_{s,c} = -10$ and ● $\chi_{s,c} = -15$ and three salt concentrations $10^{-3}$ M; $10^{-2}$ M and $10^{-1}$ M.

31

Both components are titrated due to the interaction with the charged segments of the other component. Although an increasing specific adsorption energy increases the charge adjustment, it is observed that these effects also occur in the situation where the adsorption is purely electrostatic. The two main effect of the specific adsorption energy on the surface charge/ pH curves are a shift of the p.z.c. to higher pH values and an increased absolute surface charge. Due to the charge associated with the adsorbed polyelectrolyte the surface charge is screened very efficiently and, especially at higher pH values, no salt effect is observed. The effects of an increased specific adsorption energy on the polyelectrolyte segments is mainly revealed at the highest salt concentration. At 0.1 M salt the surface charge/ polyelectrolyte charge attraction is screened resulting in a significantly lower adsorption with decreasing adsorption energy. Further the adsorbed polyelectrolyte charge is less significantly titrated by the surface sites due to the pronounced screening (see also Figure 3 and Figure 6). This results for low pH values in an increased degree of dissociation of the chargeable polyelectrolyte segments. For the lowest salt concentration the effects on the degree of dissociation of the polyelectrolyte segments are considerable, 2 pH units below the pK of the polyelectrolyte segments about 60% of the segments are dissociated whereas only 1% is dissociated in the absence of the surface. Now at all pH values the effect of an increasing specific adsorption energy is a decreasing degree of dissociation. Due to the increased adsorbed amount a lower fraction of polyelectrolyte segments is required to compensate the surface charge.

Comparison of the effects observed in Figure 7 and Figure 8 reveals the following trends. At low pH values (< pK 5) the surface sites are only slightly effected by the adsorbed polyelectrolyte, whereas at higher values a significant amount of extra charge is induced. The concentration of indifferent electrolyte only affects the titration behaviour at low pH values, where a decreasing effect is observed with increasing salt concentration. On the contrary extra charges are induced on the polyelectrolyte segments at low pH values whereas the effect at high pH is only small. These trends are explained due to the effect that both components have on the potential profile developed around the surface. At low pH the surface sites determine the potential decay and consequently the polyelectrolyte segments are mainly adjusted. At high pH the polyelectrolyte segments are most important. The effect of an increasing specific interaction energy is an increasing effect of the adsorbed polyelectrolyte on the decay of the potential profile.

*Hydrophobic effects*

Finally we will briefly consider the effects due to hydrophobic interactions. To mimic these interactions the Flory-Huggins interaction parameters between the water monomers and both polyelectrolyte segments, C and U were set at a value of 3. Thus the polyelectrolyte molecules in the uncharged state are expelled from the solution, and even the charged polyelectrolyte accumulates at the surface. Within the SCF calculations the observed effects due to specific adsorption and hydrophobic interactions are related, both effects result in a more profound accumulation of the polyelectrolyte molecules at the surface. Calculations have shown that comparable effects on the titration curves were obtained for hydrophobic polyelectrolyte molecules. The adjustment of chargeable segments in the vicinity of oppositely charge species is not affected by the type of interaction but by the degree of accumulation close to the

interface. This again emphasises that the most important effect is the decay of the electrostatic potential profile developed due to the interaction. The component that influences this decay most significantly determines to a large extent the degree of dissociation of the other species.

## Conclusions

The incorporation of a variable surface charge within the self consistent field calculations was shown to be a major contribution for the description of the interactions that are important in many applied fields. It was shown that both components were able to titrate each other. The electrostatic potential developed around the different components affects the overall electrostatic potential profile which vice versa influences the degree of dissociation of the single components. The segment type that is most important for the developed potential profile determines the degree of dissociation of the other segments. At low pH the surface charge is dominant and consequently the polyelectrolyte segments are titrated strongly, whereas, at high pH the surface sites are mainly titrated. With decreasing salt concentration and low pH the surface charge/polyelectrolyte charge is screened to a lesser extend, the adsorption is increased and the charge adjustment is even more profound.

Outside the p.z.c. of the surface these effects were even observed for the situation where the adsorption was purely electrostatic, due to the fact that the effective valence of the polyelectrolyte is high. With increasing specific adsorption energy the adsorption was increased, even at pH values above the p.z.c. of the surface sites. This results in a shift of the p.z.c. to higher pH values which is commonly observed for specific adsorption on oxide surfaces (*32*). The effect of the interaction parameter is best observed at high salt concentration where the adsorption at low pH is diminished strongly due to screening effects. Due to a specific adsorption energy the molecules now accumulate at the surface which affects the degree of dissociation strongly. With an increasing interaction parameter the overcompensation of the surface charge by the adsorbed polyelectrolyte charge is also manifested. This results in a significant lateral repulsion compared with the situation where the adsorption was purely electrostatic and the surface charge was slightly higher than the adsorbed polyelectrolyte charge.

Regarding the described results it can be concluded that the theoretical description of weak polyelectrolytes in contact with a surface with a variable charge requires a most delicate description. The adsorbed amount, its conformation and the charge associated with the different units is determined by a subtle balance of the local conditions; pH, salt concentration and specific adsorption energy. The classification as proposed by Van der Steeg et al. (*9*) between screening enhanced and screening reduced adsorption can be applied also within a system consisting of weak polyelectrolytes segments and surface sites with a variable charge. As long as the surface charge exceeds the charge associated with the adsorbed polyelectrolyte molecules screening reduced adsorption is observed If the surface charge is overcompensated the adsorption is screening enhanced.

## Appendix I

*List of symbols*

| | |
|---|---|
| c | concentration (mol $l^{-1}$) |
| C | Stern layer capacitance |
| $C_i$ | normalisation constant for molecules i |
| d | distance between two lattice layers |
| e | elementary charge |
| E(z) | field strength in layer z |
| $G_x(z)$ | segment weighting factor for segment x in layer z |
| $G_i(z,s)$ | segment weighting factor for segment s of molecule i in layer z |
| $G_i(z,s|1)$ | end-segment distribution function in layer z of molecules i (s segments long), with segment 1 in an arbitrary layer |
| $G_i(z,s|N)$ | end-segment distribution function in layer z of molecules i (N-s segments long), with segment N in an arbitrary layer |
| i,j | index for molecule |
| k | Boltzmann's constant |
| $K_c$ | dissociation constant of polyelectrolyte segment |
| $K_a$ | dissociation constant of surface segment |
| M | number of lattice layers |
| N | chain length of a molecule |
| $N_A$ | number of Avogadro |
| $q_{i,ads}^{exc}$ | the excess charge associated with the adsorbed polyelectrolyte molecules of type i |
| s | segment ranking number |
| T | absolute temperature |
| $u_x(z)$ | potential for segments of type x in layer z |
| u'(z) | hard-core potential in layer z |
| $V_{cell}$ | volume of a lattice cell (l) |
| $V_m$ | molar Volume (l $mol^{-1}$) |
| x,y | index for segment type |
| z | layer number |
| $\alpha_x(z)$ | degree of dissociation of segments of monomer x in layer z |
| $\alpha_x^b$ | degree of dissociation of segments of monomer x in the bulk solution |
| $\beta$ | parameter indicating the state of a segment; dissociated ($\beta = 1$) or not ($\beta = 0$) |
| $\delta_{i,x}^s$ | Kroniker delta function, which is 1 if segment s of molecule i is of type x and 0 otherwise |
| $\varepsilon$ | $\varepsilon_0 \varepsilon_r$ |
| $\varepsilon_0$ | dielectric permittivity in vacuum |
| $\varepsilon_r$ | relative dielectric permittivity of a specific segment |
| $\varepsilon(z)$ | dielectric permittivity in layer z |
| $\theta_i$ | amount of molecules i (in equivalent monolayers) in the system |
| $\lambda_0$ | fraction of neighbouring lattice sites in the same layer |
| $\lambda_1$ | fraction of neighbouring lattice sites in the adjacent layers |
| $\rho_i(z)$ | volume fraction of molecule i in layer z |
| $\sigma(z)$ | charge on a plane in the centre of layer z expressed per unit area |

34

$\sigma_0$       surface charge, charge located at layer 0

$\upsilon_x$       valence of segment x

$\Phi_i$       volume fraction of molecule i in the bulk solution

$\chi_{x,y}$       Flory-Huggins interaction parameter between the segments x and y

$\psi(z)$       electrostatic potential in layer z

$\psi_0$       surface potential

## References

(1) Durand, G.; Lafuma, F.; Audebert, R. Adsorption of cationic polyelectrolytes at clay-colloid interface in dilute aqueous suspensions - effect of the ionic strength of the medium. *Prog. Colloid Polym. Sci.* **1988**, *76*, 278 -282.

(2) Wang, T.K.; Audebert, R. Adsorption of Cationic Copolymers of Acrylamide at the Silica-Water Interface: Hydrodynamic Layer Thickness Measurements. *J.Colloid Interface Sci.* **1988**, *121(1)*, 32 - 41.

(3) Meadows, J.; Williams, P.A.; Garvey, M.J.; Harrop, R.A.; Phillips, G.O. Enhanced Polyelectrolyte Adsorption. *Colloids Surf.* **1988**, *32*, 275 -288.

(4) Meadows, J.; Williams, P.A.; Garvey, M.J.; Harrop, R.A.; Phillips, G.O. Characterization of the Adsorption-Desorption Behaviour of Hydrolyzed Polyacrylamide. *J.Colloid Interface Sci.* **1989**, *132(2)*, 319 -328.

(5) Van der Steeg, H.G.M.; De Keizer, A.; Bijsterbosch, B.H. The adsorption of cationic starch on microcrystalline cellulose. *Nordic Pulp Pap. Res. J.* **1989**, *4(2)*, 173 -178.

(6) Cohen Stuart, M.A.; Fleer, G.J.; Lyklema, J.; Norde, W.; Scheutjens, J.M.H.M. Adsorption of Ions, Polyelectrolytes and Proteins. *Adv.Colloid Interface Sci.* **1991**, *34*, 477 -535.

(7) Dahlgren, A.G.; Waltermo, A.; Blomberg, E.; Claesson, P.M.; Sjostrom, L.; Akesson, T.; Jonsson, B. Salt Effects on the Interaction between Adsorbed cationic Polyelectrolyte Layers - Theory and Experiment. *J.Phys.Chem.* **1993**, *97(45)*, 11769 -11775.

(8) Muthukumar, M. Adsorption of a polyelectrolyte chain to a charged surface. *J. Chem. Phys.* **1987**, *86(12)*, 7230 -7235.

(9) Van der Steeg, H.G.M.; Cohen Stuart, M.A.; De Keizer, A.; Bijsterbosch, B.H. Polyelectrolyte Adsorption: A Subtle balance of Forces. *Langmuir* **1992**, *8(10)*, 2538 -2546.

(10) Van der Schee, H.A.; Lyklema, J. A lattice theory of polyelectrolyte adsorption. *J.Phys.Chem.* **1984**, *88(26)*, 6661 -6667.

(11) Roe, R.J. Multilayer theory of adsorption from a polymer solution. *J. Chem. Phys.* **1974**, *60(11)*, 4192 -4207.

(12) Evers, O.A.; Fleer, G.J.; Scheutjens, J.M.H.M.; Lyklema, J. Adsorption of Weak Polyelectrolytes from Aqueous Solution. *J.Colloid Interface Sci.* **1986**, *111(2)*, 446 -453.

(13) Böhmer, M.R.; Evers, O.A.; Scheutjens, J.M.H.M. Weak Polyelectrolytes between Two Surfaces: Adsorption and Stabilization. *Macromolecules* **1990**, *23(8)*, 2288 -2301.

(14) Scheutjens, J.M.H.M.; Fleer, G.J. Statistical Theory of the Adsorption of Interacting Chain Molecules. 2. Train, Loop, and Tail Size Distribution. *J.Phys.Chem.* **1980**, *84*, 178 -190.

(15) Scheutjens, J.M.H.M.; Fleer, G.J. Statistical theory of the adsorption of interacting chain molecules. I. Partition function, segment density distribution and adsorption isotherms. *J.Phys.Chem.* **1979**, *83*, 1619 -1635.

(16) Fleer, G.J.; Cohen Stuart, M.A.; Scheutjens, J.M.H.M.; Cosgrove, T.; Vincent, B. *Polymers at Interfaces*; Chapman & Hall: London, 1993.

(17) Blaakmeer, J.; Böhmer, M.R.; Cohen Stuart, M.A.; Fleer, G.J. Adsorption of Weak Polyelectrolytes on Highly Charged Surfaces. Poly(acrylic acid) on Polystyrene Latex with Strong Cationic Groups. *Macromolecules* **1990**, *23(8)*, 2301 -2309.

(18) Israëls, R.; Leermakers, F.A.M.; Fleer, G.J. On the Theory of Grafted Weak Polyacids. *Macromolecules* **1994**, *27(11)*, 3087 -3093.

(19) Gebhardt, J.E.; Feurstenau, D.W. Adsorption of polyacrylic acid at oxide/water interfaces. *Colloids Surf.* **1983**, *7*, 221 -231.

(20) Newcombe, G. Activated Carbon and Soluble Humic Substances: Adsorption, Desorption, and Surface Charge Effects. *J.Colloid Interface Sci.* **1994**, *164*, 452 -462.

(21) Morris, G.; Newcombe, G. Granual Activated Carbon: The Variation of Surface Properties with the Adsorption of Humic Substances. *J.Colloid Interface Sci.* **1993**, *159*, 413 -420.

(22) Van Riemsdijk, W.H.; Bolt, G.H.; Koopal, L.K.; Blaakmeer, J. Electrolyte Adsorption on Heterogeneous Surfaces: Adsorption Models. *J.Colloid Interface Sci.* **1986**, *109(1)*, 219 -228.

(23) Koopal, L.K. Ion adsorption on mineral oxide surfaces In *Adsorption on new and modified inorganic sorbents*; Dabrowski, A.; Tertykh, V.A. Eds.; Elsevier: Amsterdam, 1996; 757-796.

(24) Flory, P.J. *Principles of polymer chemistry*; Cornell University Press: London, 1953.

(25) Björling, M.; Linse, P.; Karlström, G. Distribution of Segments for Terminally Attached Poly(ethylene oxide) Chains. *J.Phys.Chem.* **1990**, *94(1)*, 471 -481.

(26) Gorichev, I.G.; Batrakov, V.V. Surface charge as a function of potential at the oxide/electrolyte interface. *Soviet Electrchemistry* **1992**, *28*, 10 -15.

(27) Hesleitner, P.; Babíc, D.; Kallay, N.; Matijevíc, E. Adsorption at Solid/Solution Interfaces. 3. Surface Charge and Potential of Colloidal Hematite. *Langmuir* **1987**, *3(5)*, 815 -820.

(28) Breeuwsma, A.; Lyklema, J. Physical and chemical adsorption of ions in the electric double layer in hematite ($a$-$Fe_2O_3$). *J.Colloid Interface Sci.* **1973**, *43*, 437 -448.

(29) Leermakers, F.A.M.; Scheutjens, J.M.H.M. Statistical Thermodynamics of associated Colloids. II. Lipid Vesicles. *J.Phys.Chem.* **1989**, *93*, 7417 -7426.

(30) Barneveld, P.A.; Scheutjens, J.M.H.M.; Lyklema, J. Bending Moduli and spontaneous Curvature. 1. Bilayers and Monolayers of pure and Mixed Nonionic Surfactants. *Langmuir* **1992**, *8(12)*, 3122 - 3130.

(31) Wijmans, C.M.; Zhulina, E.B. Polymer Brushes at Curved Surfaces. *Macromolecules* **1993**, *26(26)*, 7214 -7224.

(32) Lyklema, J. Electric Double Layers In *Fundamentals of Interface and Colloid Science*; Academic Press: London, 1995;

(33) Koopal, L.K. Mineral Hydroxydes: from homogeneous to heterogeneous modelling. *Electrochim. Acta* **1996**, *41(14)*, 2293 -2306.

Chapter 3

# Characterisation and classification

# of purified Aldrich humic acid

## Abstract

The characteristics of purified Aldrich humic acid were studied and compared with those of naturally occurring humic substances. Literature data on humic and fulvic acids isolated from fresh water, marine water, soil and peat are used as reference to decide whether or not purified Aldrich humic acid can be used in laboratory experiments as an analogue for one of these types of natural humic substances. The following analytical techniques were applied; Elemental analyses, Fluorescence, UV and FT-IR spectroscopy, liquid and solid state $^1$H and $^{13}$C NMR, Viscosity measurements, Gel Permeation Chromatography and Ellipsometry. The results for purified Aldrich humic acid show strong similarities with the literature data. On the basis of these similarities the purified Aldrich humic acid can be classified as a representative of a soil humic acid, although it has to be mentioned that it is slightly more hydrophobic. In view of this classification and the fact that Aldrich humic acid is easily available we conclude that it can be used as a representative of soil type humic acids in further laboratory studies, provided it is further purified.

## Introduction

In environmental and soil science, the adsorption behaviour of toxic chemicals, and in particular metal ions (1) to soil components, is important with respect to the bio-availability of these chemicals. The soil-solution system is a complex system, consisting of a variety of sorbents for metal ions, such as mineral oxides, clay particles and humic substances. For well defined studies of the adsorption of toxic chemicals to soil components, the characteristics of these components have to be known. Here we will concentrate on humic substances. Humic substances are described as a mixture of polydisperse, heterogeneous, polyelectrolytes (2,3). A generally applied method to study the binding of metal ions to humics are laboratory studies. Recently Benedetti et al. (4) reported that model parameters for the description of ion adsorption to purified peat humic acid, calibrated under well defined conditions, gave good predictions of proton and metal ion binding in the natural systems. In general, both "naturally" occurring and "commercial" humic substances are used, in these type of studies. We denote the humic acid samples extracted from specific soil types as "natural", and those obtained from suppliers of chemicals as "commercial". The extraction of humic substances from natural systems is a time-consuming process. Especially humic substances in natural waters are difficult to isolate, due to their low concentrations as compared to the concentration of humics in soils and sediments. To avoid the laborious work of extraction, isolation and purification, commercial humic substances are used. The quality of commercial humic acid is however, sometimes criticised (5-7).

A thorough comparison of the physicochemical and ion binding characteristics of natural and commercial humic substances has not been conducted, although several studies dealing with separate aspects are available. Cornel et al. (8,9) discussed the molecular size distribution and spectroscopic characterisation of Aldrich humic acid together with the effect of environmental conditions (pH and ionic strength) on the diffusion coefficient. Beckett et al. (10) and Chin et al. (11) compared the molecular weight and polydispersity of Aldrich humic acid with several natural humic substances and reported comparable results. Florence (12) described the toxicity of metal ions towards aquatic media, using Aldrich humic acid as a representative for water humic substances, but did not characterise the Aldrich humic acid. Beveridge and Pickering (13) studied metal ion binding both to Aldrich humic acid and natural soil humics, but they did not discuss any differences between the two samples. They showed by measuring adsorption isotherms that metal ion adsorption on Aldrich humic acid can be used to develop metal ion speciation models, although no justification was presented for the extrapolation of these metal-complexation data to the natural environment.

The use of commercial humic substances in environmental studies has been criticised by Malcolm and MacCarthy (6), who compared seven commercial humic acids, among which Aldrich humic acid, with several natural humics. The general lack of information relating to source, extraction and pre-treatment method was considered as a major limitation of the commercial humics. Also the inconsistency from batch to batch, even with samples from the same supplier, was undesirable. The ash content and the $^{13}C$ NMR spectra of the different samples were given as prove that the commercial products were distinctly different from natural organics. Finally Malcolm and MacCarthy

concluded that all commercial humics were quite similar regardless of the supplier and can not be used as a representative of soil or aquatic humic or fulvic acid. Qiang et al. (5) compared two commercial humic acids with a series of natural humic substances. In this case the commercial samples were found to be different from each other, and both less aromatic than soil humics. They concluded that the commercial humics from different suppliers have different discrete origins and could not be recommended as analogues of natural systems. Finally Chiou et al. (7) reported a larger water solubility of organic solutes in the presence of commercial humic acids than with natural humics and concluded that the hydrophobicity of the commercial humic substances was significantly higher than that of natural samples.

Considering the above, it is possible that the differences reported by Malcolm and MacCarthy (6) and Qiang et al. (5) are due to differences in ash content rather than to the primary characteristics of the humic acids. Moreover, the reported differences are comparable to those due to small variations in accepted extraction procedures (Gregor and Powell (14) and Lowe (15)). The advantage that commercial humic substances are readily available may therefore still balance the disadvantage that some properties of commercial humic substances are different from otherwise obtained humics. Part of the disadvantages can probably be minimised by performing an additional purification step to remove salts and minerals.

The aim of this study is to compare the properties of Purified Aldrich Humic Acid (PAHA) with generally accepted natural humic substances. To this aim, PAHA will be characterised and classified by Elemental analyses, Fluorescence, UV and FT-IR spectroscopy, $^1$H and $^{13}$C NMR, Viscosity measurements, Gel Permeation Chromatography and Ellipsometry.

## Material and methods

All chemicals used were p.a. quality. The Purified water was obtained by percolating tab water through a mixed bed ion exchange column followed by an active carbon column and a micro filter.

### Humic acid purification method

One batch of Purified Aldrich Humic Acid (PAHA) was used in all experiments, the obtained amount was large enough to perform both the characterisation and classification described here and the adsorption studies to be described later.

For the purification (2,16) 10 g of Aldrich humic acid (Aldrich Chemie; code:H1,675-2) was added to a 1 l aqueous solution containing 5 ml concentrated HF and 5 ml concentrated HCl. The solution was stirred for 8 hours and afterwards filtrated over a Whatman Cellulose filter, grade 2, to remove silica and other soluble minerals. The humic acid residue was washed several times with 1 M HCl, neutralised and dissolved in a NaOH solution of pH 9 for 24 hours. The suspension was brought to pH 2 with 1 M HCl, stirred for 24 hours and centrifuged using a Beckman JS-7.5 centrifuge at 7500 rpm for one hour. The humic acid precipitate was then dialysed against slowly, flowing purified water for about one week. Finally the sample was shaken with an acid Dowex

50W-X8 resin for two weeks to remove all trace metals. The humic acid obtained in this way is in its proton form, it is freeze dried and stored in a glass container.

Before use the PAHA was resuspended overnight in a KOH solution with pH approximately 10, to a concentration of 2 g l^{-1}. Results of potentiometric proton titrations (*17,18*) have shown the necessity of this procedure to completely resuspend the sample. Other PAHA solutions were made from this stock solution.

*Analytical methods*

The elemental content measurements were performed on a Carlo Erba Elemental Analyser Model 1106, at the Organic Chemistry department, Wageningen Agricultural University[*].

Fluorescence spectra were recorded with a Perkin Elmer LS-5 Luminescence spectrometer; management of the spectrophotometer and all data acquisition were under PC control. In all experiments, the emission and excitation slits were set at a band width of 5 nm and a scan speed of 120 nm min^{-1} was selected for the monochromator. Emission spectra were obtained at an excitation wavelength of 360 nm, monitoring the emission over the range of 380 - 600 nm. Excitation spectra were recorded over a range of 270 - 500 nm at a constant emission wavelength of 520 nm. The synchronous-scan excitation fluorescence spectra were measured by changing simultaneously both wavelengths from 390 - 600 nm, with a constant wavelength difference of 18 nm.

All UV measurements were performed with a Hitachi U-3210 spectrophotometer. To characterise the type of humic matter, the $E_4/E_6$ ratio of optical absorbencies of solutions of humic matter at 465 and 665 nm was measured following the procedure recommended by Chen et al. (*19*).

Fourier Transform Infrared spectra were recorded with a Perkin Elmer 1725X FT-IR spectrometer, at a resolution of 4 and 1000 co-added scans.

Solid state CPMAS ^{13}C-NMR was recorded on a AMX 300 NMR spectrometer (Bruker G.M.B.H., Karlsruhe, Germany) at 75.5 MHz at the Wageningen NMR centre, Wageningen Agricultural University[†]. The parameters employed, included a contact time of 1 ms, a delay time of 2 s and collecting 1 K scans utilising a spinning speed of 5 kHz. The spectra were smoothed with a 50 Hz line broadening function. Both liquid state ^{1}H-NMR and ^{13}C-NMR were recorded on a AC-E 200 NMR spectrometer (Bruker) at the Organic Chemistry department, Wageningen Agricultural University[†].

Gel permeation (or size exclusion) chromatography was measured on a TSK G4000 SWXL and a TSK C2000 SWXL silica gel column in series at the Netherlands Institute Diary Research (NIZO), Ede[‡]. Instrumentation includes a Waters 616 solvent pump, a Waters 600s controller, a Waters In line degasser and a Gilson 231 Bio sample injector. 100 μl was brought onto the column. A flowrate of 0.8 ml min^{-1} and a pressure of 1400 psi were used for all experiments. The eluent used was a phosphate buffer of pH 6.5

and 0.1 M NaSO$_4$. Signals were detected with a UV spectrophotometer at 254 nm (LKB Bromma 2140 Rapid Spectral Detector), a RI detector (ERC-7510 Erma Optical Works Ltd) and a static light scattering apparatus; (DAWN DSP-F laser photometer Wyatt Technology Corp.). Molecular weights were measured directly by static light scattering and indirectly by calibration with protein standards.

The dn/dc of PAHA was measured using a Shodex RI-71 Refractive index detector in combination with a ABI 785A Absorbence detector and was 0.28 cm$^3$g$^{-1}$. The Refractive index detector was calibrated using solutions of known NaCl concentration.

The viscosities were measured with an Ubbelohde type capillary viscometer with automatic time recording (Viscosometric MS type 53 000).

Ellipsometry experiments were measured using a revised ellipsometer from DRE-Dr. Riss Ellipsmeterbau GmbH (DRE ELX1) as described by Boerboom et al. (20).

## Results and discussion

### Elemental analyses

The elemental analysis on an ash free basis of PAHA is as follows (wt%): C, 55.8 %; O, 38.9 %; H, 4.6 %; N, 0.6 %. The H:C ratio for the PAHA was 0.99; the O:C ratio was 0.52. The concentration of trace metals was below the detection limit of ICP measurements. The concentrations of Si and P were much smaller than 0.01 %. The oxygen content was not determined directly; it was obtained as the difference from 100% and the sum of the other elements. The measured elemental content is representative for humic substances, although the nitrogen content is low.

A convenient method to study the relation between the elemental content and the origin of the humic material is based on the graphical method developed by Van Krevelen (21). Van Krevelen used diagrams in which the atomic hydrogen to carbon ratio was plotted as a function of the atomic oxygen to carbon ratio. These diagrams have been used frequently to illustrate compositional differences (22,23) between fulvic acid, humic acid and humin, and also to show variations in humic substances as a function of their origin (24): fresh water, marine water, soil or peat.

Rice et al. (24) composed several Van Krevelen diagrams for humic substances based on 650 samples isolated from sites all over the world. One diagram differentiated between the type of humic substances, and another gives information on the origin of humic acids. Comparing the presented H:C and O:C ratios with the previously mentioned diagrams shows a clear correlation between PAHA and soil humic acids. Based on the values reported by Rice (24) and summarised in Table I, PAHA is classified as humic acid. According to the Van Krevelen diagram differentiating between the origin of the humic acids (24), PAHA is positioned in the middle of the soil humic acid area, whereas it is only on the edge of the marine and fresh water humic acid areas. Regarding this diagram, PAHA can also be classified as a peat humic acid, although the area depicted to peat was based on only 23 samples. Next to the classification some structural information is obtained from the H:C ratio. The high H:C ratio suggests a high degree of aliphaticity (21).

**Table I:** Mean elemental compositions of different humic substances from different origin expressed as weight percentage. Adapted from Rice et al. (24) (All values are on an ash free basis).

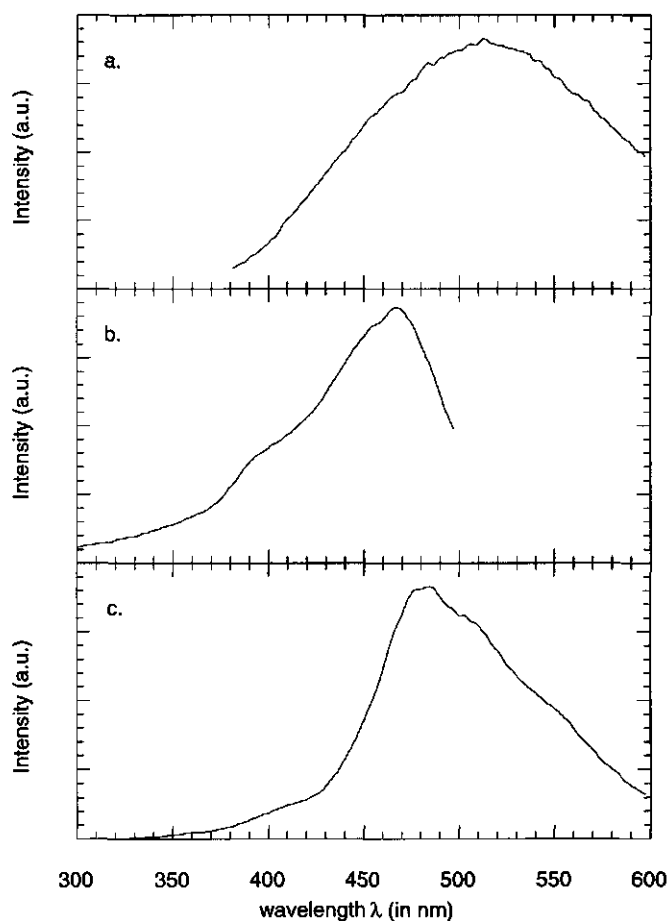|                        | C    | H   | O    | O:C  | H:C  |
|------------------------|------|-----|------|------|------|
| Fulvic acid            | 46.2 | 4.9 | 45.6 | 0.76 | 1.28 |
| Humin                  | 56.1 | 5.5 | 34.7 | 0.46 | 1.17 |
| Soil humic acid        | 55.4 | 4.8 | 36.0 | 0.50 | 1.04 |
| Fresh water humic acid | 51.2 | 4.7 | 40.4 | 0.60 | 1.12 |
| Marine humic acid      | 56.3 | 5.8 | 31.7 | 0.45 | 1.23 |
| Peat humic acid        | 57.1 | 5.0 | 35.2 | 0.47 | 1.04 |

## Fluorescence spectroscopy



**Figure 1:** Fluorescence spectra of PAHA, for an aqueous solution (100 mg l$^{-1}$, pH 8). At the Y axis the intensity is given in arbitrary units. **a:** Emission spectrum ($\lambda_{exc}$ = 360 nm) **b:** Excitation spectrum ($\lambda_{em}$ = 520 nm). **c:** Synchronous-scan excitation spectrum ($\lambda_{em} = \lambda_{ex}$ + 18 nm).

Figure 1, b and c present, an emission, excitation and synchronous-scan excitation spectrum of PAHA, respectively. The conditions used in these experiments were 100 mg $l^{-1}$, pH 8 and no corrections for scattering effects, such as Raman (25) scattering, were applied. The spectra are comparable to those of natural humic substances as reported by Senesi et al. (26,27).

The position of $\lambda_{max}$ in an emission spectrum is related to the degree of condensation and/or substitution of the aromatic ring. The high value of 510 nm observed in the emission spectrum (Figure 1) is representative for soil humic acid (26). The two main excitation peaks (Figure 1b) at 450 and 465 nm are typical for soil humic acids (Class II) as defined by Senesi et al. (27). The synchronous-scan excitation spectrum (Figure 1c) also shows that PAHA can be classified as soil humic acid. Soil humic acids are characterised by a main peak at 475 nm and shoulders at both lower (about 400 nm) and longer (about 490 nm) wavelength (27,28).

Based on this comparison, PAHA is classified as a soil humic acid. For all three fluorescence methods a remarkable resemblance of PAHA with Mollic Epipedon soil (27,29) (an IHSS-reference sample), is observed. However, Alluvial soils (27,30) and Terra Rossa soils (27,31) are similar as well.

## UV spectroscopy, $E_4/E_6$ ratios

The $E_4/E_6$ ratio of PAHA was 5.17. According to the classification by Qiang et al. (5), who reported that $E_4/E_6$ ratios for soil humic acids ranged from 4.93 to 6.05 while those of the commercial humics were much lower, PAHA is classified as a soil humic acid.

The $E_4/E_6$ ratio is also employed to indicate differences in molecular size (humic acid versus fulvic acid) and it reflects the degree of condensation. $E_4/E_6$ ratios for humic acids range from 3 to 6, whereas fulvic acid ratios range between 6 and 8.5 (32). Based on these values an intermediate molecular size and a low degree of condensation (relatively large proportion of aliphatic structures) can be ascribed to PAHA.

## FT-IR

The FT-IR spectrum of PAHA is given in
Figure 2. The major absorption bands are in agreement with the attributions reported in literature (33,34); an overview is given in Table II. The bands at 3425 cm$^{-1}$, 3275 cm$^{-1}$, 2650 cm$^{-1}$, 1720 cm$^{-1}$, 1385 cm$^{-1}$ and 1230 cm$^{-1}$ are mainly associated with either OH-stretching and C=O vibrations of the carboxylic groups or CO stretching of the phenolic OH. The bands at 2920 cm$^{-1}$, 2850 cm$^{-1}$ and 1450 cm$^{-1}$ are mainly associated with aliphatic CH stretching or bending, whereas the bands at 3115 cm$^{-1}$, 1620 cm$^{-1}$ and 1425 cm$^{-1}$ can be ascribed to aromatic contributions. All these bands appear for PAHA and they are common for humic substances.
The ratio of the intensities at 1720 cm$^{-1}$ to that at 1620 cm$^{-1}$ is often regarded as an indication of the content of carboxylic groups. The high ratio for PAHA classifies this humic acid as relatively acidic (35).
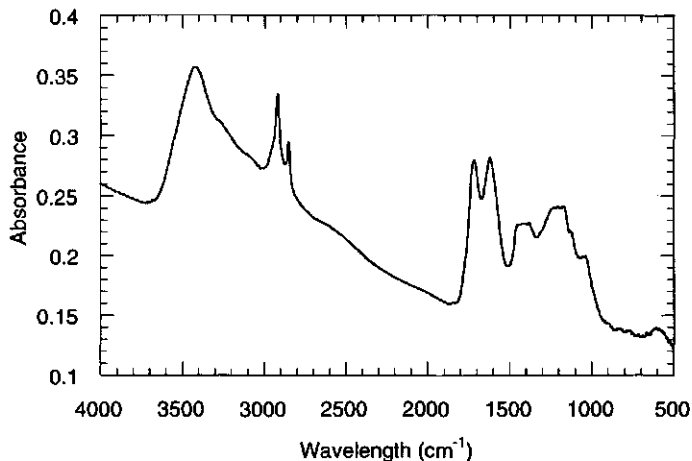
**Figure 2:** FT-IR spectrum of PAHA.

According to the overall shape of the FT-IR spectra it is possible to make a distinction between humic and fulvic acids (*36,37*). Based on such a comparison PAHA resembles a humic acid. Especially the absence of a band at 2000 cm$^{-1}$ (which always occurs in fulvic acid spectra) and the presence of a band at 1050 cm$^{-1}$, representing aromatic ethers, indicates a humic acid character. Although a distinction between fulvic and humic acid can be made, differences among different spectra of humic substances from various geographical areas are not significant enough to classify PAHA in this respect.

**Table II:** FT-IR band of PAHA.

| PAHA wavenumber (in cm$^{-1}$) | Assignment |
|---|---|
| 3425 | OH stretching of phenolic OH |
| 3275 | intra H bounded phenolic OH stretching |
| 3115 | aromatic CH stretch |
| 2920 | asymmetric CH stretching of $CH_2$, $CH_3$ |
| 2850 | asymmetric CH stretching of CH |
| 2650 | OH stretching vibrations of hydrogen-bounded COOH |
| 1720 | C=O stretch of COOH (mainly aliphatic) |
| 1620 | aromatic C=C |
| 1450 | $CH_2$, $CH_3$ bending |
| 1425 | aromatic ring stretching |
| 1385 | OH and CO bending of phenolic OH |
| 1230 | CO stretching and OH bending deformation |
| 1125 | secondary aliphatic OH |
| 1050 | aromatic ethers |

## NMR

A solid state CPMAS $^{13}$C NMR spectrum is given in Figure 3. The spectrum of PAHA is almost identical to the spectra reported by Malcolm and MacCarthy (6). The spectrum of PAHA is characterised by four groups of signals, that are attributed to the presence of aliphatic carbon (32.66 ppm), aromatic carbon (130.54 ppm), carboxyl carbon (173.24 ppm) and carbonyl carbon (195.25 ppm). The high intensity of the aliphatic peak is partly attributed to the CPMAS technique. Using CPMAS it is not possible to use the peak intensity to quantify the different groups. Liquid state NMR is more suitable for this purpose, although the resolution of the recorded liquid state NMR spectra was not very high.
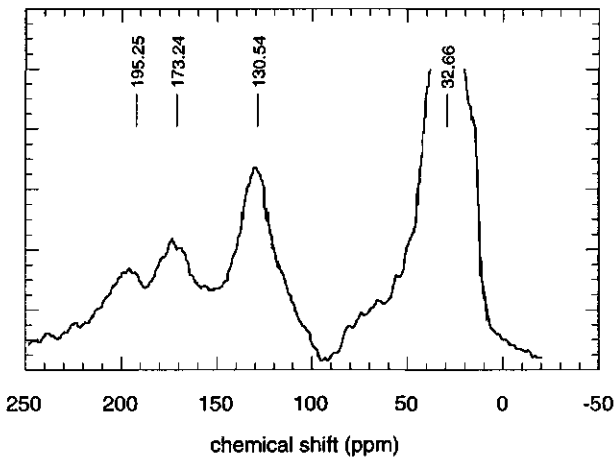


**Figure 3:** CPMAS $^{13}$C NMR spectrum of PAHA.

The PAHA liquid state $^{13}$C-NMR spectrum was characterised following Steelink et al. (38). The average areas of the major peaks can be assigned to aliphatic carbons 20-40 ppm, aromatic carbons 110-150 ppm and carboxyl carbons at 170-190 ppm. Two minor peaks are assigned to aliphatic carbon singly bounded to one oxygen at 50-95 ppm and non carboxylic carbonyl carbons at 190-220 ppm.

The PAHA $^1$H-NMR spectrum is mainly characterised, following Wilson et al. (39,40), by three broad peaks accompanied by some shoulders; 0.5-1.8 ppm (aliphatic protons), 1.8-3.0 ppm (protons attached to carbon α to aromatic rings and carboxylic groups) and 6.4-9 ppm (aromatic protons). The peak fractions were respectively, 42.9, 37.6 and 19.5%. Only a very faint peak was observed in the 3.0-4.75 ppm area (protons attached to carbon α to oxygen).

Based on the NMR spectra PAHA is classified as a simple humic acid with a high degree of aliphatic groups. Only a small number of groups like ethers, esters, aliphatic carbons singly bounded to one oxygen or to dioxygenated carbons were found. According to Lowe (15), this could be an effect of the purification procedure. Due to the low resolution of the $^{13}$C-NMR spectra it was not possible to differentiate on the origin of the humic acid as described by Malcolm (41).

*Hydrophobicity*

The degree of hydrophobicity of a protein or polymer can be evaluated by measuring the accumulation of the sample at the water-air interface using ellipsometry. The amounts of PAHA adsorbed at the water-air interface at pH 4, 6 and 8 were respectively 3.3, 1.7 and 0.8 mg PAHA $m^{-2}$. These values indicate a rather hydrophobic character as compared with the adsorbed amounts of different hydrophobic proteins (*42,43*) onto the water-air interface. The decrease in adsorption as a function of pH can be explained by the increase in polyelectrolyte charge with increasing pH. Further classification based on the degree of hydrophobicity is not possible since no literature data, as a function of the origin of humics substances, are available.

*Molecular weight determination*

The average molecular weight of PAHA was estimated by viscosity measurements and gel permeation chromatography. The viscosity average $M_v$ was $(19.6 \pm 0.5)$ $10^3$. This value was obtained using the Mark-Houwink relation and the constants K and $\alpha$, as described by Clapp et al. (*44*). For humic acids $\alpha = 0.5$ may be used in concentrated salt solutions and at low pH ($\theta$ solvent), an appropriate value for K = 5 $10^{-4}$ dl $g^{-1}$. The molecular weights measured with gel permeation chromatography were determined by calibration with protein standards. This gave a weight averaged molecular weight of $M_w$ = $(21 \pm 2)$ $10^3$. It is possible that calibration with globular proteins may slightly overestimate the molecular weight, to overcome this problem calibration with another coiled polymer, poly-styrenesulfonate is proposed (*45,46*). The elution pattern measured by GPC is given in Figure 4, it can be observed that the polydispersity was only modest and ranges from some thousand to about fifty thousand.
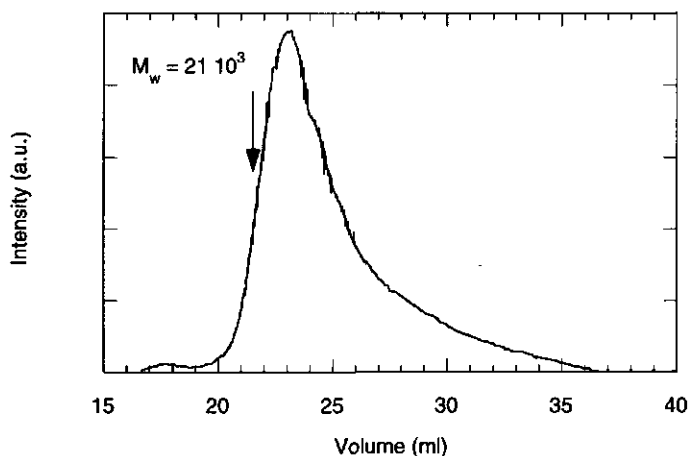


**Figure 4:** Molecular weight distribution determined by gel permeation chromatography. The weight average molecular weight was determined by calibration with proteins standards.

The molecular weight distribution of the Aldrich humic acid was also determined by Van den Hoop and Van Leeuwen (47) and Beckett and Hart (48), using flow field flow fractionation, and by several other authors (9-11). Although different techniques were used, the mean molecular weights were also around 20 $10^3$. Aldrich humic acid was classified as a rather polydisperse sample with an average molecular weight comparable to that measured by Van den Hoop and Van Leeuwen (47). Due to the purification procedure described previously, PAHA consists of a smaller molecular weight distribution compared with the unpurified material. A more extended discussion about various molecular weight determinations is given in a later paper (49).

The molecular weight distributions of natural humic substances reported in the literature vary from 500 to 200000 (3,50,51). Most data were obtained on fulvic acids, for which the molecular weight ranges from 500-1000 (3), and some analyses have been reported for humic acids (M > 1000) (10,50,51). Beckett et al. (10) reported that the order of size and polydispersity of humic acids was as follows: aquatic < soil < peat < lignite. It was mentioned that the variation in molecular weight for fulvic acids of different origin was small whereas the variation for humic acids was considerable.

Considering the molecular weight as determined by viscosity measurements and gel permeation chromatography, and according to the order reported by Beckett et al. (10), PAHA is classified as a soil or peat humic acid.


## Conclusions


Considering the present results it is concluded that PAHA reflects many characteristics normally found for naturally occurring humic acids. Elemental analysis, the E4/E6 ratio, the molecular weight and especially fluorescence spectroscopy support the classification as soil humic acid, although the elemental analyses and the molecular weight do not exclude a peat character. Based on the different analytical results it can be concluded that PAHA is a relatively simple humic acid with a low content of N, S and P and it contains only a small number of groups like ethers, esters, aliphatic carbons singly bounded to one oxygen or dioxygenated carbons. The E4/E6 ratio, which is relatively high for a humic acid, sustains the molecular weight determined by viscosity measurements and gel permeation chromatography. The high H:C ratio, the E4/E6 ratio and the FT-IR and NMR spectra indicate a relatively high degree of aliphaticity. The relatively high aliphaticity corresponds with the relatively large hydrophobicity measured with ellipsometry. The latter aspect was already mentioned by others, and is commonly observed for commercial humic substances.

It is shown that classification of humic substances solely based on it solid state $^{13}$C NMR spectra, as reported by Malcolm and MacCarthy (6), is not sufficient to fully understand the properties of these substances. The application of different analytical techniques clearly shows the resemblance between commercial and natural humic substances. Once a commercial humic acid is characterised and classified as a specific type of humic acid, it can be used as a alternative for its natural analogues. A major advantage of these commercial humics is the lack of the laborious and time consuming work of extraction and isolation. A second point mentioned by Malcolm and MacCarthy (6) was the discrepancy between different batches of commercial humic substances.

Therefore laboratory studies for environmental applications should preferably be based on one batch of purified, classified and well-characterised humic acid.

Overall it may be concluded that PAHA can be used as an analogue for soil and peat type humic acids in speciation studies. In a subsequent paper (*49*) both the proton and cadmium ion binding characteristics of PAHA will be studied and compared with results obtained by Milne et al. (*18,52*) on a peat humic acid.

### References

(1) Buffle, J. *Complexation in aquatic systems: an analytical approach*; Horwood: Chichester, 1988.

(2) Aiken, G.R.; McKnight, D.M.; Wershaw, R.L.; MacCarthy, P. *Humic Substances in Soil, Sediment, and Water*; Wiley Interscience: New York, 1985.

(3) Hayes, M.H.B.; MacCarthy, P.; Malcolm, R.L.; Swift, R.S. *Humic Substances II: In search of structure*; Wiley Interscience: New York, 1989.

(4) Benedetti, M.F.; Van Riemsdijk, W.H.; Koopal, L.K.; Kinniburgh, D.G.; Gooddy, D.C.; Milne, C.J. Metal ion binding by natural organic matter: From the model to the field. *Geochim.Cosmochim.Acta* **1996**, *60(14)*, 2503 -2513.

(5) Qiang, T.; Xiao-quan, S.; Zhe-ming, N. Comparative characteristic studies on soil and commercial humic acids. *Fresenius Anal.Chem.* **1993**, *347*, 330 -336.

(6) Malcolm, R.L.; MacCarthy, P. Limitations in the Use of Commercial Humic Acids in Water and Soil. *Environ.Sci.Technol.* **1986**, *20*, 904 -916.

(7) Chiou, C.T.; Kile, D.E.; Brinton, T.I.; Malcolm, R.L.; Leenheer, J.A. A Comparison of Water Solubility Enhancements of Organic Solutes by Aquatic Humic Materials and Commercial Humic Acids. *Environ.Sci.Technol.* **1987**, *21(12)*, 1231 -1234.

(8) Cornel, P.K.; Summers, R.S.; Roberts, P.V. Diffusion of Humic Acid in Dilute Aqueous Solution. *J.Colloid Interface Sci.* **1986**, *110(1)*, 149 -165.

(9) Summers, R.S.; Cornel, P.K.; Roberts, P.V. Molecular size distribution and spectroscopic characterization of humic substances. *Sci.Total Environ.* **1987**, *62*, 27 -37.

(10) Beckett, R.; Jue, Z.; Giddings, C. Determination of Molecular Weight Distributions of Fulvic and Humic Acids Using Flow Field-Flow Fractionation. *Environ.Sci.Technol.* **1987**, *21*, 289 -295.

(11) Chin, Y.; Aiken, G.R.; O'Loughlin, E. Molecular Weight, Polydispersity, and Spectroscopic Properties of Aquatic Humic Substances. *Environ.Sci.Technol.* **1994**, *28(11)*, 1853 -1858.

(12) Florence, T.M. Development of physico-chemical speciation procedures to investigate the toxicity of copper, lead, cadmium and zinc towards aquatic biota. *Anal.Chim.Acta* **1982**, *141*, 73 -94.

(13) Beveridge, A.; Pickering, W.F. Influence of humate-solute interactions on aqueous heavy metal ion levels. *Water,Air,Soil Pollut.* **1980**, *14*, 171 -185.

(14) Gregor, J.E.; Powell, H.K.J. Effects of extraction procedures on fulvic acid properties. *Sci.Total Environ.* **1987**, *62*, 3 -12.

(15) Lowe, L.E. Carbohydrates in Soil In *Soil Organic Matter*; Schnitzer, M.; Khan, S. U. Eds.; Elsevier Scientific Publishing Company: Amsterdam, 1978; 65-94.

(16) Thurman, E.M.; Malcolm, R.L. Preparative Isolation of Aquatic Humic Substances. *Environ.Sci.Technol.* **1981**, *15(4)*, 463 -466.

(17) Vermeer, A.W.P. this Thesis. Appendix I: Potentiometric proton titrations, experimental set-up and data treatment.

(18) Milne, C.J.; Kinniburgh, D.G.; De Wit, J.C.M.; Van Riemsdijk, W.H.; Koopal, L.K. Analysis of proton binding by peat humic acid using a simple electrostatic model. *Geochim.Cosmochim.Acta* **1995**, *59(6)*, 1101 -1112.

(19) Chen, Y.; Senesi, N.; Schnitzer, M. Information Provided on Humic Substances by $E_4/E_6$ Ratios. *Soil Sci.Soc.Am.J.* **1977**, *41*, 352 -358.

(20) Boerboom, F.J.G.; De Groot-Mostert, A.E.A.; Prins, A.; Van Vliet, T. Bulk and Surface rheological behaviour of aqueous milk protein solutions. A comparison. *Neth.Milk Dairy J.* **1996**, *50(2)*, 183 -198.

(21) Van Krevelen, D.W. Graphical-statistical method for the study of structure and reaction processes of coal. *Fuel* **1961**, *29*, 269 -284.

(22) Kawatsuka, K.; Tsutsuki, K.; Kumada, K. Chemical studies on soil humic acids I. Elementary Composition of Humic Acids. *Soil Sci.Plant Nutr.* **1978**, *24(3)*, 337 -347.

(23) Visser, S.A. Application of Van Krevelen's Graphical-Statistical Method for the Study of Aquatic Humic Material. *Environ.Sci.Technol.* **1983**, *17(7)*, 412 -417.

(24) Rice, J.A.; MacCarthy, P. Statistical evaluation of the elemental composition of humic substances. *Org.Geochem.* **1991**, *17(5)*, 635 -648.

(25) Ewald, M.; Belin, C.; Berger, P.; Weber, J.H. Corrected Fluorescence Spectra of Fulvic Acids Isolated from Soil and Water. *Environ.Sci.Technol.* **1983**, *17*, 501 -504.

(26) Senesi, N. Molecular and quantitative aspects of the chemistry of fulvic acid and its interactions with metal ions and organic chemicals. *Anal.Chim.Acta* **1990**, *232*, 77 -106.

(27) Senesi, N.; Miano, T.M.; Provenzano, M.R.; Brunetti, G. Characterization, Differentiation, and classification of humic substances by fluorescence spectroscopy. *Soil Sci.* **1991**, *152(4)*, 259 -271.

(28) Pullin, M.J.; Cabaniss, S.E. Rank Analysis of the pH-Dependent Synchronous Fluorescence Spectra of Six Standard Humic Substances. *Environ.Sci.Technol.* **1995**, *29*, 1460 -1467.

(29) Senesi, N.; Miano, T.M.; Provenzano, M.R.; Brunetti, G. Spectroscopic and compositional comparative characterization of I.H.S.S. reference and standard fulvic and humic acids of various origin. *Sci.Total Environ.* **1989**, *81/82*, 143 -156.

(30) Yonebayashi, K.; Hattori, T. Chemical and biological studies on environmental humic acids I. Compositional Elemental and Functional Groups of Humic Acids. *Soil Sci.Plant Nutr.* **1988**, *34(4)*, 571 -584.

(31) Chen, Y.; Senesi, N.; Schnitzer, M. Chemical and Physical characterization of humic and fulvic acids extracted from soils of the mediterranean region. *Geoderma* **1978**, *20*, 87 -104.

(32) Kononova, M.M. *Soil organic matter*; Pergamon Press: Oxford, 1966.

(33) Stevenson, F.J. *Humus Chemistry. Genesis, Composition, Reactions*; Wiley Interscience: New York, 1982.

(34) Tao, Z.; Yang, Y.; Sheng, F. Spectroscopic and structural characterisation of fulvic acid from weathered coal. *Toxic.Environ.Chem.* **1995**, *49*, 45 -56.

(35) Cabaniss, S.E. Carboxylic acid content of a fulvic acid determined by potentiometry and aqueous Fourier transform infrared spectrometry. *Anal.Chim.Acta* **1991**, *255*, 23 -30.

(36) Tao, S.; Deng, B.; Hermosin, B.; Saiz-Jimenez, C. Application of principle component-clustering analysis to classification of FTIR spectra of aquatic, sediment and soil humic and fulvic acids from main rivers of China. Humic Subst. Global Environ. Implic. Hum. Health, Proc. Int. Meet. Int. Humic Subst. Soc., 6th.Senesi N and Miano TM. Amsterdam. Elsevier. 1994 367-372.

(37) Ricca, G.; Severini, F. Structural investigations of humic substances by IR-FT, $^{13}$C-NMR spectroscopy and comparison with a maleic oligomer of known structure. *Geoderma* **1993**, *58*, 233 -244.

(38) Steelink, C.; Wershaw, R.L.; Thorn, K.A.; Wilson, M.A. Application of liquid-state NMR spectroscopy to humic substances In *Humic Substances II: In search of structure*; Hayes, M. H. B.; MacCarthy, P.; Malcolm, R. L.; Swift, R. S. Eds.; Wiley Interscience: New York, 1989; 281-309.

(39) Wilson, M.A.; Gillam, A.H.; Collin, P.J. Analysis of the structure of dissolved marine humic substances and their phytoplanktonic precursors by $^{1}$H and $^{13}$C Nuclear Magnetic Resonance. *Chem.Geo.* **1983**, *40*, 187 -201.

(40) Wilson, M.A.; Collin, P.J.; Tate, K.R. $^{1}$H-nuclear magnetic resonance study of a soil humic acid. *J.Soil Sci.* **1983**, *34*, 297 -304.

(41) Malcolm, R.L. Application of solid-state $^{13}$C NMR spectroscopy to geochemical studies of humic substances In *Humic Substances II: In search of structure*; Hayes, M. H. B.; MacCarthy, P.; Malcolm, R. L.; Swift, R. S. Eds.; Wiley Interscience: New York, 1989; 339-372.

(42) Graham, D.E.; Phillips, M.C. Proteins at Liquid Interfaces II. Adsorption Isotherms. *J.Colloid Interface Sci.* **1979**, *70*, 415 -426.

(43) Damodaran, S. Interrelationship of Molecules and Functional Properties of Food Proteins In *Food Proteins*; Kinsella, J. E.; Soucie, W. G. Eds.; The American Oil Chemists Society Campaign: Illinois, 1989; 21-51.

(44) Clapp, C.E.; Emerson, W.W.; Olness, A.E. Size and Shapes of Humic Substances by Viscosity Measurements In *Humic Substances II: In Search of Structure*; Hayes, M. H. B.; MacCarthy, P.; Malcolm, R. L.; Swift, R. S. Eds.; Wiley Interscience: New York, 1989; 497-514.

(45) Kilduff, J.E.; Weber, W.J.J. Transport and Separation of Organic Macromolecules in Ultrafiltration. *Environ.Sci.Technol.* **1992**, *26*, 569 -577.

(46) Chin, Y.; Gschwend, P.M. The abundance, distribution, and configuration of porewater organic colloids in recent sediments. *Geochim.Cosmochim.Acta* **1991**, *55*, 1309 -1317.

(47) Van den Hoop, M.A.G.T.; Van Leeuwen, H.P. Influence of molar mass distribution on the complexation of heavy metals by humic materials studied by stripping voltammetry. *J.Colloid Interface Sci.* **1996**,

(48) Beckett, R.; Hart, B.T. Use of Field-Flow Fractionation Techniques to characterize aquatic particles, colloids and macromolecules In *Environmental particles*; Buffle, J.; van Leeuwen, H. P. Eds.; CRC Press: Florida, 1993; 165-206.

(49) Vermeer, A.W.P. this Thesis. Chapter 4: Proton and Cadmium binding to purified Aldrich humic acid, exploration of the NICA-Donnan model.

(50) Visser, S.A. Viscosimetric studies on molecular weight fractions of fulvic and humic acids of aquatic, terrestrial and microbial origin. *Plant Soil* **1985**, *87*, 209 -221.

(51) Cameron, R.S.; Thornton, B.K.; Swift, R.S.; Posner, A.M. Molecular weight and shape of humic acid from sedimentation and diffusion measurements on fractionated extracts. *J.Soil Sci.* **1972**, *23(4)*, 394 -408.

(52) Milne, C.J.; Kinniburgh, D.G.; De Wit, J.C.M.; Van Riemsdijk, W.H.; Koopal, L.K. Analysis of Metal-Ion Binding by Peat Humic Acid Using a Simple Electrostatic Model. *J.Colloid Interface Sci.* **1995**, *175*, 448 -460.

Chapter 4

# Proton and cadmium binding to purified Aldrich humic acid,

# exploration of the NICA-Donnan model

## Abstract

Proton and cadmium ion binding to a purified Aldrich humic acid has been measured as a function of pH and salt concentration. For the interpretation of the results the NICA-Donnan model is applied. The Donnan volumes are obtained independently by measuring the hydrodynamic volumes of the humic acid at the conditions at which the isotherms are measured. The Donnan volume can be obtained directly at high (0.1 M) salt concentration by viscosity measurements, whereas at lower salt concentrations the extension of the double layer is also important. The measured Donnan volumes correspond with a humic acid molecule that is much larger than its dry volume. This type of behaviour can be compared with the random coil model, commonly used for simple polyelectrolytes. The observed volumes are considerably larger than those used by Benedetti et al. in their Donnan treatment of humic substances. The insight obtained by describing humic substances as flexible polyelectrolyte may be of use for interpreting metal ion speciation within the natural environment.

## Introduction

A powerful method to study the characteristics of humic substances in relation to ion binding makes use of potentiometric proton titrations (1,2). The acid-base properties of humic substances are determined by a variety of functional groups (3-5). In principle each type of group in a given chemical environment has its own intrinsic affinity for proton and/ or metal ion binding. However, due to electrostatic interactions these intrinsic affinities can not be determined directly from a series of proton adsorption isotherms. To "remove" the electrostatic interaction, a model is required that accounts for the salt effect on the proton adsorption. With such an electrostatic model and under the assumption of random heterogeneity, the isotherms measured at different salt concentrations can be recalculated. When the electrostatic model is adequate the recalculated isotherms should merge into a "Master Curve". The Master Curve reflects the chemical heterogeneity of the material studied. Its derivative can be used as a fingerprint describing the intrinsic affinities that in turn is related to the chemical composition (6-9).

De Wit et al. (1,9,10) and Milne et al. (2) have described the procedure to calculate the Master Curve in more detail. In their treatment the humic colloids were considered as rigid impermeable, charged spheres or cylinders. The surface potentials were derived by solving the Poisson Boltzmann equation; the average radius of the spheres or the cylinders was used as an adjustable parameter. The description as impermeable spheres or cylinders is however, not necessarily an adequate presentation for all humic substances. The rigid sphere model seems appropriate for strongly hydrophobic humics, whereas the cylinder model can be seen as a first order approximation for worm like chains for which only the primary radius of curvature is considered, i.e. for highly charged chain type of humics. An alternative presentation of the humic colloids is proposed by Marinsky and co-workers (11-13), who described the humic acid molecules as a Donnan gel. Later this approach was used by Benedetti et al. (14) in a simple form. The order of magnitude of the Donnan gel volume was estimated using literature values of viscosity measurements of humic substances. Final values were found by using a fitting procedure. Benedetti et al. noted that it is impossible to obtain a unique estimation of the Donnan volume based on fitting alone, and that preferably the Donnan volume of a humic acid sample should be measured independently. The radii of the humic acid molecules proposed by Benedetti et al. in their Donnan treatment are of the order of a few nanometers (1.9 - 3.9 nm).

An argument against the use of the simple Donnan model with a relatively small Donnan volume is that in this model it is assumed that the charge density on the polyelectrolyte chain is compensated by electrolyte ions within the Donnan volume. To a first approximation this is correct when the radius of the hydrated polyelectrolyte particles is much larger than the Debye length ($\kappa^{-1}$). At $10^{-2}$ mol $l^{-1}$ electrolyte $\kappa^{-1}$ is of the order of 3 nm, hence only at high ionic strength the Donnan model can be applied to such small particles. In view of this and the fact that the volumes used by Benedetti et al. are fitted rather than measured it is worthwhile to consider both the structure and size of humic acid molecules in solution in some more detail.

Environmental factors like pH, ionic strength and the concentration of the humic substances themselves affect the size and shape of the dissolved humics. Several studies have been performed to investigate these dependencies. It was reported by Cornel et al. (15) that the diffusivity of humic acid entities increased with increasing ionic strength and decreasing pH. These observations were attributed to a coil structure of the organic molecules, the expansion of the coil depending on pH and/ or ionic strength. This type of model that describes the variation of the conformation of humic substances with changes in the solution properties, was first proposed by Ghosh and Schnitzer (16). These authors described the humic molecules at high pH, low salt and low sample concentration as flexible linear colloids with an extended worm like conformation. When the charge of the humic substances is decreased or the screening of the charges is enhanced by increasing the electrolyte concentration, a random coil conformation is obtained. A similar model was proposed by Cameron et al. (17), who described a humic acid as a randomly coiled strand with charge distributed along its length at all salt concentrations and pH values. In this view the molecule is always enclosed by a spherical shape within which the distribution of mass is Gaussian. Depending on the conditions the molecules are described as tightly or loosely coiled. In support of this approach, Hayes and Swift (18) reported that the shape of humic molecules in solution is essentially spheroidal but not condensed or rigid.

Considering a humic acid as a more or less randomly coiled molecule has consequences for the segment density inside the coil boundaries. Tanford (19) in his treatment of random coiled polymers has shown that the molecule itself occupies only a very small fraction of the volume that it pervades. Chain molecules may be coiled over a region of space that is more than hundred times greater than the volume actually occupied by their segments. The space given by the hydrodynamic boundary of the coil will be largely filled by solvent. Applying this concept to humic acids would result in a water content larger than 90 % in the humic acid domains and an effective volume per molecule substantially larger than that of the dry humic molecule. This would mean that for such hydrophilic humic acids the Donnan gel model is more appropriate than the rigid sphere or cylinder model. Moreover the Donnan volume of such a humic acid molecule should be much larger than its dry volume.

Data on radii of humic acid molecules vary from several angstroms (10,14,20) to a few hundred nanometers (21,22). The discrepancy between these radii has been a major topic of discussion. The very small values (10,14) are typical equivalent particle radii, not based on direct physical measurements. Generally techniques as Field Flow Fractionation (23), Viscosity measurements (24) and Gel Permeation Chromatography (25) yield larger radii whereas with the different scattering techniques (21,26,27) very large radii are found. These differences can, at least partly, be explained due to the polydispersity of the samples and aggregation effects. In general different type of averages are obtained with the different techniques. For instance, in the case of dynamic light scattering the average is strongly determined by the largest particles, whereas in the case of viscosity measurements the weight of all size fractions is nearly equal. Östenberg and Mortensen (28) measured the radii of humic acid solutions using small-angle neutron scattering and concluded that the humic acid particles can be described by building units of a radial size, smaller than 2.5 nm, aggregated into clusters with an average radius of 40 - 50 nm. Reid et al. (29) also discussed the

aggregation of humic substances in aqueous media and mentioned that aggregates of approximately 20 smaller molecules existed. They have shown that the aggregates partly dissociate due to the addition of detergent, indicating that the aggregation is at least partially reversible. The reversibility of humic acid aggregation was also investigated by Powell and Town (30) who applied Gel Permeation Chromatography of samples fractionated by equilibrium dialysis. They concluded that humic acid occurred as dynamic aggregates which can dissociate, pass through the dialysis membrane and then reform.

From this discussion it may be concluded that in general it is difficult to assign a certain size to humic acids in solution. In order to obtain, for a given humic acid, an independent estimation of the average size of the hydrated molecules one will have to do additional measurements. If relatively large volumes are found it may be conclude that the random coil model for humics is realistic and that the simple Donnan model can be applied. For intermediate volumes one may still have to use the Donnan approach, but in this case the approximation is rather crude and the characteristic length of the gel phase will depend strongly on $\kappa^{-1}$. For small volumes the rigid sphere or rigid rod model used by De Wit et al. (1) and Milne et al. (2) is to be preferred to describe the electrostatics.

The aim of this paper is to analyse ion adsorption to humic acids and to base the heterogeneity analysis not only on the proton binding isotherms at different salt concentrations, but also on independent measurements of the hydrodynamic volumes of the humic acid at the conditions at which the isotherms are obtained. The size of the dissolved humic acid molecules will be studied by Viscosity measurements, Gel Permeation Chromatography, and by Static and Dynamic Light Scattering. Once the volumes are known the electrostatic model can be chosen, the Master Curve can be calculated and conclusions can be drawn about the chemical heterogeneity of the humic acid. Based on these observations further modelling of measured proton and metal ion adsorption isotherms can be done. The methods will be illustrated and discussed using Purified Aldrich Humic Acid (PAHA). As shown previously, PAHA may be considered as a soil and/ or peat type humic acid (31). The experimental results and the model parameters will be compared with the results obtained by Benedetti et al. (32) and Kinniburgh et al. (33), who used a well-characterised purified peat humic acid (PPHA).

## Electrostatic interactions: the Donnan approach

In the Donnan model each humic acid molecule is considered as a micro gel phase with fixed charges due to the dissociation of the functional groups of the humics. In the simple Donnan model all fixed charges are assumed to be compensated by salt ions within the gel phase. The electroneutrality of the gel phase is given by Eq. (4.1):

$$\frac{Q}{V_D} + \sum z_i (c_{i,D} - c_i) = 0 \qquad (4.1)$$

where $Q$ (mol $kg^{-1}$) equals the net fixed charge of the humic acid, $V_D$ ($m^3$ $kg^{-1}$) is the Donnan gel volume, $z_i$ is the valence of the different ions and $c_{i,D}$ and $c_i$ (mol $m^{-3}$) are the molar concentrations of the different ions present in the Donnan phase and the bulk, respectively. Due to the charge of the humic acid molecules the gel phase exhibits an electrostatic potential relative to the bulk solution. In the simple Donnan model this potential, $\psi_D$, is assumed to be independent of the position within the gel. The concentration of an ion i within the Donnan gel can now simply be related to its bulk concentration by a Boltzmann factor, based on $\psi_D$:

$$c_{i,D} = c_i \exp\left(-\frac{z_i F}{RT}\psi_D\right)$$ (4.2)

where all constants have the usual meaning. In the presence of a simple 1:1 electrolyte at not too high or too low pH values Eqs. (4.1) and (4.2) reduce to:

$$\frac{Q}{V_D} = c_S\left(e^{+F\psi_D/RT} - e^{-F\psi_D/RT}\right)$$ (4.3)

where $c_S$, is the salt concentration. For a series of values of $Q$ as a function of pH and a given salt concentration, $\psi_D$ can now be calculated if $V_D(pH,c_s)$ is known.

The Donnan volume $V_D$ ($pH,c_s$) is defined as:

$$V_D = \frac{(V_{hy} - V_{HA})N_A}{M} = \frac{V_{hy}N_A}{M} - \frac{1}{\rho_{HA}}$$ (4.4)

where M (kg $mol^{-1}$) is the measured average molecular weight, $N_A$ ($mol^{-1}$) the number of Avogadro, $V_{hy}(pH,c_s)$ ($m^3$) is the measurable hydrodynamic volume of a humic acid molecule, $V_{HA}$ ($m^3$) the volume of a dry humic acid molecule, and $\rho_{HA}$ (kg $m^{-3}$) the dry bulk density for humic substances (3,34). Hence, in order to calculate $V_D$ both $V_{hy}$ and M have to be known. For a strongly hydrated molecule Eq. (4.4) reduces to $V_D = V_{hy}N_A/M$.

The Debye length, $\kappa^{-1}$ (m), (Eq. (4.5)) may be taken as a measure of the thickness of the compensating ionic atmosphere (35).

$$\kappa^{-1} = \frac{F^2 \sum_i z_i^2 c_i}{\varepsilon_0 \varepsilon RT}$$ (4.5)

In order to satisfy the assumption that all fixed charges of the gel are compensated within the volume of the humic acid phase (neglecting the dry volume of the humic acid) the condition is that the hydrodynamic radius $(V_{hy})^{1/3} \gg \kappa^{-1}$. For values of $(V_{hy})^{1/3} \le \kappa^{-1}$, a crude approximation is to assume that $V_D$ is of the order of $(\kappa^{-1})^3 N_A/M$ to make sure that most of the diffuse charge is enclosed by the Donnan volume (36).

In general only limited information will be present on $V_D$ ($pH,c_s$). In favourable cases $(V_{hy})^{1/3} \gg \kappa^{-1}$, i.e. $V_D$ values have been measured at relatively high ($\sim$ 0.1 M) salt concentration. With the thus obtained values of $V_D$ the measured Q(pH) curve at this

high salt concentration can be recalculated to a $Q(pH_D)$ curve using Eq. (4.2) and the definition of $pH_D$:

$$pH_D = pH - \log\left\{\exp\left(-\frac{z_i F}{RT}\psi_D\right)\right\} \qquad (4.6)$$

As all electrostatic effects are incorporated in $\psi_D$, the resulting curve should be free of salt effects (provided the simple Donnan model holds) and is called the Master Curve. $Q(pH_D)$ curves for the lower background electrolyte concentrations should merge with the Master Curve. As the value of $\psi_D$ $(pH,c_s)$ can be found from the difference between the initial $Q(pH)$ curve and the Master Curve, the only unknown for the calculation of the other $Q(pH_D)$ curves is $V_D$ $(pH,c_s)$. $V_D$ values obtained in this way should be reasonable as compared to those measured at the highest salt concentration and they should not exceed the upper limit of $4/3\pi(\kappa^{-1})^3 N_A/M$.

## Molecular weight and size of humic acid molecules in solution

The size or volume of a particle in solution can be obtained by, for instance, viscosity measurements, Static Light Scattering (SLS), Dynamic Light Scattering (DLS) and Gel Permeation Chromatography (GPC). Below these methods will be briefly discussed.

### Viscometry

Under the assumption that the particles are spherical the hydrodynamic volume of a particle can be obtained from the intrinsic viscosity, $[\eta]$ $(m^3 kg^{-1})$ and the particle mass, m (kg), using the Einstein equation (4.7):

$$V_{hy} = \frac{m[\eta]}{2.5} \qquad (4.7)$$

For non-spherical molecules the factor 2.5 has to be replaced by a number > 2.5, the actual value being dependent on the axial ratio of the molecule. The expression most commonly used for the calculation of this number is that given by Simba (37) and was applied for humics by Chen and Schnitzer (24), who evaluated different geometries.

For a polydisperse humic acid with a viscometric average molecular weight, $M_v$ (kg mol$^{-1}$), a viscometric average hydrodynamic volume $V_{hy,v}(pH,c_s)$ is obtained and Eq. (4.7) may be written as:

$$V_{hy,v} = \frac{M_v[\eta]}{2.5 N_A} \qquad (4.8)$$

By combining Eqs. (4.4) and (4.8) a very simple relation is found for $V_D$ (Eq. (4.9)).

$$V_D = \frac{[\eta]}{2.5} - \frac{1}{\rho_{HA}}$$ (4.9)

Hence, by measuring $[\eta]$, $V_D$ can be found using tabulated values for $\rho_{HA}$ (3,34). The intrinsic viscosity of the humic acid at the specified solution conditions can be found by measuring the viscosity of the humic in solutions as a function of the humic acid concentration and by measuring the blank solution. The relative viscosity is defined as:

$$\eta_r = \frac{\eta_{HA}}{\eta_0}$$ (4.10)

where $\eta_{HA}$ (N m$^{-2}$ s) equals the viscosity of the humic acid solution and $\eta_0$ (N m$^{-2}$ s) of the pure solvent. Both viscosities are proportional to the flow time. The specific viscosity is defined as:

$$\eta_{sp} = \frac{\eta_{HA} - \eta_0}{\eta_0} = \eta_r - 1$$ (4.11)

The reduced viscosity as:

$$\eta_{red} = \frac{\eta_r - 1}{c} = \frac{\eta_{sp}}{c}$$ (4.12)

The intrinsic viscosity (Eq. (4.13)) is found by extrapolation of the reduced viscosity to zero concentration:

$$[\eta] = \lim_{c \to 0} \frac{\eta_{sp}}{c}$$ (4.13)

Viscosity measurements can also be used to obtain molecular weights. The viscosity averaged molecular weight, $M_v$, can in principle be evaluated from the Mark Houwink relation (Eq. (4.14)), where $K$ and $\alpha$ are two constants.

$$[\eta] = K \times M_v^{\alpha}$$ (4.14)

In general the value of $\alpha$ lies between 0.5 and 0.8. For poor solvents $\alpha$ approximates 0.5 and for very good solvents $\alpha = 0.8$ (19). According to Clapp et al. (38) in salt solutions of 0.1 M a value of $\alpha = 0.5$ in combination with $K = 5 \ 10^{-4}$ dl g$^{-1}$ may be used for humic acids extracted from soil. These averaged values are based on data of Piret et al. (39), Chen and Schnitzer (24) (pH 7 and higher, no extra salt) and Visser (40) (pH 7 and different salt concentrations). Visser (40) also measured these parameters for Aldrich humic acid. $K$ and $\alpha$ were calculated based on different fractions separated by ultrafiltration. Values of $\alpha = 0.34$ and $K = 7.7 \ 10^{-4}$ dl g$^{-1}$ were obtained for Aldrich humic

acid. A disadvantage of the calibration with separated humic acid fractions is that the cut-off speciations of ultrafiltration membranes may not hold for humic acids as was discussed by Kilduff and Weber (*41*) and Chin and Gschwend (*25*), we therefor neglect these values of K and α.

Once the molecular weight and [η] are determined, a the hydrodynamic volume can be calculated and $(V_h)^{-1/3}$ can be compared with $\kappa^{-1}$ to judge which double layer model is most appropriate.

## Dynamic Light Scattering

DLS is a modern technique to obtain the average radius of particles dispersed in a solution. The method uses the fluctuations of the scattered light intensity due to Brownian motion of the particles, which in turn is related to the diffusion coefficient of the hydrated particles. From these intensity fluctuations a time dependent autocorrelation function can be obtained. The diffusion coefficient (D) is obtained by fitting a second cumulant fit through the autocorrelation function. From the diffusion coefficient the radius of the particles is calculated with the Stokes-Einstein relation (*35*) (Eq. (4.15)), which has been derived for isolated spherical particles. It may also be applied to solutions of macromolecules in which case the radius a should be replaced by the hydrodynamic radius $r_{hy}$ of the macromolecule, in which η is the solvent viscosity:

$$D = \frac{kT}{6\pi\eta a} \qquad (4.15)$$

For polydisperse samples an "intensity weighted average" diffusion coefficient is obtained. This average depends approximately quadratic on the volume of the particles. The intensity weighted average hydrodynamic radius, is therefore strongly determined by the larger particles of the distribution.

## Static Light Scattering

SLS is a light scattering technique that can provide information about the radius of gyration and the molar mass of the particles under investigation. This technique uses the angular dependence of the scattered intensity to determine both properties by constructing a so called Debye plot. A Debye plot is obtained by plotting $R_\theta/K^*c$ vs. $\sin(\theta/2)$, where $R_\theta$ is the excess Rayleigh ratio, $K^*$ is an optical constant, c is the humic acid concentration (measured by the RI detector) and θ equals the angle at which the scattering is detected. By fitting a first order polynomial in $\sin(\theta/2)$ to the data, the intercept and the slope at zero angle can be determined. Under certain assumptions (e.g. infinity low sample concentration) the molecular weight equals the intercept and the mean square radius of gyration can be calculated from the slope, once the molecular weight is known. The various averaged molecular weight can be calculated from the measured distribution.

## Gel Permeation Chromatography

In general the hydrodynamic volume of a molecule can also be determined with GPC. In principle GPC is based on size exclusion: the larger the size of the particle is the shorter is the retention time. An elution chromatogram therefore reflects the size distribution. As this volume is related to the molecular weight, see Eq. (4.8), the elution pattern also reflects the molecular weight distribution. Two approaches are used to obtain the molecular weight distribution, indirectly by using a calibration with protein standards and directly by static in line light scattering. For these proteins a linear relation was found between log (M) and the retention time. As a first approximation this calibration curve was used without adaptation for PAHA. For an accurate calibration one can use the approximation that log ([η] M) versus the retention time should be the same for all polymers. For a given column combination, solvent elution rate, temperature and retention time, the unknown molecular weight $M_x$ now can be found as:

$$M_x = \frac{[\eta]_{cal}}{[\eta]_x} M_{cal} \qquad (4.16)$$

Equating $M_x$ and $M_{cal}$ for a given retention time thus assumes that also the intrinsic viscosities are the same. Note that for the $V_{hy}$ distribution of the unknown only M and [η] of the standards are required. Direct determination of $V_{hy}$ at the relevant conditions is however in practice hampered by the fact that a good operation of the column system often requires its own solvent conditions.

The second approach used to obtain the molecular weights and radius distribution is SLS (see above). The SLS measurements are done "on line" with the GPC fractionation.

## Material and methods

All experiments have been performed in a thermostatted room at 21 ± 1 °C and with $KNO_3$ as indifferent electrolyte, all chemicals used were p.a. quality and the Purified water was obtained by percolating tab water through a mixed bed ion exchange column followed by an active carbon column and a micro filter.

Within the experiments, purified Aldrich humic acid (denoted as PAHA) was used. The purification and characterisation of PAHA are described elsewhere (31). It has been shown that PAHA reflects many characteristics normally found for humic substances and that it may be classified as a soil and/ or peat humic acid. The humic acid is in its proton form and was freeze dried and stored in a glass container.

Before use PAHA was resuspended overnight in a KOH solution with pH approximately 10, to a concentration of 2 g l$^{-1}$. Results of potentiometric proton titrations have shown the necessity of this procedure to completely resuspend the sample. Slow redispersion effects were also reported by Milne et al. (2) and Pinheiro et al. (26)

studying purified peat humic acid and by Paxéus and Wedborg (42), studying fulvic acid. Other PAHA concentrations used were made from this stock solution.

*Titration set-up and electrode calibration*

Titrations were performed using the Wallingford titration system (43-45). This titrator consists of a thermostatted titration cell, four Metrohm burettes and a Microlink PH4 module (Bio-data Ltd). This module measures the electrode potential down to 0.1 mV and is capable of monitoring up to four electrodes simultaneously. The burettes and PH4 module were interfaced to a PC with a Microlink MF18 interface unit and all control and data acquisition was under PC control. The equipment is especially built for colloid titrations and pH-STAT (constant pH) experiments on colloidal systems.

Prior to the titrations the solutions were freed from carbon dioxide by bubbling water saturated nitrogen gas (Hoekloos 5.0 $N_2$) through the solution at pH 4, for at least one hour. During a titration the reaction vessel was maintained at a slight overpressure (~1 cm $H_2O$) of nitrogen in order to exclude atmospheric carbon dioxide. The pH was monitored with duplicate glass electrodes (Ingold U272-S7), against a double junction Ag/AgCl reference electrode (Ingold 363-S7). The salt-bridge was filled with a 1 M $KNO_3$ solution. It was observed that leakage of the salt changed the salt concentration in the vessel less than $10^{-3}$ M per 24 hours.

Titrants were prepared from commercial volumetric standards (Tritrisol); 0.1 M $HNO_3$ was used as acid titrant and 0.1 M KOH as base. The base solutions were found to be prone to contamination with carbon dioxide. In order to minimise this problem the demineralised water was boiled for several hours prior to the preparation of the basic solutions. The exact base concentration was determined by titration with the $HNO_3$ solution.

Typical proton titrations used 30 ml. The concentrations of the solutions were in the order of 0.4 to 2 g PAHA $l^{-1}$. After equilibration, successive acid and base titrations were performed at different salt concentrations. Provided PAHA is thoroughly redispersed at a high pH a stable equilibrium conformation is reached and successive titrations hardly show hysteresis. The salt concentration was adjusted at pH 3, using one of the burettes. After each addition the cell is equilibrated for 30 minutes, before continuation of the titration. After addition of titrant, the rate of drift was measured over a 2 minute interval after an initial delay of 20 seconds to allow adequate mixing. The electrode readings were accepted when the drift was less than 0.2 mV $min^{-1}$. A maximum reading time of 20 minutes was set for two successive additions of titrant. The doses of $HNO_3$ and KOH were calculated by the interface to obtain a constant mV change of 5 mV for each addition, to obtain a good distribution of datapoints over the pH range studied.

The calibration of the potentiometric titration cell was done by both buffer calibration and by blank acid-base titrations of various values for the ionic strength. The volume of titrant required for a pH change of an equivalent volume of the blank electrolyte solution was calculated for, and subtracted from, each datapoint. Activity coefficients were derived from the calculated ionic strength using the Davies equation. The relatively high proton consumption of the samples (about 5 times that of the blank) meant that the blank correction was only small at moderate pH. At low and high pH values the blank becomes a significant component of the potentiometric titration and is responsible for a

larger uncertainty in the calculated charge-pH curves. A more extensive discussion of the calibration and subtraction procedure has been described elsewhere (43).

Cadmium titrations in the presence of PAHA were done by pH-STAT measurements at pH 4, 6 and 9 and 0.01 and 0.1 M $KNO_3$. The cadmium concentration and the pH were simultaneously measured while the solution was stirred continuously.

The cadmium ion measurements were made in a polypropylene beaker, which fits inside the titration cell and prevents the loss of cadmium by adsorption to the glass walls. The cadmium ion concentrations were measured using a solid state sulphide based cadmium ion specific electrode (Orion 9448) against a double junction Ag/AgCl reference electrode. The cadmium ion selective electrode was calibrated routinely before each experiment at comparable salt concentration and pH. Calibration of the cadmium ion selective electrode was done by the addition of small, accurate doses of a cadmium stock solution. The calibration curves were found to be linear and reproducible within the concentration range studied in this work. The concentration of the cadmium ion stock solution was determined by an endpoint titration with ethylene-diamine-tetraacetic acid (EDTA).

*Viscometric set-up*

The viscosities were measured with an automatic viscometer (Viscosometric MS type 53 000). Two Ostwald type Ubbelohdes were used with a flow time $(t_0)$ of 97.58 ± 0.04 and 275.2 ± 0.8 sec of demineralised water (25 °C), respectively. The presented viscosities are averages of 10 readings.

*Dynamic Light Scattering set-up*

The equipment used for the DLS experiments was built from standard components: an ALV-125 laser light spectrometer/ goniometer, an ALV-5000 digital correlator, an ALV-800 transputerboard and a spectro physics 35 mW, 632.8 nm HeNe laser. The wavelength of the laser used is in a part of the spectrum of the colloids studied which is free of absorption peaks.

*Static Light Scattering set-up*

For on-line light scattering detection a DAWN DSP-F laser photometer (Wyatt Technology Corporation) was used, equipped with a K5 flowcell and a 632.8 nm HeNe laser. A parameter needed to obtain molecular weight information is the refractive increment index (dn/dc). The dn/dc of PAHA was measured using a Shodex RI-71 Refractive index detector in combination with a ABI 785A Absorbence detector and was 0.28 $cm^3g^{-1}$. The Refractive index detector was calibrated using NaCl solutions of known concentration.

*Gel Permeation Chromatography* set-up

The sample (1.0 g l^{-1}) was injected (100 µl) into the gel permeation chromatographic system. Prior to injection the PAHA solutions were filtered through a 0.45 µm filter (Whatmann). Separation was achieved using a TSK G4000 SWXL and a TSK C2000 SWXL silica gel column in series. Instrumentation includes a Waters 616 solvent pump, a Waters 600s controller, a Waters In line degasser and a Gilson 231 Bio sample injector. The columns were eluted with a filtered (0.2 µm) and degassed phosphate buffer of pH 6.5 with an indifferent salt concentration of 0.1 M $Na_2SO_4$ at a flowrate of 0.8 ml min^{-1} and a pressure of 1400 psi. Sample quantification was done with a UV spectrophotometer at 254 nm (LKB Bromma 2140 Rapid Spectral Detector) and a RI detector (ERC-7510 Erma Optical Works Ltd). The molecular characteristics were measured indirectly by calibration with protein standards and directly using on-line multi angle static laser light scattering detection.

## Results

### Molecular weights, hydrodynamic radii and Donnan gel volumes

*Molecular weights of PAHA*

The viscometric average molecular weight of PAHA, calculated from the intrinsic viscosity data at pH 3 in 0.1 M NaCl, using the Mark-Houwink relation (Eq. (4.14)) with $\alpha = 0.5$ and $K = 5 \cdot 10^{-4}$ dl g^{-1}, $M_v$, is $20 \cdot 10^3$.

The weight averaged molecular weight of PAHA as determined by GPC and calibration with monodisperse proteins equals $M_w = (21 \pm 2) \cdot 10^3$. This value corresponds well with the viscosity based average molecular weight.

Figure 1 presents the elution pattern and the corresponding molecular weight distribution as determined by SLS after separation by the gel permeation chromatographic system. The distribution was measured in duplo and was reproducible within experimental error. The molecular weights of the different PAHA fractions were calculated from a Debye plot. The different averaged molecular weights are: $M_n = (34 \pm 3) \cdot 10^3$, $M_w = (42 \pm 4) \cdot 10^3$ and $M_z = (51 \pm 10) \cdot 10^3$. It is observed that these molecular weights are considerably larger than the values obtained by viscometry and the protein calibration. These differences are attributed to the possible aggregation of the humic molecules. As mentioned before, the dynamic aggregation of humics was also described by Powell et al. (*30*), for humics passing membranes.

Regarding the aggregation it can be concluded that the binding between the different molecules is only weak. The aggregates are in dynamic equilibrium: they can dissociate and reform easily. For the single PAHA molecules we therefore prefer to use the average value of $20 \cdot 10^3$. Similarly the Donnan volume required for the description of

potentiometric titrations has to be the volume of the single molecules, not of the aggregates. So that also for the calculation of $V_{hy}$ we prefer to use $20 \cdot 10^3$.
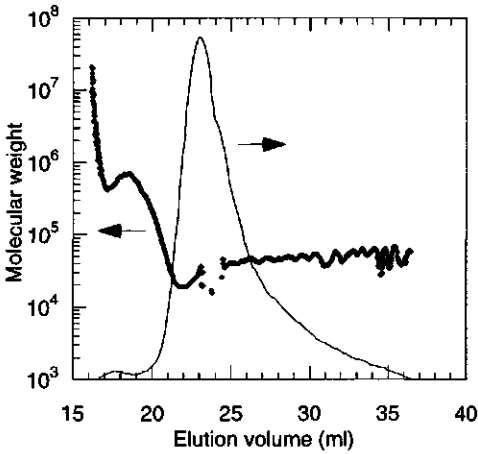


**Figure 1:** Molecular weights as determined by SLS after separation by GPC, as a function of the retention time (pH 6.7, $10^{-1}$ M $KNO_3$). At the second Y-axis the GPC spectrum is given in arbitrary units.
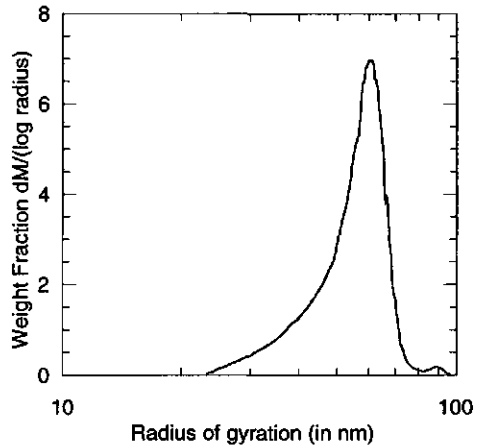


**Figure 2:** Distribution of the radius of gyration of PAHA measured by SLS after separation by GPC. At pH 6.7 and $10^{-1}$ M $KNO_3$.
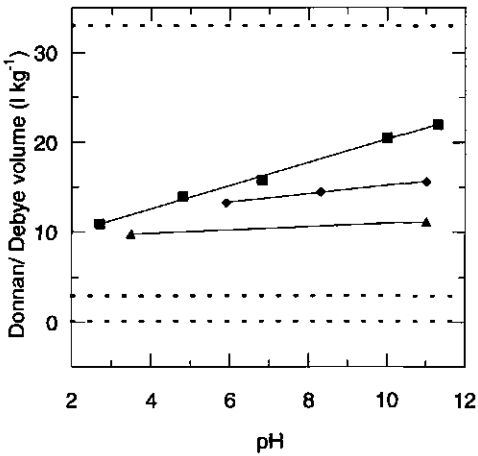


**Figure 3:** $V_D$ calculated from viscosity data (neglecting $1/\rho_{HA}$), as a function of pH: $\blacksquare = 10^{-3}$ M; $\blacklozenge = 10^{-2}$ M; $\blacktriangle = 10^{-1}$ M $KNO_3$. The dotted lines presents the "Debye volumes" $3/4\pi(\kappa^{-1})^3$ at the different salt concentrations.



**Figure 4:** Average hydrodynamic radii of PAHA, measured by DLS, as a function of pH and salt concentration: $\blacksquare = 10^{-3}$ M; $\blacklozenge = 10^{-2}$ M; $\blacktriangle = 10^{-1}$ M $KNO_3$.

*The effective size of PAHA*
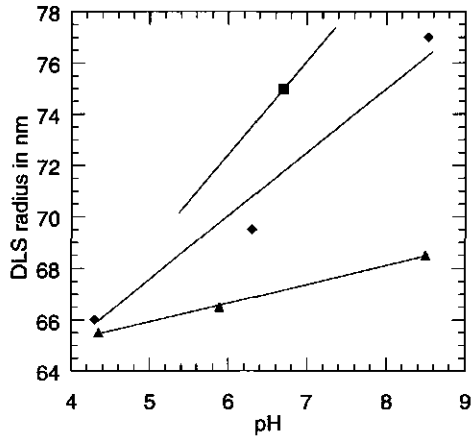
The intrinsic viscosity was determined as a function of pH and salt concentration. The hydrodynamic volumes of the PAHA molecules based on the measured intrinsic viscosities, are given in Figure 3, were calculated by the Einstein equation (4.8), where M equals $20 \cdot 10^3$.

Figure 2 presents the radii of gyration of the different PAHA fractions separated by GPC as measured by SLS measurements in a buffered 0.1 M $Na_2SO_4$ solution. The peak of the distribution is at about 60 nm. As expected the radii as determined with the light scattering technique are substantially larger than the radii calculated from the viscosity data.

The PAHA radii measured by DLS at different pH values and $10^{-1}$, $10^{-2}$ and $10^{-3}$ M $KNO_3$ are also given in Figure 4. The major trends observed are an increasing radius with increasing pH and decreasing salt concentration, similarly as found with the viscometry. At a salt concentration of 0.1 M $KNO_3$ the pH effect on the colloidal size was small compared to that at lower salt concentrations. The magnitude of the DLS radii are comparable to those measured by SLS. As explained above the differences between the results obtained with the light scattering methods and the viscometry are probably due to aggregation effects.

*Donnan volumes of PAHA molecules and their water content*

As discussed, both the average molecular weight and the hydrodynamic volume of PAHA, as a function of pH and ionic strength, have been measured. A first approximation of the Donnan volume is based on these data. Once $\kappa^{-1}$ exceeds the radius measured by viscometry, the viscosity based volume will be an underestimation compared with the Debye volume. Regarding this aspect, the experimental $V_D$ at the lower salt concentrations are preferably approximated by the Debye volume. At a high salt concentration the Donnan volume was measured directly by viscometry and was, at a salt concentration of 0.1 M $KNO_3$, 10.9 l kg$^{-1}$.

The dry bulk densities ($\rho_{HA}$) for humic substances range from 1400 to 2000 kg m$^{-3}$ (3,34), and by combination of these values with Eqs. (4.4), (4.7) and (4.9) the water content of the Donnan gel domains can be calculated once the Donnan volume is known. The water content at 0.1 M $KNO_3$ is about 90 %. Thus the space given by the hydrodynamic boundary of the gel is largely filled by solvent and the effective volume per molecule is substantially larger than that of the dry molecule. Such high solvent contents are normal for random coil polymers (19). The high water content and the fact that the extension of the humic acid molecules increases with improving solvent conditions, supports the structure model proposed by Cameron et al. (17).

**Proton adsorption and the Donnan Model**

The proton adsorption isotherms at different salt concentrations are shown in Figure 5 by the filled symbols. The reproducibility of these curves at a given salt concentration was very good.
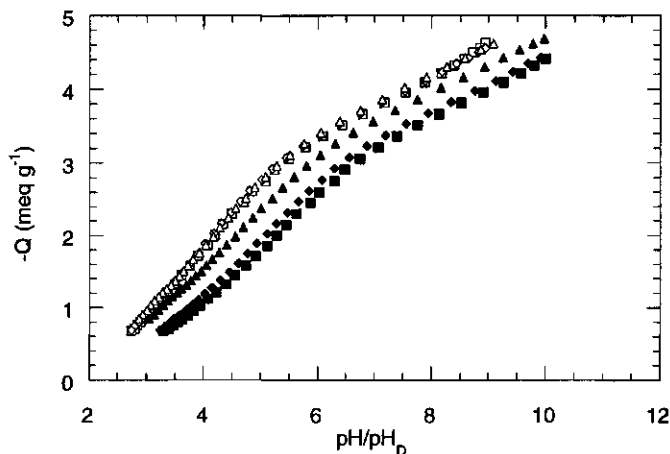
**Figure 5:** PAHA proton adsorption isotherms. Experimental Q(pH) curves (solid symbols) and Master Curve Q(pH$_D$) (open symbols) for the Donnan gel model. ■ = $10^{-3}$ M; ◆ = $10^{-2}$ M; ▲ = $10^{-1}$ M KNO$_3$.

The addition of indifferent electrolyte between the successive titrations causes a redistribution of protons which changes both the humic acid charge and the pH of the solution. The relative positions of the three surface charge/ pH curves has therefore been fixed by independent pH STAT titrations (*43*).

The absolute position of the curves can be determined by measuring the consumption of 0.1 M HNO$_3$ by PAHA brought into its acid form, using a back titration (*43,46,47*). In this way the PAHA charge at the pH of the acidic solution (0.1 M) can be calculated. The titration curve in 0.1 M salt can now be fixed to this point. Following Milne et al. (*2*) a check was made on the position of the curve by fitting a model isotherm through the data points (*48*). The best value obtained for the initial charge at pH 3 and 0.1 M salt was 0.6 Eq. kg$^{-1}$, which corresponds very well to other reported values (*2,14*). The curves for the different ionic strengths remain nearly parallel throughout the pH range, a phenomenon that was also reported by Milne et al. (*2*). A relatively small salt effect is observed at low salt concentrations. At the higher salt concentrations the reactive groups are more easily dissociated due to the more profound screening of the indifferent electrolyte.

The obtained curves can be further analysed by the Master Curve procedure in which the Donnan model was used to convert the Q(pH) curves to the Q(pH$_D$) curves. The position of the Master Curve was established, using the experimentally determined Donnan volume at $10^{-1}$ M KNO$_3$, that is within experimental error independent of pH. The Q(pH) curves at the other salt concentrations were adjusted to this Q(pH$_D$) curve by adjusting the Donnan volume. Both the fitted and measured Donnan volumes are shown in Table I. The Master Curve data are shown in Figure 5 by the open symbols. At $10^{-2}$ M KNO$_3$ a fitted Donnan volume of 15.7 results. This value corresponds very well with the measured values, see Table I. At $10^{-3}$ M KNO$_3$ a fitted Donnan volume of 59 is found. This value is about three times the measured value. This is due to the fact that in this case $(V_{hy})^{1/3} < \kappa^{-1}$. The Donnan volume measured by viscometry has to be enlarged

to enclose most of the diffusely bound ions that compensate the polyelectrolyte charge. It may be concluded that there exists a clear dependence of the fitted $V_D$, on the salt concentration, whereas the fitted $V_D$ may be taken independent of pH. At a salt concentration of $10^{-3}$ M the volume measured by viscometry depends strongly on pH, but the fact that the $4/3\pi(\kappa^{-1})^3$ is much larger than the measured $V_D$ leads to a fitted $V_D$ value compensating for this dependence.

**Table I:** Hydrodynamic radius, Donnan volume and the corresponding water contents as a function of the salt concentration.

| | measured | | | fitted |
|---|---|---|---|---|
| ionic strength | radius (in nm) | $V_D$ (l kg$^{-1}$) | % water | $V_D$ (l kg$^{-1}$) |
| $10^{-1}$ M | 4.4 | $10 \pm 1$ | 93 | 10.9 |
| $10^{-2}$ M | 5.0 | $15 \pm 2$ | 95 | 15.7 |
| $10^{-3}$ M | 8 | $17 \pm 6$ | 96 | 59 |

The calculated PAHA Donnan potential as a function of pH is shown in Figure 6. In general the potential increases with increasing pH. The behaviour is however far from being pseudo Nernstian, (59 mV/pH). With increasing ionic strength, a decreasing Donnan potential is observed. Due to the increased salt concentration the screening of the charges becomes more profound, resulting in a decreased electrostatic interaction or a decreased electrostatic potential.



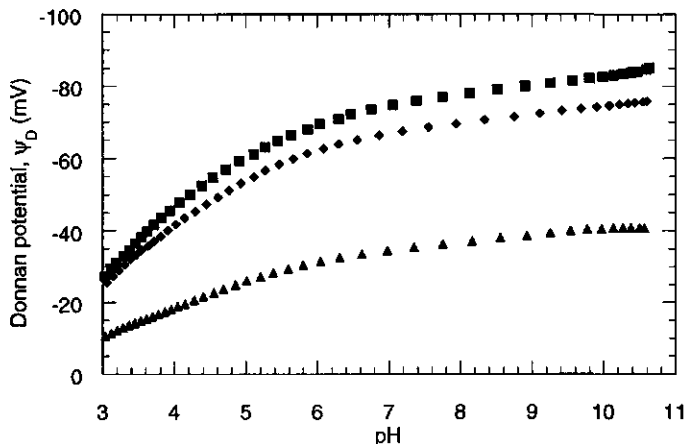**Figure 6:** Calculated Donnan potentials for PAHA as a function of pH and salt concentration. ■ = $10^{-3}$ M; ♦ = $10^{-2}$ M; ▲ = $10^{-1}$ M KNO$_3$.

The Master Curve reflects the intrinsic chemical heterogeneity of PAHA. The intrinsic affinity distribution can be approximated by taking the first derivative of the Master Curve (6-8), using the heterogeneity analysis software developed by Nederlof. The

affinity distribution is shown in Figure 7. The intrinsic affinity distribution reflects a bimodal distribution consisting of two mayor peaks, one at a pK of about 4.5, reflecting carboxylic type of groups and a second distribution at about pK 9, that can be assigned to more weakly acid groups such as phenols, alcohols and enols (49).
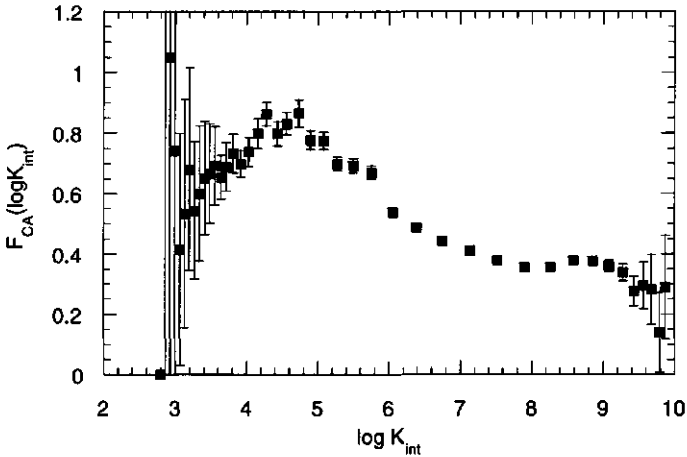


**Figure 7:** Non-normalised intrinsic CA affinity distribution of PAHA. Error bars indicate a 66% confidence interval (6).

## Cadmium adsorption

The measured cadmium binding onto PAHA is given in Figure 8a and 8b for 0.1 and 0.01 M $KNO_3$, respectively and for pH 4, 6 and 9.
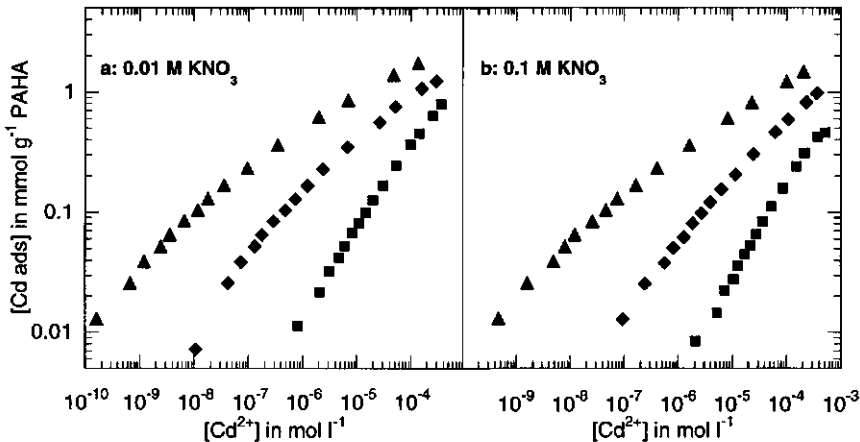


**Figure 8:** PAHA-cadmium binding data as a function of the equilibrium cadmium concentration for 3 different pH values and 2 salt concentrations: ■ pH = 4; ♦ pH = 6; ▲ pH = 9. a: 0.01 M $KNO_3$ b: 0.1 M $KNO_3$.

The cadmium binding is strongly dependent on the salt concentration and pH. Cadmium binding decreases with increasing salt concentration and increases with increasing pH. The shape of the adsorption isotherms and the pH dependence of the cadmium binding are qualitatively in good agreement with other published data (50,51).

## Modelling of proton and cadmium binding

### General aspects

In order to model proton and metal ion binding to humic substances in a consistent way, a multi component heterogeneous site binding model is required. Different models for multicomponent adsorption have been proposed in the past (32,51,52). A discussion of several models has been given by Milne et al. (51). For well studied systems first the proton adsorption at different salt concentrations has been considered. As shown above such data can be used to separate electrostatic (e.g. Donnan potentials) and "chemical" (intrinsic affinity distribution) effects. This separation will also be followed here, describing the electrostatics with the Donnan model. For the site binding part that has to account for the intrinsic heterogeneity, the proton and metal ion binding and the proton/ metal ion site competition, several options are open. Firstly the stoichiometry of the metal ion binding has to be considered. In order to keep the situation relatively simple monodentate binding is often assumed. The next assumption relates to the heterogeneity effects. Initially in literature two limiting situations have been considered (1): (1) proton and metal ion binding are fully correlated and (2) the proton and metal ion are fully independent. In the fully correlated case the affinity distribution for the metal ions is the same as that for the protons, except for a shift along the affinity axis. In the fully uncorrelated case, the affinity distributions are entirely independent, but the competition for the sites remains. An equation for this situation has been derived by Rudzinski et al. (53). An elegant kind of intermediate between these isotherms is the NICA model (52). Koopal et al. derived this non ideal competitive adsorption model, in which the affinity distributions for the metal ions are not necessarily of identical shape as the proton affinity distributions. Apart from a general heterogeneity that is equal for all ions, the NICA model also includes an ion specific heterogeneity or non-ideality that in principle can vary with each ion.

According to the measured affinity distribution the binding sites of PAHA (as well as other humic acids) are composed of carboxylic and phenolic type of groups (Figure 7). This can be incorporated in the NICA model by using a bimodal distribution and considering the binding to both site types as independent, except for the electrostatic interactions (that are accounted for in the Donnan part of the model). Below such a bimodal NICA model will be used in combination with the Donnan model.

The bimodal NICA-Donnan equation can be written as Eq. (4.17), where $\Gamma_{i,t}$ is the total adsorbed amount of component i, $\Gamma_{max,x}$ is the maximal adsorbed amount, $\tilde{K}_{i,x}$ equals the mean intrinsic affinity constant of component i and x relates to the two peaks of the affinity distribution. The concentration of i in the Donnan phase, $c_{i,D}$, is related to the its bulk concentration by Eq. (4.2).

$$\Gamma_{i,t} = \Gamma_{max,1} \cdot \frac{(\tilde{K}_{i,1} c_{i,D})^{n_{i,1}}}{\sum_i (\tilde{K}_{i,1} c_{i,D})^{n_{i,1}}} \frac{\left\{\sum_i (\tilde{K}_{i,1} c_{i,D})^{n_{i,1}}\right\}^{P_1}}{1 + \left\{\sum_i (\tilde{K}_{i,1} c_{i,D})^{n_{i,1}}\right\}^{P_1}}$$

$$+ \Gamma_{max,2} \cdot \frac{(\tilde{K}_{i,2} c_{i,D})^{n_{i,2}}}{\sum_i (\tilde{K}_{i,2} c_{i,D})^{n_{i,2}}} \frac{\left\{\sum_i (\tilde{K}_{i,2} c_{i,D})^{n_{i,2}}\right\}^{P_2}}{1 + \left\{\sum_i (\tilde{K}_{i,2} c_{i,D})^{n_{i,2}}\right\}^{P_2}}$$

(4.17)

The parameter $p_x$ accounts for the intrinsic chemical heterogeneity which is the same for all components ($0 < p \leq 1$). The parameter $n_{i,x}$ accounts for the ion specific heterogeneity or non-ideality that is not accounted for by $p_x$ and/ or the electrostatic model ($n \neq 1$ non-ideal, $n = 1$ ideal).

If only protons are present in a solution of an indifferent electrolyte, the NICA model reduces to the double Langmuir Freundlich model (2,52).

$$\Gamma = \Gamma_{max,1} \cdot \frac{\left\{\tilde{K}_{H,1} c_{H,D}\right\}^{m_{H,1}}}{1 + \left\{\tilde{K}_{H,1} c_{H,D}\right\}^{m_{H,1}}} + \Gamma_{max,2} \cdot \frac{\left\{\tilde{K}_{H,2} c_{H,D}\right\}^{m_{H,2}}}{1 + \left\{\tilde{K}_{H,2} c_{H,D}\right\}^{m_{H,2}}}$$

(4.18)

In Eq. (4.18), the heterogeneity parameter $m_H$ describes the combined effect of $n_H$ and $p$ ($m_H = n_H p$).

A general scheme used to derive the various parameters of the NICA model for a multicomponent set of proton and metal ion adsorption data is described elsewhere (32). Briefly the procedure is as follows. The Master Curve data are used to derive values for the parameters of Eq. (4.18): $\Gamma_{max,1}$, $\Gamma_{max,2}$, $\tilde{K}_{H,1}$, $\tilde{K}_{H,2}$, $m_{H1}$ and $m_{H2}$. The values are also assumed to apply in the presence of other cations. The competitive character of the NICA model requires the assumption that $\Gamma_{max,H} = \Gamma_{max,i}$ where $i$ is a metal ion. The values of the six additional parameters for the metal ion ($p_x$, $\tilde{K}_{M,x}$, $n_{i,x}$) are derived from the metal ion adsorption isotherms at different pH values. It is assumed that the Donnan volume is not effected by the metal ion adsorption. The validity of this assumption can be checked by calculating the metal ion parameters for each of the different salt concentrations. Since the metal ion parameters ($p_x$, $\tilde{K}_{M,x}$, $n_{i,x}$) are independent on the salt concentration, the fitted values should be the same within the experimental error. Only if this precondition is fulfilled, we may use the measured Donnan volumes to model the metal ion binding.

## Modelling the proton adsorption isotherms

The Master Curve (Figure 5) was fitted to Eq. (4.18) using a non-linear least-squares procedure (48). Figure 9 presents (1) the fitted curve and (2) the intrinsic affinity distribution. As expected, the intrinsic affinity distribution reflects a bimodal distribution with two peaks at an intrinsic pK of about 4 and 8.5, respectively.
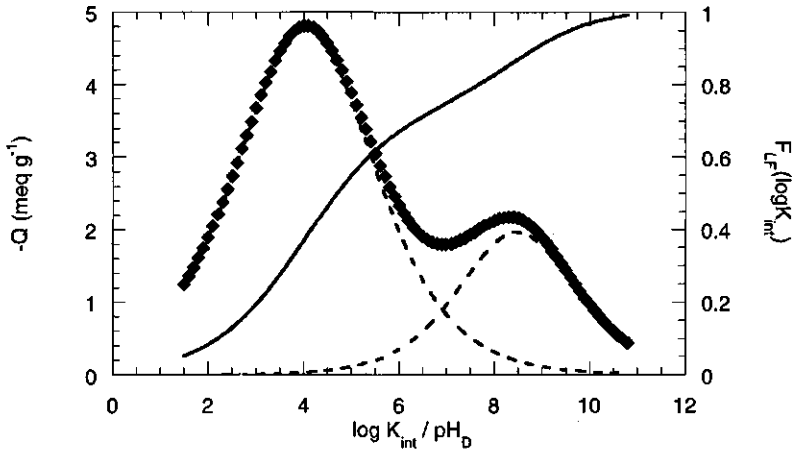


**Figure 9:** (1) Double Langmuir Freundlich isotherm corresponding to the Master Curve and (2) the Non-normalised intrinsic affinity distribution, derived from this isotherm. The one y-axis gives Q (solid line), the other $F(logK_{int})$ (♦). The two broken lines represent the distributions of the carboxylic and phenolic type of groups, respectively.
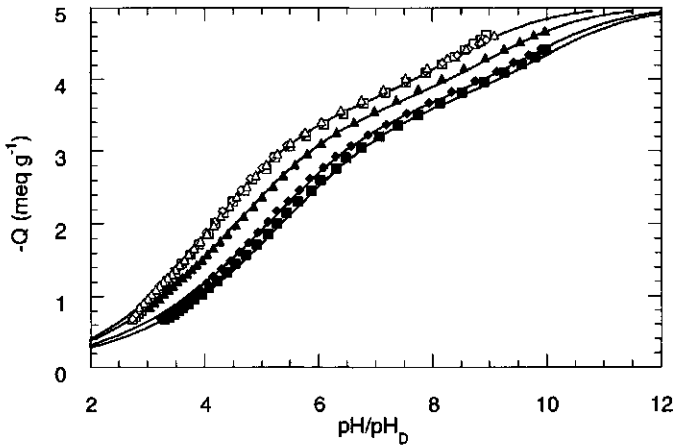


**Figure 10:** Calculated and experimental PAHA proton adsorption isotherms. The solid lines correspond to the double Langmuir Freundlich Donnan model. Symbols are as given in Figure 5. Similar symbols are used for the different salt concentrations for the experimental (solid) and Master Curve (open). ■ = $10^{-3}$ M; ♦ = $10^{-2}$ M; ▲ = $10^{-1}$ M $KNO_3$.

By applying the NICA-Donnan model at a specific salt concentration, the experimental Q(pH) curves can be recalculated. The results are compared with the experimental datapoints in Figure 10. It can be observed that the model fits very well to the experimental datapoints. In particular, it accounts for the near-parallel nature of the proton adsorption isotherms at different salt concentrations and is able to predict the shifts of the curves due to changes in pH and salt concentration very accurately. The double Langmuir Freundlich parameters used to describe the Q(pH) curves, are given in Table II.

**Table II:** Assessed parameters describing the PAHA Master Curve and the surface charge/ pH curves at different salt concentrations. Data obtained by the double Langmuir Freundlich Donnan model. The PPHA parameters are given for comparison.

|          | I     | $\log \tilde{K}_1$ | $\Gamma_{max1}$ | $m_1$ | $\log \tilde{K}_2$ | $\Gamma_{max2}$ | $m_2$ |
|----------|-------|--------|--------|------|--------|--------|------|
| PAHA     | Intr. | 4.03   | 3.74   | 0.44 | 8.48   | 1.30   | 0.53 |
| PAHA     | 0.001 | 5.46   | 4.02   | 0.34 | 10.22  | 0.94   | 0.65 |
| PAHA     | 0.01  | 5.15   | 4.01   | 0.34 | 9.92   | 0.96   | 0.64 |
| PAHA     | 0.1   | 4.52   | 3.90   | 0.36 | 9.35   | 1.14   | 0.55 |
| PPHA (14)| Intr. | 2.99   | 2.76   | 0.46 | 8.62   | 3.33   | 0.32 |
| PPHA (32)| 0.1   | 4.60   | 2.48   | 0.44 | 9.34   | 1.93   | 0.39 |

## Modelling the cadmium adsorption isotherms

The cadmium data were also fitted using Kinniburgs numerical routine (48). As discussed by Benedetti et al. (32), it is preferred to derive an initial estimate of the metal ion parameters in order to minimise the failure of convergence in the fitting routine. The initial value for $p_1$ values was derived graphically from the cadmium binding isotherms, as described by Benedetti et al. and was 0.6. For $p_2$, a large uncertainty was observed. This can be easily understood since the second peak contributes relatively little to the total cadmium binding (33). Cadmium is bound mainly to the carboxylic groups at high cadmium concentrations ($[Cd^{2+}] > 10^{-6}$), but the weak acid groups do contribute at lower cadmium concentrations. As described by Benedetti et al. (32), copper adsorption occurs on both type of groups. Therefore a set of copper adsorption data is better suited to determine $p_2$. Based on such data, Benedetti et al. concluded that the values of $p_1$ and $p_2$ are comparable. Unfortunately there were no copper binding data available for PAHA, but following Benedetti et al. a starting value of $p_2 = 0.6$ has been used.

The final set of Cd binding parameters is given in Table III. The tabulated values are the average of the values calculated using the Donnan volumes at the two different salt concentrations; 0.1 and 0.01 M $KNO_3$. The values obtained for the different salt concentrations were the same within the experimental error as indicated by Kinniburgs numerical routine. The coefficients of determination ($R^2$) were 0.994 and 0.989 for the high and low salt concentration, respectively. Figure 11 a and b present the cadmium

binding data and the fitted NICA-Donnan isotherms. It can be observed that the model fits very well to the experiments. Both the pH and salt dependence are calculated accurately. Comparison of Figure 11a and 11b shows that a significant increase in cadmium binding is obtained with decreasing ionic strength.
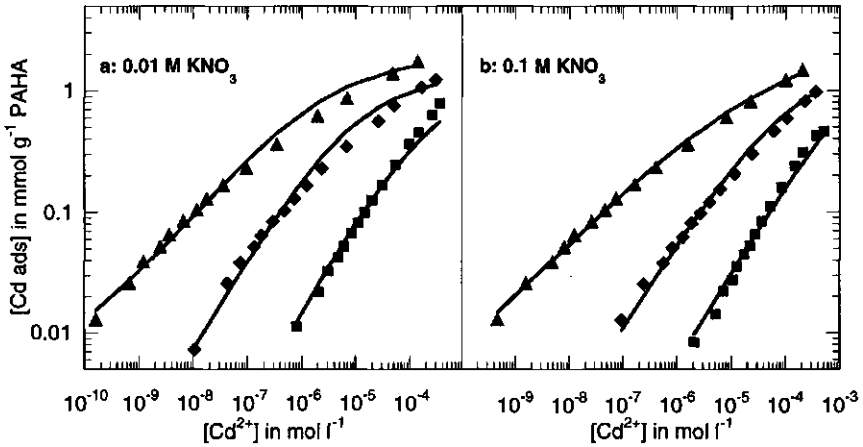


**Figure 11:** PAHA-cadmium binding data as a function of the equilibrium cadmium concentration for 3 different pH values: ■ pH = 4; ♦ pH = 6; ▲ pH = 9 and 2 salt concentrations. The solid lines represent the calculated cadmium binding isotherms according to the NICA-Donnan volumes. **a:** 0.01 M KNO$_3$ **b:** 0.1 M KNO$_3$.

**Table III:** Assessed parameters describing the cadmium binding to PAHA at different salt concentrations, using the NICA-Donnan model. The PPHA parameters are given for comparison.

|  | $\log \tilde{K}_{Cd,1}$ | $p_1$ | $n_{Cd,1}$ | $\log \tilde{K}_{Cd,2}$ | $p_2$ | $n_{Cd,2}$ |
|---|---|---|---|---|---|---|
| PAHA | 2.24 | 0.70 | 0.76 | 4.1 | 0.72 | 0.37 |
| PPHA (32) | 2.89 | 0.49 | 0.75 | 4.9 | 0.68 | 0.5 |

## Discussion

It has been shown that the Donnan volume of a humic acid sample as a function of pH and ionic strength can be obtained by Viscosity measurements, provided $p_{HA}$ is known and molecules are assumed to be spherical. At 0.1 M and 0.01 M KNO$_3$ the measured Donnan volumes were used directly for the model calculations. At the low salt concentration the extension of the double layer resulted in a Debye length much larger than the viscometric radii of the PAHA molecules and consequently the Donnan volume required for the model approaches is the Debye volume instead of the measured hydrodynamic volume. For the calculation of the radii the viscosity average molecular weight has been used.

The observed trends in the hydrodynamic volume of the PAHA molecules can be explained by electrostatic effects. With increasing electrostatic repulsion the hydrodynamic radius of the PAHA molecules increases. With increasing ionic strength the charge is shielded and consequently the radius of the colloids decreases. These observations support the model proposed by Cameron et al. (17), who described the hydrated humics as roughly spherical molecules that can be tightly or loosely coiled, depending on the conditions. The measured hydrodynamic volume corresponds with a volume that is much larger than the dry volume of a PAHA molecule. The resulting water content of the PAHA domains are compared with the values described by Tanford (19) for a Gausian polymer coil. Although elipsometry experiments (31) show that PAHA has also some characteristics of a hydrophobic humic, we have to conclude from the above observations that in solution PAHA molecules can be described with a flexible strongly hydrated structure. As PAHA has many characteristics in common with soil and peat type humic acids most of these humics can probably also be described as flexible strongly hydrated gels.

Comparison of the Master Curve and the intrinsic proton affinity spectra for PAHA, obtained with (1) the directly measured Donnan volumes and (2) the Donnan volume relation for humic substances proposed by Benedetti et al. (14), shows the following differences. Due to the fact that the measured volumes are considerably larger than the volumes used by Benedetti et al. the position of the Master Curve based on the measured volumes is roughly 1 pH unit higher than that obtained with the Benedetti relation. The two peak positions of the present affinity spectrum are therefore shifted to pK values that are about 1 pK unit higher than the peak positions of the affinity spectrum obtained with the Benedetti method. Further the Donnan potentials calculated following the Benedetti approach, are relatively high. At pH 3 the calculated potentials are -60, -90 and -110 mV for $10^{-1}$, $10^{-2}$ and $10^{-3}$ M $KNO_3$, respectively, whereas in the present treatment we find -10, -25 and -27 mV.

Based on the experimental Donnan volumes it was shown to be possible to model both proton and metal ion binding to PAHA as a function of pH and salt concentration, with the NICA-Donnan model. Especially the description of the cadmium binding at the lowest salt concentration is better than that obtained by Benedetti et al. for cadmium binding on PPHA.

Comparison of the results of the PAHA proton and metal ion binding isotherms with those of a well-characterised Purified Peat Humic Acid (PPHA) (2,14,32,33,51) shows that the shape of the proton and cadmium isotherms, as well as the effects due to changes in pH and ionic strength are in good agreement. The model parameters of the proton and cadmium binding onto PPHA are summarised in Table II and Table III, respectively. The average molecular weight of PPHA is 23 $10^3$ as determined by Milne et al. (2) by equilibrium UV-scanning ultracentrifugation (34). This value is very similar to the value of PAHA.

By comparing the intrinsic affinity constants it should be realised that these values depend on the gel volumes used in the Donnan model. As shown above the Benedetti gel volumes lead to $pK_H$ values that are roughly 1 pK unit lower than those obtained with the viscosity gel volumes. Comparison of the apparent affinity constants, obtained by applying the NICA model only, is more straight forward. These constants are however, more difficult to interpret.

The results obtained within this study emphasise that the well-characterised PAHA (31) can be used as an analogue for soil and peat type humic acids in speciation studies in natural environments. Regarding the different origin of both humics the resemblance of the model parameters supports the findings of Benedetti et al. (54) that the set of constants obtained for a given humic (e.g. PAHA or PPHA) can be used more generally.

## Conclusions

The viscometricaly determined gel volumes can be successfully applied (1) to calculate the Master Curve with the Donnan model and (2) in the NICA-Donnan model for the description of both proton and cadmium ion binding to PAHA. It was shown that the double Langmuir Freundlich parameters derived from the Master Curve described the pH and salt dependence of the proton binding data very well. The non-ideal competitive adsorption (NICA) model, based on the thus obtained parameters and the newly derived metal parameters fits the cadmium binding data reasonably well. Also the salt dependence of the cadmium binding was modelled successfully. The latter was much less well possible by the earlier version of the Donnan approach (14,33). Considering these findings we have to conclude that the strongly hydrated spherical particle model for PAHA is realistic. The effective hydrodynamic volume contains a large amount of water, the humic acid segments itself occupy only a small fraction of this volume. This type of model can be compared with a random coil model, commonly used for polyelectrolytes. Depending on the environmental conditions the water content can be even 98 %, which results in an effective volume per humic acid molecule that is orders of magnitude larger than that of the dry humic acid molecule. Due to changes in pH and salt concentration the molecules are tightly or loosely coiled, which causes the radii of the PAHA molecules to vary between approximately 4 and 8 nm. The description of humic molecules as a coiled polyelectrolyte can also be of help for the understanding of the adsorption behaviour of humics onto mineral soil particles. We will return to this in the next chapters (55,56).

**References**

(1) De Wit, J.C.M.; Van Riemsdijk, W.H.; Nederlof, M.M.; Kinniburgh, D.G.; Koopal, L.K. Analysis of ion binding on humic substances and the determination of intrinsic affinity distributions. *Anal.Chim.Acta* **1990**, *232*, 189 -207.
(2) Milne, C.J.; Kinniburgh, D.G.; De Wit, J.C.M.; Van Riemsdijk, W.H.; Koopal, L.K. Analysis of proton binding by peat humic acid using a simple electrostatic model. *Geochim.Cosmochim.Acta* **1995**, *59(6)*, 1101 -1112.
(3) Stevenson, F.J. *Humus Chemistry. Genesis, Composition, Reactions*; Wiley Interscience: New York, 1982.
(4) Aiken, G.R.; McKnight, D.M.; Wershaw, R.L.; MacCarthy, P. *Humic Substances in Soil, Sediment, and Water*; Wiley Interscience: New York, 1985.
(5) Hayes, M.H.B.; MacCarthy, P.; Malcolm, R.L.; Swift, R.S. *Humic Substances II: In search of structure*; Wiley Interscience: New York, 1989.

(6) Nederlof, M.M.; Van Riemsdijk, W.H.; Koopal, L.K. Determination of Adsorption Affinity Distributions: A General Framework for Methods Related to Local Isotherm Approximations. *J.Colloid Interface Sci.* **1990**, *135(2)*, 410 -425.

(7) Nederlof, M.M.; Van Riemsdijk, W.H.; Koopal, L.K. Comparison of semi-analytical Methods To Analyze Complexation with Heterogeneous Ligands. *Environ.Sci.Technol.* **1992**, *26(4)*, 763 -771.

(8) Nederlof, M.M.; Van Riemsdijk, W.H.; Koopal, L.K. Heterogeneity Analysis for Binding Data Using an Adapted Smoothing Spline Technique. *Environ.Sci.Technol.* **1994**, *28(6)*, 1037 -1047.

(9) De Wit, J.C.M.; Van Riemsdijk, W.H.; Koopal, L.K. Proton Binding to Humic Substances. 2. Chemical Heterogeneity and Adsorption Models. *Environ.Sci.Technol.* **1993**, *27*, 2015 -2022.

(10) De Wit, J.C.M.; Van Riemsdijk, W.H.; Koopal, L.K. Proton Binding to Humic Substances. 1. Electrostatic Effects. *Environ.Sci.Technol.* **1993**, *27(10)*, 2005 -2014.

(11) Marinsky, J.A.; Wolf, A.; Bunzl, K. The binding of trace amounts of Lead (II), Copper (II), Cadmium (II), Zinc (II) and Calcium (II) to soil organic matter. *Talanta* **1980**, *27*, 461 -468.

(12) Marinsky, J.A.; Reddy, M.M. Proton and metal ion binding to natural organic polyelectrolytes-II. Preliminary investigations with a peat and a humic acid. *Org.Geochem.* **1984**, *7(3/4)*, 215 -221.

(13) Ephraim, J.H.; Alegret, S.; Mathuthu, A.; Bicking, M.; Malcolm, R.L.; Marinsky, J.A. A United Physicochemical Description of the Protonation and Metal Ion Complexation Equilibria of Natural Organic Acids (Humic and Fulvic Acids). 2. Influence of Polyelectrolyte Properties and Functional Group Heterogeneity on the Protonation Equilibria of Fulvic Acid. *Environ.Sci.Technol.* **1986**, *20(4)*, 354 -366.

(14) Benedetti, M.F.; Van Riemsdijk, W.H.; Koopal, L.K. Humic substances considered as a heterogeneous Donnan gel phase. *Environ.Sci.Technol.* **1996**, *30(6)*, 1805 -1813.

(15) Cornel, P.K.; Summers, R.S.; Roberts, P.V. Diffusion of Humic Acid in Dilute Aqueous Solution. *J.Colloid Interface Sci.* **1986**, *110(1)*, 149 -165.

(16) Ghosh, K.; Schnitzer, M. Macromolecular structures of humic substances. *Soil Sci.* **1980**, *129(5)*, 266 -276.

(17) Cameron, R.S.; Thornton, B.K.; Swift, R.S.; Posner, A.M. Molecular weight and shape of humic acid from sedimentation and diffusion measurements on fractionated extracts. *J.Soil Sci.* **1972**, *23(4)*, 394 -408.

(18) Hayes, M.H.B.; Swift, R.S. The chemistry of soil organic colloids In *The Chemistry of Soil Constituents*; Greenland, D. J.; Hayes, M. H. B. Eds.; Wiley: New York, 1978; 179-320.

(19) Tanford, C. *Physical chemistry of macromolecules*; Wiley Interscience: New York, 1967.

(20) Thurman, E.M.; Wershaw, R.L.; Malcolm, R.L.; Pinckney, D.J. Molecular size of aquatic humic substances. *Org.Geochem.* **1982**, *4*, 27 -35.

(21) Caceci, M.S.; Billon, A. Evidence for large organic scatters (50-200 nm diameter) in humic acid samples. *Org.Geochem.* **1990**, *15(3)*, 335 -350.

(22) Ledin, A.; Karlsson, S.; Düker, A.; Allard, B. Application of photon correlation spectroscopy for measurement of concentration and size distribution of colloids in natural waters. *Anal.Chim.Acta* **1993**, *281*, 421 -428.

(23) Beckett, R.; Hart, B.T. Use of Field-Flow Fractionation Techniques to characterize aquatic particles, colloids and macromolecules In *Environmental particles*; Buffle, J.; van Leeuwen, H. P. Eds.; CRC Press: Florida, 1993; 165-206.

(24) Chen, Y.; Schnitzer, M. Viscosity Measurements on Soil Humic Substances. *Soil Sci.Soc.Am.J.* **1976**, *40*, 866 -872.

(25) Chin, Y.; Gschwend, P.M. The abundance, distribution, and configuration of porewater organic colloids in recent sediments. *Geochim.Cosmochim.Acta* **1991**, *55*, 1309 -1317.

(26) Pinheiro, J.P.; Mota, A.M.; d'Oliveira, J.M.R.; Martinho, J.M.G. Dynamic properties of humic matter by dynamic light scattering and voltametry. *Anal.Chim.Acta* **1996**, *329*, 15 -24.

(27) Ren, S.Z.; Tombácz, E.; Rice, J.A. Dynamic light scattering from power-law polydisperse fractals: Application of dynamic scaling to humic acid. *Phys. Rev. E* **1996**, *53(3)*, 2980 -2983.

(28) Österberg, R.; Mortensen, K. Fractal dimension of humic acids A small angle neutron scattering study. *Eur.Biophys.J.* **1992**, *21*, 163 -167.

(29) Reid, P.M.; Wilkinson, A.E.; Tipping, E.; Jones, M.N. Aggregation of humic substances in aqueous media as determined by light-scattering methods. *J.Soil Sci.* **1991**, *42*, 259 -270.

(30) Powell, H.K.J.; Town, R.M. Solubility and fractionation of humic acid; effect of pH and ionic medium. *Anal.Chim.Acta* **1992**, *267*, 47 -54.

75

(31) Vermeer, A.W.P.; Koopal, L.K. submitted to *Environ.Sci.Technol*, this Thesis. Chapter 3: Characterisation and classification of purified Aldrich humic acid.

(32) Benedetti, M.F.; Milne, C.J.; Kinniburgh, D.G.; Van Riemsdijk, W.H.; Koopal, L.K. Metal Ion Binding to Humic Substances: Application of the Non-Ideal Competitive Adsorption Model. *Environ.Sci.Technol.* **1995**, *29(2)*, 446 -456.

(33) Kinniburgh, D.G.; Milne, C.J.; Benedetti, M.F.; Pinheiro, J.P.; Filius, J.; Koopal, L.K.; Van Riemsdijk, W.H. Metal Ion Binding by Humic Acid: Application of the NICA-Donnan Model. *Environ.Sci.Technol.* **1996**, *30(5)*, 1687 -1698.

(34) Reid, P.M.; Wilkinson, A.E.; Tipping, E.; Jones, M.N. Determination of molecular weights of humic substances by analytical (UV scanning) ultracentrifugation. *Geochim.Cosmochim.Acta* **1990**, *54*, 131 -138.

(35) Lyklema, J. *Fundamentals of Interface and Colloid Science*; Academic Press: London, 1991.

(36) Davies, J.T.; Rideal, E.K. *Interfacial Phenomena*; Academic Press: New York, 1961.

(37) Simba, R. The influence of Brownian movement on the viscosity of solutions. *J.Phys.Chem.* **1940**, *44*, 25 -34.

(38) Clapp, C.E.; Emerson, W.W.; Olness, A.E. Size and Shapes of Humic Substances by Viscosity Measurements In *Humic Substances II: In Search of Structure*; Hayes, M. H. B.; MacCarthy, P.; Malcolm, R. L.; Swift, R. S. Eds.; Wiley Interscience: New York, 1989; 497-514.

(39) Piret, E.L.; White, R.G.; Walther, H.C.J.; Madden, A.J.J. Some physicochemical properties of peat humic acids. *Sci.Proc.R.Dublin Soc.,Ser.1A*, **1960**, , 69 -79.

(40) Visser, S.A. Viscosimetric studies on molecular weight fractions of fulvic and humic acids of aquatic, terrestrial and microbial origin. *Plant Soil* **1985**, *87*, 209 -221.

(41) Kilduff, J.E.; Weber, W.J.J. Transport and Separation of Organic Macromolecules in Ultrafiltration. *Environ.Sci.Technol.* **1992**, *26*, 569 -577.

(42) Paxéus, N.; Wedborg, M. Acid-base properties of aquatic fulvic acid. *Anal.Chim.Acta* **1985**, *169*, 87 -98.

(43) Vermeer, A.W.P. this Thesis. Appendix I: Potentiometric proton titrations, experimental set-up and data treatment.

(44) Kinniburgh, D.G.; Milne, C.J. Guide to the Wallingford Titrator; Technical report. WD/93/23. British Geological Survey: Keyworth, Nottinghamshire. 1993.

(45) Kinniburgh, D.G.; Milne, C.J.; Venema, P. Design and Construction of a Personal-Computer-Based Automatic Titrator. *Soil Sci.Soc.Am.J.* **1995**, *59(2)*, 417 -422.

(46) Boehm, H.P.; Diehl, E. Untersuchung an sauren Oberflächenoxyden des Kohlenstoffs. *Z. Electrochem.* **1962**, *66(8/9)*, 642 -647.

(47) Boehm, H.P. Chemical Identification of Surface Groups In *Advances in Catalysis (and related subjects)*; Acad. Press: New York, 1966; 179-273.

(48) Kinniburgh, D.G. Fit User Guide; Technical Report WD/93/23. British Geological Survey: Keyworth, Nottinghamshire. 1993.

(49) Perdue, E.M.; Reuter, J.H.; Parrish, R.S. A statistical model of proton binding by humus. *Geochim.Cosmochim.Acta* **1984**, *48*, 1257 -1263.

(50) Saar, R.A.; Weber, J.H. Complexation of cadmium(II) with water- and soil-derived fulvic acids: effect of pH and fulvic acid concentration. *Can.J.Chem.* **1979**, *57(11)*, 1263 -1268.

(51) Milne, C.J.; Kinniburgh, D.G.; De Wit, J.C.M.; Van Riemsdijk, W.H.; Koopal, L.K. Analysis of Metal-Ion Binding by Peat Humic Acid Using a Simple Electrostatic Model. *J.Colloid Interface Sci.* **1995**, *175*, 448 -460.

(52) Koopal, L.K.; Van Riemsdijk, W.H.; De Wit, J.C.M.; Benedetti, M.F. Analytical Isotherm Equations for Multicomponent Adsorption to Heterogeneous Surfaces. *J.Colloid Interface Sci.* **1994**, *166*, 51 -60.

(53) Rudzinski, W.; Charmas, R.; Partyka, S.; Bottero, J.Y. On the Nature of the Energetic Surface Heterogeneity in Ion Adsorption at a water/Oxide Interface: Theoretical Studies of Some Special Features of Ion Adsorption at Low Ion Concentrations. *Langmuir* **1993**, *9(10)*, 2641 -2651.

(54) Benedetti, M.F.; Van Riemsdijk, W.H.; Koopal, L.K.; Kinniburgh, D.G.; Gooddy, D.C.; Milne, C.J. Metal ion binding by natural organic matter: From the model to the field. *Geochim.Cosmochim.Acta* **1996**, *60(14)*, 2503 -2513.

(55) Vermeer, A.W.P. this Thesis. Chapter 5: Interactions between humic acid and mineral particles.

(56) Vermeer, A.W.P. this Thesis. Chapter 6: Adsorption fractionation of humic substances at mineral surfaces, experiments compared with theory.

Chapter 5

# Interactions between humic acid and mineral particles

## Abstract

The adsorption of purified Aldrich humic acid onto mineral particles has been measured as a function of pH and salt concentration as well as in the presence of several cadmium concentrations. Next to the adsorbed amount the thickness of the adsorbed layer has been studied. The characteristics of these isotherms and the conformation of the adsorbed layer are discussed in relation to the polyelectrolyte behaviour of purified Aldrich humic acid in combination with several interaction mechanisms. At high pH and low salt concentration the humic acid molecules are adsorbed relatively flat on the surface, which can be described by a relatively large fraction of "trains". At low pH and high salt concentration a large fraction of the adsorbed polyelectrolyte is not in direct contact with the surface. Due to this a significant amount of adsorbed polyelectrolyte can be described as adsorbed in "loops" and "tails". This results in a high adsorbed amount. A further understanding of the interactions between humic substances and mineral surfaces has been obtained by doing model calculations using a polyelectrolyte adsorption theory. Both electrostatic interactions and specific adsorption energy are essential to explain the measured adsorption isotherms and layer thicknesses. Under most conditions a large fraction of the adsorbed polyelectrolyte is not directly bound to the surface and extends into the solution. Due to the charges associated with the extending molecules an electrostatic barrier is developed. Once this electrostatic barrier is developed, further adsorption is inhibited. The results indicate that calculations based on the SCF theory are helpful to gain insight into the binding characteristics of humic acid onto mineral particles.

## Introduction

Within the natural soil system a distinction can be made between a mobile and an immobile fraction. The mobile fraction consists of components that are soluble and transportable by groundwater. The non-dissolvable or settled particles and the material bound to these particles belong to the immobile soil fraction. The mobility of natural organic matter is influenced by its colloidal stability and by binding to components of the solid matrix, like metal(hydr)oxides. It is generally accepted that most contaminants form complexes with the functional groups of the humic substances (1-4), and that with contaminant binding to mineral particles the adsorbed humic material plays an important role (5-8). The adsorptive properties of both the natural organic matter and the oxide can be altered by the interaction between the two components when the humics are adsorbed on the soil minerals (9,10). The transport of contaminants that bind to the mobile colloids may be enhanced strongly in the environment, this phenomenon is known as colloid facilitated transport. To be able to evaluate the speciation of these contaminants a better understanding of the interactions between the different soil components is essential. To obtain a better understanding of these interactions a model system consisting of hematite and purified Aldrich humic acid (PAHA) (11) will be studied.

Humic substances are a mixture of naturally occurring, polydisperse, heterogeneous polyelectrolytes (12-14) that can be divided into three fractions; fulvic acid, humic acid and humin. These fractions are differentiated on the basis of their solubility at different pH (15). Humic acids remain in solution at pH 2 and higher, fulvics even at lower pH and humin is not soluble under alkaline or acid conditions. Humic substances are predominantly negatively charged due to the abundance of carboxylic and phenolic type of groups. Hydration of the charged groups and the electrostatic repulsion between the charges results in an extended conformation of the humic acid molecules (16-18). Due to the addition of indifferent electrolyte the charges are shielded, resulting in a reduction of the electrostatic repulsion and a more tightly coiled configuration.

Based on the structural features of humic substances, humic acids molecules are often describe as fairly flexible polyelectrolytes (16,17,19-22). Chen and Schnitzer (20) mentioned that fulvic and humic acids behave like flexible, linear, synthetic polyelectrolytes, and concluded that the humics are not exclusively composed of condensed rings, but that there must be numerous linkages about which relatively free rotation occurs. Ghosh and Schnitzer (17) showed that humic acids can be described as flexible linear colloids under the conditions that normally prevail in natural soils. Cameron et al. (16) visualised the humic acid molecules in solution as a series of charged, occasionally branched strands. They concluded that the strands coil and wind randomly with respect to both space and time so that the mean distribution of molecular mass is spherical and Gaussian about the centre. Branching results in an increased coil density within the molecule giving rise to more compact spheres than for a linear molecule of equivalent weight. Cameron et al. described the humic acid molecules as a structure that is perfused with solvent molecules that are able to exchange with bulk solvent molecules. It has been shown by Vermeer (18) that the proton and cadmium binding to PAHA could be modelled accurately by assuming that the humic acid molecules are strongly hydrated, fairly flexible, polyelectrolyte molecules. Within the

described approach the humics also occupy only a very small fraction of the volume they pervade and consequently the space given by the hydrodynamic boundary of the coil is largely filled by water.

In view of these results we can approximate humic acid molecules as flexible linear polyelectrolyte molecules and compare their properties with those of synthetic polyelectrolytes. It has to be emphasised that the humics are not described as simple polyelectrolytes, only the properties of both components are assumed to be similar. Naturally the degree of branching affects these similarities, but this is supposed to be a second order effect. Due to a high degree of branching these rearrangements will be less pronounced, but are still significant. For fulvic acid this description may be less appropriate since these molecules are relatively small.

Only in a limited number of studies the adsorption of humic material has been described based on its polyelectrolyte properties (22). Summers and Roberts studied the effects of the polydispersity of the humic substances on the adsorption isotherms and reported that previously developed concepts for well defined synthetic polymers (23-26) were also applicable to macromolecules of natural origin whose chemical composition was less well defined.

On model calculations with simple polyelectrolytes and on the adsorption of synthetic polyelectrolytes numerous literature data are available. A brief review of polyelectrolyte adsorption has been given by Cohen Stuart et al. (27). In general, linear polyelectrolytes behave similar to neutral polymers at high ionic strength and low degrees of dissociation. At low salt concentration and strong dissociation the polyelectrolyte nature is very dominant.

Within the above mentioned model calculations it is widely an accepted practice to describe the adsorption of chain molecules in terms of trains (several succeeding segments of a macromolecule which are attached to the surface) and loops and tails (sections extending into the solution, where the loops and tails are respectively attached to the surface at two and one end) (28). Vermeer (29) has shown, on the basis of Self Consistent Field (SCF) calculations for the adsorption of weak polyelectrolyte on variably charged surface that: the adsorbed amount and the conformation of the adsorbed molecule are influenced by electrostatic interactions between the different segments of the polyelectrolyte, and electrostatic and specific interactions between the polyelectrolyte and the adsorbent. The charges on both the surface and the adsorbed polyelectrolyte were determined by a local association-dissociation equilibrium that depends on pH and salt concentration within the local environment of the chargeable groups. At low pH, where the polymer was only weakly charged or even neutral, the conformation of the adsorbed polyelectrolyte was extended and a high adsorbed amount resulted. The adsorption is now driven by the specific affinity of the polyelectrolyte for the surface, and loops and tails determine the conformation of the adsorbed molecules. On the other hand, at high pH values a flat conformation with a relatively high fraction of trains was obtained. If a specific adsorption energy between the surface and the polyelectrolyte was introduced, the surface charge was overcompensated by the adsorbed polyelectrolyte. These extra charges are associated with the extending polyelectrolyte segments and cause the development of a negative potential profile around the particles. Due to such a negative potential an electrostatic barrier arises that causes the occurrence of a depletion zone, as was described by

Dahlgren and Leermakers (30), based on SCF calculations. Comparable effects were reported by De Laat and Van Den Heuvel (31), who studied the adsorption/ desorption of polyacrylic acid onto barium titanate, and Meadows et al. (32) who mentioned that the extra polyelectrolyte charge and the resulting potential barrier are the predominant factors in limiting the amount of adsorbed polyelectrolyte.

According to Spostito different interaction mechanisms for the adsorption of humic substances to mineral particles have to be considered (33), the major ones are: ion exchange or physical adsorption (purely coulombic interactions), ligand exchange or surface complexation (specific segment surface interactions), divalent cation bridging and hydrophobic interactions. It is generally accepted that all of these interactions may be important rather than only one of them. The importance of the different mechanisms for a given system depends on the mineral particles under investigation and the solution conditions during the experiments (22,34,35).

For the adsorption of humic acids on positively charged minerals, in general, an increase in adsorption is observed with decreasing pH and increasing salt concentration (6,22,34-36). This behaviour is explained in various ways. According to Summers and Roberts (22), physical adsorption occurs next to specific binding and the differences in the adsorbed amount are mainly due to the charge difference between the mineral particles and the organic matter, and shielding of the lateral interactions by the indifferent electrolyte.

In addition to physical adsorption, specific binding of the organic molecules is suggested to be involved (6,7,36,37). Parfitt et al. (38) gave spectroscopic evidence for specific interactions via a "ligand exchange" between a surface hydroxyl or bound water molecule and the oxygen of the carboxylic group. With increasing pH the adsorbed humic molecules may become more negatively charged which leads to a repulsion of the negative groups of the adsorbed humic that are not involved in ligand exchange, decreasing the overall affinity for the surface. The net energy for bond formation via ligand exchange will also decrease due to the change of the surface potential with increasing pH. Tipping (6,39) measured adsorption isotherms on different iron oxides. For a 1:1 background electrolyte plateau values of adsorbed humic acid were found in the range 20 - 80 mg g$^{-1}$, depending on the pH. Tipping described the adsorption by a ligand exchange mechanism and modelled the adsorption as a Langmuir isotherm. Murphy et al. (7,40) measured the adsorption of different humic substances to hematite particles and used the same mechanism and isotherm equation as Tipping. Tipping and Murphy et al. concluded that differences in adsorption were due to differences between the humics and found that humic acid adsorption is higher than fulvic acid adsorption. Gu et al. (37) studied the reversibility of the adsorption of Natural Organic Matter (NOM) to iron oxide particles and reported a strong hysteresis between adsorption and desorption. An ligand exchange mechanism was proposed and the isotherms were described using a modified Langmuir equation in which a hysteresis parameter was incorporated.

Divalent cation binding also affects the adsorption of humic acid onto mineral particles (6,41,42). In the presence of divalent ions, like $Ca^{2+}$ and $Mg^{2+}$, Tipping (6) reported slightly higher values for the adsorption. It was shown that the extra capacity was associated with coadsorption of $Ca^{2+}$ and/ or $Mg^{2+}$ ions. Tipping postulated that the

cations compete with the oxide for the anionic groups on the humic acid molecules, causing fewer contacts per humic acid molecule and consequently an increased adsorption. Due to the formation of metal ion-humic acid complexes also the lateral electrostatic repulsion is decreased and this also may contribute to the increased adsorption. Tipping mentioned that a non Langmuir behaviour was observed in the case where $Ca^{2+}$ and $Mg^{2+}$ were present, which was ascribed to the screening by the divalent ions. McKnight et al. (41) also mentioned the importance of the trace metal adsorption associated with the organic fraction and showed a correlation between adsorbed trace metals and adsorbed fulvic acid. Engebertson and Wandruszka (42) showed that humic acid undergoes a number of organisational rearrangements when subjected to metal ions in solution. According to these authors the formation of intramolecular humic acid/ metal ion pseudomicelles precedes intermolecular interactions. Aggregates of humic acid molecules in the presence of metal ions should be regarded as more compact and more micelle-like in nature than analogous hydrophobic moieties that exist in dissolved humic acid when no metal ions are present. Due to such a compact structure the increased adsorption was explained.

A final aspect concerning the characteristics of the adsorption isotherms are hydrophobic interactions. Humic substances are of amphiphilic nature; they contain both hydrophobic and hydrophilic moieties. Due to these interactions the shape and the absolute adsorbed amount of the adsorption isotherms may be influenced. For instance Amal et al. (43), suggested for the adsorption of fulvic acid to hematite particles first coverage in a monolayer due to electrostatic interaction, followed by further adsorption or "hemimicelle" formation through hydrophobic effects between the first and successive layers. This type of adsorption was reflected by the fact that the adsorption isotherms described by Amal, first show a pseudo plateau, followed by a second step.

To gain a better insight into the binding characteristics between humic acid molecules and mineral particles it is useful to compare the experimental adsorption isotherms and the measured layer thicknesses with calculations based on the self consistent field theory for polyelectrolyte adsorption. In this work adsorption isotherms of Purified Aldrich Humic Acid (PAHA) on crystalline iron oxide particles (hematite $\alpha$-$Fe_2O_3$) were measured and the influence of pH, salt concentration and the presence of $Cd(NO_3)_2$ was studied. The adsorption of PAHA on hematite was investigated at a broad range of humic acid concentrations using depletion measurements and reflectometry. The trend in the adsorbed amount is compared with that of the layer thickness of the humic acid layer as measured by dynamic light scattering. The importance of the four different interaction mechanisms and phenomena as conformational changes and preferential adsorption will be discussed. The applicability of Langmuir type equations is questioned and the polyelectrolyte behaviour (44) of the organic matter will be emphasised in discussing the adsorption process. Finally some calculations are performed using the Self Consistent Field theory for the adsorption of (weak) polyelectrolytes (45-47) on a variably charged surface (29).

## Material and methods

All experiments have been performed at room-temperature (21°C) and with $KNO_3$ as indifferent electrolyte. Chemicals used were p.a. quality and the water used was purified by percolating tab water through a mixed bed ion exchange column followed by an active carbon column and a micro filter.

Oxides surfaces

Different hematite ($\alpha$-$Fe_2O_3$) suspensions were used within this study. Particles were prepared as described by Breeuwsma and Lyklema (48) and by Penners and Koopal (49) and will be denoted with the letter B and P, respectively. The suspensions have been aged for several years at room temperature. Before use the suspensions were washed with HCl and dialysed thoroughly against purified water. The BET ($N_2$) surfaces have been measured with a NOVA 1000 Quantachrome. The hematite B particles have a mean size of 50 nm and a BET surface of 43 $m^2$ $g^{-1}$. The BET surfaces of the hematite P particles with diameters of 212, 402 and 570 nm were respectively 6.8, 4.3 and 2.6 $m^2$ $g^{-1}$. The porosity of all the hematite samples was studied by the $N_2$ gas adsorption isotherms and revealed that the samples were only slightly micro porous.

Some adsorption measurements were made on silicon wafers coated with either a rutile ($TiO_2$) layer or a silica layer. The rutile layer has an isoelectric point of 5. The negative charge of the silica layer is negligible below pH 3.

Humic acid

For all experiments, a purified Aldrich humic acid (Aldrich-Chemie; code:H1,675-2) denoted as PAHA was used. Purification and characterisation of PAHA are described elsewhere (11,15,50). PAHA reflects many characteristics normally found for naturally occurring humic substances and is classified as a soil humic acid. PAHA in its proton form is freeze dried and stored in a glass container. The concentration of trace metals was below the detection limit of ICP measurements.

Before use PAHA was resuspended overnight in a KOH solution with pH approximately 10, to a concentration of 2 g $l^{-1}$. Results of potentiometric proton titrations (18,51) have shown the necessity of this procedure to completely resuspend the sample. Other PAHA solutions were made from this stock solution.

Surface characterisation of the hematite particles

Titrations were performed using the automated Wallingford titration system (52,53). Typically potentiometric proton titrations used 30 ml of suspension. The concentrations of the suspensions were in the order of 20 g $l^{-1}$ hematite. After removal of possible carbon dioxide at pH 3 for about two hours, successive acid and base titrations were performed at different $KNO_3$ concentrations. The $KNO_3$ concentration was adjusted at

pH 3, using one of the burettes and after addition an equilibration time of 30 minutes was allowed. A polypropylene basket was used to prevent adsorption of hematite to the glass vessel. The suspension was stirred continuously to prevent settling of the suspension. After addition of titrant, the rate of drift was measured over a 2 minute interval after an initial delay of 20 seconds to allow adequate mixing. The electrode readings were accepted when the drift was less than 0.5 mV min$^{-1}$. A maximum reading time of 20 minutes was set for two successive additions. The doses of $HNO_3$ and KOH were calculated by the interface to obtain a constant mV change of about 5 mV for each addition, to obtain a good distribution of data points over the pH range studied. A detailed description of the potentiometric proton titration and data treatment are given elsewhere (54).

## PAHA adsorption

### Depletion measurements

PAHA adsorption isotherms onto hematite B were measured at three different pH values (4, 6, 9) and two different $KNO_3$ concentrations (0.01 M, 0.1 M). In a separate series of experiments the influence of the size of the hematite P particles on the adsorption of PAHA was measured at pH 6 and 0.01 M $KNO_3$. The adsorption measurements were carried out batchwise in polyalymere tubes, each containing about 0.5 m$^2$ of hematite and varying initial concentrations of PAHA (5 mg l$^{-1}$ to 500 mg l$^{-1}$).

The H, $KNO_3$ and $Cd(NO_3)_2$ concentrations in the tubes were made by adding the required amount of stock solutions with Metrohm 665 Dosimat burettes. Hematite was added by weighing an amount of stock suspension in the tubes (approximately 8 g l$^{-1}$). PAHA was added using a volumetric pipette. Especially at high pH precautions against carbon dioxide were taken, PAHA solutions were ultrasoned for several minutes before they were brought into the tubes.

After adding all components the pH was adjusted to the desired pH within 0.1 unit. The suspension was shaken, head over head, for about 18 hours. From kinetic experiments it was found that the equilibrium concentrations became constant after 14 hours. Then the pH was readjusted and suspensions were shaken for a short period (about 1 hour), the final pH was measured and the analyses took place.

The humic acid content of the supernatant was measured after centrifugation for 30 minutes at 7500 rpm using a Beckman JA-21 or JA-20 centrifuge. Control experiments without the oxide showed that no loss of humic acid occurred during this procedure. Concentrations of humic acid were determined with a Hitachi U-3210 spectrophotometer UV spectrophotometry at 254 nm. The absorbance at 254 nm for a given humic acid concentration is pH and salt dependent. This problem was solved by making a calibration line for each required pH and salt level.

### Reflectometry

Adsorption measurements of PAHA on rutile and silica were made with a reflectometer according to the procedure described by Dijt et al. (55). The PAHA solutions were

83

delivered at the oxide surface using a stagnation-point flow-cell. A He/ Ne laser with a wavelength of 632.8 nm was used to detect the adsorption. At the wavelength of the laser PAHA shows no absorption peaks. The laser emits a polarised beam, which is reflected by the surface. At the Brewster angle the reflectivity of the parallel polarised beam will be minimal, whereas the perpendicular beam will still reflect significantly (55). The intensities of both polarisation directions are measured continuously by means of photodiodes (56). The relative change in the ratio between the parallel and perpendicular reflectivity with respect to the initial ratio is proportional to the adsorbed amount.

The proportionality factor $A_s$ was calculated by the method of Hansen (57). Its value is proportional to the dn/dc of the polyelectrolyte. The dn/dc of PAHA was 0.28 $cm^3g^{-1}$ (11).


Dynamic Light Scattering measurements


Two kinds of experiments were performed; (1) determination of the radii of the isolated components: hematite P and PAHA and (2) measurements of the radii of the PAHA covered hematite P particles. The equipment used for the dynamic light scattering experiments was built from standard components: an ALV-125 laser light spectrometer/ goniometer, an ALV-5000 digital correlator, an ALV-800 transputerboard and a Spectro Physics 35 mW HeNe laser. The wavelength of the laser was 632.8 nm. The scattering angle θ was 90° for all the performed experiments. A detailed description of the experimental set-up has been described by Lyklema (58).

During a dynamic light scattering experiment the Brownian motion of the scattering particles leads to time dependent fluctuations in the detected scattering intensities. From these intensity fluctuations a time dependent autocorrelation function can be obtained. The diffusion coefficient (D) was obtained by fitting a second cumulant fit through the autocorrelation function. From the diffusion coefficient the radius of the particles is calculated with the Stokes-Einstein relation for isolated spherical particles. This method may also be applied to solutions of macromolecules if the radius $a$ is replaced by the hydrodynamic radius $r_h$ of the macromolecule. The required viscosity of the PAHA solutions was measured with an automatic viscometer (Viscosometric MS type 53 000).

The radii of bare hematite particles were measured at low pH (between pH 2 and 4) and without the addition of any salt (addition of indifferent electrolyte or increasing the pH will partly aggregate t' e hematite particles). The radii of the PAHA molecules were measured at different pH, salt concentration at a PAHA concentration of 50 mg l⁻¹ (18). Prior to the measurements the solutions were filtered using a 300 nm Millipore filter.

For the coated particles the following procedure is used. A small amount of hematite P was added, while stirring strongly, to a filtered PAHA solution adjusted to the required pH and salt concentration. PAHA concentrations were chosen to be on the adsorption plateau of the adsorption isotherms. After equilibration for 14 hours, while stirring strongly, the mixture was filtered through a 600 nm Millipore filter and the hydrodynamic radius was measured. This special procedure is required to avoid particle aggregation during the sample preparation (59,60). The hydrodynamic radius of the coated particles

was calculated from several hundred measurements, experiments with a high rms error were withdrawn and an average radius was calculated from the remaining datapoints. The layer thickness was calculated from this average radius by subtracting the radius of the bare particles.

## Results

Characterisation of the hematite particles

The surface charge/ pH curves of hematite B for three salt concentrations are given in Figure 1. Its points of zero charge (p.z.c.) as determined by pH-STAT titrations upon addition of indifferent electrolyte (54) is 8.9. These curves are comparable to the titration curves described previously (48).

The electron micrographs of hematite B and P were used to study their size and geometry. The hematite B particles resembled parallelograms with an included angle of 60° and a mean size of 50 nm, as observed by electron microscopy. The hematite P particles are nearly spherical with diameters of 86, 212, 402 and 570 nm (measured with dynamic light scattering). The magnitude of these measured diameters agreed well with those calculated from electron micrographs.
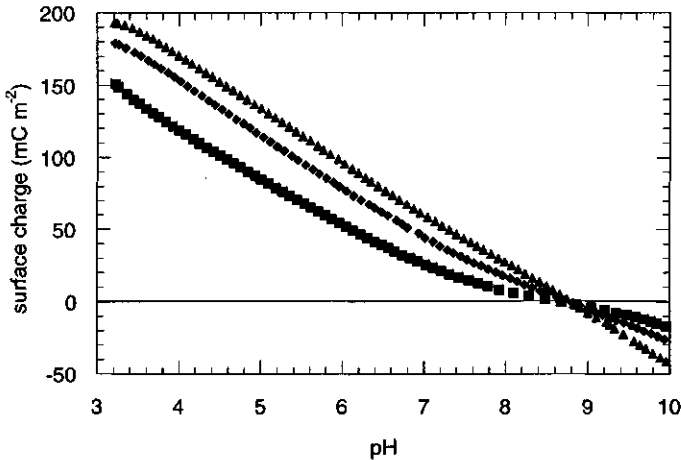


**Figure 1:** The surface charge of hematite B as a function of pH in the presence of different concentrations $KNO_3$: ■ = $10^3$ M; ♦ = $10^2$ M; ▲ = $10^{-1}$ M.

Adsorption of humic acid on hematite particles

Adsorption isotherms of PAHA on hematite B at 0.1 M and 0.01 M $KNO_3$ are shown in Figure 2 and Figure 3, respectively. It is observed that the humic acid adsorption

increases with decreasing pH A slightly increasing adsorption, especially at pH 4, was measured with increasing ionic strength. This type of adsorption is classified as screening enhanced, following Van der Steeg (61), that is the nonelectrostatic attraction between humic acid groups and the surface sites dominates. Salt mainly screens the lateral repulsion between the adsorbed humic acid segments and hence the adsorption is enhanced with increasing salt concentration. The adsorption isotherms show an initial steep slope indicating a high affinity character, followed by a pseudo plateau at elevated equilibrium concentrations. These features of the adsorption isotherms are commonly observed for the adsorption of humic substances onto mineral particles (6,35-37,41,43).
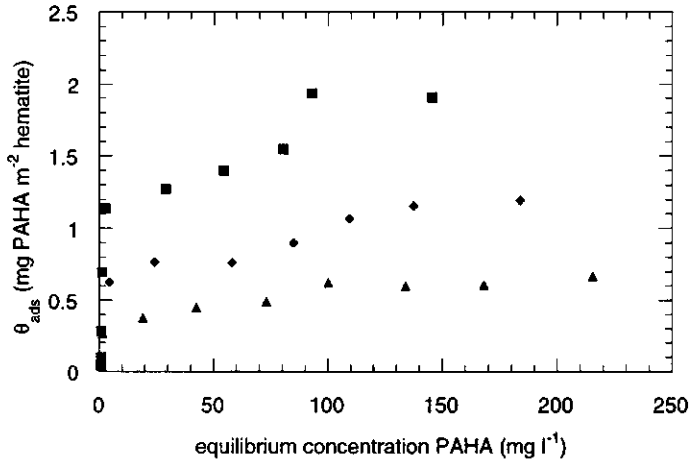


**Figure 2:** Adsorption isotherms of PAHA onto hematite B, 0.1 M $KNO_3$. Effect of pH on the adsorption: ■ pH = 4; ◆ pH = 6; ▲ pH = 9.
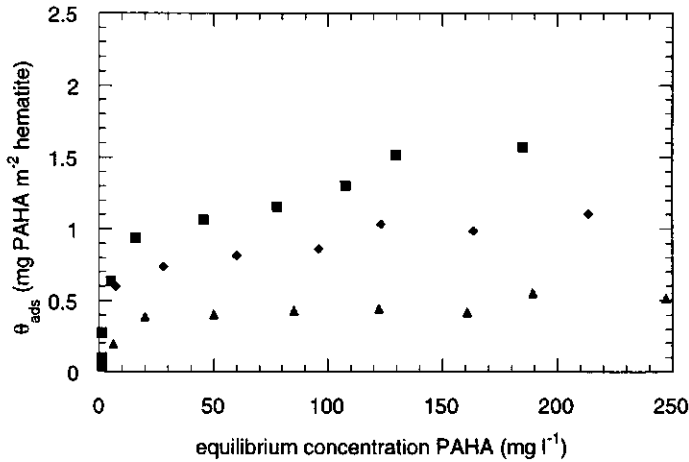


**Figure 3:** Adsorption isotherms of PAHA onto hematite B, 0.01 M $KNO_3$. Effect of pH on the adsorption: ■ pH = 4; ◆ pH = 6; ▲ pH = 9.

The charge density that is initially associated with the bare oxide and the free humic at a given pH and ionic strength is shown in Figure 1 above and a figure given in (18), respectively. If we assume that both charge densities are not affected by the adsorption of the humic onto the oxide it is possible to calculate the overall charge of the complex for a given amount of adsorbed humic. These calculations show that at pH 4 the net total charge of the oxide particles and the adsorbed humic acid remains positive. At pH 6 and 9 the net particle charge becomes negative. Qualitatively this result is in agreement with electrophoretic measurements (62,63) that show that the positive iron oxide particles become negative due to adsorption even at very low humic acid coverage. These results indicate that the adsorption can not be described by charge compensation only.

To study whether the surface curvature of the oxide particles influences the adsorbed amount, the conformation of the adsorbed layer and the overcompensation of the surface charge, the dependence of the adsorption on the radius of the adsorbent was investigated at pH 6 and 0.01 M $KNO_3$. These experiments were performed by using three different sized hematite P suspensions: P212, P403 and P570. All experiments were performed with an equal surface area per tube. The adsorption isotherms (solid symbols) are shown in Figure 4. The shape as well as the plateau value of the adsorption isotherms on the different hematite P particles are within experimental error the same. The radii of the hematite particles are not large enough to introduce conformational differences within the adsorbed layer. The hematite P isotherms are compared with the isotherm at pH 6 and 0.01 M $KNO_3$ of the much smaller, parallelogram like hematite B particles (open symbols). At the plateau level the adsorption on hematite B is about halved compared with the hematite P particles.
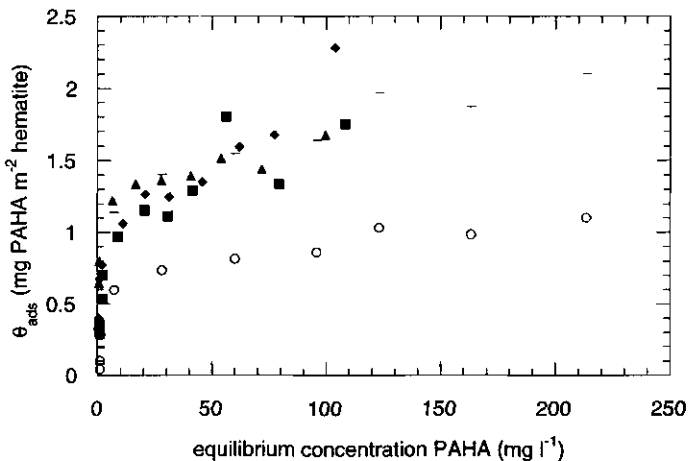


**Figure 4**: Adsorption isotherms of PAHA onto different hematite particles, pH 6 and 0.01 M $KNO_3$. The adsorption onto different sized hematite P particles is compared with that on hematite B: ■ = hematite P 212 nm (diameter); ♦ = hematite P 403 nm; ▲ = hematite P 570 nm; O = hematite B (equivalent diameter of approximately 50 nm) and - = adjusted adsorption isotherm of PAHA onto hematite B particles (the charge density of the hematite P (64) particles at pH 6 was taken as standard).

Comparison of the electron micrographs of hematite B and P shows that the shape of the different hematite particles is only slightly different and that the difference in adsorption can not be attributed to the difference in geometry of the particles. The differences in the adsorbed amount may reflect a more compact adsorption layer for the smaller hematite B particles. This seems however, very unlikely regarding the increasing available volume with decreasing radius. Alternatively, the differences in PAHA adsorption on hematite P and hematite B may arise due to the differences in surface charge density. If it is assumed that for a given humic acid at given conditions the charge on the hematite largely determines the adsorption, the adsorption on both samples should reflect the ratio between these charge values. This is indeed the case. By multiplication of the adsorption values on hematite B with a factor 1.8, which is obtained by comparison of the surface charge curves of hematite B and P that were reported previously (64), an isotherm results that corresponds with those of hematite P (Figure 4). However, as mentioned before, charge compensation only can not describe the adsorbed amount. Comparison of the charges associated with the single components showed that under the applied conditions, the surface charge is overcompensated by the adsorbed polyelectrolyte charge. Due to the charge overcompensation of the hematite particles a negative potential profile will develop around the particles. This electrostatic barrier will inhibit further adsorption of the negatively charged humics and minimise charge overcompensation.

An electrostatic barrier will also influence the reversibility of the adsorption process, changes within the adsorbed layer will be slowed down and may seem to be irreversible. The reversibility of the adsorption as a function of differences in pH, salt and PAHA concentration was studied by reflectometry using $TiO_2$ and $SiO_2$ as substrates. It was observed that the adsorption was reversible for pH changes larger than two pH units. Although for smaller pH changes, the adsorption was not reversible within the timescale of the experiment, the adsorbed amount decreased slowly as time elapsed. Comparable results were obtained upon changes in salt or PAHA concentration.

Layer thickness of the adsorbed humic acid

The layer thickness of PAHA adsorbed at hematite P86 ranges from 37 to 55 nm as was measured by dynamic light scattering. Experiments with silica particles, at a pH where no adsorption occurred, did not show an increased radius. Thus the increased radius of the hematite particles can be ascribed due to the adsorption of the PAHA molecules. The thickness of the adsorbed layer indicates that the adsorbed molecules protrude strongly into the solution. Experiments with hematite P570 particles gave comparable layer thicknesses, indicating that the increased radius was not caused by aggregation of the hematite particles. The adsorption level at the plateau of the isotherms, the thickness of the adsorbed layer and the diameter of dissolved PAHA domains are shown in Table I. A relevant procedure to compare these properties for the different pH values is by comparing ratios of the measured values, using pH = 4 as a standard. It is observed that the layer thickness decreases less pronounced with increasing pH, than does the adsorbed amount. The diameter of the humic acid

molecules even increases with increasing pH. Considering these trends we may conclude that the adsorbed layer becomes less compact with increasing pH. At pH 9 the surface charge is negligible whereas the charge of the adsorbed polyelectrolyte is significant. Due to the lateral repulsion between the different adsorbed polyelectrolyte segments some of the polyelectrolyte segments will protrude relatively far into the solution. The dependence of the adsorbed amount and the hydrodynamic layer thickness on pH observed in the present experiments compares well with results reported by Wang and Audebert (65) for the adsorption of a cationic polyelectrolyte on silica.

**Table I:** Experimental data from depletion and dynamic light scattering experiments.

| pH | surface concentration $\Gamma_{max}$ (mg g$^{-1}$) | ratio | thickness PAHA adsorbed layer $\delta_{PAHA}$ (nm) | ratio | diameter PAHA in solution $d_{PAHA}$ (nm) | ratio |
|---|---|---|---|---|---|---|
| 4 | 52 | 1.00 | 55 | 1.00 | 130 | 1.00 |
| 6 | 35 | 0.67 | 40 | 0.74 | 138 | 1.06 |
| 9 | 17 | 0.33 | 37* | 0.67 | 143 | 1.10 |

* This value was obtained indirectly; adsorption did not take place at pH 9 but at pH 6 and pH was increased afterwards.

Influence of cadmium adsorption

In order to study the influence of heavy metal ions on the adsorption of PAHA, adsorption isotherms were measured in the presence of a constant amount of cadmium. Further the order of addition of cadmium and PAHA on the adsorption was studied.

Adsorption isotherms in the presence of cadmium are shown in Figure 5 and 6. Several observations can be made when the isotherms in Figure 5 and 6 are compared with the isotherms of Figure 2 and 3. Especially at pH 9 the adsorption of humic acid is increased when cadmium ions are present, this was most pronounced at the highest salt concentration. It is also observed that the shape of the isotherms is changed compared to the isotherms without the divalent electrolyte. In the presence of cadmium ions the adsorption is higher at low PAHA concentrations, reflecting a higher affinity of the PAHA molecules for the surface. A slight maximum exists in the adsorption isotherms at pH 6 and 9. This maximum was also observed for the adsorption of PAHA on rutile in the presence of cadmium, as measured by reflectometry.

For high cadmium concentrations compared to the available PAHA sites, the humic will be saturated with cadmium, resulting in more compact PAHA entities. As a consequence of this the adsorbed amount is increased. At higher PAHA concentrations and with a low amount of cadmium, the humic will still be negatively charged. This leads to a repulsion between the segments and thus a more extended configuration, which gives rise to a less profound adsorption. These two features are reflected in the shape

of the adsorption isotherm and cause the observed maximum. The observed maximum was also reported for the adsorption of synthetic polyelectrolytes in the presence of divalent ions on kaolinite (66) and anatase (67).
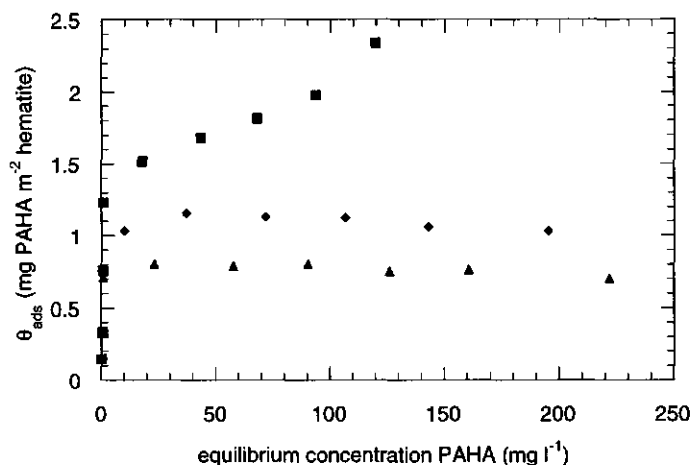


**Figure 5:** Adsorption isotherms of Purified Aldrich Humic Acid onto hematite, 0.1 M $KNO_3$ and $10^{-4}$ M $Cd(NO_3)_2.10H_2O$. Effect of pH on the adsorption: ■ pH = 4; ♦ pH = 6; ▲ pH = 9.



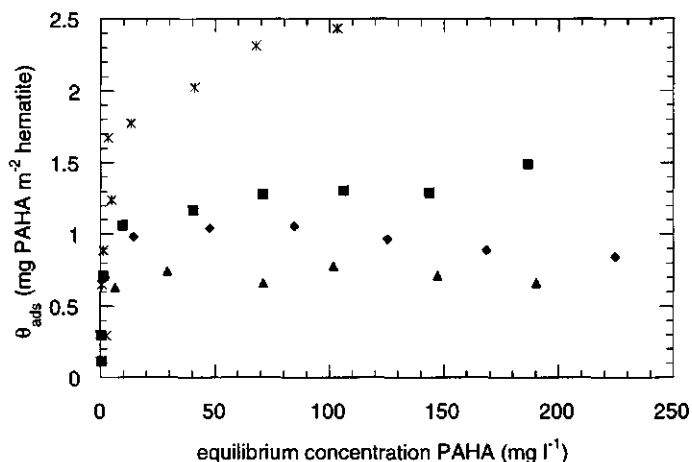**Figure 6:** Adsorption isotherms of Purified Aldrich Humic Acid onto hematite, 0.01 M $KNO_3$ and $10^{-4}$ M $Cd(NO_3)_2.10H_2O$. Effect of pH and cadmium concentration on the adsorption: ■ pH = 4; ♦ pH = 6; ▲ pH = 9, ✳ pH = 4 and $10^{-3}$ M $Cd^{2+}$.

At pH 4 and 0.01 M $KNO_3$ experiments with a constant amount of hematite, PAHA and a total Cd concentration of $10^{-3}$ M showed that the PAHA fraction removed from the solution upon centrifugation increased strongly as compared to the situation at $10^{-4}$ M cadmium. At this point the difference between adsorption and aggregation has to be

emphasised. At pH 4, 0.01 M KNO$_3$ and $10^{-3}$ M Cd$^{2+}$, the isotherm shown in Figure 6 reflects both PAHA adsorption and aggregation. From dynamic light scattering experiments it was found that PAHA aggregated strongly at pH 4 and such a high cadmium concentration, whereas the radius of the PAHA molecules decreased upon addition of small amounts of cadmium ($< 10^{-5}$ M). At these low cadmium concentrations the humic acid/ Cd$^{2+}$ entities are more compact than the dissolved humic acid molecules in the absence of cadmium as was also shown by Engebertson and Wandruszka (42). Due to these two contradicting effects aggregation and compression, the description of the adsorption isotherms at low pH and high salt concentration may become somewhat arbitrary. Results reported by Tipping (6) and McKnight et al. (41) showed comparable effects of cadmium on the humic acid adsorption isotherms and their adsorption plateaux.

The effects of the order of addition on the PAHA adsorption were studied by depletion measurements and reflectometry. The results on rutile as measured by reflectometry were comparable with those on hematite B as measured by depletion measurements. Two adsorption experiments were performed; with the first experiment cadmium was spiked to an oxide/ PAHA equilibrated system and within the second experiment PAHA was spiked to an oxide/ Cd$^{2+}$ equilibrated system. Results are compared with the previously shown adsorption isotherms (Figure 5 and 6) where Cd$^{2+}$ and PAHA were added simultaneously to the hematite system. The adsorbed amounts of PAHA of the Cd$^{2+}$ spiked experiments were comparable with the adsorption isotherms of the experiments without any cadmium (Figure 3), thus indicating that the cadmium ions do not influence the PAHA adsorption once the PAHA adsorption took place. Upon several cycles of adsorption and desorption, by adjusting the pH, the adsorbed amount of PAHA approached the level of the isotherms where PAHA and cadmium were added simultaneously.

When PAHA was spiked, the adsorption level was slightly lower or at most equal to the level of the isotherms where both components were added simultaneously. Based on the equilibrium concentrations of PAHA and cadmium, compared with experiments where these components were added simultaneously, it was concluded that a competition effect between Cd$^{2+}$ and PAHA for the oxide surface groups could be observed. The effect was only small since the exchange of cadmium ions between the surface and the solution was much faster than the kinetics of the PAHA adsorption/ desorption process. Again it has to be emphasised that the conformation of the humics in solution is important for the adsorbed amount.

**SCF theory, polyelectrolyte adsorption on a surface with a variable charge**

Outline

As was already discussed in the introduction of this paper humic acids are often described as fairly flexible, linear polyelectrolytes. The use of a model describing the adsorption of simple polyelectrolytes will be useful in gaining insight into the described binding characteristics of humic acids. Again we emphasise that the humics are not

simple polyelectrolytes, only the properties of both type of polyelectrolytes are assumed to be similar.

The adsorption of weak polyelectrolytes onto a surface with a variable charge can be modelled with the SCF theory (29). The SCF theory for the adsorption of chain molecules (28) is an extension of the homogeneous Flory-Huggins lattice theory for chain molecules in solution. Basically the theory evaluates the probabilities of all possible chain configurations on a lattice in a non-homogeneous potential field near a surface and determines the most favourable. As the potential field is also determined by the positions of the segments and the solvent monomers the self consistent equilibrium distribution of segments can only be found by numerical calculation. In the SCF theory for polyelectrolyte adsorption a polyelectrolyte molecule i is considered as a chain of $N_i$ segments numbered $s=1....N_i$. The polyelectrolyte molecules are dissolved in an aqueous electrolyte solution composed of monomeric water, W, and salt ions, $Na^+$ and $Cl^-$. All these components are placed in a lattice consisting of M layers parallel to the surface (S) and numbered from $z = 1$ to $z = M$. The distance between two adjacent layers is denoted by d. The protons present are dimensionless and determine the pH of the system. The total amount of polyelectrolyte in the system is expressed in equivalent monolayers, $\theta$. On one side of the system the surface (an impenetrable wall) is placed at $z = 0$. At the other boundary at $z = M + 1$, reflecting conditions are assumed. Each segment type x ($x = U, C, P, Na^+, Cl^-, W, S$) experiences a potential $u_x(z)$ at a distance z·d from the surface. $u_x(z)$ is normalised with respect to the bulk solution. Thus $u_x(\infty) = 0$. The potential $u_x(z)$ is a free energy composed of all energetic and entropic interactions a segment undergoes, it depends on the average surroundings, electrostatic interactions and nearest neighbour segment-segment interactions. Flory-Huggins (68) parameters, $\chi_{x,y}$, are used to quantify the segment-segment and segment-solvent interactions The long range Coulombic interactions are introduced in the lattice model as a series of parallel plate condensers (multi-Stern-layer model) (45,46). The charges on the surface and the polyelectrolyte are created by introducing segments that can dissociate into a charged segment and a proton, governed by a proton dissociation constant, $pK_H$. The so-called two state approach (47,69) is used to describe the acid-base equilibrium of the weak polyelectrolytes and the surface. With a mean field approximation the weighted probability $G_i(z,s)$ of finding a segment s of component i in a layer z is calculated using Boltzman equations. To evaluate the probabilities of all possible conformations a first order Markov approach is used. On the basis of these probabilities equilibrium volume fractions $\rho_i(z)$ are calculated for all components in the system and from these the adsorbed amounts can be obtained.

Choice of parameters

The calculations were performed using a lattice of simple cubic symmetry with a cell size d of 0.311 nm. This cell size corresponds with a water density of 55.2 mol $l^{-1}$. The system is built of 100 layers. This value was chosen to assure that all concentration and potential profiles were relaxed in the bulk of the system. The surface (S) is composed of two types of groups, a charged and a neutral one in the ratio of 1:1. Both types of sites are equal except for their charge. All units in the system have a dielectric constant $\varepsilon_r$ of

80 and are considered to be hydrophilic. The charged group has a $pK_H$ of 9 and is titrated from 0.5 to -0.5 according to the one pK model introduced by Van Riemsdijk et al. (70) and reviewed by Koopal (71)). For the present choice of the lattice cell this results in a maximum density of 5.2 charged sites $nm^{-2}$. A completely hydroxylated hematite surface would accommodate about 9 hydroxide groups $nm^{-2}$ whereas the experimental values vary from 4.5 through 5.9 to 9 OH $nm^{-2}$ as measured by Jurinak (72), McCafferty and Zettlemoyer (73) and Morimoto et al. (74), respectively.

To study the effect of some characteristic humic acid properties, different polyelectrolytes were studied. The influence of both electrostatic and specific interactions on the adsorbed amount and the shape of the polyelectrolyte isotherms, are modelled. Three forms of special effects related to the polymer are considered: a specific adsorption energy, chemical heterogeneity and hydrophobicity. The properties of the four different polyelectrolyte molecules used in the calculations are summarised in Table II. The chainlength of these polyelectrolytes is 200. Polyelectrolyte 5 is intended to represent a pseudo fulvic acid, its chainlength is about a factor 10 smaller than that of polyelectrolyte 3 and the proportion of chargeable segments is relatively high. In all cases the polyelectrolyte is taken to be linear with at least two types of segments; U, C or P, where the U segment is uncharged and C is a segment with a pK of 4, representing carboxylic type of groups and P is a segment with a pK of 10, representing phenolic type of groups. The chargeable segments of the polyelectrolyte are titrated from 0 to -1. The specific effects are introduced by giving the segments in the polyelectrolyte chain different characteristics. For these interactions, Flory-Huggins (68) $\chi$ parameters can be defined. By definition $\chi = 0$ for molecules of the same kind and $\chi_{x,y} = \chi_{y,x}$. A $\chi$ of 0.5 indicates a $\theta$ solvent.

**Table II**: Polyelectrolytes used in the SCF calculations.

| polyelectrolyte type | | Chain composition | $\chi$ parameters (in solution) | $\chi$ parameters (with surface) |
|---|---|---|---|---|
| pure electrostatic | 1 | $U_{100}C_{100}$ | all $\chi_{x,y} = 0$ | $\chi_{c,s} = 0$, $\chi_{u,s} = 0$ |
| 1 + specific adsorption | 2 | $U_{100}C_{100}$ | all $\chi_{x,y} = 0$ | $\chi_{c,s} = -15$, $\chi_{u,s} = 0$ |
| 2 + heterogeneity | 3 | $U_{100}C_{68}P_{32}$ | all $\chi_{x,y} = 0$ | $\chi_{c,s} = -15$, $\chi_{u,s} = 0$, $\chi_{p,s} = 0$ |
| 3 + hydrophobicity | 4 | $U_{100}C_{68}P_{32}$ | $\chi_{P,W} = 3$, $\chi_{U,W} = 3$ all other $\chi_{x,y} = 0$ | $\chi_{c,s} = -15$, $\chi_{u,s} = 0$, $\chi_{p,s} = 0$, |
| 3, but low molecular weight | 5 | $U_{11}C_{9}P_{4}$ | all $\chi_{x,y} = 0$ | $\chi_{c,s} = -15$, $\chi_{u,s} = 0$, $\chi_{p,s} = 0$ |

## Results

The surface modelled in the present calculations can be classified as pseudo hematite. The calculated charge/ pH curves of the model surface (Figure 7) are comparable with the experimental hematite curves (Figure 1), although the overall charge density is somewhat higher.
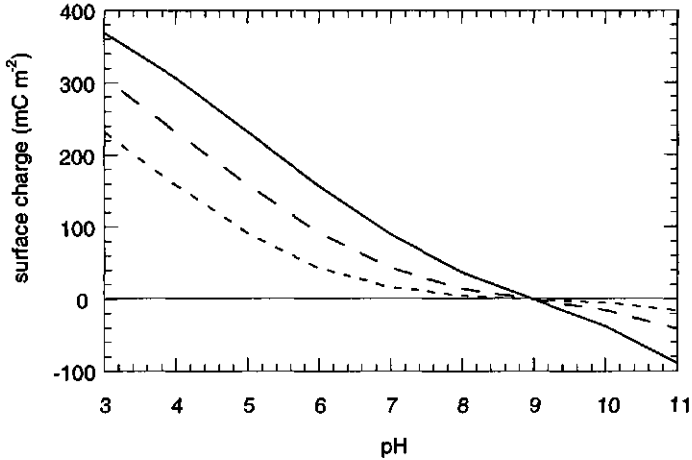
**Figure 7:** Calculated surface charge as a function of pH in the presence of different salt concentrations: $\cdots\cdots$ $= 10^{-3}$ M; $----$ $= 10^{-2}$ M; $\underline{\hspace{1cm}}$ $= 10^{-1}$ M. The pK of the surface sites is 9 and the sites are titrated from 0.5 to -0.5 according to the one pK model (70).

Different polyelectrolytes have been studied to obtain a pseudo humic acid. The effects of the differences in composition and nearest neighbour interactions of these polyelectrolytes on the level of adsorption are shown in Figure 8. All adsorption isotherms were calculated at pH 4 and a salt concentration of 0.01 M.
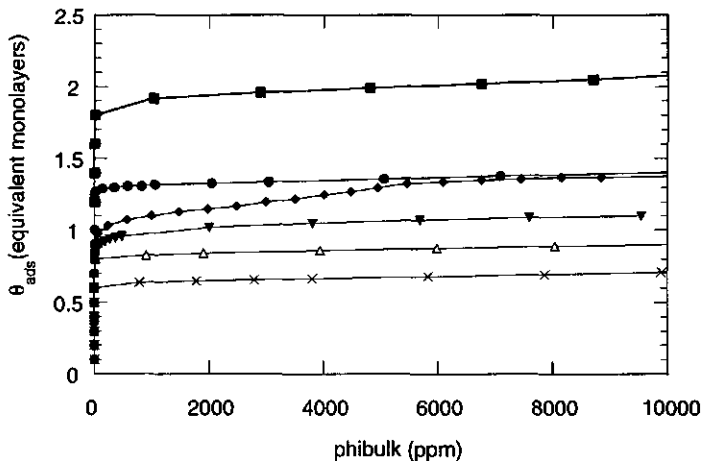


**Figure 8:** Calculated adsorption isotherms at pH 4 and a salt concentration of 0.01 M. At the Y axis the adsorbed amount is given in equivalent monolayers, the bulk equilibrium concentration is given in ppm. x = polyelectrolyte 1; $\triangle$ = polyelectrolyte 2; $\bullet$ = polyelectrolyte 3; $\blacksquare$ = polyelectrolyte 4; $\blacktriangledown$ = polyelectrolyte 5;. $\blacklozenge$ = a bimodal mixture of polyelectrolyte 3 and 5, the weight fraction of polyelectrolyte 3 = 5/7.

The interaction between polyelectrolyte 1 and the surface sites is pure Coulombic. Calculations at pH 9 with polyelectrolyte 1 (not shown) showed that no adsorption

occurred at the p.z.c. of the surface groups. Considering the observed screening enhanced PAHA adsorption (Figure 2 and 3), it is concluded that a specific interaction energy between the surface and the polyelectrolyte is necessary to model the adsorption of humic acid.

The effect of a specific interaction energy on the adsorption isotherm is shown in Figure 8 (polyelectrolyte 2). Due to the specific interaction energy between the surface sites and the C segments the adsorbed amount is increased by about 25%.

To mimic the fact that most humic acid molecules contain carboxylic and phenolic groups, polyelectrolyte 3 was introduced. As is shown in Figure 8 partial replacement of C segments by P segments in the polyelectrolyte chain leads to an increase in adsorption. The adsorption of polyelectrolyte 3 is increased by a factor 2 as compared to polyelectrolyte 1. This is due to two aspects (1) the decreased charge per polymer and (2) the presence of fewer groups with an attractive energy towards the surface.

The effects of a specific adsorption energy and the chemical heterogeneity on the adsorbed amount as a function of pH and salt concentration can be summarised by the following trends (results are not shown). With increasing pH the increased adsorption (expressed as a fraction of the adsorption for the pure electrostatic case) increases due to the introduction of a specific adsorption energy. At pH 9 the adsorption of polyelectrolyte 1 is absent due to the absence of electrostatic polymer surface attraction. Consequently at the p.z.c. a specific adsorption energy causes the most significant increase in adsorption. With increasing salt concentration the effect of the coulombic interaction diminishes and the role of the specific adsorption energy increases.

Regarding the shape of the calculated isotherms it is observed that all curves level of at higher equilibrium concentrations. The experimental isotherms show a slowly increasing (Figure 2 and 3). Regarding the calculated adsorption isotherms this may not be due to specific interactions or the composition of the humic acid. Two effects that can affect the shape of the adsorption isotherm are proposed (1) the formation of hemimicelles or a bilayer through a hydrophobic effect (43) and (2) the occurrence of adsorption fractionation due to polydispersity (25).

Calculations using a different type of lattice (29,75) that made it possible to calculate the properties of the polyelectrolyte in solution, showed that the partially "hydrophobic" polyelectrolyte 4 only formed micelles at pH values lower than the pK of polyelectrolyte segment C. The charge associated with the polyelectrolyte seems to be a limiting factor.

Adsorption isotherms of the "hydrophobic" polyelectrolyte show a considerable increase in adsorption as compared to polyelectrolyte 3 (Figure 8). Due to the increased polyelectrolyte charge the extra adsorption of the more hydrophobic polyelectrolyte 4 decreases with increasing pH. The increase of adsorption is proportional to the Flory-Huggins interaction parameter. The more hydrophobic the polyelectrolyte segments, the more the molecules are repelled from the solution and this promotes adsorption. Calculation of the layer thickness and the volume fraction profile of the adsorbed molecules (not shown) indicated that the adsorbed layer was composed of only single molecules and that a bilayer was not formed. The shape of the isotherms was not influenced (Figure 8).

The polydispersity of humic substances was approximated by a mixture of two polyelectrolytes (polyelectrolyte 3 and 5) with comparable characteristics (Table II). The adsorption isotherms of polyelectrolyte 3, 5 and that of the mixture, with a weight fraction of polyelectrolyte 3 of 5/7, are given in Figure 8. It is observed that the slowly increasing adsorption at the plateau level of the experimental adsorption isotherms can be modelled by polydispersity effects. A detailed discussion on adsorption fractionation is given elsewhere (76).

Comparison of the different polyelectrolytes and regarding the fact that the shape of the experimental isotherms can be explained by polydispersity effects, polyelectrolyte 3 is accepted as pseudo humic acid and further calculations are performed with polyelectrolyte 3.

The adsorption isotherms of polyelectrolyte 3 are given in Figure 9 for different pH values (4, 6 and 9) and 0.01 M salt. The adsorption increases with decreasing pH and the pH effect is similar to that shown in Figure 3.
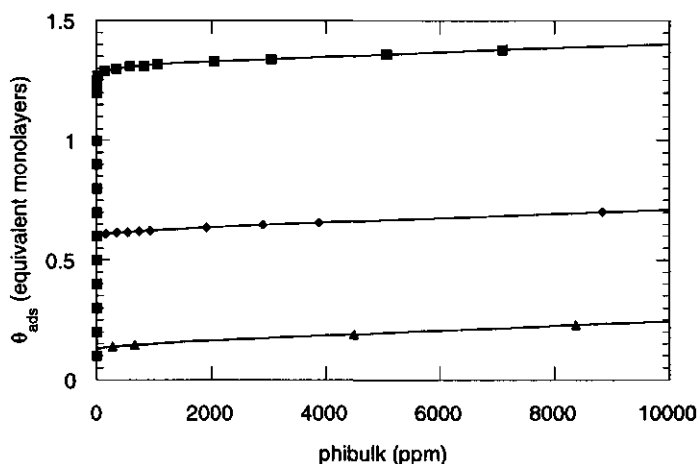


**Figure 9:** Adsorption isotherms of polyelectrolyte 3 for three pH values: ■ = pH 4; ♦ = pH 6; ▲ = pH 9 and a salt concentration of 0.01 M.. At the Y axis the adsorbed amount is given in equivalent monolayers, the bulk equilibrium concentration is given in ppm.

The calculated hydrodynamic layer thickness and the adsorbed amount as a function of pH are given in Figure 10. The hydrodynamic layer thickness was calculated following Scheutjens et al. (77). The conformation of the adsorbed polyelectrolyte has been studied by comparing the volume fraction profiles and is reflected in the hydrodynamic layer thickness. A relatively small decrease of the hydrodynamic layer thickness as compared to that of the adsorbed amount is observed for increasing pH. The maximum in the adsorbed amount as a function of pH was already discussed (29,45,46) based on SCF calculations and has been measured for synthetic polyelectrolytes (65) and for humic substances (6,36,62). At high pH the surface coverage is very low and the charged groups of the polyelectrolyte adsorb relatively flat to the surface. The

polyelectrolyte segments with a low pK value are almost fully dissociated and strong polyelectrolyte behaviour is observed. As discussed above the adsorbed amount is, roughly speaking, proportional to the surface charge of the oxide and decreases with increasing pH. At lower pH values the polyelectrolyte molecules extend further into the solution compared with pH values close to the p.z.c. of the surface sites. At pH values near the pK of the polyelectrolyte the degree of dissociation ($\alpha$) of the polyelectrolyte in the first layers adjusts itself to compensate and sometimes even overcompensate for the surface charge. Particularly at pH values below the pK of the polyelectrolyte the degree of dissociation of the segments not in contact with the surface is very low and consequently the lateral interaction is very small. At pH values much lower than the pK, the attractive electrostatic interaction between the polyelectrolyte and the oxide surface vanishes and the adsorbed amount decreases.
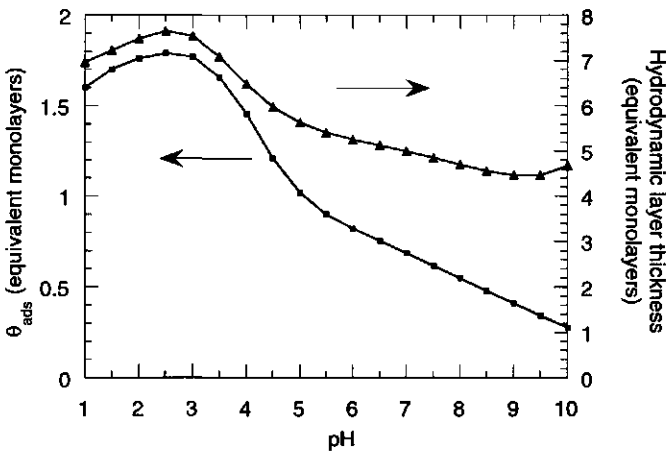


**Figure 10:** Calculated adsorption isotherm for polyelectrolyte 3 as a function of pH. At the left Y axis the adsorbed amount is given as equivalent monolayers. At the right Y axis the calculated hydrodynamic layer thickness is given.

An impression on the distribution of the charges in the adsorbed polyelectrolyte layer and of the surface in the presence of polyelectrolyte 3 is shown in Figure 11. Note that the surface charge is multiplied by a factor -1 to obtain a more convenient comparison with the polyelectrolyte charge. The curves were calculated for a salt concentration of 0.01 M. It is shown that the charge on the adsorbed polyelectrolyte, in the first few layers, overcompensates the surface charge at pH values higher than the pK of the polyelectrolyte molecules. The surface itself has a variable charge that is increased due to the adsorption. For comparison the (negative) surface charge curve of the bare surface is given as a dashed line. The charge associated with the adsorbed polyelectrolyte overcompensates the initially positive charge of the surface and thereby generates an electrostatic barrier for further adsorption of negatively charged polyelectrolytes.

The electrostatic potential profile for different pH values as a function of the distance from the surface ($\psi_z$), is given in Figure 12. It can be seen that at pH values below or

equal to the pK of the polyelectrolyte, the overall potential close to the surface is still positive. At higher pH values a negative potential is developed. At not too high pH values (pH < 10) the negative potential is associated with the adsorbed negatively charged polyelectrolyte.
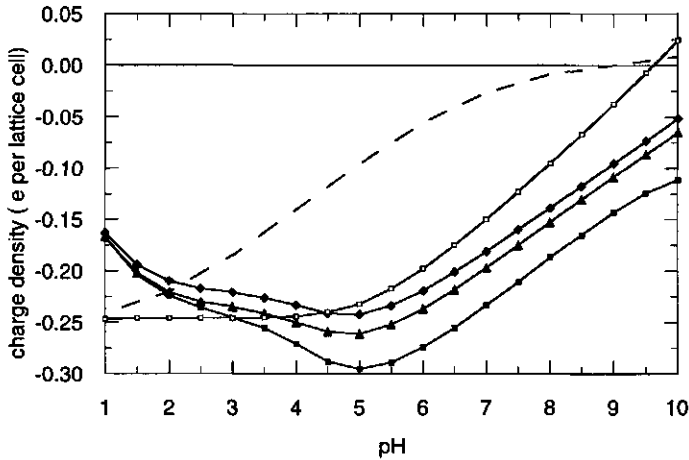


**Figure 11:** Calculated titration charge of the separate components for polyelectrolyte 3 in interaction with the surface. The salt concentration was 0.01 M and the total amount of polyelectrolyte 3 was 3 equivalent monolayers. The charges are given as elementary charge per lattice cell. The broken line shows the negative surface charge of the bare surface (note that the surface charge is multiplied by a factor -1), □ shows the negative charge on the surface in the presence of polyelectrolyte 3. The other curves represent the charge on the polyelectrolyte, ♦ of the adsorbed polyelectrolyte in the first layer next to the surface; ▲ in the first three layers; ■ of the adsorbed polyelectrolyte molecules.
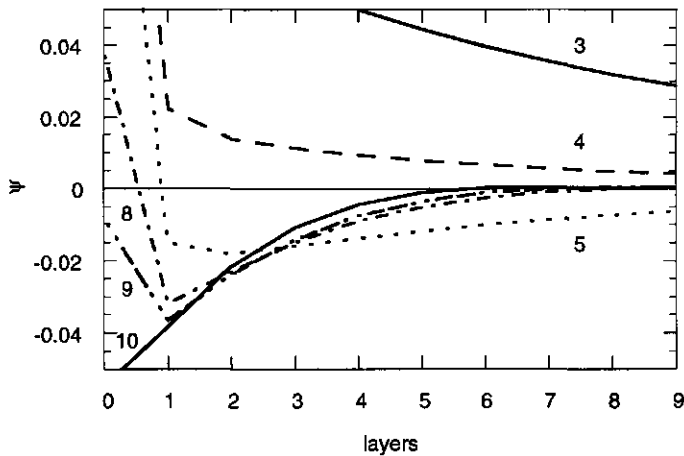


**Figure 12:** Calculations of $\psi_z$, as a function of pH for polyelectrolyte 3. The salt concentration was 0.01 M and the total amount of polyelectrolyte was 3 equivalent monolayers. All other conditions are the same as in Figure 8. The upper solid line = pH 3; $----$ = pH 4; $\cdots\cdots$ = pH 5; $-\cdot-\cdot\cdot$ = pH 8; $-\cdot\cdot-\cdot$ = pH 9; the lower solid line = pH 10.

As can be seen from the decay of the different potential profiles given in Figure 12, the thickness of the adsorbed polyelectrolyte layer decreases with increasing pH. This electrostatic barrier rather than the available surface area seems to be the limiting factor determining the adsorbed amount. The importance of such an arising electrostatic barrier on the adsorption of synthetic polyelectrolytes was already mentioned by other authors (31,78).

## Discussion

The adsorption isotherms of PAHA onto hematite particles show an increased adsorption with decreasing pH, increasing salt concentration and increasing concentration of cadmium. The hydrodynamic radius, measured by dynamic light scattering, shows a decreasing thickness with increasing pH. A relatively small decrease of the hydrodynamic layer thickness is observed as compared to the decrease in the adsorbed amount.

It has been described previously that the conformation of an adsorbed polyelectrolyte layer and the conformation of the polyelectrolyte molecules in solution are related (32,79). For instance, Meadows et al. (32) showed that adsorption at a high salt concentration followed by redispersion in a more diluted medium leads to a significant enhancement in the amount adsorbed and a much lower proportion of segments in loops and tails compared to direct adsorption at the latter salt concentration. Regarding the analogy between humic substances and simple polyelectrolytes it seems probable that also the conformation of the humic acid molecules in solution influences the conformation of the adsorbed layer. As an example two cases with extreme environmental conditions are discussed. The conditions of the first situation are a low indifferent electrolyte concentration combined with a high pH. At high pH values most PAHA groups are dissociated causing a high charge density. Due to electrostatic repulsion between the different groups of a PAHA molecule, these molecules have an extended conformation in the bulk solution (18). Such an extended configuration is emphasised due to the absence of indifferent electrolyte; no screening by the salt ions occurs. After adsorption the majority of the charged groups of the PAHA molecules are in the vicinity of the surface, leading to a relatively flat conformation and a relatively low adsorbed amount. The other extreme is a high concentration of indifferent electrolyte combined with a low pH. The few charges associated with PAHA, due to the low degree of dissociation, are screened by the salt ions and consequently the humic molecules show a tightly coiled and compact conformation in solution (18). The humics adsorb as coiled entities and retain their structure. The adsorption is high, due to an increased contribution of humic acid segments protruding into the solution.

The effect of cadmium ions on the adsorption of humic acid onto the hematite particles is reflected in the binding characteristics of these divalent ions to the humic acid molecules in solution. It is commonly observed (18,80,81) that the cadmium adsorption to humic acid increases with increasing pH, thus causing a more profound additional adsorption of the organic matter onto the mineral phase. Cadmium bound to dissolved humic substances determines the size and conformation of the dissolved humic acid molecules. As described by Engebertson and Wandruszka (42), the humic

99

acid/ $Cd^{2+}$ entities should be regarded as more compact than dissolved humic acid in the absence of metal ions. Next to the overall size of these entities, the number of contacts per humic acid molecule with the surface is decreased due to the competition of the divalent cations with the oxide for the anionic groups on the humic acid. The importance of the conformation of dissolved PAHA was also reflected in the experiments where one of the components was spiked to a mixture of the other components. When cadmium was spiked, the PAHA adsorption was not influenced, when both components were added simultaneously, PAHA adsorption increased.

These observations suggest that the conformation of the adsorbed layer is not sensitive to changes of the conditions (pH, salt and cadmium concentration) once adsorption took place. After adsorption of the humics, changes only occur due to large differences. These effects were also mentioned for the adsorption of synthetic polyelectrolytes (32,79). The observed apparent irreversibility can be explained due to the negative electrostatic potential developed due to the charges associated with the adsorbed molecules. The rearrangements that may occur on changing conditions are relatively slow due to such a barrier and are not observed within the timescale of the experiments.

The observed characteristics of the PAHA adsorption isotherms can be understood by applying a polyelectrolyte adsorption theory. Within this theory the adsorption of chain molecules is described in terms of trains and loops or tails. The adsorbed amount as a function of the conditions can be elucidated following such a description. It also predicts the thickness of the adsorbed layer, mainly by the length of the adsorbed tails (77,82).

At high pH and low salt concentration the polyelectrolyte molecules are adsorbed relatively flat on the surface which can be described by a large fraction of train segments. The few segments of the molecule that are not in direct contact with the surface protrude relatively far into the solution due to lateral repulsion effects. Consequently the adsorbed layer formed is very dilute. At low pH and high salt concentration the adsorbed polyelectrolyte layer can be described by a large fraction of adsorbed segments in loops and tails. Due to the high fraction of segments adsorbed in loops the adsorbed amount per surface area is relatively high. The relatively small decrease of the hydrodynamic layer thickness with increasing pH as compared to that of the adsorbed amount is caused by the relatively pronounced reduction in loop segments. The length of the tails only decreased slightly.

A model in which the adsorption is based on electrostatic compensation only can not explain the characteristics of the PAHA adsorption isotherms. Specific interactions are essential to describe the measured adsorption isotherms. Under certain conditions most of the adsorbed polyelectrolyte is not directly bound to the oxide surface, a significant amount is adsorbed in loops and tails extending away from the surface into the solution. As a consequence the overall charge of the initially positively charged particles may become negative. The adsorption capacity is not determined solely by the available surface area, the accumulation of negative charge associated with the adsorbed polyelectrolyte is an important factor in limiting the adsorbed amount. With increasing pH the overcompensation of the surface charge by the adsorbed humics is increased and this is reflected in the increased electrostatic barrier. The depth of this barrier is important concerning the adsorbed amounts (31).

The results obtained by the SCF calculations compares qualitatively very well with the measured adsorption isotherms and layer thicknesses. The dependencies on pH and salt concentration are calculated reasonably well. Both experiments and theory show that the decrease in the layer thickness is less pronounced with increasing pH as compared with the adsorbed amount.

## Conclusions

The adsorption of PAHA molecules onto mineral surfaces is determined by two opposite processes, charge compensation and specific adsorption energy enhance the adsorption and the adsorption is inhibited by lateral interactions and loss of entropy in the adsorbed state. Adsorption occurs in the screening enhanced regime; nonelectrostatic attraction between polyelectrolyte and surface dominates and salt mainly screens the repulsion between the charged polyelectrolyte segments. Under most conditions (pH > 4) the surface charge is overcompensated by the charge associated with the adsorbed humic acid. Due to the surplus of negatively charged humic acid groups a negative potential is developed around the initially positively charged hematite particles.

The general conclusion of this study is that qualitatively the adsorption of naturally occurring humic substances onto mineral oxide particles can be understood as a function of pH and salt concentration using an advanced polyelectrolyte adsorption theory. A clear resemblance is observed between the behaviour of PAHA and that of simple linear polyelectrolytes near a surface with a variable charge. In analogy with the polymer adsorption theory of Scheutjens and Fleer (28), the conformation of adsorbed polyelectrolytes can be described by loop, tail and train segments. Due to the charges associated with the adsorbed molecules not in direct contact with the surface an electrostatic barrier is developed, which results in relatively thick PAHA layers. Once this electrostatic barrier is developed, further adsorption is inhibited and a depletion zone arises. Due to such a barrier the adsorption/ desorption equilibrium is not affected, adsorption is still reversibility. It is supposed that the kinetics are slowed down.

Some of the mechanisms discussed before are reflected in the polyelectrolyte behaviour of the humic substances; anion exchange (electrostatic interaction), an entropic effect (e.g. adsorption fractionation) and cation binding are observed and influence the binding properties. Further Ligand exchange (specific adsorption energy) is used to introduce specific interactions. Next to an extra adsorption energy, hydrophobic interactions can be seen as a specific adsorption mechanism.

Based on the proposed electrolyte adsorption model it is concluded that the adsorbed humics can be described as a dynamic layer, extending into the solution. Limited rearrangements may occur due to changes in the environmental conditions and the fraction of humic acid groups protruding into the solution (loops or tails) can be adjusted. It may be clear that based on the previous mentioned characteristics of the adsorption process, Langmuir-type isotherms are not suitable for the modelling of humic substances onto mineral particles. And that the calculations based on the SCF theory can be applied to help to understand in a mechanistic manner the interaction mechanisms between the different soil components.

## References

(1) Buffle, J. Natural organic matter and metal-organic interactions in aquatic systems In *Metal ions in biological systems*; Sigel, H. Ed.; Marcel Dekker: New York, 1984; 165-221.

(2) Ephraim, J.H.; Marinsky, J.A.; Cramer, S.J. Complex-forming properties of natural organic acids. *Talanta* **1989**, *36(4)*, 437 -444.

(3) Sposito, G. Sorption of trace metals by humic materials in soils and natural waters. *CRC Crit.Rev.Environ.Control* **1986**, *16(2)*, 193 -229.

(4) Gerke, V.J.; Ziechmann, W. Die Bindung des kationischen Tensids Laurylpyridiniumchlorid an Modelhuminstoffe und Extrakte eines humuspodsols. *Chem.Erde* **1991**, *51*, 23 -28.

(5) Tipping, E.; Griffith, J.R.; Hilton, J. The Effect of Adsorbed Humic Substances on the Uptake of Copper(II) by Goethite. *Croat.Chem.Acta* **1983**, *56(4)*, 613 -621.

(6) Tipping, E. The adsorption of aquatic humic substances by iron oxides. *Geochim.Cosmochim.Acta* **1981**, *45*, 191 -199.

(7) Murphy, E.M.; Zachara, J.M.; Smith, S.C.; Philips, J.L. The sorption of humic acids to mineral surfaces and their role in contaminant binding. *Sci.Total Environ.* **1992**, *117/118*, 413 -423.

(8) Zhou, J.L.; Rowland, S.J.; Braven, J.; Mantoura, R.F.C.; Harland, B.J. Tefluthrin sorption to mineral particles: role of particle organic coatings. *Int.J.Env.Anal.Chem.* **1995**, *58*, 275 -285.

(9) Amirbahman, A.; Olson, T.M. Transport of Humic Matter-Coated Hematite in Packed Beds. *Environ.Sci.Technol.* **1993**, *27(13)*, 2807 -2813.

(10) Amirbahman, A.; Olson, T.M. The role of surface conformations in the deposition kinetics of humic matter-coated colloids in porous media. *Colloids Surf.A* **1995**, *95*, 249 -259.

(11) Vermeer, A.W.P.; Koopal, L.K. submitted to *Environ.Sci.Technol.*, this Thesis. Chapter 3: Characterisation and classification of purified Aldrich humic acid.

(12) Stevenson, F.J. *Humus Chemistry. Genesis, Composition, Reactions*; Wiley Interscience: New York, 1982.

(13) Hayes, M.H.B.; MacCarthy, P.; Malcolm, R.L.; Swift, R.S. *Humic Substances II: In search of structure*; Wiley Interscience: New York, 1989.

(14) Schnitzer, M.; Khan, S.U. *Humic substances in the environment*; Marcel Decker Inc. New York, 1972.

(15) Aiken, G.R.; McKnight, D.M.; Wershaw, R.L.; MacCarthy, P. *Humic Substances in Soil, Sediment, and Water*; Wiley Interscience: New York, 1985.

(16) Cameron, R.S.; Thornton, B.K.; Swift, R.S.; Posner, A.M. Molecular weight and shape of humic acid from sedimentation and diffusion measurements on fractionated extracts. *J.Soil Sci.* **1972**, *23(4)*, 394 -408.

(17) Ghosh, K.; Schnitzer, M. Macromolecular structures of humic substances. *Soil Sci.* **1980**, *129(5)*, 266 -276.

(18) Vermeer, A.W.P. this Thesis. Chapter 4: Proton and Cadmium binding to purified Aldrich humic acid, exploration of the NICA-Donnan model.

(19) Datta, C.; Mukherjee, S.K. Viscosity Behaviour of Natural Humic Acids Isolated from Diverse Soil Types. *J, Indian Chem. Soc.* **1970**, *47(11)*, 1105 -1108.

(20) Chen, Y.; Schnitzer, M. Viscosity Measurements on Soil Humic Substances. *Soil Sci.Soc.Am.J.* **1976**, *40*, 866 -872.

(21) Cornel, P.K.; Summers, R.S.; Roberts, P.V. Diffusion of Humic Acid in Dilute Aqueous Solution. *J.Colloid Interface Sci.* **1986**, *110(1)*, 149 -165.

(22) Summers, R.S.; Roberts, P.V. Activated Carbon Adsorption of Humic Substances. *J.Colloid Interface Sci.* **1988**, *122(2)*, 367 -381.

(23) Cohen Stuart, M.A.; Fleer, G.J.; Bijsterbosch, B.H. The Adsorption of Poly(vinyl pyrrolidone) onto Silica. I. Adsorbed Amount. *J.Colloid Interface Sci.* **1982**, *90(2)*, 310 -320.

(24) Koopal, L.K. The Effect of Polydispersity on the Adsorption Isotherm. *J.Colloid Interface Sci.* **1981**, *83(1)*, 116 -129.

(25) Cohen Stuart, M.A.; Scheutjens, J.M.H.M.; Fleer, G.J. Polydispersity Effects and the Interpretation of Polymer Adsorption Isotherms. *J.Polym.Sci.Polym.Phys.Ed.* **1980**, *18*, 559 -573.

(26) Hlady, V.; Lyklema, J.; Fleer, G.J. Effect of Polydispersity on the Adsorption of Dextran on Silver Iodide. *J.Colloid Interface Sci.* **1982**, *87(2)*, 395 -406.

(27) Cohen Stuart, M.A.; Cosgrove, T.; Vincent, B. Experimental aspects of polymer adsorption at solid/solution interfaces. *Adv.Colloid Interface Sci.* **1986**, *24*, 143 -239.

(28) Fleer, G.J.; Cohen Stuart, M.A.; Scheutjens, J.M.H.M.; Cosgrove, T.; Vincent, B. *Polymers at Interfaces*; Chapman & Hall: London, 1993.

(29) Vermeer, A.W.P. this Thesis. Chapter 2: Adsorption of a weak polyelectrolyte on a surface with a variable charge, Self Consistent Field calculations.

(30) Dahlgren, A.G.; Leermakers, F.A.M. Depletion Zones in Polyelectrolyte Systems: Polydispersity Effects and Colloidal Stability. *Langmuir* **1995**, *11(8)*, 2996 -3006.

(31) De Laat, A.W.M.; Van den Heuvel, G.L.T. Molecular weight fractionation in the adsorption of polyacrylic acid salts onto $BaTiO_3$. *Colloids Surf.A* **1995**, *98*, 53 -59.

(32) Meadows, J.; Williams, P.A.; Garvey, M.J.; Harrop, R.A.; Phillips, G.O. Enhanced Polyelectrolyte Adsorption. *Colloids Surf.* **1988**, *32*, 275 -288.

(33) Sposito, G. *The surface chemistry of soils*; Oxford Press: New York, 1984.

(34) Schlautman, M.A.; Morgan, J.J. Adsorption of aquatic humic substances on colloidal-size aluminum oxide particles: Influence of solution chemistry. *Geochim.Cosmochim.Acta* **1994**, *58(20)*, 4293 -4303.

(35) Zhou, J.L.; Rowland, S.J.; Fauzi, R.; Mantoura, R.F.C.; Braven, J. The formation of humic coatings on mineral particles under simulated estuarine conditions - A mechanistic study. *Water Res.* **1994**, *28(3)*, 571 -579.

(36) Davis, J.A. Adsorption of natural dissolved organic matter at the oxide/water interface. *Geochim.Cosmochim.Acta* **1982**, *46*, 2381 -2393.

(37) Gu, B.; Schmitt, J.; Chen, Z.; Liang, L.; McCarthy, J.F. Adsorption and Desorption of Natural Organic Matter on Iron Oxide: Mechanisms and Models. *Environ.Sci.Technol.* **1994**, *28(1)*, 38 -46.

(38) Parfitt, R.L.; Fraser, A.R.; Farmer, V.C. Adsorption on hydrous oxides. III. Fulvic acid and humic acid on goethite, gibbsite and imogolite. *J.Soil Sci.* **1977**, *28*, 289 -296.

(39) Tipping, E. Adsorption by goethite of humic substances from three different lakes. *Chem.Geo.* **1981**, *33*, 81 -89.

(40) Murphy, E.M.; Zachara, J.M.; Smith, S.C. Influence of Mineral-Bound Humic Substances on the Sorption of Hydrophobic Organic Compounds. *Environ.Sci.Technol.* **1990**, *24*, 1507 -1516.

(41) McKnight, D.M.; Wershaw, R.L.; Bencala, K.E.; Zellweger, G.W.; Feder, G.L. Humic substances and trace metals associated with Fe and Al oxides deposited in an acidic mountain stream. *Sci.Total Environ.* **1992**, *117/118*, 485 -498.

(42) Engebertson, R.R.; Wandruszka, R.v. Microorganization in Dissolved Humic Acids. *Environ.Sci.Technol.* **1994**, *28(11)*, 1934 -1941.

(43) Amal, R.; Raper, J.A.; Waite, T.D. Effect of Fulvic Acid Adsorption on the Aggregation Kinetics and Structure of Hematite Particles. *J.Colloid Interface Sci.* **1992**, *151(1)*, 244 -257.

(44) Cohen Stuart, M.A. Polyelectrolyte adsorption. *J.Phys.France* **1988**, *49*, 1001 -1008.

(45) Böhmer, M.R.; Evers, O.A.; Scheutjens, J.M.H.M. Weak Polyelectrolytes between Two Surfaces: Adsorption and Stabilization. *Macromolecules* **1990**, *23(8)*, 2288 -2301.

(46) Evers, O.A.; Fleer, G.J.; Scheutjens, J.M.H.M.; Lyklema, J. Adsorption of Weak Polyelectrolytes from Aqueous Solution. *J.Colloid Interface Sci.* **1986**, *111(2)*, 446 -453.

(47) Israëls, R.; Leermakers, F.A.M.; Fleer, G.J. On the Theory of Grafted Weak Polyacids. *Macromolecules* **1994**, *27(11)*, 3087 -3093.

(48) Breeuwsma, A.; Lyklema, J. Interfacial electrochemistry of haematite. *Discussions of The Faraday Soc.* **1971**, *52*, 324 -333.

(49) Penners, N.H.G.; Koopal, L.K. Preparation and optical properties of homodisperse heamatite hydrosols. *Colloids Surf.* **1986**, *19*, 337 -349.

(50) Thurman, E.M.; Malcolm, R.L. Preparative Isolation of Aquatic Humic Substances. *Environ.Sci.Technol.* **1981**, *15(4)*, 463 -466.

(51) Milne, C.J.; Kinniburgh, D.G.; De Wit, J.C.M.; Van Riemsdijk, W.H.; Koopal, L.K. Analysis of proton binding by peat humic acid using a simple electrostatic model. *Geochim.Cosmochim.Acta* **1995**, *59(6)*, 1101 -1112.

(52) Kinniburgh, D.G.; Milne, C.J.; Venema, P. Design and Construction of a Personal-Computer-Based Automatic Titrator. *Soil Sci.Soc.Am.J.* **1995**, *59(2)*, 417 -422.

(53) Kinniburgh, D.G.; Milne, C.J. Guide to the Wallingford Titrator; Technical report. WD/93/23. British Geological Survey: Keyworth, Nottinghamshire. 1993.

(54) Vermeer, A.W.P. this Thesis. Appendix I: Potentiometric proton titrations, experimental set-up and data treatment.

(55) Dijt, J.C.; Cohen Stuart, M.A.; Fleer, G.J. Reflectometry as a tool for adsorption studies. *Adv.Colloid Interface Sci.* **1994**, *50*, 79 -101.

(56) Dijt, J.C.; Cohen Stuart, M.A.; Hofman, J.E.; Fleer, G.J. Kinetics of polymer adsorption in stagnation point flow. *Colloids Surf.* **1990**, *51*, 141 -158.

(57) Hansen, W.N. Electric Fields Produced by the Propagation of Plane Coherent Electromagnetic Radiation in a Stratified Medium. *J. Opt. Soc. Am.* **1968**, *58(3)*, 380 -390.

(58) Lyklema, J. *Fundamentals of Interface and Colloid Science*; Academic Press: London, 1991.

(59) Liang, L.; Morgan, J.J. Coagulation of Iron Oxide Particles in the Presence of Organic Materials. *ACS Symp.Ser.,416,Chemical modelling of aqueous systems II*, **1990**, , 293 -308.

(60) Tipping, E.; Higgins, D.C. The effect of adsorbed humic substances on the colloid stability of haematite particles. *Colloids Surf.* **1982**, *5*, 85 -92.

(61) Van der Steeg, H.G.M.; Cohen Stuart, M.A.; De Keizer, A.; Bijsterbosch, B.H. Polyelectrolyte Adsorption: A Subtle balance of Forces. *Langmuir* **1992**, *8(10)*, 2538 -2546.

(62) Davis, J.A.; Gloor, R. Adsorption of Dissolved Organics in Lake Water by Aluminum Oxide. Effect of Molecular Weight. *Environ.Sci.Technol.* **1981**, *15(10)*, 1223 -1229.

(63) Tipping, E.; Cooke, D. The effects of adsorbed humic substances on the surface charge of goethite in freshwaters. *Geochim.Cosmochim.Acta* **1982**, *46*, 75 -80.

(64) Penners, N.H.G.; Koopal, L.K.; Lyklema, J. Interfacial Electrochemistry of Haematite: Homodisperse and Heterodisperse Sols. *Colloids Surf.* **1986**, *21*, 457 -468.

(65) Wang, T.K.; Audebert, R. Adsorption of Cationic Copolymers of Acrylamide at the Silica-Water Interface: Hydrodynamic Layer Thickness Measurements. *J.Colloid Interface Sci.* **1988**, *121(1)*, 32 - 41.

(66) Järnstrom, L.; Stenius, P. Adsorption of Polyacrylate and Carboxy Methyl Cellulose on Kaolinite: Salt Effects and Competitive Adsorption. *Colloids Surf.* **1990**, *50*, 47 -73.

(67) Böhmer, M.R.; El Attar Sofi, Y.; Foissy, A. Calorimetry of Poly-(Acrylic Acid) Adsorption on $TiO_2$. *J.Colloid Interface Sci.* **1994**, *164*, 126 -135.

(68) Flory, P.J. *Principles of polymer chemistry*; Cornell University Press: London, 1953.

(69) Björling, M.; Linse, P.; Karlström, G. Distribution of Segments for Terminally Attached Poly(ethylene oxide) Chains. *J.Phys.Chem.* **1990**, *94(1)*, 471 -481.

(70) Van Riemsdijk, W.H.; Bolt, G.H.; Koopal, L.K.; Blaakmeer, J. Electrolyte Adsorption on Heterogeneous Surfaces: Adsorption Models. *J.Colloid Interface Sci.* **1986**, *109(1)*, 219 -228.

(71) Koopal, L.K. Ion adsorption on mineral oxide surfaces In *Adsorption on new and modified inorganic sorbents*; Dabrowski, A.; Tertykh, V.A. Eds.; Elsevier: Amsterdam, 1996; 757-796.

(72) Jurinak, J.J. Surface Chemistry of Hematite: Anion Penetration Effect on Water Adsorption. *Soil Sci.Soc.Amer.Proc.* **1966**, *30*, 559 -562.

(73) Zettlemoyer, A.C.; McCafferty, E.M. Heat of immerion of alpha iron oxide in water. *Z.Phys.Chem.* **1969**, *64(1-4)*, 41 -48.

(74) Morimoto, T.; Nagao, M.; Tokuda, F. The Relation between the Amounts of Chemisorbed and Physisorbed Water on Metal Oxides. *J.Phys.Chem.* **1969**, *73(1)*, 243 -248.

(75) Barneveld, P.A.; Scheutjens, J.M.H.M.; Lyklema, J. Bending Moduli and spontaneous Curvature. 1. Bilayers and Monolayers of pure and Mixed Nonionic Surfactants. *Langmuir* **1992**, *8(12)*, 3122 - 3130.

(76) Vermeer, A.W.P. this Thesis. Chapter 6: Adsorption fractionation of humic substances at mineral surfaces, experiments compared with theory.

(77) Scheutjens, J.M.H.M.; Fleer, G.J.; Cohen Stuart, M.A. End Effects in Polymer Adsorption: a Tale of Tails. *Colloids Surf.* **1986**, *21*, 285 -306.

(78) Bain, D.R.; Cafe, M.C.; Robb, I.D.; Williams, P.A. The Fractionation of Polyelectrolytes by Adsorption onto Ionic Crystals. *J.Colloid Interface Sci.* **1982**, *88(2)*, 467 -470.

(79) Tjipangandjara, K.F.; Huang, Y.; Somasundaran, P.; Turro, N.J. Correlation of Alumina Flocculation with Adsorbed Polyacrylic Acid Conformation. *Colloids Surf.* **1990**, *44*, 229 -236.

(80) Saar, R.A.; Weber, J.H. Complexation of cadmium(II) with water- and soil-derived fulvic acids: effect of pH and fulvic acid concentration. *Can.J.Chem.* **1979**, *57(11)*, 1263 -1268.

(81) Milne, C.J.; Kinniburgh, D.G.; De Wit, J.C.M.; Van Riemsdijk, W.H.; Koopal, L.K. Analysis of Metal-Ion Binding by Peat Humic Acid Using a Simple Electrostatic Model. *J.Colloid Interface Sci.* **1995**, *175*, 448 -460.

(82) Scheutjens, J.M.H.M.; Fleer, G.J. Statistical Theory of the Adsorption of Interacting Chain Molecules. 2. Train, Loop, and Tail Size Distribution. *J.Phys.Chem.* **1980**, *84*, 178 -190.

Chapter 6

# Adsorption fractionation of humic substances

# at mineral surfaces,

## experiments compared with theory

**Abstract**

The effects of polydispersity on the shape of the adsorption isotherms and on the adsorption/ desorption hysteresis, of humic substances adsorbed onto mineral surfaces, have been studied. Studying the adsorption isotherm of purified Aldrich humic acid it is observed that after an initial steep rise the adsorbed amount of the humic acid gradually further increases with increasing concentrations. The mechanism that is responsible for this gradual increase is studied using an artificial polydisperse mixture of different humic substances. Natural polyelectrolytes studied include a purified Aldrich humic acid and Laurentian fulvic acid. Both humics have similar physical chemical behaviour but differ significantly in molecular size. The humic acid adsorbed preferentially over the fulvic acid. Both on experimental and theoretical grounds this behaviour is ascribed to adsorption fractionation. Self Consistent Field calculations indicate that the apparent adsorption/ desorption hysteresis is a result of adsorption fractionation.

## Introduction

Humic substances dissolved in natural waters may be removed from solution by adsorption onto the mineral phase. McKnight et al. (1) investigated the association of humic substances with colloidal particles in a mountain stream and mentioned that a clear correlation was observed between the deposited oxide and the organic carbon content. Further is was mentioned that the iron oxide particles precipitated preferentially compared to other oxides. In general there is considerable evidence from field observations that interactions exists between natural organics and iron oxides such as, for example, hematite (2-7). Considering these interactions it is obvious that the mobility of the organic fraction is diminished to a large extent by the adsorption onto the mineral phase of the soil system.

Studying the adsorption behaviour of humic substances it is important to realise that in general humic matter is a polydisperse mixture of heterogeneous polyelectrolytes (8-10). The humics can be divided into several fractions. Considering adsorption phenomena the two most important fractions are fulvic and humic acid. These two fractions are differentiated by their solubility at different pH (11). Humic acid remains in solution at pH 2 and higher and is composed of the higher molecular weight fraction of the humic matter, while fulvic acid has a lower molecular weight and remains in solution under all pH conditions. Furthermore fulvic acid is slightly more acidic. Under the applied experimental conditions both humic and fulvic acids are dissolved, unless they are bound to the mineral phase.

In a previous paper (7) the adsorption of PAHA onto hematite particles has been investigated as a function of the environmental conditions (pH and electrolyte composition). The adsorption isotherms showed an initial steep slope indicating a high affinity character followed by a gradually increasing isotherm at elevated equilibrium concentrations. The extent of adsorption as a function of pH and salt concentration was explained using a polyelectrolyte adsorption theory (12-14). The shape of the isotherms was however, only briefly discussed. In general it is known from polymer adsorption that the shape of the isotherm is affected by the polydispersity of the polymer (15-18). For non-porous surfaces this behaviour is mostly explained by preferential adsorption of the higher molecular weight fraction.

Davis and Gloor (19) reported the effect of molecular weight on the adsorption of different molecular size fractions (of lake water organics) onto non-porous alumina suspensions. They reported the preferential adsorption of the highest molecular weight fraction and concluded that this effect influenced the molecular weight distribution of dissolved organic materials in lakes. However, they did not discuss the mechanism responsible for the observed separation. Summers and Roberts (18) investigated the adsorption of humic substances onto activated carbon under laboratory conditions and concluded that on the basis of the assessable surface area the larger molecules have a greater extent of adsorption. They described that modifying the adsorption isotherm to account explicitly for adsorbent dose by explicitly taking into account the surface to volume ratio, resulted in a unique isotherm (this phenomenon is also known as a particle concentration effect).

Contrarily to these studies, Kilduff et al. (20) reported that the smaller humic acid molecular size fraction adsorbed to a greater extent onto porous activated carbon on an adsorbent mass basis. The preferential adsorption of an intermediate molecular weight fraction of synthetic polyelectrolyte molecules was described by De Laat and Van den Heuvel (21). They mentioned that the adsorption of polyelectrolytes as compared to uncharged polymers goes together with some additional effects. Due to adsorption of the charged polymer molecules an electrostatic barrier is developed, which hinders the approach of further charged chains (21). Due to this barrier a depletion zone arises. A strong dependence of the chain length on the depth of this barrier was found. The importance of such an arising electrostatic barrier on the adsorption of synthetic and model polyelectrolyte was also mentioned by other authors (22-24). Ramachandran and Somasundaran (25) reported the effect of the order of addition of different synthetic polyelectrolytes on the displacement of the initially adsorbed polymer. It was concluded that only the smaller molecular weight fraction could be displaced by the higher molecular weight fraction.

Naturally the exchange of adsorbed molecules at the surface is only possible if the already adsorbed molecules can be desorbed. Therefore comprehension of the (ir)reversibility of the adsorption process is inevitable. In relation to this it was suggested by Di Toro and Horzempa (26) that it is essential for environmental modelling to describe the adsorption process as a mixture of reversible and irreversible contributions. A distinction was made between a reversibly adsorbed and an irreversibly bound fraction and based on this difference it was possible to approximate the resistant, (humic acid) sediment fractions. A more mechanistic approach was proposed by Vaccari and Kaouris (27) who attributed the difference in reversibility to surface heterogeneity. The model described by Vaccari and Kaouris is based on the assumption that two types of sites are available on the sorbent; at the first site type adsorption is irreversible at the other sites adsorption is completely reversible and non-hysteric. Gu et al. (6) reported that natural organic matter adsorbed onto hematite showed some adsorption/ desorption hysteresis. A Langmuir equation was used in combination with a hysteresis coefficient to describe the hysteresis. Within this model the adsorbed layer was described as completely collapsed on the surface to allow for a maximum of interaction points. The main explanation given for the observed hysteresis was the existence of multiple binding sites between the adsorbed natural organic matter and the iron oxide, so that desorption required simultaneous detachment of all bound segments. As a consequence of this only the molecules adsorbed by a single bond are easily desorbed. Differences in desorption capacities between different humics were investigated by Zhou et al. (28), who explained the differences and the hysteresis by a variance in the interaction mechanism; humic acid was described as adsorbed chemically and irreversibly by forming a chemical bond with the surface, while (hydrophilic) fulvic acid was adsorbed physically by pure electrostatic forces.

Regarding the number and differences between the proposed mechanisms describing the adsorption/ desorption hysteresis it may be clear that a final description is not yet available. The observed hysteresis and adsorption fractionation of humic substances are not specific for humic substances, to the contrary as described above, they are quite generally observed with the adsorption of polydisperse polymers (15,16) and hysteresis and adsorption fractionation are closely related (16-18). For a

polydisperse polymer the initial slope of the isotherm is inversely proportional to the surface-to-volume ratio (S/V) (15), resulting in an increased adsorption under equal circumstances. It was discussed that the exchange of these polymers due to adsorption fractionation occurred in full thermodynamic equilibrium. In general the high molecular weight fraction is bound to the surface and the lower molecular weight fraction remains in solution. As a consequence of the multicomponent character of the system the adsorption when expressed as total amount of polymer adsorbed against the total polymer concentration in solution depends on the available area per unit volume; the S/V ratio. Dilution changes this ratio and therefore it is to be expected that the adsorption and desorption isotherms differ. This (apparent) hysteresis will disappear when the adsorption of the individual molecular weight fractions in the mixture are measured individually and when an appropriate multicomponent adsorption isotherm is used. Measurement of the individual molecular weight fraction is often not done and hysteresis will be observed. The described mechanism is general, but for adsorption onto porous sorbents the pore size distribution and geometry are also important. Sample size constrictions easily can give rise to preferential adsorption of the lower molecular weight fraction (20).

The main objectives of this paper are to investigate the effect of (1) the adsorption fractionation of humic substances on non-porous hematite particles on the shape of the PAHA adsorption isotherms and (2) the influence of adsorption fractionation on the adsorption-desorption hysteresis. The former is done by introducing artificial polydispersity to the humic sample. A mixture of PAHA and Laurentian fulvic acid is used for this purpose. It will be shown that using different spectroscopic analysis methods it is possible to differentiate between PAHA and LFA. Using this technique the adsorption from the PAHA/ LFA mixture onto hematite B particles will be followed in time. As was discussed previously (7) humic acids are often described as fairly flexible, polyelectrolytes. Therefore we can use model calculations to gain insight into the binding characteristics of the separate components to support the measurements. Some calculations will be presented using the Self-Consistent-Field theory originally developed for polymer adsorption (14,29,30) and later extended for the adsorption of weak polyelectrolytes (31-33) onto a surface with a variable charge (34). Based on these calculations we will show that adsorption fractionation occurs and is responsible for the often observed adsorption/ desorption hysteresis.

## Materials and methods

All experiments were performed in a constant temperature room at 21 °C. Chemicals used were p.a. quality. The water was purified by percolating tab water through a mixed bed ion exchange column followed by an activated carbon column and a micro filter.

### Iron oxides

Hematite B ($\alpha$-$Fe_2O_3$) was prepared as described by Breeuwsma (35). The suspension has been aged for several years at room temperature. Before use the suspension was

washed with HCl and dialysed thoroughly against purified water. Electron microscopy photographs showed that the particles were well developed with a mean size of 50 nm. The BET ($N_2$) surface has been measured with a NOVA 1000 Quantachrome and was 43 $m^2$ $g^{-1}$. The porosity of the hematite sample was negligible.


Humic substances


Two different humic substances were used, Purified Aldrich Humic Acid (Aldrich-Chemie; code:H1,675-2) (PAHA) and Laurentian Fulvic Acid[*] (LFA).

The purification and characterisation of PAHA are described elsewhere (36). It has been shown that PAHA reflects many characteristics normally found for naturally occurring humic substances and is classified as a soil humic acid. The humic acid obtained is in its proton form and was freeze dried and stored in a glass container. The element analysis[†] of the (PAHA) is (wt%): C, 55.8 %; O, 38.9 %; H, 4.6 %; N, 0.6 %, that of LFA is: C, 45.14 %; O, 49.68 %; H, 4.11 %; N, 1.07 %. LFA was derived from a sample of a podzol collected in the Laurentian Forest Preserve of Laval University, Québec, Canada (37). The H:C ratio for LFA was 1.09 and the ratio for PAHA was 0.99. These values correspond to organic matter of which the basic unit consists of an aromatic nucleus with aliphatic side chains up to 10 carbon atoms (38). Since the H:C ratios differ only slightly it may be assumed that both humic substances show a similar basic carbon structure. The O:C ratios for LFA and PAHA were respectively 0.83 and 0.52; the higher O:C ratio for LFA indicates a greater richness in oxygenated groups such as COOH and OH in LFA than in PAHA (38).

According to Langford LFA has a total acidity of 11.6 mmol $g^{-1}$; of which 8.6 mmol are carboxylic groups and 3.0 mmol phenolic groups. For PAHA the total acidity was 5.0 mmol $g^{-1}$ of which 3.7 mmol $g^{-1}$ are carboxylic groups and 1.3 mmol $g^{-1}$ phenolic groups (39). It can be concluded that (1) LFA has more reactive sites per mass of substance than PAHA and (2) carboxylic sites are the most abundant in both LFA and PAHA. In spite of these differences the chemical composition of both humic substances is comparable. The main difference between LFA and PAHA is the molecular size. Dynamic light scattering results showed that the diffusion coefficient of LFA ($6*10^{-11}$ $m^2s^{-1}$) is about ten times larger than that of PAHA ($4*10^{-12}$ $m^2s^{-1}$). The corresponding hydrodynamic radius of LFA is about 2 nm and that of PAHA is in the order of 50 nm.

A stock solution of PAHA was prepared with a concentration of 2 mg $l^{-1}$ by bringing the solution at pH 10 and shaking it overnight to fully dissolve the PAHA (39,40). The final solutions were then made from this stock solution by dilution.


UV spectrophotometry and Fluorescence spectroscopy


All UV measurements were performed with a Hitachi U-3210 spectrophotometer; concentrations were measured at 254 nm.

Fluorescence spectra in the emission mode were recorded with a Perkin Elmer LS-5 Luminescence spectrometer, management of the spectrophotometer and all data

acquisition were under PC control. Experiments were performed following Senesi et al. (41). In all experiments, the emission and excitation slits were set at a band width of respectively 5 and 10 nm and a scan speed of 60 nm min$^{-1}$ was selected for the monochromator. Emission spectra were obtained at an excitation wavelength of 340 nm, monitoring the emission over the range of 365 - 650 nm.

## Adsorption measurements

Isotherms of single PAHA onto hematite were measured as described elsewhere (7).

The course of adsorption of PAHA and LFA from a mixture as a function of time at pH 6 (± 0.1) and 0.01 (± 0.002) M KNO$_3$ was investigated. Using a stock solution containing 23 mg l$^{-1}$ natural organic matter of which 7 mg l$^{-1}$ was LFA and 16 mg l$^{-1}$ PAHA. The experiments were performed in polyalymere tubes of 10 ml and closed from atmosphere. To each of the tubes an amount of hematite was added resulting in a surface area per experiment of 0.13 m$^2$. Hematite was added by weighing of the suspension; KNO$_3$, HNO$_3$ and KOH were added with Metrohm 665 Dosimat burettes and the humic mixture with a 7 ml pipette. The suspensions were shaken, head over head, for different times and centrifuged immediately hereafter for 15 minutes at 7500 rpm. After separation of the supernatant, pH was checked and minor adjustments were made prior to the spectroscopic measurements. These adjustments were made since fluorescence spectroscopy is very sensitive to pH. The adsorption of both components was followed in time by combining the data of UV spectrophotometry and fluorescence spectroscopy.

## Results

### Adsorption isotherms of PAHA

Figure 1 shows the adsorption isotherms of PAHA on hematite B at three pH levels and 0.01 M KNO$_3$. The adsorption increases with decreasing pH. This feature is commonly observed for the adsorption of humic substances onto mineral particles (2,3,6,42,43). The adsorbed amount is determined by two opposite processes, charge compensation and specific adsorption enhance the adsorption and the adsorption is prohibited due to lateral interactions and loss of entropy in the adsorbed state. Nonelectrostatic attraction between polyelectrolyte and surface dominates and salt mainly screens the repulsion between the charged polyelectrolyte segments. A further discussion on the adsorbed amount is given elsewhere (7).

Depending on the pH, the initial overall charge on the adsorbed PAHA molecules is larger in absolute amount than the initial charge of the hematite particles. Due to the charge associated with the adsorbed polyelectrolyte molecules an electrostatic barrier is developed, this electrostatic barrier was shown to be important and diminishes further adsorption (7). Several authors (2,3,19,43) have shown with electrophoretic measurements that the positive charge of the iron oxide particles becomes negative

due to adsorption even at very low humic acid coverage, which supports the existence of such an electrostatic barrier.
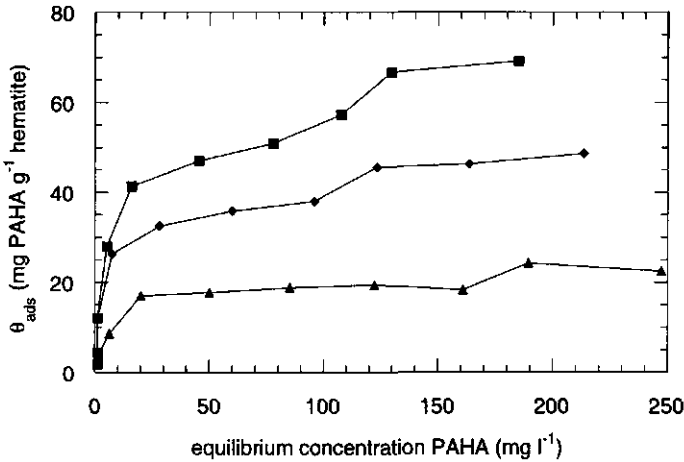


**Figure 1:** Adsorption isotherms of PAHA on hematite B at 0.01 M $KNO_3$, effect of pH on the adsorption isotherms: ■ = pH 4; ♦ = pH 6; ▲ = pH 9.

## Calibration procedures

### UV spectroscopy

To discriminate between the different components in a mixture, use was made of the adherence to the Lambert-Beer law so that a spectrum of any mixture of the two components is a linear combination of their individual spectra. The absorptivity at a wavelength of 254 nm is taken as a well-established reference (9). Figure 2 shows that the relation between the concentration and absorbance is linear upto 20 mg l-1 of both humics. As a check on the additivity the absorbance of a series of mixtures is measured. As can be seen in Table I a good correlation is observed between the measured and the calculated absorbance. All calculated points deviated less than 2 % from the measured results.

**Table I:** The correlation between the measured and the calculated UV absorbances and FS intensities, based on the extinction coefficients (Table II) of the individual components.

| PAHA : LFA* | $UV_{measured}$ (abs. at 254 nm) | $UV_{calculated}$ (abs. at 254 nm) | $FS_{measured}$ (I at 460 nm) | $FS_{calculated}$ (I at 460 nm) |
|---|---|---|---|---|
| 3 : 1 | 0.598 | 0.583 | 93.2 | 91.5 |
| 2 : 1 | 0.558 | 0.550 | 99.2 | 102.3 |
| 1 : 1 | 0.500 | 0.484 | 110.7 | 113.8 |
| 1 : 2 | 0.427 | 0.418 | 124.4 | 126.2 |
| 1 : 3 | 0.376 | 0.385 | 131.8 | 132.5 |

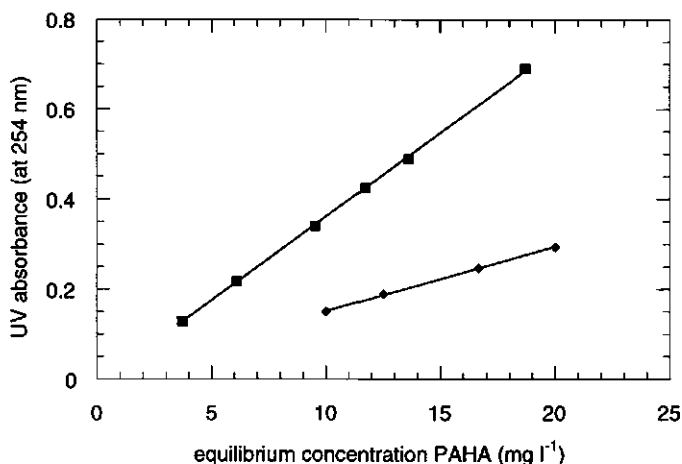* The overall concentration of the mixtures was 20 mg l-1 humic substance

**Figure 2:** Calibration lines and experimental results of UV-visible spectrophotometry measurements at pH 6, 0.01 M $KNO_3$ and various humic substances: ■ = PAHA; ♦ = LFA; the lines are obtained by linear regression. The extinction coefficients are given in Table II.

## Fluorescence spectroscopy

Fluorescence is a technique for the selective study of chromophores. The technique is sensitive to environmental conditions, therefore an accurate control of pH and salt concentration is essential. Ewald et al. (44) showed that some corrections are necessary to compare different humic substances. The main correction is for background scattered light.
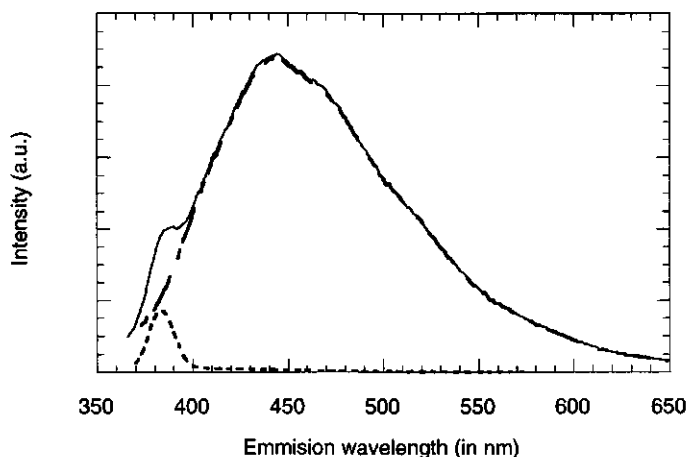


**Figure 3:** Fluorescence emission spectra ($\lambda_{ex}$ = 340 nm) of LFA showing the effects of correcting for Raman scattering (Ewald et al. (44)). The solid line, uncorrected spectrum; dotted line, component due to the Raman scattering; broken line, corrected spectrum.
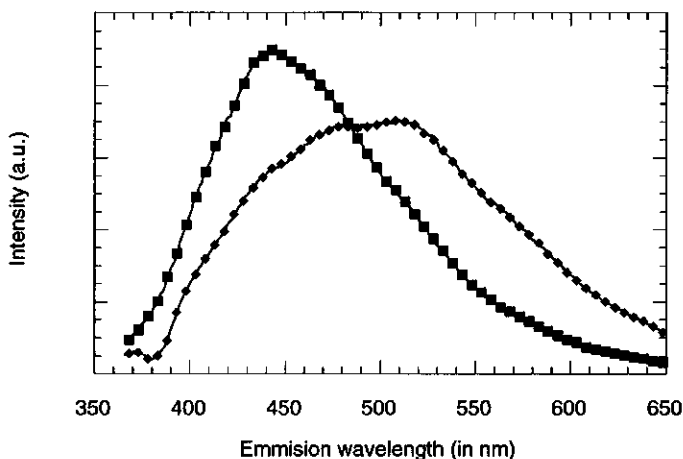
**Figure 4:** Corrected fluorescence emission spectra ($\lambda_{ex}$ = 340 nm) of PAHA and LFA at pH 6, 0.01 M KNO$_3$ (■ = PAHA; ♦ = LFA).

This scattered light includes Raman and coherent scattering. Raman scattering can produce a peak in the emission spectrum in the region within 50 nm of the excitation wavelength. Once these corrections are applied, fluorescence spectroscopy is a sensitive technique to differentiate between different fulvic and humic acids (*45,46*). Figure 3 shows the corrected and uncorrected fluorescence emission spectrum of LFA. Figure 4 shows the two corrected spectra of LFA and PAHA used in our experiments.

Spectra with different concentrations were measured and the intensities at 460 nm are shown in Figure 5. Linear relations between concentration and fluorescence intensity were obtained for both humics.
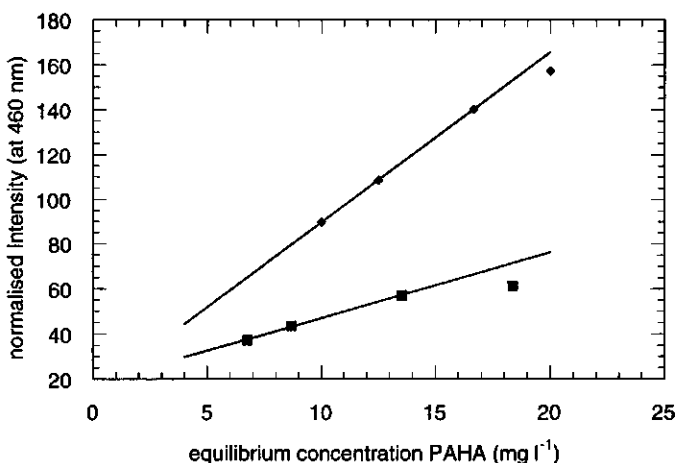


**Figure 5:** Fluorescence spectroscopy calibration lines and experimental results for PAHA and LFA at pH 6, 0.01 M KNO$_3$: ■ = PAHA; ♦ = LFA; the lines are obtained by linear regression through the lower concentrations only. The regression coefficients are given in Table II.

At higher concentrations some molecules will prohibit others from being excitated and thus disturb the linearity between concentration and intensity. In practice one can say that the signal is linearly proportional to the concentration when the optical density is lower than 0.1 at the excitation wavelength. Following this rule the linearity should hold up to a concentration of 18 mg l$^{-1}$ LFA and about 16 mg l$^{-1}$ PAHA.

The composition of a mixture can be analysed using the regression coefficients of the individual lines. Five test samples show a good correlation between the measured and the calculated intensities, see Table I, a deviation less than 3 % is obtained. Compared with the UV results the accuracy is slightly decreased.

The course of adsorption of PAHA and LFA

Due to the small differences between the fluorescence spectra of the different mixtures, with ratios PAHA : LFA that were applied in this study, the accuracy of fluorescence spectroscopy as a multicomponent mixing tracer was small. Combining fluorescence and UV spectroscopy significantly improved the results. According to the Lambert-Beer law the following equations. hold for the mixtures:

$$UV_{mix} = S_{UV}^{HA} * [HA] + I_{UV}^{HA} + S_{UV}^{FA} * [FA] + I_{UV}^{FA} \tag{6.1}$$

$$FS_{mix} = S_{FS}^{HA} * [HA] + I_{FS}^{HA} + S_{FS}^{FA} * [FA] + I_{FS}^{FA} \tag{6.2}$$

where $UV_{mix}$ and $FS_{mix}$ are the measured intensities and [HA] and [FA] are the concentrations of respectively PAHA and LFA. The values of the constants S and I are given in Table II. Combining these equations results in Eq. (6.3) giving the actual humic acid concentration from the measured UV and FS signals. The constants $C_1$ and $C_2$ are explained in Eqs. (6.4) and (6.5) respectively. For known values of $UV_{mix}$ and $FS_{mix}$, [HA] is found from Eq. (6.3) , whereafter Eq. (6.1) can be used to calculate the fulvic acid concentration. On the basis of these concentrations both the individual and the total adsorption can now be calculated.

$$[HA] = \frac{FS_{mix} - S_{FS}^{FA} * UV_{mix} - C_1}{C_2} \tag{6.3}$$

where:

$$C_1 = -I_{FS}^{HA} - I_{FS}^{FA} + S_{FS}^{FA} * (I_{UV}^{HA} + I_{UV}^{FA}) \tag{6.4}$$

and

$$C_2 = S_{FS}^{HA} - S_{FS}^{FA} * S_{UV}^{HA} \tag{6.5}$$

**Table II:** Regression coefficients of the spectroscopy calibration lines.

|          | Slope (S) | Intercept (I) | Correlation coefficient |
|----------|-----------|---------------|-------------------------|
| $HA_{uv}$ | 0.037108 | -0.00971 | 0.9998 |
| $FA_{uv}$ | 0.014316 | 0.008717 | 0.9995 |
| $HA_{FS}$ | 2.899351 | 18.15465 | 0.9997 |
| $FA_{FS}$ | 7.590612 | 13.85867 | 0.999 |

UV stands for UV-visible spectrophotometry, FS for Fluorescence Spectrometry, The constants were obtained by linear regression where the intercept of the Y axis was not imposed to be 0.

In Figure 6 the adsorption (as a percentage of the total available amount of the humics) of both LFA and PAHA is given as a function of time. Initially LFA is preferentially withdrawn from the solution, as was expected on the basis of the diffusion coefficients. After 15 minutes 50 % of the available LFA is adsorbed compared to 5 % of PAHA. However, in time the adsorbed amount of PAHA increases and that of LFA decreases. The larger PAHA molecules displace the smaller LFA molecules that are adsorbed initially because of their fast diffusion rates. It may be concluded that PAHA adsorbs preferentially. It should be stressed that even after 25 hours the adsorbed amounts of the single components still change significantly. The total adsorption is however increasing only slightly.
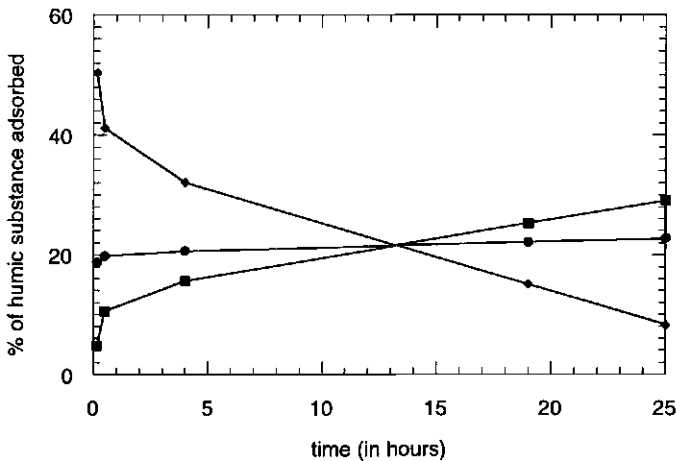


**Figure 6:** Preferential adsorption of the higher molecular weight fraction of a mixture of 16 mg $l^{-1}$ PAHA and 7 mg $l^{-1}$ LFA, at pH 6 and 0.01 M $KNO_3$. At the y-axis the percentage adsorbed of the total concentration is given as a function of the time the suspension was allowed to equilibrate. ■ = PAHA; ♦ = LFA and ● = the mixture of both humic substances.

## Modelling the adsorption

*Outline*

In order to gain insight into the binding characteristics of humic acids we will model the adsorption of weak polyelectrolytes onto a surface with a variable charge using the extended SCF theory (*34*). To model the effects of a polydisperse mixture upon the adsorption/ desorption hysteresis, the surface-to-volume ratio (S/V) is adjusted. The effects of a polydisperse polyelectrolyte mixture on the adsorption/ desorption to a surface with a variable charge were modelled using the approach for a bimodal mixture as was described by Roefs et al. (*47*).

*System description and choice of parameters*

In the SCF theory all components are placed in a lattice consisting of M layers parallel to the surface (S) and numbered from $z = 1$ to $z = M$. The distance between two adjacent layers is denoted by d. The protons present are dimensionless and determine the pH of the system. The total amount of polyelectrolyte in the system is expressed in equivalent monolayers, $\theta$. On one side of the system the surface (an impenetrable wall) is placed at $z = 0$. At the other boundary at $z = M + 1$, reflecting conditions are assumed. Each segment type x (x = U, C, P, $Na^+$, $Cl^-$, W, S) experiences a potential $u_x(z)$ at a distance z·d from the surface. $u_x(z)$ is normalised with respect to the bulk solution. Thus $u_x(\infty) = 0$. The potential $u_x(z)$ is a free energy composed of all energetic and entropic interactions a segment undergoes, it depends on the average surroundings, electrostatic interactions and nearest neighbour segment-segment interactions. For a detailed description of the system under investigation is referred to a previous paper (*7*), here we will only give the most important parameters.

The calculations were performed using a lattice of simple cubic symmetry with a cell size d of 0.311 nm. The cell size corresponds with a water density of 55.2 mol $l^{-1}$. The system is built of 100 layers. This value was chosen to assure that all concentration and potential profiles could attain their bulk values. The surface (S) is composed of two types of groups, a charged and a neutral one in the ratio of 1:1. For the present choice of the lattice cell this results in a density of 5.2 charged segments $nm^{-2}$. The charged group has a pK of 9 and is titrated from 0.5 to -0.5 according to the one pK model (*48,49*). The polyelectrolytes are taken to be linear with three types of segments; U, C and P where segment U is uncharged, segment C has a pK of 4 and P a pK of 10. The chargeable segments of the polyelectrolyte are titrated from 0 to -1. All units have a dielectric constant $\varepsilon_r$ of 80. The Flory-Huggins $\chi$ parameters (*50*) describing the interactions between the different units in the bulk are all equal to zero. Due to this the salt ions are treated as indifferent. The $\chi$ parameters of all segments with the surface are also zero, except $\chi_{C,S}$ that is set to -15. Indicating that the C segments have a specific affinity for the surface.

Polyelectrolyte I is a chain with the following composition:

$$U_{12}\left(C_4U_2P_2U\right)_{16}U_{40}C_4$$
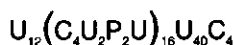
polyelectrolyte I is intended to mimic a simple humic acid with two type of charged segments representing carboxylic and phenolic type of groups (7) together with two blocs of uncharged segments. Also this polyelectrolyte intends to mimic a simple humic acid it has to be emphasised that it is not our purpose to model PAHA, we just study the properties of model polyelectrolytes to gain insight into the importance of certain interaction mechanisms.

The effect of the polydispersity on the adsorption is illustrated by the isotherms for a mixture of two monodisperse samples. Two chainlengths are chosen for which the adsorption plateaux differ notably. The composition of polyelectrolyte II is:

$$U_1\left(C_4U_2P_2U\right)_2U_4C$$
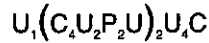
where the number of the repeating block is decreased from 16 to 2 compared to polyelectrolyte I. Polyelectrolyte II is intended to represent a fulvic acid, its molecular weight is about a factor 10 smaller than that of polyelectrolyte I and the proportion of C and P segments (chargeable) is relatively high.

To model the adsorption/ desorption isotherms, the surface-to-volume ratio (S/V ) is adjusted. The surface-to-volume ratio is given by $S/V = (M\ell)^{-1}$, where $\ell$ is the thickness of a lattice layer and M the number of layers.

## Results

The adsorption isotherms of polyelectrolyte I and polyelectrolyte II at three different pH values and a salt concentration of 0.01 M are given in Figure 7 as well as that of the mixture of polyelectrolyte I and II. The mixture with a weight fraction 5/7 for Polyelectrolyte I, shows adsorption isotherms with an initial high affinity part, where the surface accommodates practically speaking all available polyelectrolyte molecules. When the polyelectrolyte concentration starts to build up the isotherm first increases gradually due to replacement of polyelectrolyte II by polyelectrolyte I and than reaches a pseudo plateau, where only the longer molecules are adsorbed. At lower pH this effect is most profound, due to the high adsorption complete displacement of the small molecule fraction occurs only at a high equilibrium concentration. The rounded shape of the isotherm is most clearly seen at this pH.

Figure 8 demonstrates the displacement in a somewhat different way, by showing the adsorption isotherms of polyelectrolyte II of the mixture at three pH values. The isotherm of polyelectrolyte II at pH 6 is shown as reference. As can be seen, the adsorbed amount of polyelectrolyte II decreases with increasing overall concentration of the mixture. At high concentrations nearly the entire adsorption is due to pure polyelectrolyte I. It can be seen in Figure 7 that the plateau does not coincide with that of pure polyelectrolyte I, the adsorption is always lower than that of pure polyelectrolyte I. This is due to the fact that the total equilibrium concentration is plotted rather than the equilibrium concentration of polyelectrolyte I.
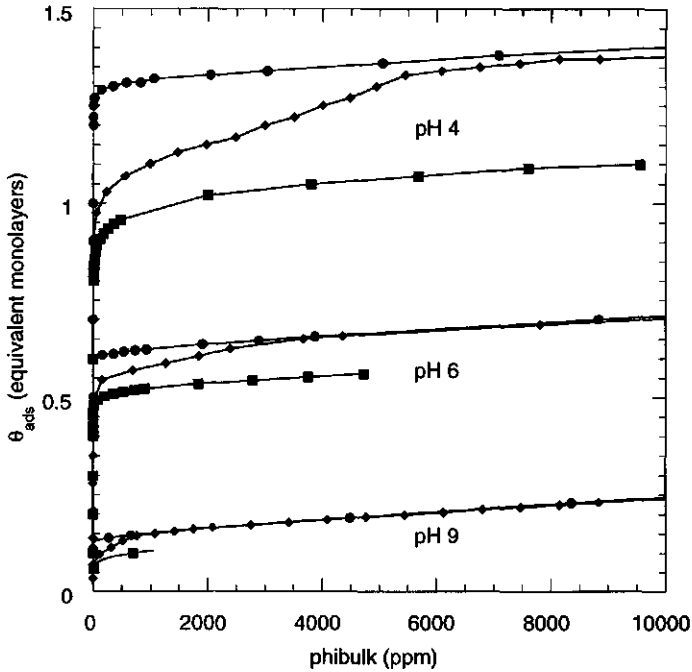
**Figure 7:** Calculated adsorption isotherms for polyelectrolyte I and II and a bimodal mixture of polyelectrolyte I and II at 0.01 M salt. ● = polyelectrolyte I, ■ = polyelectrolyte II; ♦ = mixture of polyelectrolyte I and II. The isotherms are given for three different pH values as indicated.


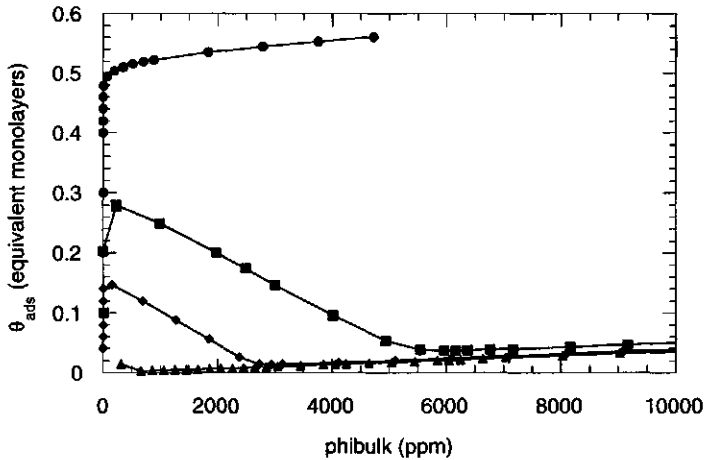
**Figure 8:** Calculated adsorption isotherms of polyelectrolyte II for a bimodal mixture of both polyelectrolytes. ■ = pH 4; ♦ = pH 6; ▲ = pH 9; ● adsorption isotherm of a monodisperse solution of polyelectrolyte II at pH 6.

It follows from the calculations that desorption by dilution hardly occurs because this does not affect the equilibrium concentration of the adsorbed fraction but rather

decreases the bulk concentration of the non-adsorbed polyelectrolyte. Such an adsorption desorption sequence is simulated by adjusting the surface-to-volume ratio S/V. In Figure 9a the adsorption isotherms for four S/V ratio's are given together with one desorption isotherm. The S/V ratio is varied from $(100\ell)^{-1}$ till $(100.000\ell)^{-1}$. It can be observed that with increasing S/V almost all molecules are adsorbed and that the small molecules are only withdrawn from the surface at very high equilibrium concentrations. The solid line represents a desorption isotherm, with a total amount of polyelectrolyte of one equivalent monolayer and a surface-to-volume ratio gradually increasing from $(100\ell)^{-1}$ to $(100.000\ell)^{-1}$. The desorption isotherm follows a high affinity isotherm as hardly any desorption of the longer molecules occurs; as one can see in Figure 9b the desorption isotherm does not coincide with the adsorption isotherm and even crosses all the isotherms with different S/V ratio's. This is related to the fact that overall concentrations are plotted at the x-axis.
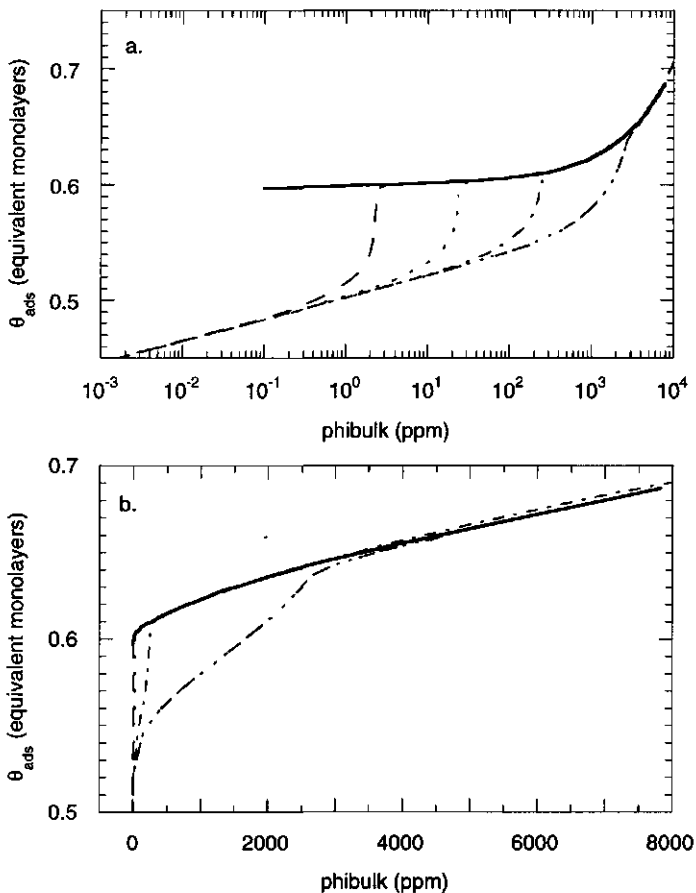


**Figure 9a:** Four adsorption isotherms and one desorption isotherm for a bimodal mixture of both polyelectrolytes. The adsorption isotherms are given for different S/V ratio's: ⁻⁻⁻⁻⁻ S/V = $(100\ell)^{-1}$; ⁻⁻⁻⁻⁻ S/V = $(1000\ell)^{-1}$; ·········· S/V = $(10000\ell)^{-1}$; ⁻⁻⁻⁻⁻⁻⁻ S/V = $(100000\ell)^{-1}$; ———— desorption isotherm. **b:** The adsorbed amount as a function of the bulk concentration at a linear scale, to emphasise the difference between the adsorption and desorption isotherms at the plateau level.

## Discussion

Following the adsorption of a mixture of LFA and PAHA in time it was observed that LFA adsorbs initially, due to the higher diffusitivity. At longer timescales the initially adsorbed LFA is replaced by the larger PAHA. This can be explained by the lower loss of translational entropy of the largest molecules upon adsorption. It was found that the timescale of this rearrangement is large. Equilibrium was not yet reached within the 25 hours used in the experiments. Although the overall adsorbed amount seems constant within the time of the experiment, the adsorbed amount of the single components was not.

Even though the adsorption experiments with the mixture reflected an artificial polydispersity, the observed trends can be extrapolated to experiments where only one type of humic is present. It is generally excepted that humic substances by itself can be described as a polyelectrolyte mixture with a broad molecular weight distribution (36,51-53). Therefore we may explain the gradually increasing adsorption isotherm at higher equilibrium concentrations, observed for the PAHA adsorption, by adsorption fractionation. It is clear that the second plateau as is observed for the calculated mixture isotherms in Figure 7 may not be expected for the adsorption isotherms of natural humic substances. The model calculations assumed a bimodal distribution whereas the natural humic acid sample contains a continuous distribution. Although we are aware of this difference we can conclude that the higher molecular weight fraction adsorbed preferentially and causes the gradual increase of the measured adsorption isotherms at higher equilibrium concentrations.

At first sight the results reported by Kilduff et al. (20) seem to be in contradiction with our results, but if the porosity of the oxide particles is taken into account both studies are in agreement. Within their study the smaller molecules accumulate in the pores of the activated carbon particles, where the larger molecules can not. Only due to this fact the smaller molecules are adsorbed to a larger extent. Thus the preferential adsorption of the smaller molecules reported by Kilduff does not reflect process described in this paper but has to be attributed to the structure of the surface. Even the adsorption of the intermediate molecular weight fraction as discussed by De Laat and Van der Heuvel (21) does not reflect the preferential adsorption of this molecular weight fraction. Thermodynamically the largest molecules would adsorb preferentially, however, the timescale needed to achieve this is probably beyond the timescale of the experiment. It was reported by Koopal (16) that for polymer adsorption an equilibrium time of about 160 hours was required. Regarding the extra complications associated with polyelectrolyte adsorption, the development of an electrostatic barrier that inhibits further adsorption and desorption, even longer equilibrium times are expected.

Using the SCF theory it is possible to model the adsorption of a mixture of polydisperse polyelectrolytes to a surface with a variable charge in full equilibrium. It was observed that the larger molecular weight fraction accumulates at the surface and that the smaller polyelectrolytes remain in solution.

Simulation of a desorption isotherm showed that hysteresis with the adsorption isotherm was developed. It is stated that the observed hysteresis is not an indication that the polyelectrolyte adsorption is irreversible but can be explained by adsorption

fractionation due to the polydispersity of the organic substances, with each component desorbing according to its own isotherm.

The relevance of this study for environmental applications is clear. By applying the proposed mechanistic model a better insight is obtained in the importance of adsorption fractionation as a mechanism controlling the speciation of natural organic substances. A step forward has been made to improve predictive capabilities with respect to the transport of natural organic matter and co-transport of associated contaminants. For example it can be understood that the adsorption of hydrophobic organic compounds to the river sediment was increased (5), since the affinity of the sediment for hydrophobic contaminants is influenced by the nature of the adsorbed organic material.

Finally we may conclude that both on experimental and theoretical grounds preferential adsorption is observed, even for systems where the smaller particles undergo a more pronounced attraction. The hysteresis observed by several authors can be explained by the preferential adsorption of the largest polyelectrolytes and does not have to be due to irreversible interactions.

**References**

(1)  McKnight, D.M.; Wershaw, R.L.; Bencala, K.E.; Zellweger, G.W.; Feder, G.L. Humic substances and trace metals associated with Fe and Al oxides deposited in an acidic mountain stream. *Sci.Total Environ.* 1992, *117/118*, 485 -498.
(2)  Tipping, E. The adsorption of aquatic humic substances by iron oxides. *Geochim.Cosmochim.Acta* **1981**, *45*, 191 -199.
(3)  Davis, J.A. Adsorption of natural dissolved organic matter at the oxide/water interface. *Geochim.Cosmochim.Acta* **1982**, *46*, 2381 -2393.
(4)  McKnight, D.M.; Bencala, K.E.; Zellweger, G.W.; Aiken, G.R.; Feder, G.L.; Thorn, K.A. Sorption of Dissolved Organic Carbon by Hydrous Aluminum and Iron Oxides Occurring at the Confluence of Deer Creek with the Snake River, Summit County, Colorado. *Environ.Sci.Technol.* **1992**, *26(7)*, 1388 -1396.
(5)  Murphy, E.M.; Zachara, J.M.; Smith, S.C.; Philips, J.L. The sorption of humic acids to mineral surfaces and their role in contaminant binding. *Sci.Total Environ.* **1992**, *117/118*, 413 -423.
(6)  Gu, B.; Schmitt, J.; Chen, Z.; Liang, L.; McCarthy, J.F. Adsorption and Desorption of Natural Organic Matter on Iron Oxide: Mechanisms and Models. *Environ.Sci.Technol.* **1994**, *28(1)*, 38 -46.
(7)  Vermeer, A.W.P. this Thesis. Chapter 5: Interactions between humic acid and mineral particles.
(8)  Stevenson, F.J. *Humus Chemistry. Genesis, Composition, Reactions*; Wiley Interscience: New York, 1982.
(9)  Hayes, M.H.B.; MacCarthy, P.; Malcolm, R.L.; Swift, R.S. *Humic Substances II: In search of structure*; Wiley Interscience: New York, 1989.
(10)  Schnitzer, M.; Khan, S.U. *Humic substances in the environment*; Marcel Decker Inc. New York, 1972.
(11)  Aiken, G.R.; McKnight, D.M.; Wershaw, R.L.; MacCarthy, P. *Humic Substances in Soil, Sediment, and Water*; Wiley Interscience: New York, 1985.
(12)  Cohen Stuart, M.A. Polyelectrolyte adsorption. *J.Phys.France* **1988**, *49*, 1001 -1008.
(13)  Cohen Stuart, M.A.; Fleer, G.J.; Lyklema, J.; Norde, W.; Scheutjens, J.M.H.M. Adsorption of Ions, Polyelectrolytes and Proteins. *Adv.Colloid Interface Sci.* **1991**, *34*, 477 -535.
(14)  Fleer, G.J.; Cohen Stuart, M.A.; Scheutjens, J.M.H.M.; Cosgrove, T.; Vincent, B. *Polymers at Interfaces*; Chapman & Hall: London, 1993.
(15)  Cohen Stuart, M.A.; Scheutjens, J.M.H.M.; Fleer, G.J. Polydispersity Effects and the Interpretation of Polymer Adsorption Isotherms. *J.Polym.Sci.Polym.Phys.Ed.* **1980**, *18*, 559 -573.

(16) Koopal, L.K. The Effect of Polydispersity on the Adsorption Isotherm. *J.Colloid Interface Sci.* **1981**, *83(1)*, 116 -129.

(17) Hlady, V.; Lyklema, J.; Fleer, G.J. Effect of Polydispersity on the Adsorption of Dextran on Silver Iodide. *J.Colloid Interface Sci.* **1982**, *87(2)*, 395 -406.

(18) Summers, R.S.; Roberts, P.V. Activated Carbon Adsorption of Humic Substances. *J.Colloid Interface Sci.* **1988**, *122(2)*, 367 -381.

(19) Davis, J.A.; Gloor, R. Adsorption of Dissolved Organics in Lake Water by Aluminum Oxide. Effect of Molecular Weight. *Environ.Sci.Technol.* **1981**, *15(10)*, 1223 -1229.

(20) Kilduff, J.E.; Karanfil, T.; Chin, Y.; Weber, W.J.J. The adsorption of natural organic polyelectrolytes by activated carbon: a size exclusion chromatography study. *Environ.Sci.Technol.* **1996**, *30(4)*, 1336 -1343.

(21) De Laat, A.W.M.; Van den Heuvel, G.L.T. Molecular weight fractionation in the adsorption of polyacrylic acid salts onto BaTiO$_3$. *Colloids Surf.A* **1995**, *98*, 53 -59.

(22) Bain, D.R.; Cafe, M.C.; Robb, I.D.; Williams, P.A. The Fractionation of Polyelectrolytes by Adsorption onto Ionic Crystals. *J.Colloid Interface Sci.* **1982**, *88(2)*, 467 -470.

(23) Meadows, J.; Williams, P.A.; Garvey, M.J.; Harrop, R.A.; Phillips, G.O. Enhanced Polyelectrolyte Adsorption. *Colloids Surf.* **1988**, *32*, 275 -288.

(24) Dahlgren, A.G.; Leermakers, F.A.M. Depletion Zones in Polyelectrolyte Systems: Polydispersity Effects and Colloidal Stability. *Langmuir* **1995**, *11(8)*, 2996 -3006.

(25) Ramachandran, R.; Somasundaran, P. Polyelectrolyte Interactions at the Hematite/Water Interface. Part I. *Colloids Surf.* **1988**, *32*, 307 -318.

(26) Di Toro, D.M.; Horzempa, L.M. Reversible and Resistant Components of PCB Adsorption-Desorption: Isotherms. *Environ.Sci.Technol.* **1982**, *16(9)*, 594 -602.

(27) Vaccari, D.A.; Kaouris, M. A model for irreversible adsorption hysteresis. *J.Environ.Sci.Health* **1988**, *A23(8)*, 797 -822.

(28) Zhou, J.L.; Rowland, S.J.; Fauzi, R.; Mantoura, R.F.C.; Braven, J. The formation of humic coatings on mineral particles under simulated estuarine conditions - A mechanistic study. *Water Res.* **1994**, *28(3)*, 571 -579.

(29) Scheutjens, J.M.H.M.; Fleer, G.J. Statistical theory of the adsorption of interacting chain molecules. I. Partition function, segment density distribution and adsorption isotherms. *J.Phys.Chem.* **1979**, *83*, 1619 -1635.

(30) Scheutjens, J.M.H.M.; Fleer, G.J. Statistical Theory of the Adsorption of Interacting Chain Molecules. 2. Train, Loop, and Tail Size Distribution. *J.Phys.Chem.* **1980**, *84*, 178 -190.

(31) Evers, O.A.; Fleer, G.J.; Scheutjens, J.M.H.M.; Lyklema, J. Adsorption of Weak Polyelectrolytes from Aqueous Solution. *J.Colloid Interface Sci.* **1986**, *111(2)*, 446 -453.

(32) Böhmer, M.R.; Evers, O.A.; Scheutjens, J.M.H.M. Weak Polyelectrolytes between Two Surfaces: Adsorption and Stabilization. *Macromolecules* **1990**, *23(8)*, 2288 -2301.

(33) Israëls, R.; Leermakers, F.A.M.; Fleer, G.J. On the Theory of Grafted Weak Polyacids. *Macromolecules* **1994**, *27(11)*, 3087 -3093.

(34) Vermeer, A.W.P. this Thesis. Chapter 2: Adsorption of a weak polyelectrolyte on a surface with a variable charge, Self Consistent Field calculations.

(35) Breeuwsma, A.; Lyklema, J. Interfacial electrochemistry of haematite. *Discussions of The Faraday Soc.* **1971**, *52*, 324 -333.

(36) Vermeer, A.W.P.; Koopal, L.K. submitted to *Environ.Sci.Technol.* this Thesis. Chapter 3: Characterisation and classification of purified Aldrich humic acid.

(37) McKeague, J.A.; Scheldrick, B.H.; Desjardin, J., G. Compilation of Data for CSSC Reference Soil Samples. Land Resources Research Centre: Ottawa. 1978.

(38) Visser, S.A. Application of Van Krevelen's Graphical-Statistical Method for the Study of Aquatic Humic Material. *Environ.Sci.Technol.* **1983**, *17(7)*, 412 -417.

(39) Vermeer, A.W.P. this Thesis. Chapter 4: Proton and Cadmium binding to purified Aldrich humic acid, exploration of the NICA-Donnan model.

(40) Milne, C.J.; Kinniburgh, D.G.; De Wit, J.C.M.; Van Riemsdijk, W.H.; Koopal, L.K. Analysis of proton binding by peat humic acid using a simple electrostatic model. *Geochim.Cosmochim.Acta* **1995**, *59(6)*, 1101 -1112.

(41) Senesi, N.; Miano, T.M.; Provenzano, M.R.; Brunetti, G. Characterization, Differentiation, and classification of humic substances by fluorescence spectroscopy. *Soil Sci.* **1991**, *152(4)*, 259 -271.

(42) Tipping, E. Adsorption by goethite of humic substances from three different lakes. *Chem.Geo.* **1981**, *33*, 81 -89.

(43) Tipping, E.; Cooke, D. The effects of adsorbed humic substances on the surface charge of goethite in freshwaters. *Geochim.Cosmochim.Acta* **1982**, *46*, 75 -80.

(44) Ewald, M.; Belin, C.; Berger, P.; Weber, J.H. Corrected Fluorescence Spectra of Fulvic Acids Isolated from Soil and Water. *Environ.Sci.Technol.* **1983**, *17*, 501 -504.

(45) Miano, T.M.; Sposito, G.; Martin, J.P. Fluorescence Spectroscopy of Humic Substances. *Soil Sci.Soc.Am.J.* **1988**, *52*, 1016 -1019.

(46) Ghosh, K.; Schnitzer, M. Fluorescence excitation spectra of humic substances. *Can.J.Soil Sci.* **1980**, *60*, 373 -379.

(47) Roefs, S.P.F.M.; Scheutjens, J.M.H.M.; Leermakers, F.A.M. Adsorption Theory for Polydisperse Polymers. *Macromolecules* **1994**, *27(17)*, 4811 -4816.

(48) Van Riemsdijk, W.H.; Bolt, G.H.; Koopal, L.K.; Blaakmeer, J. Electrolyte Adsorption on Heterogeneous Surfaces: Adsorption Models. *J.Colloid Interface Sci.* **1986**, *109(1)*, 219 -228.

(49) Koopal, L.K. Ion adsorption on mineral oxide surfaces In *Adsorption on new and modified inorganic sorbents*; Dabrowski, A.; Tertykh, V.A. Eds.; Elsevier: Amsterdam, 1996; 757-796.

(50) Flory, P.J. *Principles of polymer chemistry*; Cornell University Press: London, 1953.

(51) Evans, H.E.; Evans, R.D.; Lingard, S.M. Factors Affecting the Variation in the Average Molecular Weight of Dissolved Organic Carbon in Freshwaters. *Sci.Total Environ.* **1989**, *81/82*, 297 -306.

(52) Chin, Y.; Aiken, G.R.; O'Loughlin, E. Molecular Weight, Polydispersity, and Spectroscopic Properties of Aquatic Humic Substances. *Environ.Sci.Technol.* **1994**, *28(11)*, 1853 -1858.

(53) Beckett, R.; Jue, Z.; Giddings, C. Determination of Molecular Weight Distributions of Fulvic and Humic Acids Using Flow Field-Flow Fractionation. *Environ.Sci.Technol.* **1987**, *21*, 289 -295.

Chapter 7

# Proton binding to a heterogeneous system

# effects due to the interactions

# between the different components

## Abstract

Proton adsorption to a mixture of purified Aldrich humic acid and hematite is measured and discussed. The combination of humic acid and metal(hydr)oxide is of relevance in many environmental systems like soils. The proton binding to the mixed system is influenced by the interactions between the humic and the hematite, and the proton adsorption isotherm is not a simple summation of the proton isotherms to the humic and the hematite separately. Both hematite and humic acid molecules have a variable charge that is affected by mutual interactions between these particles. An estimate of the differences in proton charge caused by these interactions is obtained by comparison of the proton charge of the individual samples and their mixtures. From this comparison it can be concluded that in the adsorbed state some of the carboxylic groups of the humic acid are bound to protonated surface sites of hematite. These groups are less available for further proton binding. Opposite to this an increased proton adsorption on the oxide surface is deducted. The negative potential field of the adsorbed humic acid layer promotes protonation of the hematite surface. The experiments are compared with Self Consistent Field (SCF) calculations of a weak polyelectrolyte adsorbed on a variably charged surface. Within the calculations surface charge/ pH curves are obtained as a function of the adsorbed amount of polyelectrolyte. The calculations show that both components titrate each other.

## Introduction

The natural environment is a complex heterogeneous system consisting of mineral oxides, clay particles and organic substances in an aqueous electrolyte solution. In this system organic and inorganic complexing materials play a role in regulating the speciation of toxic metal ions. For instance, the bioavailability of metal ions is strongly related to the binding of these ions to the different soil components. Increasing the salt concentration may enhance the binding of cations to the mineral and organic soil fraction by reducing the electrostatic repulsion. Decreasing the pH will increase the proton adsorption but decrease the metal ion adsorption. Further it may by expected that cation binding is also affected by the interactions between the different components (organics and mineral particles).

To study the effects of the interactions between the organic soil fraction and mineral particles on the proton binding we will consider a model system, composed of purified Aldrich humic acid (denoted as PAHA) and hematite particles in an electrolyte solution.

The proton and metal ion binding to both humic substances (1-8) and iron oxides (9-14) as well as the interactions between these components (15-20) have been studied extensively. From electrophoretic mobility measurements it was found that superequivalent adsorption of humic acid onto the oxide particles (21-29) was commonly observed. It was mentioned that, even at pH 3 and at very low concentrations of organic matter (order of 10 mg g$^{-1}$ hematite), the surface charge of the mineral particles was overcompensated by the charge associated with the adsorbed polyelectrolyte molecules.

In a previous paper proton and metal ion adsorption to PAHA (30) have been studied and the results could be described with the NICA Donnan model, using measured Donnan volumes as a function of pH and salt concentration.

The binding of protons (31-33) and metal ions (9,10) to hematite were mainly studied by potentiometric techniques. Modelling aspects of ion adsorption to mineral surface have been discussed in some recent reviews by Koopal (34,35). He indicates that modelling with the classical two-pK model should be avoided. A discussion on the application of different site binding models commonly used to model cation adsorption onto oxides is given by Venema et al. (36).

The adsorption of PAHA onto hematite B was studied by Vermeer (33,37) using an advanced polyelectrolyte adsorption theory (38,39). In these papers the PAHA molecules were described as fairly flexible polyelectrolyte molecules that were able to adjust their conformation upon adsorption. Comparison of the experimental results with Self Consistent Field (SCF) calculations on polyelectrolyte adsorption were used to gain better insight into the interaction mechanisms between PAHA and hematite B. It was concluded that both coulombic and specific interactions were essential to describe the observed pH and salt concentration dependencies of the PAHA adsorption. Due to the specific adsorption energy superequivalent adsorption may occur. Because of the excess negative charge associated with the adsorbed PAHA molecules, superequivalent adsorption gives rise to an electrostatic barrier for further adsorption of PAHA.

The proton adsorption of interacting (weak) polyelectrolytes and particles with a variable charge has not been discussed very thoroughly in the literature. Newcombe (40) and Morris and Newcombe (22) described the titration curves of mixtures of soluble humic substances adsorbed onto granular activated carbon. They assumed that the substrate charge was not affected by the adsorbed material, the difference in proton adsorption was attributed solely to the organic matter. It was described that in particular the carboxylic groups of the humic matter showed a decreased degree of dissociation. This was ascribed to the lower pH close to the surface compared with the bulk pH, due to the accumulation of positive ions, including protons, in the vicinity of the adsorbed polyelectrolyte layer. Newcombe (40) described a shift of the point of zero charge (p.z.c.) of the complex to a lower pH value. Baker (41) described the interactions between fulvic acid and alumina particles. Adsorption of fulvic acid was observed over the entire pH range studied (pH 3-10), where the p.z.c. of the alumina suspension was 5.3. The actual titration data of the mixture displayed a lower number of titrateable groups compared with the non-interacting sum and the difference between the two isotherms increased with decreasing ionic strength. These differences were explained, assuming that two groups (one fulvic and one alumina) are involved in the adsorption reaction. After adsorption these two groups are no longer available for proton binding, which diminishes the overall number of titrateable groups. The fraction of fulvic groups involved with the adsorption was estimated from fulvic acid/alumina adsorption isotherms. This fraction was in good agreement with the differences measured, without considering any reduction in titrateable sites due to steric effects and adjustment of the surface charge.

Both studies described the interaction between the two components by assuming that the particle surface charge was not affected by the adsorbed polyelectrolyte. Baker even assumed both components to preserve their non-interacting charge. It may be clear that these assumptions are questionable. It is well known from other literature data that the surface charge of particles with a variable charge depends on the local conditions. For instance, adsorption of small ions (e.g. cadmium, copper or phosphate) (9,42) or molecules with a variable charged group (e.g. phthalic or salicylic acid) (43) cause a shift of the point of zero charge of the surface.

The aim of this paper is to gain insight into the availability of the proton binding sites in a mixture of PAHA and hematite B particles, as compared to their availability in the single components. To this aim proton adsorption isotherms of these mixed systems will be measured and compared with the proton isotherms of the single components and the non-interacting mixture curve. Differences between the actual and the non-interacting proton isotherms of the mixture will be investigated as a function of pH and salt concentration. It will be shown that it is possible to differentiate between the effects on the PAHA groups and those on the hematite sites. Finally we will compare the experimental results with calculations based on the SCF theory for the adsorption of (weak) polyelectrolytes (44-46) on a variably charged surface (47). This theory is an extension of the theory of Scheutjens and Fleer (48-50) for polymer adsorption.

**Adsorption onto surfaces with a variable charge; the state of the art**

Before presenting our experiments we will briefly discuss the difficulties we may expect studying the proton adsorption of the separate components in a mixture.

Based on previous studies we may expect that both the surface and the adsorbed polyelectrolyte adapt their charge to the local conditions. Van der Schee and Lyklema (51) described that the adsorption of poly-L-lysine changed the surface charge of an AgI sol. A great advantage of such a system is that the surface charge on AgI, which is due to the adsorption of potential-determining ions ($Ag^+$ and $I^-$), is measurable and can be varied as a function of pAg, independent of the proton concentration.

Studying the adsorption of polyelectrolytes onto oxide surfaces, changes in the surface charge can not be measured directly. Both the surface charge and the charge of the adsorbed polyelectrolyte molecules depend on the same potential-determining ions ($H^+$ and $OH^-$). The effects of adsorption on the position of the point of zero charge (p.z.c.) and the isoelectric point (i.e.p.) can sometimes be obtained. The principle difference between these two points is rather relevant. The p.z.c. is defined as a surface property, whereas the i.e.p. reflects the mobility of the entire complex in an electric field. It is well known that a shift of the i.e.p. to a lower pH due to specific adsorption, corresponds with a shift of the p.z.c. to a higher pH value and vice versa (52). The procedure to obtain the p.z.c. of an amphoteric oxide is by measuring the common intersection point (c.i.p.) of surface charge/ pH curves obtained at different concentrations of indifferent electrolyte, whereas in the presence of specifically adsorbing ions (13,53,54) a c.i.p. should not be confused with the p.z.c.

Van Riemsdijk and Lyklema (42) described the adsorption of phosphate onto gibbsite and observed a co-adsorption of protons, resulting in a higher p.z.c. The co-adsorption of hydroxyl ions due to the specific adsorption of cations onto iron oxides has been investigated by several authors (9,31,36,53,55). Indeed a shift of the p.z.c. to a lower pH was observed in all studies.

When the adsorbed molecules themselves also have a variable charge, the p.z.c. of the oxide can not be obtained directly. The effects of specific adsorption of organic and inorganic weak acids on the surface charge of hydrous oxides were reported by Stumm et al. (43). Matijevíc and co-workers (56-58) also studied the adsorption of small organic acids onto hematite and mentioned significant adsorbed amounts several pH units above the p.z.c. of the uncovered hematite particles. Due to this adsorption the i.e.p. shifts to lower pH values. Gebhardt and Feurstenau (59) studied the adsorption of a polyacrylic acid onto hematite and mentioned an effect on the electrophoretic mobility upto two units above the p.z.c. Gebhardt also reported significant shifts to lower pH of the i.e.p. due to the specific adsorption of the polyelectrolyte molecules.

Studying the system presented in this paper we can also only measure the overall proton adsorption and therefore we have to make some assumptions to distinguish between the effects on the single components.

## Material and methods

All experiments have been performed in a thermostatted room at 21 ± 1 °C. Chemicals used were p.a. quality and the purified water was obtained by percolating tab water through a mixed bed ion exchange column followed by an active carbon column and a micro filter. $KNO_3$ is used as indifferent electrolyte.

### Hematite particles

Hematite B ($\alpha$-$Fe_2O_3$) was prepared as described by Breeuwsma and Lyklema (13) and was aged for several years. Before use the particles were washed with HCl and dialysed extensively against demineralised water. The particle mean size of hematite B is 50 nm, its BET ($N_2$) area is 43 $m^2g^{-1}$ and the particles are non porous.

### Humic acid

For all experiments, a purified Aldrich humic acid (Aldrich-Chemie; code:H1,675-2) denoted as PAHA was used. Purification and characterisation of PAHA are described elsewhere (60). PAHA reflects many characteristics normally found for naturally occurring humic substances and can be classified as a soil and/ or peat type humic acid (60). PAHA is obtained in its proton form and was freeze dried and stored in a glass container.

Before use a stock solution of PAHA was prepared by resuspending PAHA overnight in a KOH solution with pH approximately 10, to a concentration of 2 g $l^{-1}$, to assure complete resuspension of the sample (6,30). Other PAHA solutions were made from this stock solution.

### Potentiometric proton titrations

Titrations were performed using the Wallingford titration system (61-63). This titrator consists of a thermostatted titration cell, four Metrohm burettes and a Microlink PH4 module (Bio-data Ltd). This module measures electrode potentials down to 0.1 mV and is capable of monitoring up to four electrodes simultaneously. The burettes and PH4 module were interfaced to a PC with a Microlink MF18 interface unit and all control and data acquisition was under PC control.

Prior to the experiments all solutions were degassed thoroughly using water saturated nitrogen gas (Hoekloos 5.0 $N_2$). During a titration the reaction vessel was maintained at a slight overpressure (~1 cm $H_2O$) of nitrogen in order to exclude atmospheric carbon dioxide. The pH was monitored with duplicate glass electrodes (Ingold U272-S7), against a double junction Ag/AgCl reference electrode (Ingold 363-S7). The salt-bridge was filled with a 1 M $KNO_3$ solution. It was observed that leakage of the salt changed the salt concentration in the vessel less than $10^{-3}$ M per 24 hours.

Titrants were prepared from commercial volumetric standards (Tritrisol), 0.1 M $HNO_3$ was used as acid titrant and 0.1 M KOH as base. The base solutions were found to be prone to contamination with carbon dioxide. In order to minimise this problem the purified water was boiled for several hours prior to the preparation of the basic solutions. The exact base concentration was determined by titration with the $HNO_3$ solution.

Typically potentiometric proton titrations of the hematite B/ PAHA mixture used an initial volume of 50 ml. A polypropylene basket was used to prevent adsorption of hematite to the vessel. In general the vessel contained 1 gram of hematite. The PAHA solutions added were made to obtain overall concentrations of 0.0072, 0.036, 0.06 and 0.1 g PAHA $g^{-1}$ hematite. After equilibration at pH 4 for 90 minutes, both to reach equilibrium adsorption as well as to exclude carbon dioxide, successive acid and base titrations were performed at different salt concentrations. $KNO_3$ additions were made without opening the cell at pH 3, using a the burette and the titrations were continued after an equilibration time of 30 minutes. During the titrations the suspension was stirred continuously to prevent settling of the particles. After addition of titrant, the rate of drift was measured over a 2 minute interval after an initial delay of 20 seconds to allow adequate mixing. The electrode readings were accepted when the drift was less than 0.5 mV $min^{-1}$. A maximum reading time of 20 minutes was set for two successive readings. The doses of $HNO_3$ and KOH were calculated by the interface to obtain a constant mV change of 5 mV for each addition, to obtain a good distribution of data points over the pH range studied.

### Results and interpretation

In order to be able to illustrate the division of the added PAHA over the adsorbed amount and the amount remaining in solution the adsorption isotherms of PAHA onto hematite B at pH 4, 6 and 9 and 0.01 M $KNO_3$ as measured previously are redrawn in Figure 1 (33). The symbols present the experimental isotherms, the fitted curves extrapolate the isotherms to higher equilibrium concentration. It has to be mentioned that the lines are just a guide for the eye, they do not have any physical meaning. At the x-axis the equilibrium concentration of PAHA, normalised by the amount of hematite, is given as mg PAHA $g^{-1}$ hematite in solution. At the y-axis the adsorbed amount is given as mg PAHA $g^{-1}$ hematite. The four straight lines drawn in Figure 1 represent added PAHA concentrations of 0.0072, 0.036, 0.06 and 0.1 g PAHA $g^{-1}$ hematite, respectively. The intersection points of the (extrapolated) isotherms with these lines provide the adsorbed amount and the equilibrium concentration of PAHA at the given conditions. The 0.0072 g PAHA $g^{-1}$ hematite line crosses all PAHA adsorption isotherms in the high affinity region of the isotherm, virtually all PAHA is adsorbed at this low PAHA addition. At the highest PAHA addition the extrapolated isotherms are required to estimate the equilibrium concentrations and adsorbed amounts at all pH values. Adsorption isotherms at pH 11 (not shown) indicate that no significant PAHA adsorption occurs several pH units above the p.z.c. of the bare hematite. PAHA adsorption has been shown to be reversible within some hours for pH changes of

several pH units. For small pH changes the adsorbed amount adjusted slowly over a much longer timescale (33,37).
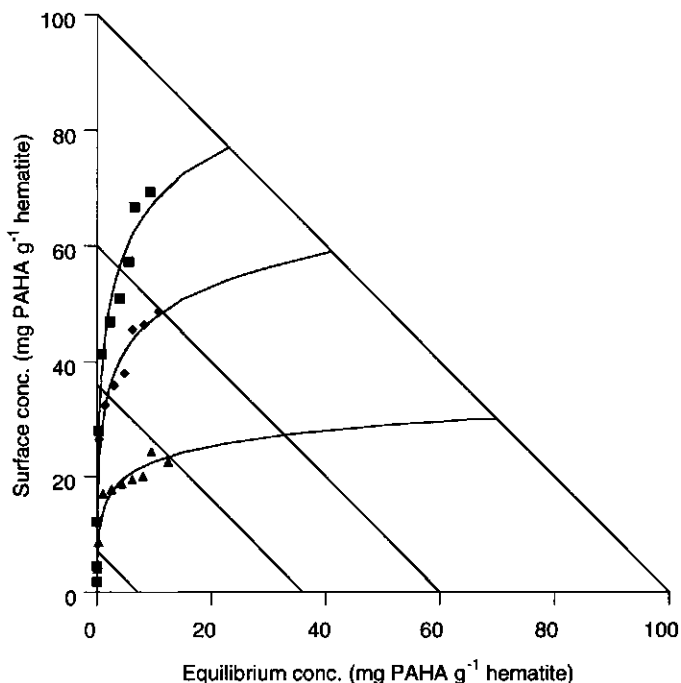


**Figure 1:** Schematic presentation of the adsorption isotherms of PAHA on hematite B, 0.01 M $KNO_3$ and different pH values: ■ pH = 4; ♦ pH = 6; ▲ pH = 9. At the x-axis the equilibrium concentration is given as mg PAHA $g^{-1}$ hematite in solution. At the y-axis the adsorbed amount is given as mg PAHA $g^{-1}$ hematite. The straight lines represent constant PAHA concentrations of 0.0072, 0.036, 0.06 and 0,1 g PAHA $g^{-1}$ hematite, respectively.

Potentiometric proton titrations of the four mixtures were measured at two salt concentrations; 0.1 M and 0.01 M $KNO_3$. Figure 2 presents the results of the different mixtures together with the proton adsorption isotherms of the single components. The titration curves at 0.1 M $KNO_3$ are shown in the left column, those at 0.01 M $KNO_3$ in the right column. At the y-axis the proton adsorption is expressed as mmol of active sites per amount of the component in the mixture. The scale of the sub-figures is the same; the decrease in size going from top to bottom reflects the decreasing total amount of PAHA in the four systems. The hematite B curves are corrected to zero at its p.z.c. The initial PAHA charge of single PAHA at pH 3 was estimated using a separate titration (61,64,65) in combination with pH STAT titrations, and was 0.6 mmol. $g^{-1}$ PAHA in 0.01 M $KNO_3$ and 0.77 mmol. $g^{-1}$ PAHA in 0. 1 M $KNO_3$. These values correspond very well to other reported values for humic acids (6,66). Regarding the fact that no adsorption was observed at pH values several pH units above the p.z.c. of the bare hematite B particles the assumption has been made that that no functional group interactions occurred at pH 10.5.
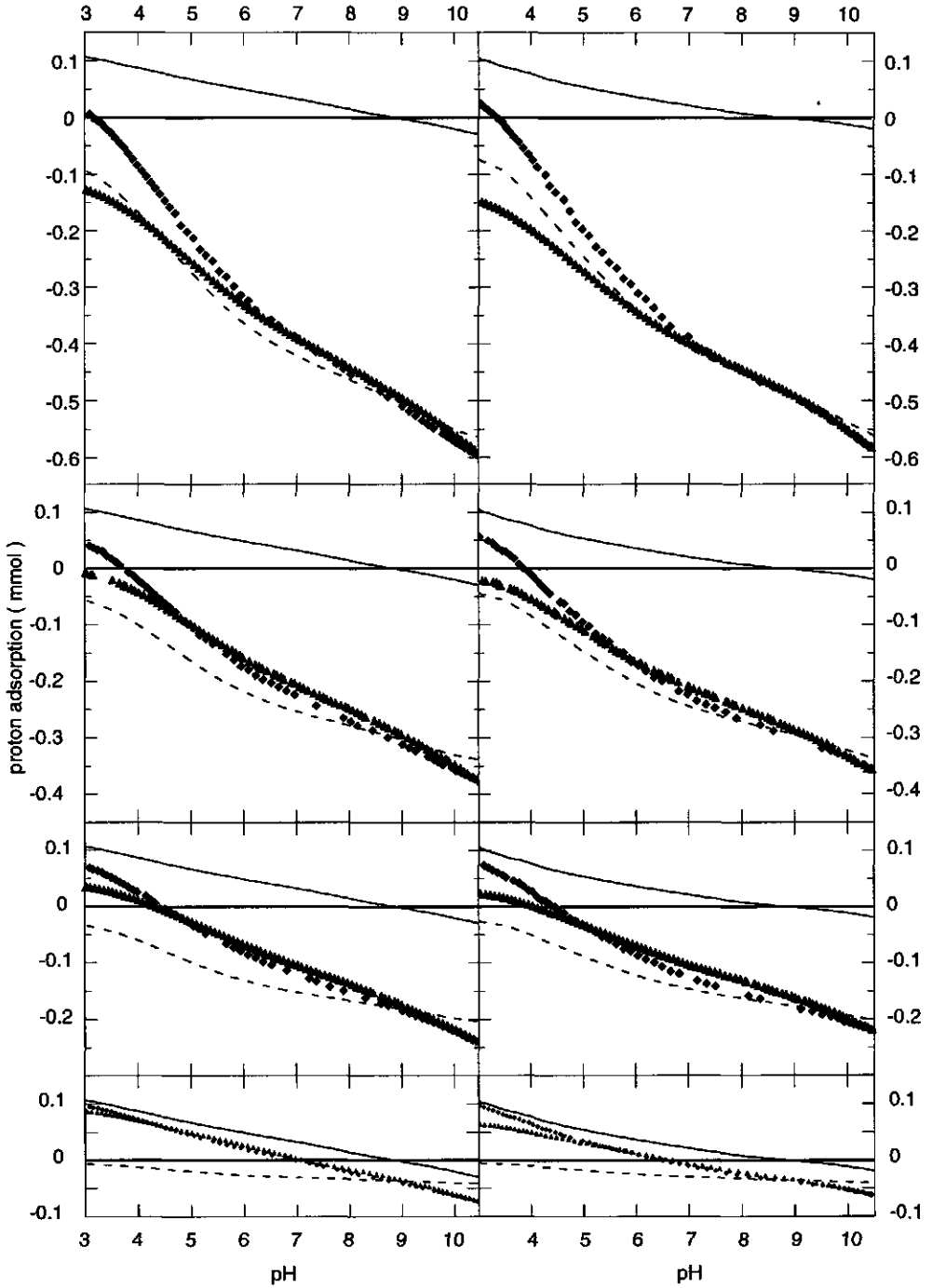
**Figure 2:** Proton adsorption isotherms of the different mixtures of PAHA and 1 g hematite B together with the isotherms of the single components. PAHA concentrations of the mixtures are, from top to bottom, 0.1,

0.06, 0.036 and 0,0072 g PAHA g$^{-1}$ hematite, respectively. Left column 0.1 M KNO$_3$; right column 0.01 M KNO$_3$. At the y-axis the proton adsorption is expressed as mmol per amount of the component in the mixture. The solid line represents the hematite B surface charge/ pH curve; the broken line the PAHA surface charge/ pH curve; ▲ = the actual mixture and ♦ = the non-interacting "PAHA + hematite B" surface charge/ pH curve.

It can be seen that the overall PAHA charge for the 0.0072 g PAHA g$^{-1}$ hematite mixture is much smaller than the hematite B charge, whereas that for the 0.1 g PAHA g$^{-1}$ hematite mixture the PAHA charge exceeds the hematite charge of the oxide by about a factor 6. In discussing the 0.1 g PAHA g$^{-1}$ hematite mixture it has to be taken into account that a significant amount of PAHA is not adsorbed. It is observed that the difference between the actual and the non-interacting mixture curves increases with decreasing salt concentration.

The extent to which the titrateable groups of PAHA and hematite B are involved in adsorption reactions is studied by comparison of the actual proton adsorption isotherms of the mixtures with the sum of the adsorption contributions of PAHA and hematite B, shortly denoted as the non-interacting proton adsorption isotherms. The non-interacting curves in Figure 2 represent the expected proton adsorption of the mixture if there are no functional group interactions between the hematite particles and the PAHA molecules.

The differences between the proton adsorption isotherms of the actual and non-interacting mixtures are quite noticeable. The total proton adsorption over the entire pH range of the actual mixture is less than the sum of the single components. Further it is observed that at low pH the proton adsorption of the mixture falls behind compared with the proton adsorption of the sum of the single components, whereas at higher pH values the sum of adsorptions exceeds the actual mixture adsorption. At the highest PAHA concentration these trends are slightly different due to the high fraction of PAHA molecules in solution. For convenience we will discuss only one of the isotherms, later we will present the final results for all curves. For the mixture of 0.06 g PAHA g$^{-1}$ hematite and 0.01 M KNO$_3$ the difference between the actual and the non-interacting proton adsorption curves is given in Figure 3 (solid symbols). The actual proton adsorption curve represents both the extra charge induced to the oxide by the adsorbed polyelectrolyte and the charge induced to the polyelectrolyte due to the interaction with the hematite surface. Some insight already exists in the behaviour of oxide surfaces due to the adsorption of molecules with a variable charge. Therefore we will use the oxide surface as a guideline throughout our discussion. If we are able to separate the proton adsorption at PAHA and hematite we can subsequently study the affinity spectra of the adsorbed PAHA and compare this spectrum with the affinity spectrum of the dissolved PAHA molecules.

As discussed above, the system under investigation is composed of a weak polyelectrolyte and a surface with a variable charge. Consequently, both components can adjust their degree of dissociation to the local conditions. Due to specific adsorption of PAHA molecules (33) the hematite surface charge is overcompensated at the high pH values by the charges associated with the adsorbed PAHA molecules, even for very low coverages. At pH values above the p.z.c. of the bare hematite particles the surface is only slightly positively or even negatively charged, whereas the PAHA molecules are highly negatively charged. Due to these differences in the charge density the degree of

dissociation of the adsorbed PAHA molecules will be hardly influenced whereas the surface sites of hematite will be strongly affected by the negative field of the PAHA present. The latter aspect is first of all reflected in a shift of the p.z.c. to a higher pH value, as was already discussed in the literature overview given above. At pH values where no adsorption is observed, the induced charge is naturally equal to zero. At low pH values the hematite B particles are highly charged whereas the charge associated with the adsorbed PAHA molecules is relatively low. Even so the adsorbed amounts are relatively high, the overcompensation of the surface charge diminishes or even vanishes with decreasing pH. These effects result in an extra induced surface charge of hematite that can be sketched as a function of pH as a curve that is zero at high pH, slowly increases with decreasing pH and than decreases again for pH values where the overcompensation of the surface charge is diminished. Using electrophoretic mobility measurements (*21-29*) it was shown that even at pH 3 and at very low concentrations of organic matter (order of 10 mg g$^{-1}$ hematite), negative mobilities were found. Due to such a low adsorbed amount it can be concluded that under these circumstances the surface charge of the mineral particles is overcompensated by the charge associated with the adsorbed polyelectrolyte molecules.
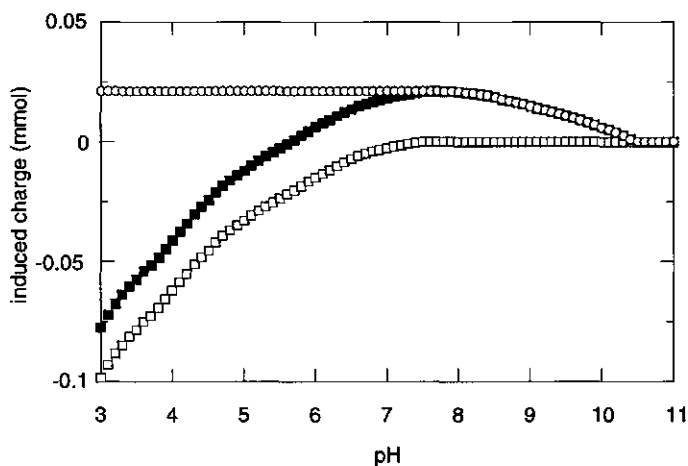


**Figure 3:** The different contributions to the induced charge for 0.06 g PAHA g$^{-1}$ hematite at 0.01 M KNO$_3$: ■ = The measured difference between the actual and the non-interacting mixtures; O = the induced charge attributed to the hematite particles and □ = the induced charge attributed to PAHA.

Based on the above reasoning the positive induced charge up to its maximum will be associated with the hematite surface, see Figure 3. For pH values higher than pH 7 the measured difference is subscribed solely to charge adjustment of the oxide. For lower pH values the charge induced on the oxide is assumed to be constant, as is shown in Figure 3 (open circles). Note that this is only a first order approximation. When the thus obtained extra charge induced on the oxide surface is subtracted from the measured difference between the actual and the non-interacting mixtures, the negative charge induced on the adsorbed polyelectrolyte is obtained. This charge is shown in

Figure 3 by the open squares. It may be noted that when the curvature of the extra induced charge attributed to the oxide is underestimated, the observed effects are even more pronounced.

The induced polyelectrolyte charge for the four different PAHA concentrations at 0.01 M $KNO_3$ is given in Figure 4. At the y-axis the extra charge is expressed as mmol $g^{-1}$ adsorbed PAHA. It is assumed that, for the two lowest PAHA concentrations, the adsorbed amounts of PAHA were maximal over the pH range studied. For the other PAHA concentrations the adsorbed amount was obtained, where necessary, by interpolation using the adsorption isotherms shown in Figure 1. A reversible adsorption/desorption was assumed. As can be seen in Figure 4 at pH values above pH 7, an accurate estimation of the adsorbed amount is not necessary since the induced charge is negligible.
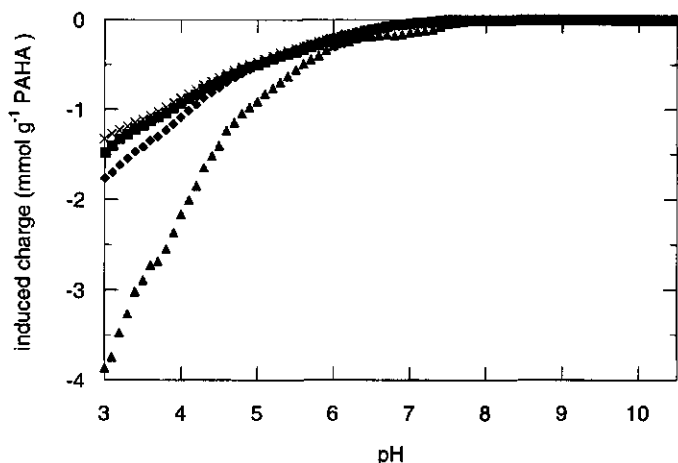


**Figure 4:** Charge induced to PAHA, for different PAHA concentrations; ▲ = 0.0072; ♦ = 0.036; ■ = 0.06 and × = 0,1 g PAHA $g^{-1}$ hematite, 0.01 M $KNO_3$.

It is observed that at low pH, the induced charge increases with decreasing PAHA concentration. At these low pH values, the polyelectrolyte molecules are only slightly charged. Due to the interaction with the hematite surface extra charges are induced to the PAHA molecules. At low PAHA concentrations this leads to a more pronounced effect per gram of PAHA. Figure 5 presents the proton adsorption of adsorbed PAHA as a function of pH. It is observed that at pH values larger than 7 the curves match the charge curve of free PAHA. At lower pH values especially at the low total PAHA amounts it is found that the negative charge of the adsorbed PAHA is increased, due to the interactions with the hematite surface. Proton adsorption isotherms at 0.1 M $KNO_3$ are given in Figure 6. It is observed that due to the more profound screening of the salt ions the induced charge is smaller than with that at 0.01 M $KNO_3$. This is especially true at the low total PAHA amount
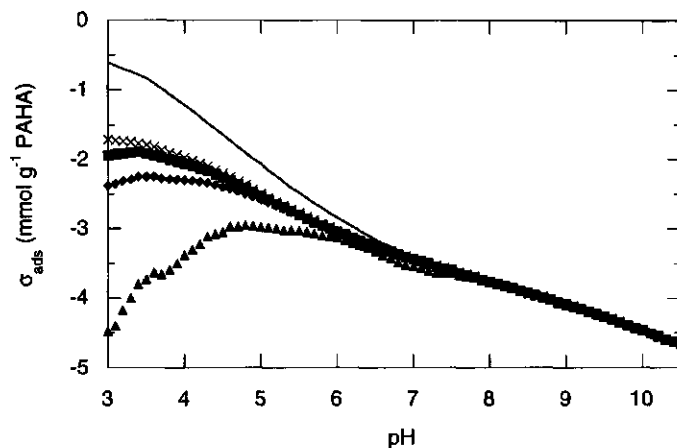
135

**Figure 5:** Proton adsorption isotherms of dissolved (solid line) and adsorbed PAHA, for different PAHA concentrations; 0.01 M $KNO_3$. ▲ = 0.0072; ♦ = 0.036; ■ = 0.06 and × = 0,1 g PAHA $g^{-1}$ hematite.
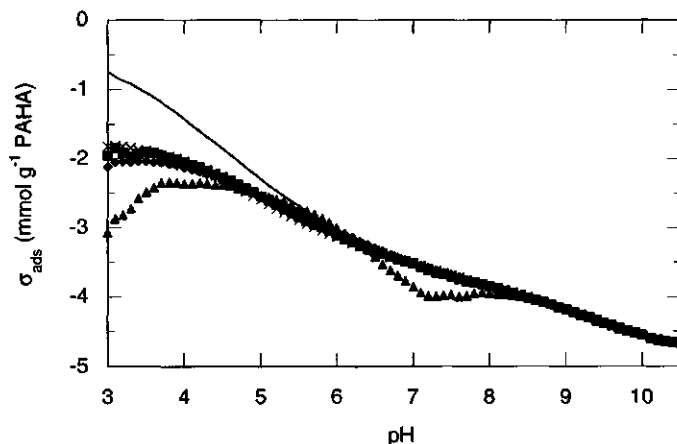


**Figure 6:** Proton adsorption isotherms of dissolved (solid line) and adsorbed PAHA, for different PAHA concentrations; 0.1 M $KNO_3$. ▲ = 0.0072; ♦ = 0.036; ■ = 0.06 and × = 0,1 g PAHA $g^{-1}$ hematite.

To study the differences in the chargeable groups of free and adsorbed PAHA, a heterogeneity analysis can be performed. The heterogeneity of the chargeable groups of free PAHA was already investigated (30). The apparent proton affinity distribution can be approximated by taking the first derivative of the charge/ pH curve (67). This distribution can be used as a fingerprint describing the chargeable groups. The apparent affinity distribution of PAHA in 0.01 M $KNO_3$ is plotted in Figure 7. The error bars indicate the accuracy of the affinity distribution. The description becomes less precise at extreme pH values where the adsorption isotherm is less accurate (61). The apparent affinity distribution reflects a bimodal distribution consisting of two mayor peaks, one at a pK of about 5, reflecting carboxylic type of groups and a second at about pK 10 reflecting phenolic type of groups.

The apparent affinity distribution of the adsorbed PAHA at 0.01 M $KNO_3$ is shown in Figure 8. The affinity distribution is calculated for the 0.1 g PAHA $g^{-1}$ hematite mixture. Although we aware that for this mixture the estimated adsorbed amount was less accurate this proton adsorption isotherm was chosen. This choice was made since it is in principle impossible to calculate an affinity spectrum for a proton adsorption isotherm showing a maximum, as was observed for the other isotherms. Because of the inaccuracy of the determination of the adsorbed amount, compared to the inaccuracy of the calculation of the affinity distribution, no error bars are shown. It is observed that the ratio between the main peaks in the two distributions is altered. Although both affinity distributions are not normalised, it can be concluded that the number of titrateable phenolic groups (distribution with a mean pK of 10) remains constant but that the titrateable carboxylic groups (distribution with a mean pK of 5) decrease significantly.
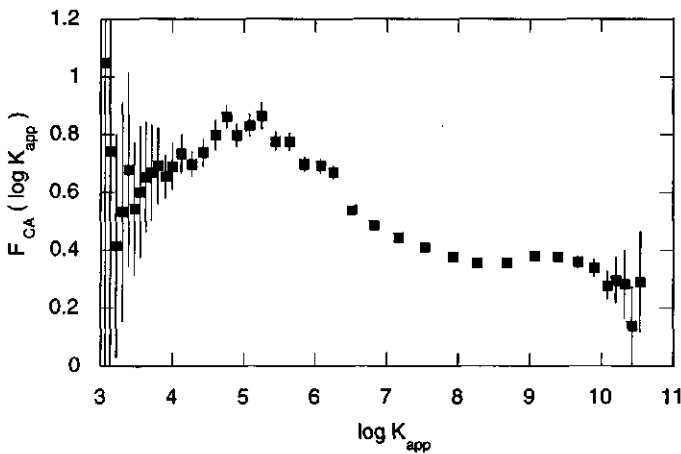


**Figure 7:** The non-normalised apparent CA affinity distribution of free PAHA at 0.01 M KNO3. This result is obtained following Nederlof et al. (67). The error bars indicate the reliability of the calculated curve.


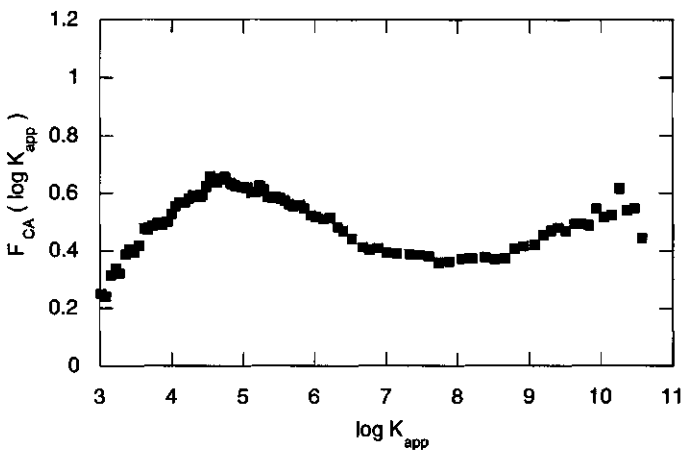
**Figure 8:** The non-normalised apparent CA affinity distribution of PAHA adsorbed onto hematite B. This result is obtained from the 0.1 g PAHA $g^{-1}$ hematite mixture at 0.01 M $KNO_3$, following Nederlof et al. (67).

**Self Consistent Field calculations**

System definition

The system studied above can be further investigated by comparing the results with calculations using the extended SCF theory for polyelectrolyte adsorption onto variably charged surfaces (47). In these calculations the humic acid molecules are modelled as fairly flexible, linear polyelectrolytes. This simplification was shown to give reasonable results in describing the shape and the pH and salt concentration dependencies of the experimental adsorption isotherms of PAHA onto hematite B (33,37).

Within the SCF theory, a polyelectrolyte molecule i is considered as a series of $N_i$ segments numbered $s=1....N_i$. All components (water (W), salt ions ($Na^+$ and $Cl^-$), polyelectrolyte molecules (with segments C, P and U) and the surface sites (S)) are placed in a lattice consisting of M layers of thickness d parallel to the surface layer and numbered from $z = 1$ to $z = M$. On one side of the system at $z = 0$ a layer surface segments is placed. The surface sites have a variable charge. At the other boundary at $z = M + 1$, reflecting conditions are assumed. In each layer, z, each segment type x (x = W, $Na^+$, $Cl^-$, C, P, U, S) of the different molecules experiences a potential u(z) which is the free energy with respect to the bulk solution. This potential is composed of all energetic and entropic interactions a segment undergoes, it depends on average surroundings, nearest neighbour segment-segment interactions and electrostatic interactions (50). The electrostatic interactions are introduced in the model as a series of parallel plate condensers (multi-Stern-layer model) (44,45). The so-called two state approach (46,68) is used to describe the acid-base equilibrium of the polyelectrolytes segments and the surface sites. To evaluate the probabilities of all possible conformations of the polyelectrolyte molecule a first order Markov approach is used. On the basis of these probabilities and the potential u(z) the equilibrium volume fractions $\rho_i(z)$ are calculated for all components in the system. Since the volume fraction of a specific component both depends on and determines the potential energy, a self consistent equilibrium solution has to be determined numerically. Once u(z) and $\rho_i(z)$ are determined other thermodynamic properties of the system can be derived.

The degree of dissociation, $\alpha_{x,\beta}$, is defined as a monomer property, where $\beta(z)$ equals the internal state ($\beta(z) = 0, 1; 1 =$ dissociated) of the chargeable unit. This internal state is determined by the local pH(z). The local pH(z) is determined by the bulk pH and the electrostatic potential in layer z. Within this theory it is possible to study separately the degree of dissociation of the surface sites and that of the adsorbed polyelectrolyte segments. A polyelectrolyte molecule is treated as adsorbed if at least one segment is in direct contact with the surface.

Choice of parameters

The calculations were performed using a lattice of simple cubic symmetry with a characteristic size d of 0.311 nm and M = 100. The latter value was chosen to assure that all concentration and potential profiles were relaxed in the bulk of the system

(equal to 0). All polyelectrolyte segments in the bulk are indistinguishable; irrespective of the position of the segment along the chain each segment feels $\psi = 0$. The surface (S) is composed of two types of hydrophilic sites a charged and a neutral one, in the ratio of 1 : 1. The charged site has a pK of 9 and is titrated from 0.5 to -0.5 according to the one pK model (34,69). For the present choice of the lattice cell this results in a maximum density of 5.2 charged segments $nm^{-2}$. The polyelectrolytes are taken to be linear with three type of segments; U, C and P where segment U is uncharged, segment C has a pK of 4 and P a pK of 10. The chargeable segments of the polyelectrolyte are titrated from 0 to -1. All segments have a dielectric constant $\varepsilon_r$ of 80. The composition of the polyelectrolyte chain is: $U_{12}(C_4U_2P_2U)_{16}U_{40}C_4$. This molecule intends to mimic the PAHA molecules, with two type of charged segments representing carboxylic and phenolic type of groups (33) together with two blocs of uncharged segments. The ratio U : C : P was based on the composition of PAHA. The C segments have a specific adsorption energy with the surface, expressed as a Flory-Huggins $\chi$ parameter (70). For all calculations $\chi_{sc} = -15$. All other $\chi$ parameters are zero.

Charge densities and electric potentials

In a simple plate condensor model the relation between the plate charge, $\sigma$, and the potential drop, $\Delta\psi$, over the plates is given by Eq. 7.1:

$$\sigma_0 = \psi_0 {}^* C \qquad (7.1)$$

where C is the electrostatic capacitance of the condensor, which is defined as:

$$C = \frac{\varepsilon_0 \varepsilon_r}{d} = \frac{\varepsilon}{d} \qquad (7.2)$$

where $\varepsilon_0 \varepsilon_r$ is the permittivity in between the condensor plates. In the lattice model the charges are placed in the mid-planes of the lattice layers. In the present calculations all permittivities are set to be equal. The condensor plates in the model may therefore coincide with the midplanes of the lattice layers. (In the case that $\varepsilon$ is not the same throughout the system the number of model condensors has to be twice the number of lattice layers to account for the jumps in $\varepsilon$. Within the presented calculations the electrostatic potential difference between two successive charge planes varies linearly with distance. This is analogous to the potential decay in the Stern layer. Now the electrical field strength (Eq.7.3) at a distance z from the surface equals:

$$E(z) = \frac{1}{\varepsilon} \sum_{z'=0}^{z} \sigma(z') \qquad (7.3)$$

and hence the electrostatic potential difference (Eq.7.4) between two successive layers is given by:

$$\psi(z) - \psi(z+1) = \int_{x=(z-\frac{1}{2})d}^{(z+\frac{1}{2})d} E(x)dx = \frac{d}{\epsilon} \sum_{x=0}^{z} \sigma(x) \qquad (7.4)$$

The charge density in each layer is calculated following Eq.7.5:

$$\sigma(z) = \sum_{x} \sum_{\beta} \upsilon_{x,\beta} \, e \, \alpha_{x,\beta}(z) \, \rho_x(z) / d^2 \qquad (7.5)$$

where e equals the elementary charge, $\upsilon_{x,\beta}$ is the valence of segment type x in reference state $\beta$, $\alpha_{x,\beta}$ the degree of dissociation of segment type x in reference state $\beta$ and $\rho_x(z)$ is the volume fraction of segment x in layer z. For the chargeable polymer units $\upsilon_{C,0} = \upsilon_{P,0} = 0$ or $\upsilon_{C,1} = \upsilon_{P,1} = -1$, for the surface $\upsilon_{S,0} = 1/2$ or $\upsilon_{S,1} = -1/2$, $\upsilon_{Na} = 1$, $\upsilon_{Cl} = -1$, $\upsilon_{U} = 0$ and $\upsilon_{W} = 0$.


Results


Figure 9a presents the calculated surface charge/ pH curves of the uncovered surface as well as that of the surface with an adsorbed polyelectrolyte layer for different overall polyelectrolyte concentrations and 0.01 M salt. It is shown that the surface charge increases with increasing polyelectrolyte concentration over the entire pH range studied and that the p.z.c. of the surface is shifted to a higher pH value due to the adsorption of polyelectrolyte molecules. At the three highest concentrations the surface is almost completely protonated at pH values lower than pH 5 and hence no further charge can be induced. The maximum surface charge for the present system is 432 mC m$^{-2}$. Due to the specific adsorption energy the charges associated with the adsorbed polyelectrolyte overcompensate the initial surface charge. The increasing surface charge is due to the lower pH close to the surface compared with that in the bulk due to the reduction of the positive field in the vicinity of the surface. The difference in surface charge between the surface in the presence and absence of polyelectrolyte is given in Figure 9b. These curves reveal the extra surface charge induced by the specific adsorption of the negatively charged polyelectrolyte molecules. All curves display a maximum that shifts to a lower pH as the polyelectrolyte concentration increases. Again the curves with the three highest concentrations coincide since the maximal surface charge is reached. The corresponding charge/ pH curves of the adsorbed polyelectrolyte are given in Figure 9c together with the charge/ pH curve of a single polyelectrolyte molecule in bulk solution at a bulk polyelectrolyte concentration of 0.01 and a salt concentration of 0.01 M salt (the procedure to calculate the bulk properties of a polyelectrolyte molecule is given elsewhere (47)). The differences observed at pH values above pH 8 are attributed to the different bulk concentrations within the calculations of the adsorbed polyelectrolyte behaviour. With decreasing bulk concentration the degree of dissociation of the adsorbed polyelectrolyte molecules is inhibited due to the electrostatic repulsion of the already dissociated polyelectrolyte segments. Figure 9d presents the extra polyelectrolyte charge induced by the interaction with the surface. It is observed that at low pH values the initial charge increases strongly with decreasing polyelectrolyte concentration. At these pH values, all the C type polyelectrolyte groups

are titrated by the highly charged surface. At the higher pH values no effect is observed on the polyelectrolyte charge. Thus it is concluded that both the surface charge and the charge of the polyelectrolyte molecules adapt strongly to the local conditions. The slightly positive apparent polyelectrolyte charge at pH 5 for the highest polyelectrolyte concentrations is a combined effect of the relatively small interaction by the surface and the low high concentration compared with the free polyelectrolyte.
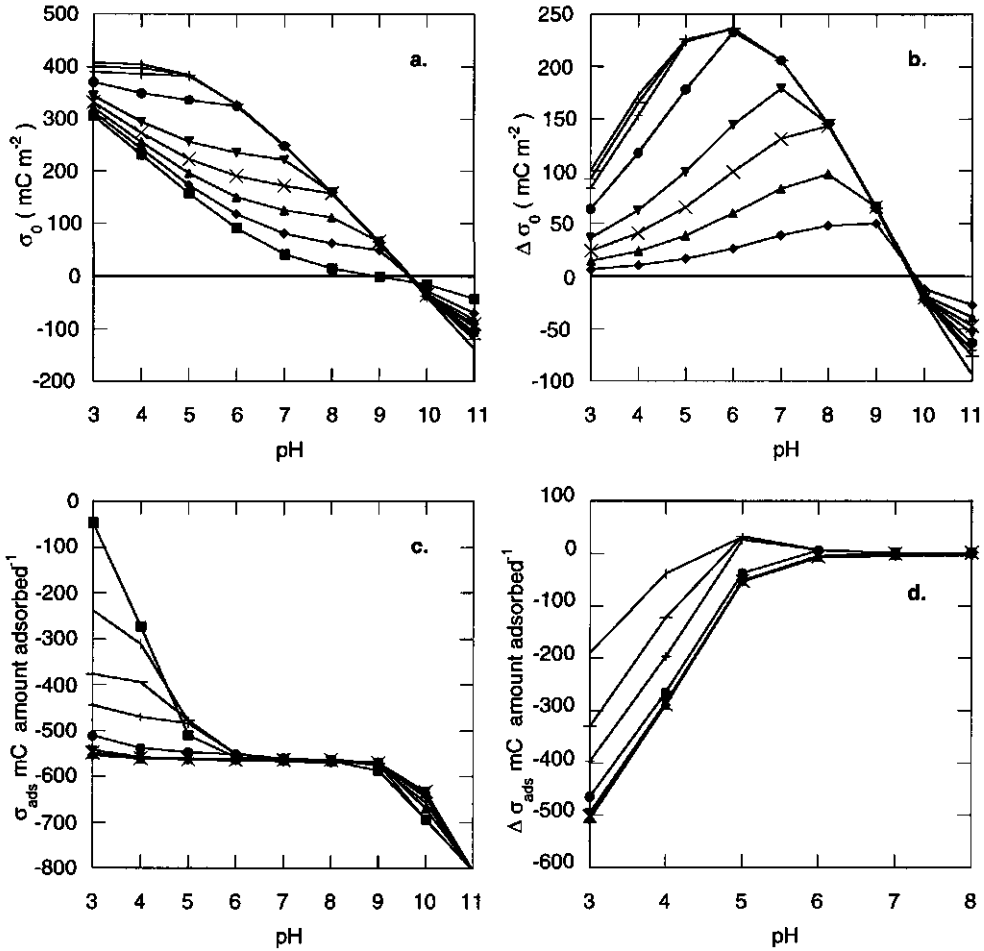


**Figure 9:** Calculated proton adsorption isotherms as a function of the polyelectrolyte concentration. The salt concentration was 0.01 M. The surface consists of segments with a pK value of 9 and is titrated from 0.5 to -0.5, the surface density is 5.2 chargeable groups $nm^{-2}$.The polyelectrolyte has two different chargeable segments with pK values of respectively 4 (C) and 10 (P) that are titrated from 0 to -1. All components have a dielectric constant $\epsilon$, of 80. Polyelectrolyte segment C has an attractive energy to the surface expressed as a Flory-Huggins parameter ($\chi_{cs} = -15$). **a)** Surface charge in the absence (■) and presence of polyelectrolyte, where the number of equivalent monolayers of polyelectrolyte ($\theta$) = 0.1 (♦), 0.2 (▲), 0.3 (×), 0.4 (▼), 0.6 (●), 0.8 (+), 1 (–) and 2 (I). **b)** Surface charge induced by the polyelectrolyte **c)** proton adsorption of the free (■) and adsorbed polyelectrolyte. **d)** charge induced by the surface.

Due to these differences in the charge densities, the electrostatic potentials are affected. The surface potential and the potential within the first layer are given in Figure 10a and b, respectively.
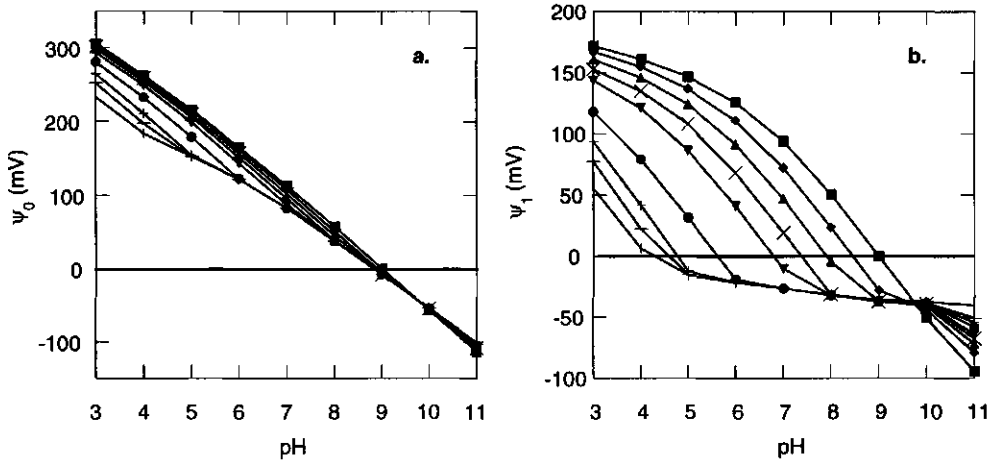


**Figure 10:** Calculated potential as a function of pH. **a)** Surface potential ($\psi_0$). **b)** Potential in the first layer ($\psi_1$). All conditions are the same as in Figure 9.

The surface potential of the uncovered surface is pseudo Nernstian (Eq. 7.6) , where all symbols have the usual meaning. At high surface coverage's the surface potential deviates seriously from the Nernst law due to the screening of the adsorbed polyelectrolyte.

$$\Psi_0 = \frac{2.3RT}{F}\left[\left(pH_{pzc} - pH\right) - \log\frac{\left[SH^{\frac{1}{2}+}\right]}{\left[S^{\frac{1}{2}-}\right]}\right] \tag{7.6}$$

The differences between the potentials within the first layer are far more pronounced due to the increasing accumulation of counter-charge in layer 1 with increasing adsorbed amount. According to Eq.7.1 combined with Eq.7.4, the potential drop over the first layer depends on the surface charge and the overall charge in the first layer. For a constant pH, $\psi_1$ is proportional to $\Delta\sigma$ and thus strongly depends on the charge associated with the adsorbed polyelectrolyte and the total amount of indifferent electrolyte in layer 1. However, the latter is negligible since the salt ions can hardly compete with the specific adsorbing polyelectrolyte segments. As a consequence; the pH at which, for a constant polyelectrolyte concentration, $\psi_1$ becomes zero must be seen as the pH at which the adsorbed polyelectrolyte compensates the surface charge. As one compares Figure 9b with Figure 10b it is observed that the pH at the maxima of Figure 9b correspond with the pH at which the adsorbed polyelectrolyte charge exceeds the surface charge. At lower pH values the number of chargeable groups associated with the polyelectrolyte molecules is not sufficient to compensate the surface charge, the segments with a pK value of 4, of the polyelectrolyte molecules are

almost completely titrated by the surface. At higher pH values the adsorbed amounts decrease whereas the charge on the polyelectrolyte molecules increases, consequently no effect is observed on the degree of dissociation of the polyelectrolyte. However, the p.z.c. of the surface shifts to a higher pH value and the surface is titrated by the adsorbed polyelectrolyte.

## Discussion

Experiments indicated that due to the adsorption of PAHA molecules onto the hematite B particles, both components were able to adjust their charge. Potentiometric proton titrations clearly showed that the actual charge found by titration of the mixture was not a simple summation of the initial charges associated with the single components as was proposed by Baker (41). Neither could the difference between the real situation and the non-interacting mixture be subscribed to the organic fraction only, as mentioned by Newcombe and Morris (22,40).

A main aspect in the adsorption process is a specific adsorption energy due to which adsorption occurred at pH values upto 1 pH unit above the p.z.c. of the bare hematite particles. Further the hematite surface charge may become overcompensated by the charges associated with the adsorbed PAHA due to the specific adsorption energy. The latter aspect is commonly observed in electrophoretic mobility measurements of oxide particles coated with humics (21-29), even for very low humic acid concentrations where the potential maximum charge of the humic hardly exceeds the surface charge.

The experimental results were compared with SCF calculations for weak polyelectrolytes near a surface with a variable charge. It was observed that at low pH extra charge was induced mainly on the polyelectrolyte, whereas at high pH extra charge was induced mainly on the surface. It was shown that the degree of overcompensation of the overall surface charge by the polyelectrolyte in direct contact with the surface determined which component was most significant titrated. The trends observed with the calculations were remarkably similar to those that were derived from the experimental data.

Considering these calculations a better insight has been obtained in the factors controlling the extra charge attributed to the oxide. In Figure 3 we assumed that the shape of the extra charge induced to the oxide was as shown by the open circles. We already recognised that this was only a crude approximation, however an approximation that was rather close to the true curvature. By combining the results of Figure 9b and Figure 10b we concluded that the charge induced to the surface increased slowly with decreasing pH until a pH was reached where the adsorbed polyelectrolyte no longer overcompensated the surface charge. At pH values lower than this pH the extra induced surface charge decreased again. It was shown that the pH value at which this inflection occurred depends on the adsorbed amount of polyelectrolyte. As mentioned above it is well known that the surface charge of oxide particles is already overcompensated by the adsorbed humics at pH values around pH 3 for very low humic acid concentrations. Based on these observations combined with

the calculated curvature of the charge induced on the surface we may conclude that the curve as shown in Figure 3 was reasonable. Although it is expected that at pH values lower than pH 7 the true curve was still slowly increasing with a maximum at about pH 3 we may expect that this extra increase was only small since we already induced about 25 % extra charge to the initial surface charge. Again it is emphasised that when the curvature of the extra induced charge attributed to the oxide is underestimated, the observed effects are even more pronounced.

Based on these results we can apply the following mechanistic model for the adsorption of humic acids onto mineral particles. As discussed before (33), the humic acid molecules adsorb onto the hematite surface forming an extended layer which can be described by trains, loops and tails. Due to such a layer numerous humic acid groups are not in direct contact with the surface and are not necessarily involved in the charge compensation of the surface. On the other hand, extra charges are induced to the acid groups of PAHA that are in the vicinity of the surface. It is clear that the induced charges can be attributed to the humic acid segments in direct contact with the surface, thus the induced charges are adsorption sites and can be described as train segments, segments bound in the first layer next to the surface. It seems very clear that these sites are less available for further cation binding. At lower PAHA concentrations an increasing number of charged groups per PAHA molecule are adsorbed at the surface and can be described as train segments. (Such an increased fraction of train segments with decreasing polymer concentration was also measured by Meadows et al. (71), studying ESR spectra of hydrolysed polyacrylamide on cationic polystyrene latex.) Further the charged PAHA segments adsorbed in loops and tails may cause the development of a negative electrostatic potential field close to the surface. Due to this negative potential the proton concentration in the vicinity of the surface will be increased compared to that in the bulk, resulting in a higher surface charge which is reflected in a shift of the p.z.c. to a higher pH, by about 1 pH unit.

## Conclusions

Analysing proton adsorption isotherms of mixed systems it was shown that extra charges are induced to the humic acid to compensate the charge associated with the oxide surface. A considerable fraction of the dissociated carboxylic groups, initially dissociated and induced, are involved as binding sites with the oxide surface and may be described as train segments, following the description commonly used in the polyelectrolyte adsorption theory. Consequently these binding sites will be less available for specific binding to other ions in the solution. They seem to be partially withdrawn from the system for proton binding, which is reflected in the affinity spectrum of adsorbed PAHA. Vice versa it is shown that extra surface charges are induced to the oxide surface due to the specifically adsorbed humic acid molecules. Charged species screen the surface charge to an extent that depends on their concentration. Due to this screening, other small ions can accumulate in the vicinity of the surface and accomplice a change in the surface charge. This is reflected in a shift of the p.z.c. of the hematite surface to a higher pH value. It may be concluded that both surface and polyelectrolyte

are titrated due to the presence of each other. The component that influences the potential in the first layers most significantly determines which process dominates. At low pH and low surface coverage the main effect can be observed on the humic acid, at high pH values the surface charge of the hematite particles is mainly affected.

## Environmental impact

Potentiometric proton titration of mixed systems are useful to estimate the impact of various environmental changes on the bioavailability of metal ions. The possible application of laboratory experiments to estimate the speciation of metal ions is improved by the described experiments. In real environmental systems, in which binding of the organic fraction and metal ions to oxides and clays is a second order effect, results have already been obtained (72). However, in numerous environmental systems some of the binding sites of the organic soil fraction may be masked or neutralised by the interaction with the metal oxide surfaces or other mineral components of the soil matrix. Within this paper, the effects of interactions between the different soil components on the available binding sites of both the organic and the mineral species have been described in detail.

The approach developed above could be of help in interpreting the bioavailability of metal ions in soils and fresh waters. Using the adsorption characteristics of these mixed systems a more sophisticated speciation model can be developed. The present understanding shows that for organics in contact with minerals binding sites are on the organics and gained on the minerals. Which process dominates; can be predicted based on the adsorbed amount and the pH and salt composition of the system.

It can be concluded that by incorporating the findings discussed in this paper, the metal ion speciation in natural systems can be better understood. In a later paper (73) we will describe the cadmium adsorption to the mixture of PAHA and hematite B based on the above described proton adsorption data.

### References

(1) Benedetti, M.F.; Milne, C.J.; Kinniburgh, D.G.; Van Riemsdijk, W.H.; Koopal, L.K. Metal Ion Binding to Humic Substances: Application of the Non-Ideal Competitive Adsorption Model. *Environ.Sci.Technol.* **1995**, *29(2)*, 446 -456.

(2) Tipping, E. Modeling ion binding by humic acids. *Colloids Surf.A* **1993**, *73*, 117 -131.

(3) Ephraim, J.H.; Marinsky, J.A.; Cramer, S.J. Complex-forming properties of natural organic acids. *Talanta* **1989**, *36(4)*, 437 -444.

(4) Dzombak, D.A.; Fish, W.; Morel, F.M.M. Metal-Humate Interactions. 1. Discrete Ligand and Continuous Distribution Models. *Environ.Sci.Technol.* **1986**, *20(7)*, 669 -675.

(5) Milne, C.J.; Kinniburgh, D.G.; De Wit, J.C.M.; Van Riemsdijk, W.H.; Koopal, L.K. Analysis of Metal-Ion Binding by Peat Humic Acid Using a Simple Electrostatic Model. *J.Colloid Interface Sci.* **1995**, *175*, 448 -460.

(6) Milne, C.J.; Kinniburgh, D.G.; De Wit, J.C.M.; Van Riemsdijk, W.H.; Koopal, L.K. Analysis of proton binding by peat humic acid using a simple electrostatic model. *Geochim.Cosmochim.Acta* **1995**, *59(6)*, 1101 -1112.

(7) Marinsky, J.A.; Reddy, M.M. Proton and metal ion binding to natural organic polyelectrolytes-II. Preliminary investigations with a peat and a humic acid. *Org.Geochem.* **1984**, *7(3/4)*, 215 -221.

(8) Bartschat, B.M.; Cabaniss, S.E.; Morel, F.M.M. Oligoelectrolyte Model for Cation Binding by Humic Substances. *Environ.Sci.Technol.* **1992**, *26(2)*, 284 -294.

(9) Fokkink, L.G.J.; De Keizer, A.; Lyklema, J. Specific Ion Adsorption on Oxides: Surface Charge Adjustment and Proton Stoichiometry. *J.Colloid Interface Sci.* **1987**, *118*, 454 -462.

(10) Venema, P.; Hiemstra, T.; Van Riemsdijk, W.H. Multiple site modelling of cadmium adsorption on goethite using an extended data set. *J.Colloid Interface Sci.* **1996**, , submitted

(11) Johnson, B.B. Effect of pH, Temperature, and Concentration on the Adsorption of Cadmium on Goethite. *Environ.Sci.Technol.* **1990**, *24(1)*, 112 -118.

(12) Gutzman, D.W.; Langford, C.H. Multicomponent kinetic analysis of trace metal binding sites on iron hydrous oxide colloids. *Water Poll.Res.J.Canada* **1988**, *23(3)*, 379 -387.

(13) Breeuwsma, A.; Lyklema, J. Interfacial electrochemistry of haematite. *Discussions of The Faraday Soc.* **1971**, *52*, 324 -333.

(14) Benjamin, M.M.; Leckie, J.O. Multiple-Site Adsorption of Cd, Cu, Zn, and Pb on Amorphous Iron Oxyhydroxide. *J.Colloid Interface Sci.* **1981**, *79(1)*, 209 -221.

(15) Tipping, E. Adsorption by goethite of humic substances from three different lakes. *Chem.Geo.* **1981**, *33*, 81 -89.

(16) Gu, B.; Schmitt, J.; Chen, Z.; Liang, L.; McCarthy, J.F. Adsorption and Desorption of Natural Organic Matter on Iron Oxide: Mechanisms and Models. *Environ.Sci.Technol.* **1994**, *28(1)*, 38 -46.

(17) McKnight, D.M.; Wershaw, R.L.; Bencala, K.E.; Zellweger, G.W.; Feder, G.L. Humic substances and trace metals associated with Fe and Al oxides deposited in an acidic mountain stream. *Sci.Total Environ.* **1992**, *117/118*, 485 -498.

(18) Davis, J.A. Adsorption of natural dissolved organic matter at the oxide/water interface. *Geochim.Cosmochim.Acta* **1982**, *46*, 2381 -2393.

(19) Murphy, E.M.; Zachara, J.M.; Smith, S.C.; Philips, J.L. The sorption of humic acids to mineral surfaces and their role in contaminant binding. *Sci.Total Environ.* **1992**, *117/118*, 413 -423.

(20) McD.Day, G.; Hart, B.T.; McKelvie, I.D.; Beckett, R. Adsorption of natural organic matter onto goethite. *Colloids Surf.A* **1994**, *89*, 1 -13.

(21) Tipping, E.; Cooke, D. The effects of adsorbed humic substances on the surface charge of goethite in freshwaters. *Geochim.Cosmochim.Acta* **1982**, *46*, 75 -80.

(22) Morris, G.; Newcombe, G. Granual Activated Carbon: The Variation of Surface Properties with the Adsorption of Humic Substances. *J.Colloid Interface Sci.* **1993**, *159*, 413 -420.

(23) Hunter, K.A. On the estarine mixing of dissolved substances in relation to colloid stability and surface properties. *Geochim.Cosmochim.Acta* **1983**, *47*, 467 -473.

(24) Beckett, R.; Le, N.P. The Role of Organic Matter and Ionic Composition in Determining the Surface Charge of Suspended Particles in Natural Waters. *Colloids Surf.* **1990**, *44*, 35 -49.

(25) Davis, J.A.; Gloor, R. Adsorption of Dissolved Organics in Lake Water by Aluminum Oxide. Effect of Molecular Weight. *Environ.Sci.Technol.* **1981**, *15(10)*, 1223 -1229.

(26) Liang, L.; Morgan, J.J. Coagulation of Iron Oxide Particles in the Presence of Organic Materials. *ACS Symp.Ser.,416,Chemical modelling of aqueous systems II*, **1990**, , 293 -308.

(27) Righetto, L.; Bidoglio, G.; Azimonti, G.; Bellobono, I.R. Competitive Actinide Interactions in Colloidal Humic Acid-Mineral Oxide Systems. *Environ.Sci.Technol.* **1991**, *25(11)*, 1913 -1919.

(28) Amirbahman, A.; Olson, T.M. Transport of Humic Matter-Coated Hematite in Packed Beds. *Environ.Sci.Technol.* **1993**, *27(13)*, 2807 -2813.

(29) Amal, R.; Raper, J.A.; Waite, T.D. Effect of Fulvic Acid Adsorption on the Aggregation Kinetics and Structure of Hematite Particles. *J.Colloid Interface Sci.* **1992**, *151(1)*, 244 -257.

(30) Vermeer, A.W.P. this Thesis. Chapter 4: Proton and Cadmium binding to purified Aldrich humic acid, exploration of the NICA-Donnan model.

(31) Breeuwsma, A.; Lyklema, J. Physical and chemical adsorption of ions in the electric double layer in hematite ($\alpha$-$Fe_2O_3$). *J.Colloid Interface Sci.* **1973**, *43*, 437 -448.

(32) Penners, N.H.G.; Koopal, L.K.; Lyklema, J. Interfacial Electrochemistry of Haematite: Homodisperse and Heterodisperse Sols. *Colloids Surf.* **1986**, *21*, 457 -468.

(33) Vermeer, A.W.P. this Thesis. Chapter 5: Interactions between humic acid and mineral particles.

(34) Koopal, L.K. Ion adsorption on mineral oxide surfaces In *Adsorption on new and modified inorganic sorbents*; Dabrowski, A.; Tertykh, V.A. Eds.; Elsevier: Amsterdam, 1996; 757-796.

(35) Koopal, L.K. Mineral Hydroxydes: from homogeneous to heterogeneous modelling. *Electrochim. Acta* **1996**, *41(14)*, 2293 -2306.

(36) Venema, P.; Hiemstra, T.; Van Riemsdijk, W.H. Comparison of Different Site Binding Models for Cation Sorption: Description of pH Dependency, Salt Dependency, and Cation-Proton Exchange. *J.Colloid Interface Sci.* **1996**, *181*, 45 -59.

(37) Vermeer, A.W.P. this Thesis. Chapter 6: Adsorption fractionation of humic substances at mineral surfaces, experiments compared with theory.

(38) Cohen Stuart, M.A.; Fleer, G.J.; Lyklema, J.; Norde, W.; Scheutjens, J.M.H.M. Adsorption of Ions, Polyelectrolytes and Proteins. *Adv.Colloid Interface Sci.* **1991**, *34*, 477 -535.

(39) Cohen Stuart, M.A. Polyelectrolyte adsorption. *J.Phys.France* **1988**, *49*, 1001 -1008.

(40) Newcombe, G. Activated Carbon and Soluble Humic Substances: Adsorption, Desorption, and Surface Charge Effects. *J.Colloid Interface Sci.* **1994**, *164*, 452 -462.

(41) Baker, A.R. Ph. D. thesis, University of Southampton, England. Proton and metal ion interactions of fulvic acid solutions and of alumina and alumina/ fulvic acid suspensions.

(42) Van Riemsdijk, W.H.; Lyklema, J. The reaction of phosphate with aluminium hydroxide in relation with phosphate bonding in soils. *J.Colloid Interface Sci.* **1980**, *76*, 55 -66.

(43) Stumm, W.; Kummert, R.; Sigg, L. A Ligand Exchange Model for the Adsorption of Inorganic and Organic Ligands at Hydrous Oxide Interfaces. *Croat.Chem.Acta* **1980**, *53(2)*, 291 -311.

(44) Böhmer, M.R.; Evers, O.A.; Scheutjens, J.M.H.M. Weak Polyelectrolytes between Two Surfaces: Adsorption and Stabilization. *Macromolecules* **1990**, *23(8)*, 2288 -2301.

(45) Evers, O.A.; Fleer, G.J.; Scheutjens, J.M.H.M.; Lyklema, J. Adsorption of Weak Polyelectrolytes from Aqueous Solution. *J.Colloid Interface Sci.* **1986**, *111(2)*, 446 -453.

(46) Israëls, R.; Leermakers, F.A.M.; Fleer, G.J. On the Theory of Grafted Weak Polyacids. *Macromolecules* **1994**, *27(11)*, 3087 -3093.

(47) Vermeer, A.W.P. this Thesis. Chapter 2: Adsorption of a weak polyelectrolyte on a surface with a variable charge, Self Consistent Field calculations.

(48) Scheutjens, J.M.H.M.; Fleer, G.J. Statistical Theory of the Adsorption of Interacting Chain Molecules. 2. Train, Loop, and Tail Size Distribution. *J.Phys.Chem.* **1980**, *84*, 178 -190.

(49) Scheutjens, J.M.H.M.; Fleer, G.J. Statistical theory of the adsorption of interacting chain molecules. I. Partition function, segment density distribution and adsorption isotherms. *J.Phys.Chem.* **1979**, *83*, 1619 -1635.

(50) Fleer, G.J.; Cohen Stuart, M.A.; Scheutjens, J.M.H.M.; Cosgrove, T.; Vincent, B. *Polymers at Interfaces*; Chapman & Hall: London, 1993.

(51) Van der Schee, H.A.; Lyklema, J. Adsorption of oligo- and polypeptides on AgI, their effects on double layer and colloidal stability. The effect of polymers on dispersion properties. Tadros TF. London. Academic Press. 1982 81-100.

(52) Lyklema, J. *Fundamentals of Interface and Colloid Science*; Academic Press: London, 1991.

(53) Ardizzone, S.; Formaro, L.; Lyklema, J. Adsorption from mixtures containing mono- and bivalent cations on insoluble oxides and a revision of the interpretation of points of zero charge obtained by titration. *J.Electranal.Chem.* **1982**, *133*, 147 -156.

(54) Formaro, L.; Giannantonio, R.; Pastorelli, C.; Carli, R. A Hydrophobic Patchwise Heterogeneous Oxide Surface. *J.Phys.Chem.* **1992**, *96(8)*, 3197 -3200.

(55) Djafer, M.; Lamy, I.; Terce, M. Interaction of metallic cations with the hydrous goethite surface. *Prog. Colloid Polym. Sci.* **1989**, *79*, 150 -154.

(56) Zhang, Y.; Kallay, N.; Matijevíc, E. Interactions of Metal Hydrous Oxides with Chelating Agents. 7. Hematite-Oxalic Acid and -Citric Acid Systems. *Langmuir* **1985**, *1(2)*, 201 -206.

(57) Torres, R.J.; Kallay, N.; Matijevíc, E. Adsorption at Solid/Solution Interfaces. 5.Surface Complexation of Iminodiacetic Acid on Hematite. *Langmuir* **1988**, *4(3)*, 706 -710.

(58) Kallay, N.; Matijevíc, E. Adsorption at Solid/Solution Interfaces. 1. Interpretation of Surface Complexation of Oxalic and Citric Acids with Hematite. *Langmuir* **1985**, *1(2)*, 195 -201.

(59) Gebhardt, J.E.; Feurstenau, D.W. Adsorption of polyacrylic acid at oxide/water interfaces. *Colloids Surf.* **1983**, *7*, 221 -231.

(60) Vermeer, A.W.P.; Koopal, L.K. submitted to *Environ.Sci.Technol.* this Thesis. Chapter 3: Characterisation and classification of purified Aldrich humic acid.

(61) Vermeer, A.W.P. this Thesis. Appendix I: Potentiometric proton titrations, experimental set-up and data treatment.

147

(62) Kinniburgh, D.G.; Milne, C.J.; Venema, P. Design and Construction of a Personal-Computer-Based Automatic Titrator. *Soil Sci.Soc.Am.J.* **1995**, *59(2)*, 417 -422.

(63) Kinniburgh, D.G.; Milne, C.J. Guide to the Wallingford Titrator; Technical report. WD/93/23. British Geological Survey: Keyworth, Nottinghamshire. 1993.

(64) Boehm, H.P.; Diehl, E. Untersuchung an sauren Oberflächenoxyden des Kohlenstoffs. *Z. Electrochem.* **1962**, *66(8/9)*, 642 -647.

(65) Boehm, H.P. Chemical Identification of Surface Groups In *Advances in Catalysis (and related subjects)*; Acad. Press: New York, 1966; 179-273.

(66) Benedetti, M.F.; Van Riemsdijk, W.H.; Koopal, L.K. Humic substances considered as a heterogeneous Donnan gel phase. *Environ.Sci.Technol.* **1996**, *30(6)*, 1805 -1813.

(67) Nederlof, M.M.; Van Riemsdijk, W.H.; Koopal, L.K. Determination of Adsorption Affinity Distributions: A General Framework for Methods Related to Local Isotherm Approximations. *J.Colloid Interface Sci.* **1990**, *135(2)*, 410 -425.

(68) Björling, M.; Linse, P.; Karlström, G. Distribution of Segments for Terminally Attached Poly(ethylene oxide) Chains. *J.Phys.Chem.* **1990**, *94(1)*, 471 -481.

(69) Van Riemsdijk, W.H.; Bolt, G.H.; Koopal, L.K.; Blaakmeer, J. Electrolyte Adsorption on Heterogeneous Surfaces: Adsorption Models. *J.Colloid Interface Sci.* **1986**, *109(1)*, 219 -228.

(70) Flory, P.J. *Principles of polymer chemistry*; Cornell University Press: London, 1953.

(71) Meadows, J.; Williams, P.A.; Garvey, M.J.; Harrop, R.A.; Phillips, G.O. Characterization of the Adsorption-Desorption Behaviour of Hydrolyzed Polyacrylamide. *J.Colloid Interface Sci.* **1989**, *132(2)*, 319 -328.

(72) Benedetti, M.F.; Van Riemsdijk, W.H.; Koopal, L.K.; Kinniburgh, D.G.; Gooddy, D.C.; Milne, C.J. Metal ion binding by natural organic matter: From the model to the field. *Geochim.Cosmochim.Acta* **1996**, *60(14)*, 2503 -2513.

(73) Vermeer, A.W.P. this thesis. Chapter 8: Cadmium binding to a heterogeneous system.

Chapter 8

# Cadmium binding to a heterogeneous system

## Abstract

In this work, the adsorption of cadmium and purified Aldrich humic acid on hematite is investigated under a range of conditions in order to determine the effects of the complex interactions in the ternary system, and also to propose a mechanism for the binding of metal ions. Cadmium concentrations are measured using different analysis techniques; ISE measurements, Flame AAS and Voltammetry. The different methods give comparable results. Depletion measurements show that the adsorption of purified Aldrich humic acid (at higher cadmium concentrations) and cadmium (at the higher pH values) are enhanced in the complex system compared with what would be predicted by the simple addition of the adsorption in the binary systems. Further, the order of addition of the humic and cadmium to the suspension appears to have the effect of increasing the adsorption of cadmium slightly when the cadmium was added first to the solution. The process was found to be reversible with respect to the cadmium adsorption within the error of the depletion measurements with changes of pH between pH 4 and pH 9. The enhanced adsorption of both cadmium and humic acid was best explained simply by the reduction of the inter and intramolecular electrostatic repulsion. Cadmium screens the repulsion between the charged groups of the humic and the charged humic screens the repulsion between cadmium and hematite. There was no evidence to indicate that bridging was occurring between the hematite and the humic acid molecules via the cadmium ions, as there was no distinct correlation between the increase in the cadmium binding and the increase in the humic acid binding.

## Introduction

The speciation of heavy metal ions in the natural environment (1,2) as well as in laboratory studies (3,4) using model soils has been the object of a great deal of study in recent times. Knowledge of the binding of the metal species to the soil matrix is of importance in predicting the movement of these elements and the way in which they are distributed in the environment under a range of conditions. The adsorption of metal ions to different humic substances (5-11) and to different iron oxides (12-19), two important components of many types of soils, has been investigated previously and several model descriptions have been proposed. Models in which both specific and electrostatic interactions were incorporated have been suggested to describe the interactions between the humic, the oxide and the metal ions in solution. Little variation was found between the adsorption of cadmium to the various iron oxides, provided the pH and the electrolyte composition are comparable. The surface heterogeneity of the materials, which is an important aspect when considering the adsorption of metal ions, has also been studied (20,21).

Studying these systems, insight has been obtained into the binding of heavy metal ions to the single components of the more complicated soil system, however, metal ion binding to the overall system is not yet understood very well. In a previous paper we discussed the proton adsorption to a mixture of purified Aldrich humic acid (further denoted as PAHA) and hematite B and found that the overall adsorption can not be described as a summation of the adsorption to the non-interacting components. At low pH values the proton binding to the mixed system was lower compared to the direct sum, at high pH values the measured proton binding was increased compared to the direct sum. These effects were explained by two additional processes; (1) a decreased proton adsorption to the humic and (2) an increased proton adsorption to the hematite particles. Which of the two processes dominates the overall proton adsorption depends on the charge density of the interacting particles. Due to the adsorption of the negatively charged humic to the mainly positively charged hematite the electrostatic potential in the vicinity of the hematite surface is changed considerably. The component that influences the potential decay most significantly determines which process dominates. If a negative potential is developed close to the surface, protons can accumulate in the vicinity of the surface sites resulting in an increased surface charge. If the potential is positive, the dissociation of the adsorbed humic is promoted in the surface region.

Metal ion binding to mixtures or even to an entire soil is complicated and it is not to be expected that the metal ion binding can be modelled by simply adding the adsorbed amounts of the single components. Several studies have been reported describing metal ion adsorption to mixtures. McLaren et al. (2) and Bibak (22) mentioned that metal ion adsorption characteristics of complete soils are controlled to a large extent by their organic matter and oxides content, whereas clay minerals are unlikely to have a significant influence on the sorption of metal ions. Numerous studies indicated that the adsorption of metal ions onto oxides was increased due to the interaction with humic substances (1,3,4,23-27). However, these studies did not take into account the charge associated with the humics. Only a few studies used the additivity of the adsorption to

the single components (4,22) to explain the adsorption to the mixture. Bibak described the adsorption of different metal ions to a soil by using the additivity principle, although he mentioned that the binding characteristics in soils may be modified due to mutual interactions between the components. The calculated adsorption capacities of the entire soil, as reported by Bibak, were only about half the measured values. Within the above mentioned studies the loss of adsorbed metal ions was mainly attributed to the decreased adsorption of these metal ions to the humic substances.

Regarding the trends observed for the proton binding to the mixture we tend to ascribe these differences to both components. Due to the interactions between the components we may expect that, depending on the pH, a decreased or increased adsorbed amount of cadmium will be observed as compared to the direct sum of the adsorptivities.

The aim of this work is to determine the behaviour of cadmium and PAHA in the ternary mixture, and to endeavour to predict and explain the observations in terms of what is known about the adsorption of cadmium to each of the other components, and the adsorption of PAHA to hematite B. We will start our discussion by a short description of the interactions in the binary systems as a function of pH and then discuss the adsorption characteristics of both cadmium and PAHA in the ternary system again for a wide pH range. We will discuss the different analysis techniques and compare their results. It will be shown that the mechanism developed for proton binding in a ternary system can also be applied very well to understand the metal ion binding. Finally we will discuss the application of the proposed model for a better understanding of the binding of metal ions and the way they are distributed in the environment.

## Adsorption in two component systems

The interactions between the individual components of our "model soil" have been previously studied and will be briefly reviewed in this section. Adsorption of cadmium to PAHA has been determined under different conditions by potentiometric titrations using a cadmium ion specific electrode (ISE) (11). The adsorption of cadmium to the hematite suspension was measured with batch experiments rather than by titration (12,13,28). Within this study some of these results were reproduced also by batch experiments and cadmium concentrations were determined by Flame AAS, ISE and Voltammetry. Adsorption isotherms of PAHA onto hematite B were measured by depletion measurements (29,30) and proton adsorption to different mixtures was studied by potentiometric proton titrations (31).

Cadmium binding isotherms to PAHA at 0.01 mol $l^{-1}$ $KNO_3$ and three different pH values are shown in Figure 1. The adsorption of cadmium to humic substances is naturally strongly affected by the pH and the salt concentration of the solution, as the degree of dissociation of the humic material determines its charge, and therefore the electrostatic interaction with the metal ions in solution. If the protons and cadmium ions are competing for the same sites on the humics, the pH will also affect the binding of the cadmium due to this competition.
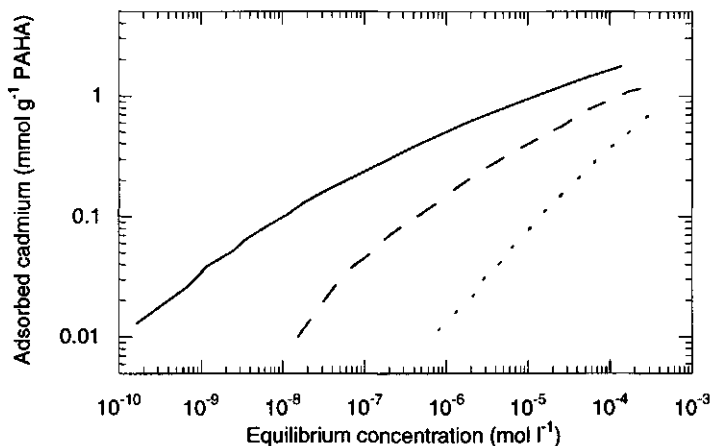
**Figure 1:** PAHA-cadmium binding data (*11*) as a function of the equilibrium cadmium concentration for 3 different pH values and 0.01 M $KNO_3$: ⋯⋯ pH = 4; - - - - pH = 6; —— pH = 9.

Potentiometric proton titrations of PAHA/ cadmium mixtures, where a fixed amount of cadmium and humic acid is titrated from pH 3 to pH 10 and back to pH 3, show no hysteresis and appear to be quite rapidly equilibrated. This indicates that the metal ion adsorption to the polyelectrolyte is reversible with changes in pH.

The Non Ideal Competitive Adsorption model in which all electrostatic interactions are incorporated by the Donnan potential (NICA Donnan model) has been most recently used in the analysis of cation binding to humic acids (*11*).

Different proton charge/ pH curves of PAHA obtained at different salt concentrations could be reduced to a Master Curve based on measured Donnan volumes. These volumes can be obtained by viscosity measurements as a function of pH and salt concentration.

The chemical heterogeneity of PAHA is mainly due to two types of groups, carboxylic type of groups and hydroxyl type of groups (*11,21,32-34*) and can be described successfully with the double Langmuir Freundlich equation. It was reported by Kinniburgh et al. (*10*) that the contribution of each of these two types of groups to the metal ion binding depends on the cation studied. In the case of cadmium binding most cadmium ions were bound to the carboxylic groups, whereas the phenolic type of groups also contributed significantly in copper binding.

The adsorption of cadmium to a range of different iron oxides comparable to the hematite used here has been measured previously (*13,17,18,28*). Cadmium adsorption isotherms on hematite B at 0.01 mol $l^{-1}$ $KNO_3$ and at three pH values are shown in Figure 2. The cadmium isotherms measured in this study and those reported in the literature were comparable within the experimental error. Data at pH 4, however, are difficult to obtain, and subject to large errors due to the small amount which is adsorbed. Based on the extended data set we extrapolated the isotherms at higher pH values to the isotherm at pH 4. The lines in Figure 2 were obtained by fitting a straight line through the extended data set. It is emphasised that the accuracy of the isotherms,
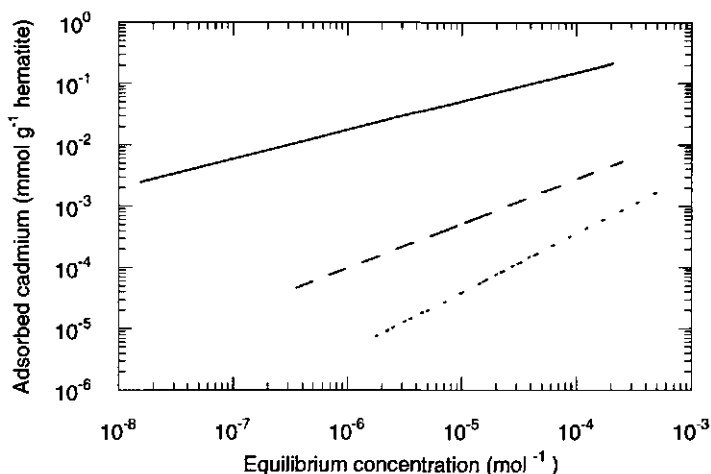
**Figure 2:** Hematite-cadmium binding data as a function of the equilibrium cadmium concentration for 3 different pH values and 0.01 M $KNO_3$: ⋯⋯ pH = 4; ---- pH = 6; ——— pH = 9. The isotherms were approximated by fitting a straight line through our data in combination with an extended data set (*13,17,18,28*) and by extrapolation of these data to pH 4.

especially at low pH is only limited. It can be observed that the adsorption increases with increasing pH as the charge on the oxide becomes less positive.

It was reported by Gunneriusson (*35*) that the adsorption of cadmium to goethite surfaces showed no significant hysteresis, the reactions were found to be nearly fully reversible. Considering this it is quite probable that the adsorption of the cadmium to the hematite B surface is also reversible.

The model that describes the ion binding to the oxide surface most accurate is the Charge Distribution MUltiple SIte Complexation model (*36*) (CD MUSIC) applied by Venema et al. (*18*), for the adsorption of cadmium on goethite. The model concept is based on the Pauling concept of charge distribution (*37*). As described in the one-pK model (*38,39*) the charge of an adsorbing ion is distributed over all its ligands both on the surface and solution side. The patchwise heterogeneity of the iron oxides was reflected by the different linkages (e.g. monodentate or bidentate) of the cadmium ions to the different crystal plains of the oxide.

The adsorption of the humic material to the oxide increases with decreasing pH. This is mainly due to charge differences, between the negatively charged humic material and positively charged hematite. Hematite is strongly positive at low pH, and becomes less positive until the p.z.c. is reached at a pH of 8.9, where the initial surface is electrically neutral. PAHA is negatively charged over the entire pH range studied. The adsorption of PAHA to the hematite at pH 4 is largely due to coulombic attractions, combined with specific adsorption of PAHA. At the p.z.c. there is no overall charge on the hematite surface, therefore the adsorption under these conditions is largely due to specific interactions. It has been shown that the adsorption of PAHA to the oxide is able to be reversed simply by dilution, or changes in pH (*29*).

Proton adsorption to PAHA/ hematite B mixtures has been compared with proton adsorption to the single components (*31*). This gives the difference in the proton

adsorption on PAHA bound to hematite B compared with free PAHA in solution, as well as the extra proton adsorption induced onto the hematite B particles. It was concluded that both components were able to titrate each other. It can be shown by comparison of the double Langmuir Freundlich parameters of the adsorbed and free PAHA that the carboxylic type of groups were involved in the adsorption process. The binding of PAHA to the hematite B surface also has the effect of shifting the p.z.c. of hematite B to a higher pH value and increase the surface charge of the hematite B particles over the entire pH range. Even at moderate coverage of humic acid, the shift is of the order of one pH unit, and therefore quite significant. The effective screening increases the effectiveness of the hematite in binding cations at a given pH value. The negative potential developed around the particles due to the presence of adsorbed polyelectrolyte attracts cations to the vicinity of the hematite surface, and this results in a more profound cation adsorption.

## Experimental procedure

### Materials

All experiments have been performed in a thermostatted room at 21 ± 1 °C and the purified water was obtained by percolating tab water through a mixed bed ion exchange column followed by an active carbon column and a micro filter. Other materials used (cadmium nitrate, potassium nitrate, hydrochloric acid and potassium hydroxide) were obtained from Fluka (p.a. quality) and used without further purification.

### Humic acid

Purification and characterisation of purified Aldrich humic acid or PAHA are described elsewhere (40). PAHA reflects many characteristics normally found for naturally occurring humic substances and is classified as a soil and/ or peat humic acid. PAHA in its proton form was freeze dried and stored in a glass container. The concentration of trace metals was below the detection limit of ICP measurements[1].

Before use PAHA was resuspended overnight in a KOH solution with pH approximately 10, to a concentration of 2 g l$^{-1}$, to assure complete resuspendation of the sample (11,34). Other PAHA solutions were made from this stock solution.

### Hematite particles

Hematite B ($\alpha$-Fe$_2$O$_3$) was prepared as described by Breeuwsma and Lyklema (41) and was aged for several years. Before use the particles were washed with HCl and dialysed extensively against demineralised water. The hematite B particles resembled parallelograms with a mean size of 50 nm. The BET (N$_2$) surface was measured with a

NOVA 1000 Quantachrome and was 43 $m^2g^{-1}$, no significant porosity of the particles was observed.


Cadmium concentration measurements

Three methods were used to determine the equilibrium cadmium concentrations within the adsorption experiments; an Ion Specific Electrode, Flame AAS and Voltammetry.

Titrations were performed using the Wallingford titration system, the experimental set up has been described elsewhere (42-44). Cadmium ion concentrations were measured using a solid state sulphide based cadmium ISE (Orion 94-48) and the pH measurements were made with an Ingold U272-S7 glass electrode. For cadmium ion and pH measurements an Ingold 363-S7 Ag/AgCl reference electrode was used. The electrode measurements are made in the closed cell of the automatic titrator. The solution is transferred to a polypropylene beaker, which fits inside the glass cell and prevents the loss of cadmium by adsorption to the glass walls. The cadmium concentration and the pH are simultaneously measured while the solution is stirred continuously. The cadmium ion selective electrode is previously calibrated (9,11) at the same salt concentration and pH at which the measurements were made.

Flame AAS measurements were taken on an S-11 atomic absorption spectrophotometer (Instrumentation Laboratory, Andover, MA)[1]. Before measurement all samples were acidified to pH 1 by the addition of 0.25 ml of concentrated $HNO_3$. This prevents any of the cadmium from adsorbing to the walls of the tubes and also causes any humic acid present in the solution to precipitate and release the bound cadmium. The samples were corrected for background Fe concentrations following Van der Lee et al. (45).

Voltammetry was performed using a Static Mercury Drop Electrode (SMDE, Metrohm) and an Ingold 363-S7 Ag/AgCl reference electrode. Both normal pulse (NPP) and reversed pulse (RPP) methods were carried out using a polarograph (Autolab, Ecochemie) controlled by a PC. A polypropylene beaker, that fits into the cell unit (Metrohm, 663 VA Stand) was used to prevent adsorption of cadmium to the cell wall. Before measurement all samples were acidified to pH 1 by the addition of 0.25 ml of concentrated $HNO_3$ to remove all humics from the solution. A more detailed description of the procedures is given by Pinheiro (46).


Adsorption of PAHA and cadmium in mixtures

Adsorption of cadmium and PAHA in the mixtures containing hematite was measured in batch experiments. Into polyallomer centrifuge tubes of 50 ml (cleaned with acid (37% HCl), steamed and washed with purified water) 2.5 ml of a 3.465 weight percent suspension of hematite B was weighed. This gives a surface area per tube of 3.7 $m^2$. PAHA (7 ml of a 0.5 g $l^{-1}$ solution) and purified water (25 ml) were added using glass pipettes. Salt (1 M $KNO_3$) was added from a 5 ml Dosimat burette to each of the tubes.

The pH was adjusted using 0.1 M $HNO_3$ and 0.1 M KOH from 5 ml Dosimat burettes. The tubes were equilibrated over several hours or overnight with continuous mixing. A cadmium stock solution was then added from a 1 ml Dosimat burette, the pH readjusted if necessary, and the suspensions again equilibrated for several hours. For the measurements at pH 9, the pH of each of the tubes was checked and readjusted after a further hour of equilibration and also just before centrifugation and extra precautions were taken to exclude carbon dioxide.

The tubes were centrifuged at 7500 rpm for one hour, to remove the suspended hematite, and the supernatant removed from the tubes by pouring into clean dry polyallomer centrifuge tubes. The UV/ Visible spectrum of the supernatant was measured from 200 nm to 500 nm using an Hitachi U3210 spectrophotometer, and the concentration of PAHA determined from the absorbance at 254 nm. This sample is then discarded. A new sample of approximately 5 ml from each tube is transferred to a clean dry sample tube, and the total cadmium amount was determined using atomic absorption spectroscopy (Flame AAS) and voltammetry. The remainder of the supernatant (approximately 30 ml) is used to determine the free cadmium using a cadmium ion selective electrode (ISE).

Order of addition of components

The effect of the order of the addition of the components to the mixture on the adsorption of both the cadmium and PAHA was determined for a number of points. In these experiments the cadmium was added first to the hematite B suspension at the appropriate pH and salt concentration (this in contrast with all other reported depletion experiments where the PAHA was added first). This mixture was equilibrated overnight. PAHA was then added, the pH adjusted where necessary, and the mixture again equilibrated overnight. The samples were centrifuged and analysed for PAHA and cadmium concentrations. PAHA was measured as described previously. The total cadmium concentrations were measured by voltammetry, without dilution, using normal and reversed pulse methods. From the measured total cadmium the free cadmium is calculated by subtraction of the amount adsorbed to the free PAHA. The latter is calculated from the adsorption isotherm of cadmium on PAHA which has been previously measured (11).

Reversibility with pH changes

The reversibility of the adsorption process with pH changes was determined by making a suspension of a large volume, and withdrawing samples after changing the pH of the suspension. Three separate experiments were performed. In the first, the suspension was prepared by first adding PAHA to hematite B at pH 9, and then adding the cadmium. The suspension was equilibrated overnight after each addition, and then a 30 ml sample was withdrawn at pH 9. The remaining suspension was adjusted to pH 4, and again equilibrated overnight. Another 30 ml sample was taken at pH 4 and the rest

adjusted again to pH 9. Analysis of PAHA and cadmium was performed on each of the three samples using UV/ Visible spectrophotometry and voltammetry.

The second experiment began at pH 4 with the addition of cadmium to hematite B and then PAHA. The suspension was again equilibrated overnight after each addition. A sample of 25 ml was taken from the mixture and the rest of the suspension adjusted to pH 9, a sample removed and the process repeated, to give in total two samples at pH 9 and two at pH 4.

The third experiment was again initiated at pH 9, and PAHA was the first addition to hematite B, as in the first experiment. The first sample was taken after equilibration overnight, and a several samples were taken at the same pH over the next 120 hours.

## Results

Comparison of cadmium measurement using different methods

Different methods have been used to measure the cadmium adsorption to the PAHA/ hematite B complexes. Atomic Absorption Spectroscopy, Voltammetry, and measurements with an Ion Specific Electrode. It is useful to have these methods as a comparison, given the difficulties experienced previously with using the cadmium ISE in samples in which iron oxides have been suspended.

Measurements from the Flame AAS give the total amount of cadmium present in the solution, which includes the cadmium bound to free PAHA. After subtraction of this amount (11) from the total amount of cadmium the quantity obtained from these measurements is the amount of cadmium adsorbed to the complex formed between PAHA and hematite B. Some solutions (test for reversibility with pH changes and order of addition) are also analysed using voltammetry. Using Voltammetry also the total cadmium was determined and the measurements were comparable to those obtained from the Flame AAS.

The electrode measurements give the total amount of unbound cadmium present in the solution. Since the amount of free humic in the solution may be measured by the UV absorption at 254 nm, the amount of cadmium in the PAHA/ hematite B complex may also be calculated from the electrode measurements using the metal ion binding to free PAHA, which is known (11).

The values obtained from Flame AAS and ISE measurements can be seen to be comparable Figure 3. At the y-axis the cadmium adsorption is expressed as mmol cadmium bound to the PAHA/ hematite B complex (where necessary corrected for the cadmium bound to the free humic acid). At the x-axis the equilibrium concentration is given (where necessary corrected for the cadmium bound to the free humic acid). It may be mentioned that the uncertainty due to the subtraction of the cadmium bound to the free PAHA is reflected in the adsorbed mmol for the ISE method, whereas it is reflected in the equilibrium concentration for the AAS method. The free humic acid was measured by UV spectroscopy as described above. At pH 4 all humic acid was bound to the hematite particles independent of the total cadmium concentration (resulting in an adsorbed amount of about 38 mg PAHA $g^{-1}$ hematite B). At pH 6 and 9 the adsorbed

amount of PAHA depends on the cadmium concentration and varied from 21 to 37 mg PAHA g⁻¹ hematite B at pH 6 and 12 to 35 mg PAHA g⁻¹ hematite B at pH 9, with increasing total cadmium.
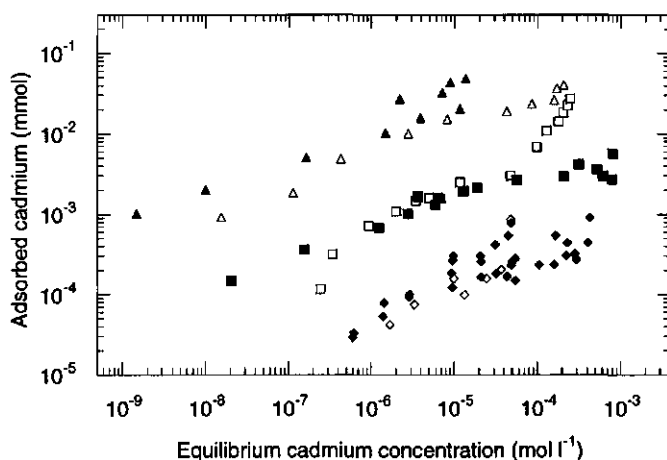


**Figure 3:** Cadmium adsorption to the PAHA hematite B complex, comparison of the different analytical methods; Flame AAS (solid symbols) and ISE (open symbols). : ♦ pH = 4; ■ pH = 6; ▲ pH = 9 at 0.01 M KNO₃.

## Electrode accuracy

The results obtained from the electrode prove to be reproducible and accurate within certain limits. The errors are such that where less than 10 % of the total cadmium is adsorbed, the accuracy of the calculated adsorption is compromised. Measurements of cadmium concentrations less than 5 10⁻⁵ M in a system in which the cadmium concentration is unbuffered are outside the limit of the electrode. It is possible to measure concentrations of cadmium lower than 10⁻⁵ M only when the system is buffered, e.g. by a significant amount of "free" PAHA present (the bound humic is taken away by centrifugation before measurement of the cadmium concentration). At pH 4, where there is very little cadmium adsorbed, and only a negligible amount of free PAHA is present, the window for the measurement of the cadmium adsorption with the electrode is quite small. At pH 6 and 9, the total adsorption of the cadmium is significant, and there is also a greater amount of free PAHA in the system for the same total amounts of PAHA and hematite B. So that the system is well buffered and the ISE measurements give reproducible results.

## Order of addition and reversibility in ternary systems

In order to obtain some insight into the mechanism of the adsorption in the mixture, the order in which each of the components were added to the mixture was investigated.

Results are summarised in Table I. In most measurements, PAHA has been added to the mixture first, and the cadmium some time later after the hematite humic mixture has equilibrated. In each of the experiments described in this paragraph, the solution was prepared by first equilibrating overnight a suspension containing hematite B and cadmium at the appropriate pH and salt concentration. At all three pH values the cadmium adsorption was at least tending to be slightly higher than in the experiments where PAHA was added first.

**Table I:** Effect of the order of addition on the cadmium adsorption to PAHA/ hematite B complexes

| Experiment | pH | [Cd] free (mol l$^{-1}$)* | Cd$_{ads}$ (total) (mol g$^{-1}$) | PAHA free (mg l$^{-1}$) | PAHA$_{ads}$ (mg g$^{-1}$) |
|---|---|---|---|---|---|
| 1 (PAHA first) | 9 | 3.1 10$^{-7}$ | 6.1 10$^{-6}$ | 75.1 | 17.6 |
| | | 1.9 10$^{-7}$ | 6.1 10$^{-6}$ | | |
| | 4 | 8.3 10$^{-5}$ | 3.0 10$^{-5}$ | 17.3 | 40.0 |
| | | 7.5 10$^{-5}$ | 3.3 10$^{-5}$ | | |
| | 9 | 7.7 10$^{-7}$ | 6.1 10$^{-6}$ | 64.9 | 21.7 |
| | | 4.7 10$^{-7}$ | 6.1 10$^{-6}$ | | |
| 2 (Cd first) | 4 | 9.3 10$^{-5}$ | 2.6 10$^{-5}$ | 8.0 | 42.2 |
| | | 8.1 10$^{-5}$ | 3.0 10$^{-5}$ | | |
| | 9 | 1.7 10$^{-7}$ | 6.0 10$^{-6}$ | 49.5 | 26.8 |
| | | 1.0 10$^{-7}$ | 6.0 10$^{-6}$ | | |
| | 4 | 8.9 10$^{-5}$ | 2.7 10$^{-5}$ | 8.2 | 42.0 |
| | | 7.9 10$^{-5}$ | 3.1 10$^{-5}$ | | |
| | 9 | 1.4 10$^{-7}$ | 6.0 10$^{-6}$ | 50.9 | 26.3 |
| | | 7.3 10$^{-8}$ | 6.0 10$^{-6}$ | | |

* The two values for each experiment were measured by NPP and RPP, respectively.

Results from the first experiment described above, where PAHA is adsorbed first at pH 9 and the cadmium second show that the adsorption of the cadmium appears to be completely reversible. Results are summarised in Table I. This is in fact almost the same as the adsorption of the cadmium in the second experiment where cadmium is adsorbed first. The adsorption of PAHA, however, is significantly lower when the humic acid is added first to the hematite at pH 9. As the pH is changed from 9 to 4, the humic acid adsorbed is slightly lower than that observed in the second experiment at pH 4. Returning to pH 9, the adsorbed amount is higher, but still not as high as that adsorbed when the cadmium is added first to the suspension at pH 4. It appears that in the absence of cadmium, the humic acid is adsorbed in a conformation that reduces the amount which may be adsorbed, and which seems at least partially irreversible.

Davis and Bhatnagar (26) found that in the adsorption of cadmium to mixtures of humic acid and hematite, a higher adsorption of the metal ion was obtained when the cadmium was added first compared with when the cadmium and humic acid were added simultaneously or the humic acid was added first. These observations compare well with our results.

The third experiment is carried out at pH 9 to determine whether the lower adsorption of PAHA at pH 9 where the addition of PAHA is the first step is a

thermodynamic or a kinetic phenomenon. The measurements of the humic acid concentration over 120 hours showed (Table II) that the adsorption of PAHA rose slightly, but was still below the level of adsorption of the experiment where the cadmium was added first at pH 4.

**Table II:** PAHA adsorption kinetics onto hematite B

| Time (hours) | PAHA free (mg l$^{-1}$) | PAHA adsorbed (mg g$^{-1}$) |
|---|---|---|
| 24.5 | 67.4 | 21.5 |
| 47.7 | 64.1 | 22.8 |
| 70.5 | 65.5 | 22.7 |
| 94.0 | 64.4 | 22.7 |
| 118.7 | 63.0 | 23.3 |

Cadmium adsorption

The cadmium adsorption to both PAHA and hematite B increases with increasing pH, as is shown in Figure 1 and Figure 2, however, some significant differences have to be mentioned. The humics are negatively charge over the entire pH range studied (11), whereas the hematite particles are predominantly positively charged (29). Hematite is strongly positive at low pH, and becomes less positive until the p.z.c. is reached, where the surface is electrically neutral. Due to this, the adsorption of cadmium ions occurs against the electrostatic repulsion between the positively charged cadmium ions and the hematite surface. Cadmium ions can, at pH values below the p.z.c., only adsorb onto the bare hematite due to specific interactions. As a consequence the cadmium adsorption at pH values around the p.z.c. of the hematite particles is increased by several orders of magnitude. This in contrast to the humic where the pH dependence of the cadmium adsorption is only small.

The increased cadmium adsorption with increasing pH is of course also observed for the adsorption to the PAHA/ hematite B complex (Figure 3). The measured adsorption to the mixture of hematite B and PAHA may be compared with the adsorption which is calculated from the addition of the adsorption to the two individual components. This is shown in **Figure 4**a, b and c for the three pH values studied. The lines represent the cadmium binding to the single components and the non-interacting sum. The non-interacting sum is virtually equal to the amount bound to the humic acid at pH 4 and 6, whereas at pH 9 the amount bound to PAHA and hematite B (without interaction) is of similar magnitude. The symbols are the data measured with the ion specific electrode, corrected for the complexation with the free PAHA. The adsorption at pH 4 can be seen to be very close to or even lower than the addition of the two non-interacting components. At pH 6, the adsorbed amount is significantly more than the predicted amount and at pH 9 the adsorbed amount is much larger than the adsorption calculated from the addition of the two components.

Regarding these observations we have to conclude that the cadmium binding to the mixed system is complicated and can not be described by a simple summation of the

binding to the single components. The actual cation binding differs from the non-interacting cation binding. In analogy with the proton binding (*31*), the deviation of the non-interacting cation binding is controlled by two opposite processes; a decreased adsorption to the humic and an increased adsorption to the hematite particles. Which process dominates the overall binding depends on the pH of the system. At low pH
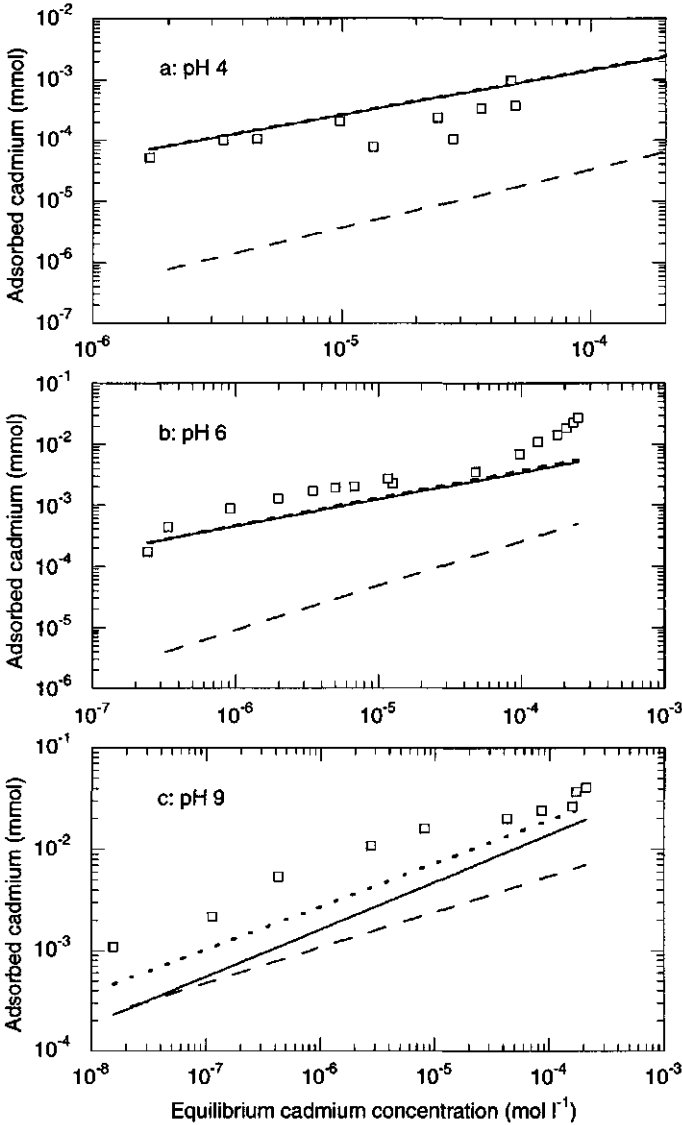


**Figure 4:** Cadmium adsorption isotherms of the PAHA hematite B complex at 0.01 M KNO$_3$ at different pH values. For comparison the adsorption isotherms of the single components and the non-interacting sum are given as well. ⋯⋯⋯ PAHA adsorption isotherm; – – – hematite B adsorption isotherm; ——— non-interacting sum of the PAHA and hematite B adsorption isotherms and □ actual measured adsorption isotherm of the complex. a: pH = 4; b: pH = 6 and c: pH = 9.

values the highly charged surface removes a significant number of groups of the humic acid, even if it is taken into account that the surface will induce a less negative or even positive potential field in the vicinity of the adsorbed polyelectrolyte resulting in an increased degree of dissociation of the humic acid segments. At higher pH values only a small fraction of the available humic acid groups is removed by binding to the surface and the remaining adsorbed humic acid charges cause a significant increase in cation binding to the oxide surface.

The increased binding to the positively charged surface is the result of a lowering of the positive potential due to the negative adsorbed charge associated with the humic acid. This lowering of the positive surface potential will enhance the binding of cadmium to the reactive sites of the oxide surface. The humic acid adsorption can even overcompensate the positive charge of the oxide. The negative potential for the humic acid molecules not in direct contact with the oxide surface (loops and tails) is equal or less negative than for the free humic acid molecules under the same conditions leading to an expected lowering of the metal ion affinity for PAHA in contact with hematite B.

This lowering of the affinity accounts for other cations (e.g. protons) as well and is also reflected in the shift of the p.z.c. of the hematite surface by about 1 pH unit (31). Regarding this fact we can describe the cadmium adsorption in a semi-quantitative way. By assuming that this increased affinity of the surface is not restricted to the p.z.c. but accounts for a wider pH range, as was discussed previously (31), we can calculated the expected cadmium adsorption.

The expected cadmium adsorption at pH 4 can be calculated by assuming that the cadmium adsorption to the oxide is increased over the entire pH range as if the pH was raised by 1 pH unit. The amount of cadmium bound to the oxide in this way is still negligible compared to the expected contribution of cadmium bound to PAHA in contact with the oxide (approximately all PAHA is adsorbed at pH 4). The bound humic is expected to be somewhat less reactive than the free PAHA and we may thus expect a slightly lower cadmium adsorption in the mixture compared to the additivity. At pH 6 (cadmium adsorption to the surface is calculated as if the pH was 7) the oxide surface starts to contribute significantly to the overall cadmium adsorption, leading to an increase of adsorption, although the affinity of PAHA for the cadmium is reduced. At pH 9 the oxide surface dominates the overall cadmium binding, resulting in a significant increase in cadmium adsorption as compared to the adsorption to the single components. This is also reflected in the cadmium binding to the single components where it was observed that the cadmium adsorption at pH values around the p.z.c. of the hematite particles is increased by several orders of magnitude compared to lower pH values, whereas the pH dependence of the cadmium adsorption to the humic is only small.

To corroborate our model we will discuss the binding of copper(II) to a mixture of humic acid and goethite. These experimental results were reported by Robertson (4,47). Robertson measured the copper adsorption to the complex at pH 4, 5 and 6 for two different salt concentrations (0.1 and 0.01 M NaClO$_4$) and for two humic acid: goethite ratios (100 : 2 and 100 : 10). Overall the observed trends were comparable to our results. The dependence of the copper adsorption on the salt concentration and the ratio between humic and goethite were comparable to our results. However, a major

difference was reported as well. At all pH values the actual copper adsorption was lower than the non-interacting copper adsorption. At pH 4 this difference was substantial; binding was as low as 15% of additive at low copper activity and approaches additivity as total (bound) copper increases (pH 6 and high copper concentration).

Such a decreased copper adsorption is expected based on the above described model. First of all it has to be mentioned that copper binding to the oxide is lower than cadmium binding to the oxide (14), whereas copper binding to the humic acid is larger compared to cadmium binding to the humic acid(48). Further the cadmium binding to the humic acid is mainly monodentate, whereas the copper binding to the humic is bidentate and requires both a carboxylic and a phenolic group (10). Regarding these two aspects and the above described model it is expected that the actual copper binding will be lower than the direct sum of the non-interacting components. It is clear that copper binds mainly to the adsorbed humic acid and only slightly to the oxide. Thus a decreased adsorption will result. This is even emphasised due to the fact that the copper ions require a specific bidentate binding site. Due to the withdrawal of carboxylic binding sites by the oxide surface, copper binding will decrease significantly.

## Conclusions

It has been shown that the proposed model, that was developed for the proton binding to the PAHA/ hematite B complex, can also semi-qualitatively explain the cadmium binding in the ternary system very well.

The model is based on the polyelectrolyte adsorption characteristics of the humic matter. The adsorbed humic acid molecules are described as a relatively thick layer with both humic acid segments in direct contact with the hematite B particles, to accomplish charge compensation of the surface, and segments protruding into the solution. The latter charged segments cause a negative or at least less positive potential field around the hematite particles. For situations where the surface charge is dominating, compared to the humic acid charge in the vicinity of the surface, even extra charges are introduced onto the humic acid molecules. The charged segments associated with the humic acid segments extending into the solution are responsible for the commonly observed charge reversal of the hematite particles upon adsorption. Due to these charges the potential profile developed around the particles is disturbed and positively charged ions may accumulate in the vicinity of the surface. This accumulation results in an adjustment of the degree of dissociation of the surface giving an increased surface charge.

Considering the discussed mechanism controlling the speciation of metal ions in ternary system, some conclusions can be drawn considering the speciation in the natural environment. It has been discussed that especially at low pH values binding sites are withdrawn from the system, which is attributed to the carboxylic groups of the adsorbed humic acid, whereas at high pH values an increased proton adsorption is observed. Based on the binding characteristics of the metal ions to the single components we may predict the overall adsorption in a qualitative way. In general, the adsorption of metal ions that bind strongly to the organic soil fraction and are only

slightly attracted by the oxides will be decreased due to the interactions between the different soil components. Whereas, the adsorption will be increased for species that bind strongly to the mineral particles. The speciation of the metal ion in an aqueous solution may also affect the adsorption. As was mentioned by Ho and Miller (27), the most predominant uranium aqueous species depend on the pH of the system. Some of these species adsorb specifically to the hematite surface, whereas other do not. Due to these differences the adsorption was increased at certain pH values, whereas it was decreased under other conditions.

Although the adsorption of heavy metal ions within a ternary system can not yet be described quantitatively, qualitatively good agreement is observed between the experimental results and the predictions from the model.

## References.

(1)   Laxen, D.P.H. Trace metal adsorption/coprecipitation on hydrous ferric oxide under realistic conditions. *Water Res.* **1985**, *19(10)*, 1229 -1236.
(2)   McLaren, R.G.; Lawson, D.M.; Swift, R.S. Sorption and desorption of cobalt by soils and soil components. *J.Soil Sci.* **1986**, *37*, 413 -426.
(3)   Tipping, E.; Griffith, J.R.; Hilton, J. The Effect of Adsorbed Humic Substances on the Uptake of Copper(II) by Goethite. *Croat.Chem.Acta* **1983**, *56(4)*, 613 -621.
(4)   Robertson, A.P.; Leckie, J.O. Humic Acid/Goethite Interactions and their Effect on Copper Binding. Humic Subst. Global Environ. Implic. Hum. Health, Proc. Int. Meet. Int. Humic Subst. Soc., 6th. Senesi N and Miano TM. Amsterdam. Elsevier. 1994 487-492.
(5)   Dzombak, D.A.; Fish, W.; Morel, F.M.M. Metal-Humate Interactions. 1. Discrete Ligand and Continuous Distribution Models. *Environ.Sci.Technol.* **1986**, *20(7)*, 669 -675.
(6)   Tipping, E. Modeling ion binding by humic acids. *Colloids Surf.A* **1993**, *73*, 117 -131.
(7)   Westall, J.C.; Jones, J.D.; Turner, G.D.; Zachara, J.M. Models for Association of Metal Ions with Heterogeneous Environmental Sorbents. 1. Complexation of Co(II) by Leonardite Humic Acid as a Function of pH and NaClO$_4$ Concentration. *Environ.Sci.Technol.* **1995**, *29(4)*, 951 -959.
(8)   Marinsky, J.A.; Reddy, M.M.; Ephraim, J.H.; Mathuthu, A.S. Computational scheme for the prediction of metal ion binding by a soil fulvic acid. *Anal.Chim.Acta* **1995**, *302*, 309 -322.
(9)   Milne, C.J.; Kinniburgh, D.G.; De Wit, J.C.M.; Van Riemsdijk, W.H.; Koopal, L.K. Analysis of Metal-Ion Binding by Peat Humic Acid Using a Simple Electrostatic Model. *J.Colloid Interface Sci.* **1995**, *175*, 448 -460.
(10)  Kinniburgh, D.G.; Milne, C.J.; Benedetti, M.F.; Pinheiro, J.P.; Filius, J.; Koopal, L.K.; Van Riemsdijk, W.H. Metal Ion Binding by Humic Acid: Application of the NICA-Donnan Model. *Environ.Sci.Technol.* **1996**, *30(5)*, 1687 -1698.
(11)  Vermeer, A.W.P. this Thesis. Chapter 4: Proton and Cadmium binding to purified Aldrich humic acid, exploration of the NICA-Donnan model.
(12)  Fokkink, L.G.J.; De Keizer, A.; Lyklema, J. Specific Ion Adsorption on Oxides: Surface Charge Adjustment and Proton Stoichiometry. *J.Colloid Interface Sci.* **1987**, *118*, 454 -462.
(13)  Ardizzone, S.; Formaro, L.; Lyklema, J. Adsorption from mixtures containing mono- and bivalent cations on insoluble oxides and a revision of the interpretation of points of zero charge obtained by titration. *J.Electranal.Chem.* **1982**, *133*, 147 -156.
(14)  Benjamin, M.M.; Leckie, J.O. Multiple-Site Adsorption of Cd, Cu, Zn, and Pb on Amorphous Iron Oxyhydroxide. *J.Colloid Interface Sci.* **1981**, *79(1)*, 209 -221.
(15)  Djafer, M.; Lamy, I.; Terce, M. Interaction of metallic cations with the hydrous goethite surface. *Prog. Colloid Polym. Sci.* **1989**, *79*, 150 -154.
(16)  Johnson, B.B. Effect of pH, Temperature, and Concentration on the Adsorption of Cadmium on Goethite. *Environ.Sci.Technol.* **1990**, *24(1)*, 112 -118.

(17) Fokkink, L.G.J.; De Keizer, A.; Lyklema, J. Temperature dependence of Cadmium Adsorption on Oxides. I. Experimental Observation and Model Analysis. *J.Colloid Interface Sci.* **1990**, *135(1)*, 118 -131.

(18) Venema, P.; Hiemstra, T.; Van Riemsdijk, W.H. Multiple site modelling of cadmium adsorption on goethite using an extended data set. *J.Colloid Interface Sci.* **1996**, , submitted

(19) Venema, P.; Hiemstra, T.; Van Riemsdijk, W.H. Comparison of Different Site Binding Models for Cation Sorption: Description of pH Dependency, Salt Dependency, and Cation-Proton Exchange. *J.Colloid Interface Sci.* **1996**, *181*, 45 -59.

(20) Gibb, A.W.M.; Koopal, L.K. Electrochemistry of a Model for Patchwise Heterogeneous Surfaces: The Rutile-Hematite System. *J.Colloid Interface Sci.* **1990**, *134(1)*, 122 -138.

(21) De Wit, J.C.M.; Van Riemsdijk, W.H.; Koopal, L.K. Proton Binding to Humic Substances. 2. Chemical Heterogeneity and Adsorption Models. *Environ.Sci.Technol.* **1993**, *27*, 2015 -2022.

(22) Bibak, A. Cobalt, Copper, and Manganese adsorption by aluminium and iron oxides and humic acid. *Commun.Soil Sci.Plant Anal.* **1994**, *25(19&20)*, 3229 -3239.

(23) Ephraim, J.H.; Ledin, A.; Allard, B. Effects of fulvic acid on the adsorption of Cd(II) on alumina. *Sci.Total Environ.* **1989**, *81/82*, 653 -660.

(24) Taylor, M.D.; Theng, B.K.G. Sorption of Cadmium by complexes of Kaolinite with humic acid. *Commun.Soil Sci.Plant Anal.* **1995**, *26(5&6)*, 765 -776.

(25) Ephraim, J.H.; Allard, B. Influence of humic substances on the uptake of metal ions by naturally occurring materials. *Ion Exch.Solvent Extr.* **1993**, *11*, 335 -367.

(26) Davis, A.P.; Bhatnagar, V. Adsorption of Cadmium and humic acid onto hematite. *Chemosphere* **1995**, *30(2)*, 243 -256.

(27) Ho, C.H.; Miller, N.H. Effect of Humic Acid on Uranium Uptake by Hematite Particles. *J.Colloid Interface Sci.* **1985**, *106(2)*, 281 -288.

(28) Van Riemsdijk, W.H.; De Wit, J.C.M.; Koopal, L.K.; Bolt, G.H. Metal Ion Adsorption on Heterogeneous Surfaces: Adsorption Models. *J.Colloid Interface Sci.* **1987**, *116(2)*, 511 -522.

(29) Vermeer, A.W.P. this Thesis. Chapter 5: Interactions between humic acid and mineral particles.

(30) Vermeer, A.W.P. this Thesis. Chapter 6: Adsorption fractionation of humic substances at mineral surfaces, experiments compared with theory.

(31) Vermeer, A.W.P. this Thesis. Chapter 7: Proton binding to a heterogeneous system, effects due to the interactions between the different components.

(32) Perdue, E.M.; Reuter, J.H.; Parrish, R.S. A statistical model of proton binding by humus. *Geochim.Cosmochim.Acta* **1984**, *48*, 1257 -1263.

(33) De Wit, J.C.M.; Van Riemsdijk, W.H.; Koopal, L.K. Proton Binding to Humic Substances. 1. Electrostatic Effects. *Environ.Sci.Technol.* **1993**, *27(10)*, 2005 -2014.

(34) Milne, C.J.; Kinniburgh, D.G.; De Wit, J.C.M.; Van Riemsdijk, W.H.; Koopal, L.K. Analysis of proton binding by peat humic acid using a simple electrostatic model. *Geochim.Cosmochim.Acta* **1995**, *59(6)*, 1101 -1112.

(35) Gunneriusson, L. Composition and Stability of Cd(II)-Chloro and -Hydroxo Complexes at the goethite (a-FeOOH)/ Water Interface. *J.Colloid Interface Sci.* **1994**, *163*, 484 -492.

(36) Hiemstra, T.; Van Riemsdijk, W.H.; Bolt, G.H. Multisite Proton Adsorption Modelling at the Solid/Solution Interface of (Hydr)oxides: A New Approach I. Model Description and Evaluation of Intrinsic Reaction Constants. *J.Colloid Interface Sci.* **1996**, *133(1)*, 91 -104.

(37) Pauling, L. The Principles Determining the Structure of Complex Ionic Crystals. *J. Amer. Chem. Soc.* **1929**, *51*, 1010 -1026.

(38) Van Riemsdijk, W.H.; Bolt, G.H.; Koopal, L.K.; Blaakmeer, J. Electrolyte Adsorption on Heterogeneous Surfaces: Adsorption Models. *J.Colloid Interface Sci.* **1986**, *109(1)*, 219 -228.

(39) Koopal, L.K. Ion adsorption on mineral oxide surfaces In *Adsorption on new and modified inorganic sorbents*; Dabrowski, A.; Tertykh, V.A. Eds.; Elsevier: Amsterdam, 1996; 757-796.

(40) Vermeer, A.W.P.; Koopal, L.K. submitted to *Environ.Sci.Technol.*, this Thesis. Chapter 3: Characterisation and classification of purified Aldrich humic acid.

(41) Breeuwsma, A.; Lyklema, J. Interfacial electrochemistry of haematite. *Discussions of The Faraday Soc.* **1971**, *52*, 324 -333.

(42) Vermeer, A.W.P. this Thesis. Appendix I: Potentiometric proton titrations, experimental set-up and data treatment.

(43) Kinniburgh, D.G.; Milne, C.J. Guide to the Wallingford Titrator; Technical report. WD/93/23. British Geological Survey: Keyworth, Nottinghamshire. 1993.

(44) Kinniburgh, D.G.; Milne, C.J.; Venema, P. Design and Construction of a Personal-Computer-Based Automatic Titrator. *Soil Sci.Soc.Am.J.* **1995**, *59(2)*, 417 -422.

(45) Van der Lee, J.J.; Temminghoff, E.; Houba, V.J.G.; Novazamsky, I. Background Corrections in the determination of Cd and Pb by Flame AAS in Plant and Soil Samples with High Fe Levels. *Appl. Spectrosc.* **1987**, *41(3)*, 388 -390.

(46) Pinheiro, J.P.; Mota, A.M.; Simoes Gonçalves, M.L. Complexation study of humic acids with cadmium(II) and lead(II). *Anal.Chim.Acta* **1994**, *284*, 525 -537.

(47) Robertson, A.P. Ph. D. thesis, Stanford University, USA. Goethite/humic acid interactions and their effects on copper(II) binding.

(48) Benedetti, M.F.; Milne, C.J.; Kinniburgh, D.G.; Van Riemsdijk, W.H.; Koopal, L.K. Metal Ion Binding to Humic Substances: Application of the Non-Ideal Competitive Adsorption Model. *Environ.Sci.Technol.* **1995**, *29(2)*, 446 -456.

## Appendix I: Potentiometric proton titrations, experimental set-up and theory (1)

### Introduction

Potentiometric proton titrations are a powerful method to study the surface characteristics of colloidal particles, water soluble polyelectrolytes and other charged systems in relation to ion adsorption. In a potentiometric proton titration the number of associated groups (surface charge) is related to the protons adsorbed by the sample. The proton consumption can be calculated by subtracting the amount of titrant required for a pH change of an equivalent volume of the blank electrolyte solution from the added amount of titrant. The concentration of protons in solution is calculated from the measured pH, using a calibration procedure. The blank consumption in the presence of a sample can not be measured directly but has to be approximated on the bases of an experimental blank and a theoretical model. In any case the ionic strength and the water equilibrium (being a function of the temperature) have to be taken into account.

Within this appendix we discuss the experimental procedures and the calculations required to obtain an accurate absolute surface charge-pH curve. We will start with describing the different procedures that are necessary for the calibration of the potentiometric titration cell. Secondly we will present three methods to obtain and subtract the blank consumption in the case of a sample titration. Then we will discuss some theoretical aspects, the experimental set-up and describe the experimental precautions that are essential for well-defined titrations and finally we describe some methods to determine the absolute position of the measured "surface" charge-pH curves.

### Control of the electrochemical cell

In order to prevent contamination of the cell, precautions have to be taken. Pollution with, for example, carbon dioxide influences the equivalence point and due to this the blank subtraction may be inaccurate. A reliable method to check the presence of carbon dioxide is the Gran plot (2,3). In a simple Gran plot of a solution containing an acid, we plot: $V_{TOT} 10^{-pH} = V_{TOT} a_H$ (proton activity/ mol) against ml of titrant added.
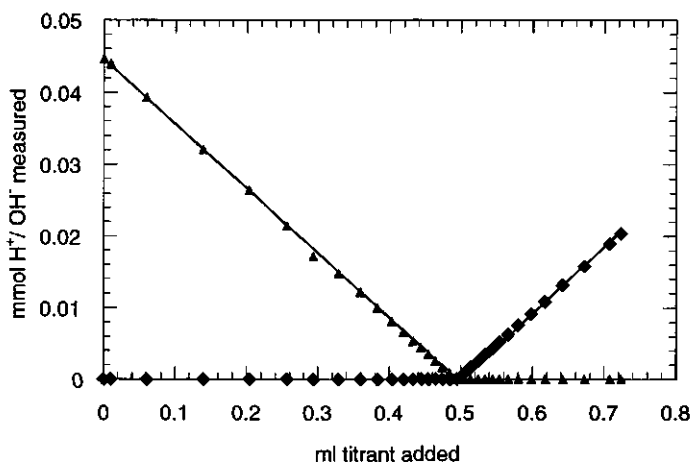


**Figure 1:** A Gran plot of a blank titration. the solid lines are based on the operational pH (buffer calibration) and the symbols on the theoretical pH.

Under not too extreme conditions the activity coefficient will be constant (constant ionic strength), and the Gran plot is composed of two straight lines, intersecting in the equivalence point. A good blank titration should give a sharp equivalence point. A flat region around the equivalence point and non-linear lines are indicative for errors in the titration (e.g. $CO_2$). Figure 1 shows an example of a Gran plot of an excellent titration.

## Calibration of the electrodes

The observed potential of the electrochemical cell, $E_{CELL}$, employed for a potentiometric measurement can be expressed in terms of the reference electrode potential, $E_{REF}$, the indicator electrode potential, $E_{IND}$, and a combined junction potential (4), that is

$$E_{CELL} = E_{REF} - E_{IND} + E_J \tag{A1.1}$$

The junction potential, $E_J$, combines the metal junction potentials inside the electrodes (which are small for a matched pair of electrodes) plus the sum of the liquid junction potentials of the cell. These are the liquid-junctions inside the reference electrode itself, the one between the reference electrode and the solution of the salt bridge and the one between the electrolyte solution of the salt bridge and the solution or suspension being analysed. In a good set-up the liquid junction potentials should be constant. This can be easily assured for the first two junctions. The third potential is constant only if the salt concentration in the cell is constant or that in the salt bridge high (3 M) and contribution of the protons to the conductivity can be neglected.

The potential of the indicator electrode (the glass electrode) is related to the activity of the protons in the solution or to the pH as show in the expression below where A and B are constants at constant temperature.

$$E_{IND} = A + B \log(a_{H^+}) \tag{A1.2}$$

Combining the Eqs. (A1.1) and (A1.2) gives for the pH in the cell:

$$pH = -\log(a_{H^+}) = \frac{E_{CELL} - (E_{REF} + E_J - A)}{B} \tag{A1.3}$$

Alternatively we may write for the cell potential:

$$E_{CELL} = E_{0,CELL} + B\, pH \tag{A1.4}$$

where the constant $E_{0,CELL}$ groups the three constants in parenthesis in Eq. (A1.3). The total junction potential cannot be evaluated by theoretical calculations, thus $E_{0,CELL}$ must be found experimentally.

Two different calibration methods are available: (1) with standard buffers of known pH values, and (2) with solutions of known proton concentration and ionic strength, I.

The pH determined by the first calibration method is a well-accepted operational pH. The calibration is done by measuring the previously described A and B constants with standard buffers. Usually the EMF's of 3, 4 or 5 different buffer solutions are measured, and a calibration line is obtained. It is important to check the calibration before and after a series of titration experiments. In general a range of calibration constants (slope and intercept) will be found for a given set up of the cell. The actual range gives information on the quality of the cell. For a proper functioning cell the value of the intercept, $E_0$, should not vary more than 5 mV (the absolute value of $E_0$ is 395 mV, strongly depending on the electrode) and the slope approximately - 58.0 ± 1.0 mV at 25 °C.

With the second method a relation between the observed pH and the concentration is obtained by measuring blank titrations. This can be accomplished using two approaches: on a pure experimental basis or by calculating a theoretical pH. The theoretical pH is defined as:

$$pH = -\log(f\, c_{H^+})$$ (A1.5)

where f is the mean activity coefficient and $c_H$ is the concentration of the protons. The mean activity coefficient can be calculated, for example, by the Davies equation (5), which is an semi-empirical extension of the Debye-Hückel equation (6). The Debye-Hückel equation is valid for values of I up to 0.1 M, whereas the Davies equation is valid for values up to 0.5 M. For even higher concentrations an empirical relation such as that suggested by Pitzer (7) must be used. Further information on these equations is given in appendix II. In not too complex electrolyte solutions the pH definition Eq. (A1.5) allows us to associate a proton concentration to its theoretical pH as long as the ionic strength is known. This is not the case with the operational definition of the pH, where the relation between pH and p[H⁺] remains vague.

*Experimental blank*

The blank solution in which a colloid is going to be suspended, usually an electrolyte solution of specified electrolyte type and concentration, is titrated in order to obtain a relation between the concentration of an acid or a base and the activity of the respective protons or hydroxyl ions in this solution. The excess concentration of acid or base at any instance is known if the solution volume, the equivalence point, as well as the amount of added titrant and its concentration, are known.

The activity of the protons or hydroxyl ions at each data point of the titration is determined from reading the calibrated pH electrode at the given temperature:

$$a_{H^+} = 10^{-pH}$$ (A1.6)

$$a_{OH^-} = 10^{-K_w + pH}$$ (A1.7)

In not too complex electrolyte solutions the curve obtained from an activity versus concentration plot for H⁺ and OH⁻ is composed of two linear sections with a slope equal to the activity coefficient of the H⁺ or the OH⁻ and an intercept at the equivalence point which indicates the proton activity at an equal concentration of added acid and base. The appropriate concentration to be plotted versus the activity is the excess concentration of H⁺ and OH⁻ ions, defined as the difference between the acid and base concentration, [H⁺] - [OH⁻]. This results in a figure that is similar to a Gran plot (Figure 1).

*Theoretical blank*

As discussed in the previous paragraph, it is important that the starting conditions of the experimental blank are equal to the solution in which the colloid is going to be suspended. This may cause some practical difficulties, since the salt concentration of subsequent titrations can not be predicted accurately and the total volume at each point of the titration is not known on forehand. Further the total amount of titrant required for the sample is considerable larger than that for the blank and thus the salt concentration is changed significantly compared to the blank titration. These problems can be solved by using a theoretical model to describe the blank titration curve. Following this procedure the experimental blank titration is used as a check, on the model applied, to calculate the blank curve.

The theoretical pH can be calculated as follows:

$$pH = -\log(f) - \log[H^+] \tag{A1.8}$$

where f is the mean activity coefficient of the proton.

For the calculation of the activity coefficients either the Davies or extended Debye-Hückel equation can be used (see appendix II). The improved Davies equation (5) for an aqueous solution of 298 K is:

$$-\log(f_D) = 0.51\left(\frac{\sqrt{I}}{1+\sqrt{I}} - 0.31\right) \tag{A1.9}$$

In Eq. (A1.9) the ionic strength is depicted with the symbol I and the procedure to calculate the ionic strength at any point of the titration will be discussed later. The advantages of Eq. (A1.9) are that, (1) it is simple; the cation and anion activity coefficient are assumed to be equal, and (2) it allows the calculation of activity coefficients in mixed electrolytes.

It is possible that (extended) Debye-Hückel type equations, in which anion and cation are treated differently, give better results for $H^+$ and $OH^-$ in salt solutions. The ordinary extended Debye-Hückel equation for T = 298 K is:

$$-\log(f_{DH}) = \frac{0.51\sqrt{I}}{1+ \text{å } 0.33\sqrt{I}} \tag{A1.10}$$

å may be thought of as the mean effective diameter of the ion. Kielland tabulated values for the parameter å. In the case of $H^+$ and $OH^-$ å is 9 and 3.5, respectively. For temperatures other than 298 K the value 0.51 has to be changed in both Eqs. (A1.9) and (A1.10).

The actual concentration of protons can be calculated, making use of the initial proton amount, the added amount of base, the ionic strength and the dissociation constant for water. Before the equivalent point the transformation of pH to $H^+$ concentration is done using the theoretical definition of pH. After the equivalence point the pH is transformed to pOH, using the Relation (A1.11). Subsequently the pOH can be transformed to [OH⁻].

$$pOH = pK_w - pH \tag{A1.11}$$

Where $pK_w$ is the water constant at the given temperature (See also appendix III).

A solution of an indifferent electrolyte with known volume and proton concentration is titrated with a base and the theoretical pH is calculated after each addition of the titrant. We start with an acid solution containing an initial amount of acid $c_A V_A$. To this acid we titrate an amount $c_{Ti} V_{Ti}$ of the base. The amounts are calculated by multiplying the concentration of the specific ion with the volume added. In the cell with a total volume of $V_{TOT}$, this leads to the following proton concentration, [H⁺], and a hydroxyl ion concentration, [OH⁻].

$$V_{TOT}\left([H^+] - [OH^-]\right) = c_A V_A - c_{Ti} V_{Ti} \tag{A1.12}$$

This can be written more simple by in terms of the actual proton excess concentration, $[H]_A$:

$$[H]_A = \frac{c_A V_A - c_{Ti} V_{Ti}}{V_{TOT}} \tag{A1.13}$$

where $[H]_A$ is defined as

$$[H]_A = [H^+] - [OH^-] \tag{A1.14}$$

In order to find $[H^+]$ the water equilibrium has to be used:

$$K_w = f^2 [H^+][OH^-] \tag{A1.15}$$

Substitution of Eq. (A1.15) into Eq. (A1.14), leads to

$$[H^+]^2 - [H^+][H]_A - \frac{K_w}{f^2} = 0 \tag{A1.16}$$

Eq. (A1.16) can be solved for the $[H^+]$, using

$$[H^+] = \frac{[H]_A + \sqrt{([H]_A)^2 + 4\dfrac{K_w}{10^{2\log(f)}}}}{2} \tag{A1.17}$$

with f obtained by Eq. (A1.9) or (A1(A1.10))

Both relations require the knowledge of the ionic strength for the calculation of f. The ionic strength depends on the initial salt concentration ($c_s$) and the added reagents. Before the equivalence point the ionic strength is about constant, addition of base only changes $V_{TOT}$, but not the amount of ions, because of the equilibrium

$$HNO_3 + KOH \leftrightarrow H_2O + KNO_3 \tag{A1.18}$$

So before the equivalence point the ionic strength can be calculated as:

$$I = \frac{V_S c_S + V_A c_A}{V_{TOT}} \tag{A1.19}$$

After the equivalence point the added base may increase the ionic strength, because all the acid will be neutralised at the equivalence point, the ionic strength becomes:

$$I = \frac{V_S c_S}{V_{TOT}} + \frac{V_A c_A + (V_{TI} c_{TI} - V_A c_A)}{V_{TOT}} \tag{A1.20}$$

Eqs. (A1.19) and (A1.20) can be combined to the following expression

$$\sqrt{I} = \frac{\sqrt{2V_S c_S + |V_A c_A - V_{TI} c_{TI}| + V_{TI} c_{TI} + V_A c_A}}{2V_{TOT}} \tag{A1.21}$$

A check on the validity of the equations used to transform concentrations in activities (pH) can be done by recording titrations at different (constant) salt concentration. If the mean activity coefficient of the proton is properly calculated, a plot of pH versus EMF, according to Eq. (A1.4), is independent of the salt concentration. When only the activity coefficient is incorrect, curves with an equal slope but different

intercept are obtained. This is illustrated by Eqs. (A1.22) and (A1.23) that give an alternative representation of Eq. (A1.4).

$$E_{CELL} = E_{0,CELL} + \frac{RT}{F} pH \tag{A1.22}$$

$$E_{CELL} = E_{0,CELL} + \frac{RT}{F} \left[ \log(f) \pm \log(c_{H^+}) \right] \tag{A1.23}$$

Different intercepts might be related to the variation of the log (f) term; that is a theoretical error is involved in the calculation of the mean activity coefficient of the proton, and/ or to the variation of the "standard potential" of the cell. Variations of the latter should be small if the salt bridge is working properly.

This calibration method has to give similar results compared to the buffer calibration, i.e. the EMF-theoretical pH equation obtained and the EMF-buffer pH equation should be very similar. This can be checked by plotting the experimental EMF versus the operational and the theoretical pH (Figure 2). Obviously both plots should be straight lines. In general the blank titration deviates somewhat from a straight line. Only when a good match between the two calibration equations is found, the experimental set-up and the procedure to calculate the activity coefficients may be considered reliable.
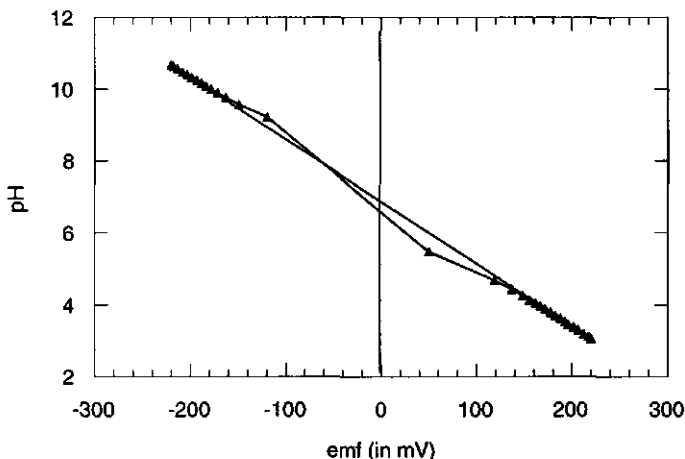


**Figure 2:** pH-EMF (mV) from blank titration. Both the operational pH that is based on a buffer calibration (straight line) and the theoretical pH (▲).

A good match between the two methods means that when plotted as EMF versus pH there should hardly be any differences between the points at the extreme pH values, whereas the middle section of the curve based on the theoretical pH may show some scatter. If the operational and the theoretical pH-EMF curves differ significantly, the cell components should be cleaned and the electrodes should be reactivated. Further improvement can be achieved by changing $E_{0,CELL}$ and B within the acceptable range of values till a good fit between operational and theoretical blank titration is observed. This procedure allows us to (semi-empirically) fit the blank curve as good as possible. It is also possible to adjust $c_{Ti}$ but this parameter is precisely known if the equivalence point is sharp (Gran plot (Figure 1)).

Another argument corroborating the validity of the calibrations can be made by plotting $V_{Ti}$ versus operational and theoretical pH (Figure 3). If the shape of both curves is identical, but the operational pH curve is shifted parallel with respect to the theoretical pH curve, this is an indication of (1) an inaccurate

value for the normality of the titrant used for the blank titration, (2) the burette is leaking or (3) the activity coefficient is systematically in error.

Note that the present procedure compares pH versus EMF plots (or pH versus ml plots), that is to say the log of the concentration is used. It is however also possible to compare $10^{-pH}$ versus EMF (or ml) plots. In this case concentrations are compared and less weight is given to the region around pH 7 in the comparison.
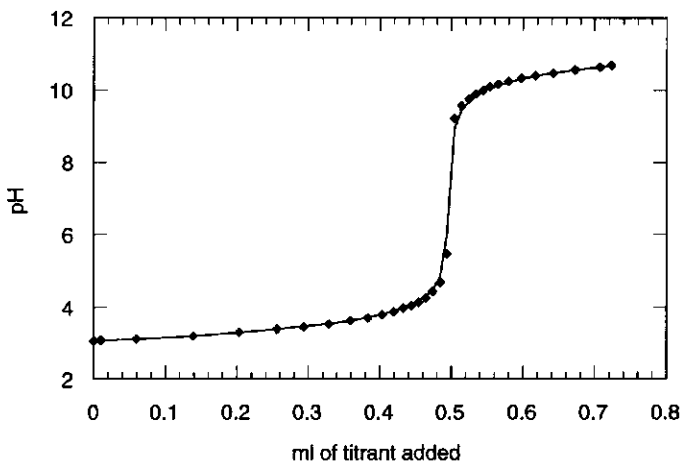


**Figure 3:** Blank titration curve as obtained using the operational pH that is based on a buffer calibration (solid line) and the theoretical pH ($\blacklozenge$).

## Calculation of the sample titrations

In order to obtain the surface charge-pH plot of a colloid, a suspension containing the colloid in a solution of known electrolyte concentration and volume is titrated. The result is a data set of measured EMF versus ml titrant. An acceptable result is obtained when the total amount of titrant required for the sample is considerably larger than that for the blank (at least twice the amount). The measured EMF can be transformed in pH by using the $E_o$ and B values based on the operational pH adjusted after calibration with the experimental blank. To obtain the acid or base consumption of the colloid from the titration result, the consumption by the solution has to be subtracted from the total consumption. A simple way to do this is by measuring a blank titration and to subtract at a given pH the blank consumption from the suspension consumption of acid or base. The disadvantage of this procedure is that in principle the volume range of the blank titration can never be the same as that of the suspension titration, the latter always requires a larger amount of titrant. To overcome this problem the "blank amount of protons in the solution" at each datapoint (pH, $V_{TOT}$) of the suspension titration in a given electrolyte solution has to be calculated. As $V_{TOT}$ is known the amount of protons in the solution can be calculated when the proton concentration corresponding with the measured pH is known. For this calculation a calibration is required. Two procedures related to the two EMF-pH calibration methods have been described in the previous section: (1) the operational pH definition is used in combination with an experimental calibration of proton activity, $a_H$, versus proton concentration, $c_H$ and (2) the theoretical pH definition is used; once the activity coefficient relation is chosen $c_H$ can be calculated using Eq. (A1.5).

In both cases blank titrations (same conditions as the sample titrations) are used to establish the $a_H$ - $c_H$ relation. In the first case the EMF is linked to the operational pH and the blank titration provides the $a_H$ - $c_H$ calibration curve. In the second case the blank is used to choose the activity coefficient relation and to

obtain the EMF-theoretical-pH calibration, subsequently each theoretical pH can be transformed in a proton concentration. With the known $a_H$ - $c_H$ or pH- $c_H$ relation the concentration of protons at a measured pH value in the solution containing the sample can be obtained. The surface charge variation of the sample in going from $(pH, V_{TOT})_1$ to $(pH, V_{TOT})_2$ in the titration is now obtained from the difference $\Delta$mmol (ads) between the actually added amount of OH⁻ and the amount of protons removed from the solution:

$$\Delta\sigma = \frac{F \, \Delta \, \text{mmol (ads)}}{m \, S} \tag{A1.24}$$

where F is the Faraday constant, m the weight of the solid and S the specific surface area. By choosing the appropriate units $\Delta\sigma$ is obtained in $C/m^2$. When S is unknown $\Delta\sigma$ can be expressed in C/g. In the next sections the third procedure to calculate $c_H$(ads) will be explained in detail.

*Subtraction of a theoretical blank*

The third calculation method is based on the theoretical pH concept as used in multiple equilibria calculations. For each addition of titrant to the solid, the amount of base that is required by a hypothetical blank solution of the same volume as the sample, to reach the pH of the sample, is calculated. Specifically, the ionic strength, the total volume and the activity coefficient for the protons are calculated.

The surface charge-pH relation can be derived from the suspension titration and a calculated theoretical blank curve. After each addition of titrant the mmoles of H⁺ adsorbed on the sample at moment t are given by

$$\text{mmol}_{TI(ADS)}(t) = V_{TI} \, c_{TI}(t) - \text{mmol}_{BLANK}(t) \tag{A1.25}$$

The $\text{mmol}_{BLANK}(t)$ is calculated as described previously for $[pH, V_{TOT}]_t$ and $[pH, V_{TOT}]_{t=0}$ observed with the suspension titration. This can be done using the following relation:

$$\text{mmol}_{BLANK}(t) = \left([H^+] - [OH^-]\right) V_{TOT}(t) - \left([H^+] - [OH^-]\right) V_{TOT}(t=0) \tag{A1.26}$$

where

$$[H^+](t) = 10^{[-pH(t)-\log(f)]} \tag{A1.27}$$

and

$$[OH^-](t) = 10^{[pH(t)-pK_w-\log(f)]} \tag{A1.28}$$

The activity coefficient, f, in Eqs. (A1.27) and (A1.28) is calculated with the Davies equation (A1.9) (or with the extended DH equation (A1(A1.10))).
From Eq. (A1.25) the surface charge increment is obtained as:

$$\sigma(t) - \sigma(t-1) = F \frac{\text{mmol}_{TI(ADS)}(t)}{m \, S} \tag{A1.29}$$

which is an alternative formulation of Eq. (A1.24). The obtained surface charge curve only shows the excess charges on the surface and not the absolute number of charges.

## Experimental set-up

Next to the methodological aspects described in the previous paragraph, the equipment itself and the operation of the titration set-up influence the correctness of the obtained data. Therefore the accuracy of the experimental set-up as well as the data treatment have to be considered. At first we will discuss the cell itself and explain the precautions that have to be taken to retrieve reliable data. Further we will describe several methods that can be used to calibrate the electrodes and we describe some experiments that have to be performed prior to any suspension titration.

*The cell*

The titrations are performed in a glass jacketed, 80 ml Duran vessel that is kept at a constant temperature using a circulating water bath. The vessel is continuously purged with high purity nitrogen gas. The titrator unit and electrode measurements are computer controlled.

The titration vessel is sealed with a polypropylene screw cap. A silicon rubber ring provides a gas-tight seal between the screw cap and the glass cell. The polypropylene screw cap is equipped with five sockets that provide access to electrodes, burette(s) and gas lines. The titration vessel with its components is shown in Figure 4 The arrangement can be changed easily for experiments that require three or more electrodes. For example, a Teflon accessory can be used that allows the addition of gas and liquids through only one socket.
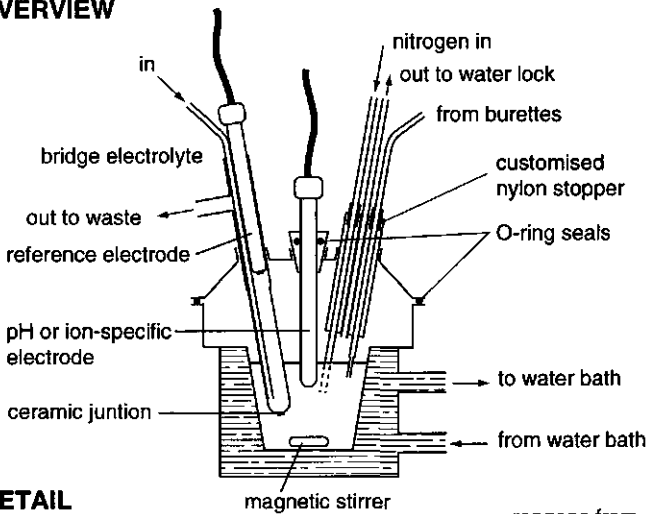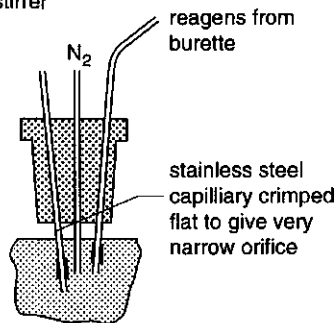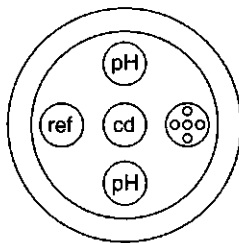


Figure 4: An overview and some detail sketches of the titration cell.

In order to prevent carbon dioxide leaks into the cell, Teflon socket joints are placed between the electrodes and the openings in the cap. Stirring is controlled by the computer program.

The entire cell plus burettes and storage bottles are placed in a thermostatted cabinet. The temperature of the cabinet is controlled independently at a slightly higher temperature than the titration cell to prevent condensation of the solutions.

The glass cell is cleaned very thoroughly, rinsed with high-purity water (mixed bed/ ion exchange/ active carbon/ micro filter) and dried before use (a polypropylene vessel must be used for the titration of a suspension and cadmium titrations, when interactions with the glass wall have to be avoided). The burette cylinders and the tubing connecting the burettes with the cell are rinsed several times with the titrant in order to eliminate contaminates and/ or trapped air bubbles. A clean dry stirrer is placed in the cell. Clean freshly rinsed electrodes, dried with a lint-free tissue, are placed in the cap that is subsequently connected to the glass cell.

Before the experiment can be started the solution is outgassed extensively. During this procedure the solution is stirred continuously. Measurement of a stable pH can be used as an indicator on the state of the cell.

Often it is advisable also to record the solution/ suspension pH before acid or base addition as this provides information on the solution/ suspension as received.

Once the cell is prepared for a titration it should remain closed, additions (titrant, reagent) have to be made through a septum in order to prevent carbon dioxide entrance.

*Exclusion of carbon dioxide*

As mentioned before the total exclusion of carbon dioxide is an essential aspect concerning the exactness of proton titrations. Precautions have to be taken to assure that the cell and the solution or suspension to be titrated are free of carbon dioxide.

To minimise the presence of carbon dioxide in the solution or suspension, prior to a titration the cell contents are outgassed under vacuum or purged with nitrogen at a cell pH of about 4. After this pre-treatment a small over pressure of nitrogen - several centimetres of water - is maintained permanently in the titration cell. In Figure 5 the nitrogen line, which is used during the experiments, is sketched.
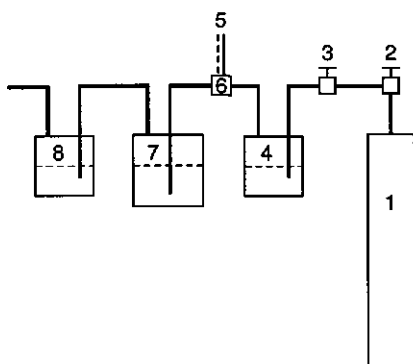


**Figure 5:** The nitrogen line (argon line): **1.** Cylinder with 99.995 $N_2$/ Ar; **2.** Pressure regulator and valve; **3.** Flow regulator; **4.** Washing flask (water); **5.** Interface (computer); **6.** Computer controlled gas flow splitter; **7.** Titration vessel and **8.** Water lock ($Ba(OH)^2$ solution).

A high-purity $N_2$ gas cylinder, equipped with pressure regulators and a fine flow regulator is used. The $N_2$ passes through a washing solution in order to remove possible impurities and to saturate the $N_2$ with the solution (it is also possible to pass the $N_2$ through a suspension of a solid similar to the one to be titrated;

the solid can adsorb possible impurities still present in the gas). Then the flow is split in two directions; one line ends above the solution in the titration cell and allows $N_2$ gas flow only during the reading of the EMF, while the other line is submerged in the solution and permits gas flow in between the EMF measurements only. The system is controlled directly by the interface. The gas outlet is dipped in a water lock filled with $Ba(OH)_2$ in order to prevent both evaporation of the solution and carbon dioxide penetration. As the narrow bore tubes are made of Teflon that is not entirely gas tight and allows a certain degree of air permeation these lines should be as short as practically possible.

Instead of nitrogen, argon gas can be used. The advantage of argon is that it forms a blanket over the solution that is less permeable to carbon dioxide. As a consequence it is not necessary to maintain a fast gas flow during the experiment.

Glass containers may be slowly dissolved by alkaline solution. When such reagents are kept in storage for an extended period of time, polypropylene bottles (Metrohm c.n.6.1608.004) should be employed. Metrohm determined three equivalents points (pH = 10.739 (alkaline), pH = 10.770 (carbonate) and pH = 10.838 (silicate)) for 0.1M alkaline solutions stored in glass bottles, whereas only two equivalent points, one for the alkali and one for the carbonate, were found for the same alkaline solution stored in polypropylene bottles. The $CO_2$ leakage for both bottles was about the same. The error involved corresponded to a variation of 0.2% in the titrant. The main problem with suspension titrations is, however, the introduction of silicates that may adsorb to the solid under study.

The alkaline solution concentration may change because of leakage of carbon dioxide into the bottles. An ulterior absorber for carbon dioxide is a bottle with a solution of KOH that reacts with the $CO_2$ present in the air (or gas supply to pressurise the bottle). The use of this type of device requires an externally applied pressure, otherwise refilling of the burette cylinder could cause problems. The set up is shown schematically in Figure 6a.
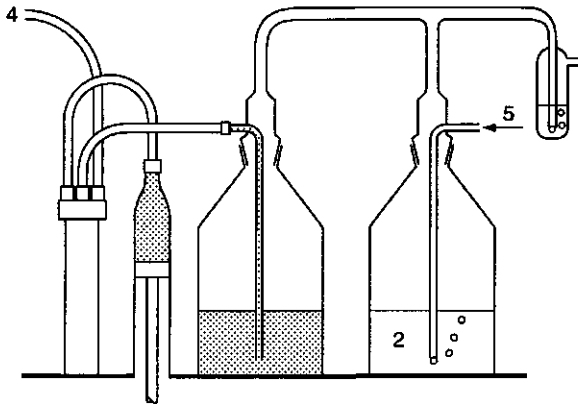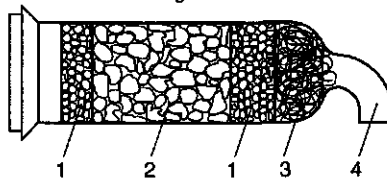


Figure 6a



Figure 6b

**Figure 6:** Several systems to prevent contamination of the stock solutions with $CO_2$; **1.** $CaCl_2$; **2.** NaOH; **3.** Glass wool; **4.** Connection to the burette bottle and **5.** $N_2$ gas flow.

An alternative arrangement that prevents contamination of solutions by atmospheric carbon dioxide is shown in Figure 6b. Two sections of a hygroscopic compound ($CaCl_2$) confine a section of supported NaOH in the centre of a drying tube. The air entering the storage vessel is contacted with the hygroscopic compound that absorbs moisture present in the air and produced in the reaction between $CO_2$ and NaOH. Tests with this set-up were not always satisfactory when applied to standard alkaline solutions but were satisfactory for acid and salt burettes.

*The salt bridge*

When leakage of electrolyte from the reference electrode can spoil the cell solution by changing the electrolyte concentration or by contaminating the cell with unwanted electrolyte, a salt bridge has to be used. In this case the contact between the reference electrode and the solution is made through the salt bridge. Several options are available: tubes with a ground glass joint, a Pt-wire (Schott) or a ceramic plug, and finally the van Laar type salt bridge with two microcapillaries. The first three bridge types can be described as a glass tube provided with a narrow opening at one end. This tube is filled with the appropriate electrolyte solution. The differences between the plugs are electrical resistance and salt leakage across the opening. The ground glass joint has the lowest resistance and the highest leakage, the ceramic plug the highest resistance and the lowest leakage. During the measurements the filling holes of the electrode and of the salt bridge must be left open to the atmosphere, otherwise the flow of liquid through the liquid junctions will stop. Also, the level of the filling solution should be higher than that of the cell. A slow leakage through the junction is needed in order to maintain electrical contact with the surrounding solution in order to prevent unstable potentials.

The salt concentration of the salt bridge has to be as invariable as possible; therefore, at low bridge concentrations ($10^{-3}$ M) a continuously slow-flowing electrolyte should be used. This prevents any changes in the bridge liquid-junction potentials due to a change in the salt concentration of the bridge solution. When a simple salt bridge is used the type of salt and the salt concentration in the bridge should preferably be the same as those in the cell. In principle the liquid junction potential between bridge and cell solution is negligible if the two solutions are identical.

The van Laar bridge consists of two capillaries having an electrical resistance of ca. 0.3 M$\Omega$ each, connected by a specially constructed "tube" to allow an overpressure in the bridge. The bridge is filled with the van Laar solution: 1.75 M $KNO_3$ and 0.25 M $NaNO_3$. Due to the high concentrations transport is dominated by the bridge solution, the composition assures equal mean mobility of anions and cations, thus limiting any diffusion potential over the bridge. An overpressure of about 0.3 bars is permanently maintained in the bridge to assure that the liquid junction takes place outside the capillaries. The van Laar bridge is used preferably when an experiment is done with varying salt concentrations, when the ions of the electrolyte used in the cell have a rather different transport number, when chloride must be seen as a contaminating ion or when experiments are carried out at a series of temperatures. In the latter case the reference electrode can be kept at a constant and different temperature than the cell. One of the disadvantages of this bridge is that crystallisation of the van Laar solution can occur and the narrow bore capillaries of the bridge can be easily blocked.

*Stirring*

Electrolyte concentration gradients in the cell are undesirable; therefore, stirring during and for a short period after the addition of acids, bases and/ or electrolyte solutions is necessary. The stirring of the sample should be vigorous enough to assure sample homogeneity without giving rise to foaming, and it should also cease before a measurement in order to assure a precise reading. On the other hand in cases where settling of the suspension occurs and resuspending is difficult continuous stirring can be the only option.

Two options are available, these are a magnetic stirrer and an impeller. Using the later requires a special "lock" and one of the openings in the polypropylene cap has to be used for this purpose; therefore, less space is available for the electrodes and the inlet and outlet of gases and liquids' lines. Using the impeller eliminates the possibility of having problems with a magnetic stirrer due to e.g. electric fields or magnetic or magnetisable suspensions such as iron oxide. Further, an impeller does not pulverise the particles in the cell. In order to keep the cell gas tight a special lock around the impeller shaft is required. To prevent pulverising of the colloidal particles using a magnetic stirrer, a stirring bar with a moulded pivot ring positioned half way along its length is used.

## Absolute position of the surface charge-pH curve

Measuring potentiometric titrations the addition of indifferent electrolyte between the successive titrations causes a redistribution of protons which changes both charge on the particles and the pH of the solution. The relative position of the curves at different salt concentrations may be established from the change in pH upon salt addition or alternatively by a pH-STAT-titration where the salt concentration is varied at constant pH. Performing a pH-STAT titration the extra surface charge induced by the added salt is calculated from the amount of titrant needed to retrieve the starting pH. In this case no activity coefficients are required. From the change in pH or the pH STAT result the change in charge upon salt addition can be calculated, provided that the volume is known. In this way the surface charge-pH curves at different salt concentrations can be positioned relative to each other.

To retrieve an absolute position of the surface charge-pH curve, the exact value of one point of a set of curves has to be known. Several possibilities are available as such a point, for example the point of zero charge (p.z.c.), isoelectric point (i.e.p.) or the maximum number of titrateable acidic or basic groups.

A first approximation can be made on the basis of the first derivative. In the absence of any specific adsorption of ions, and assuming that the surface potential is homogeneous over the entire surface, the p.z.c. corresponds to the common intersection point of successive surface charge versus pH curves of increasing ionic strength. It has been shown that due to specific adsorption a shift of the p.z.c. occurs. The p.z.c. is reflected in the surface charge-pH curve as an inflection point and thus the first derivative shows a maximum. An exact value of the p.z.c. can only be obtained experimentally. Different procedures can be attributed to determine the p.z.c. of a colloidal suspension. Which method can be used depends on the colloid of interested, more specific on the p.z.c. of the colloid of interest. Since reliable titrations can only be performed in the range of pH 3 up to 11, the p.z.c. can only be determined inside this window. Several options are available; measurement of the common intersection point of the surface charge-pH curves at different ionic strengths or by measuring the pH change on addition of the colloid to different electrolyte solutions with different pH values. Other methods like determination of the i.e.p. by measuring the zeta-potential are also possible. If the p.z.c. is located outside the accessible pH range, the total titrateable groups can be used to ascribe one absolute point to the titration curve.

Titrations performed to determine the p.z.c. use a small pH window around the p.z.c. (8), and should be performed as one continuous experiment. The titration should be started at the lowest salt concentration, checked for hysteresis and after the addition of the next salt dose a waiting time should be imposed.

An alternative procedure to determine the p.z.c. (8) is based on the fact that below and above this point addition of an uncharged colloid, to an indifferent electrolyte solution with a specific pH, influences the pH. Due to a decrease and respectively increase of the excess of protons, the pH will change. An important feature concerning this method is the fact that the colloid under investigation has to be uncharged (in the proton form). Further it is essential that the colloid does not contain any free acid or base.

Next to these measurements of the p.z.c. a method to determine the maximum number of titrateable groups can also be used to ascribe an absolute value to one point of the curve. This can be done with a so called Boehm experiment (9,10). Two types of Boehm experiments can be performed, one to determine the maximum number of acidic groups and one for the number of basic groups. As an example

we discuss the method to determine the maximum titrateable acidic groups: to a colloidal suspension in an electrolyte solution sufficient base is added to react with all the available acidic groups. The suspension is stirred and equilibrated overnight. After centrifugation the pH of the supernatant is recorded and known amounts of the supernatant are taken. To each aliquot a known excess of acid is added and after removal of the carbon dioxide the samples are back titrated to the original pH.

Following (A1.30) the number of acidic groups can be calculated. Take S mg of the suspension, add b ml of b' M base. Take s ml supernatant, add A ml of A' M acid. Titrate with B' M base to an endpoint of B ml. Then:

$$\text{\# titratable groups} = \frac{\left[\dfrac{bb'+(BB'-AA')b}{s}\right]}{S} \tag{A1.30}$$

### References

(1)  Vermeer, A.W.P.; Giatti, A.; Sunkel, J.; Koopal, L.K. Potentiometric suspension titrations, experimental set-up and data treatment; Internal Report. Wageningen Agricultural University. 1994.

(2)  Gran, G. Determination of the Equivalent Point in Potentiometric Titrations. Part II. *Analyst* **1952**, *77*, 661 -671.

(3)  Rossotti, F.J.C.; Rossotti, H. Potentiometric Titrations Using Gran Plots. *J. Chem. Ed.* **1965**, *42(7)*, 375 -378.

(4)  Skoog, D.A.; West, D.M. *Fundamentals of Analytical Chemistry*; Holt, Reinhart & Winston: London, 1970.

(5)  Davies, C.W. Activity measurements In *Ion interactions*; Butterworths: London, 1962; 34-54.

(6)  Bolt, G.H.; Bruggenwert, M.G.M. Activity coefficients of ions in aqueous solutions In *Soil chemistry 5A. Basic Elements*; Elsevier Scientific Publishing Company: Amsterdam, 1978; 16-20.

(7)  Pabalan, B.M.; Pitzer, K.S. Chemical modelling of aqueous systems II, ACS Symposium series 416. Washington, DC. American Chemical Society. 1990 44

(8)  Breeuwsma, A.; Lyklema, J. Interfacial electrochemistry of haematite. *Discussions of The Faraday Soc.* **1971**, *52*, 324 -333.

(9)  Boehm, H.P.; Diehl, E. Untersuchung an sauren Oberflächenoxyden des Kohlenstoffs. *Z. Electrochem.* **1962**, *66(8/9)*, 642 -647.

(10) Boehm, H.P. Chemical Identification of Surface Groups In *Advances in Catalysis (and related subjects)*; Acad. Press: New York, 1966; 179-273.

## Appendix II: Calculation of the activity coefficient

Using pH glass electrodes, direct access to the proton concentration [H⁺] is not obtainable. The electrodes respond to the "proton" activity, $a_H$. The relation between concentration and activity is given by:

$$a_H = f_H \times c_H \tag{A2.1}$$

where: $f_H$ = the activity coefficient of a proton.

Factors that affect the activity coefficient of an ion can be divided into salt and medium effects. The first group consists of; ionic strength, composition of the electrolyte (e.g., 1:1), and ionic charge. Temperature, dielectric constant, density of the solvent and the size of the ion are the main factors of the second group.

Debye and Hückel (*1*) introduced an expression for the ionic activity coefficient (of an ion with valence z).

$$\log(f_z) = \frac{A z^2 \sqrt{I}}{1 + B \mathring{a} \sqrt{I}} \tag{A2.2}$$

where:

$$I(\text{ionic strength}) = \frac{1}{2} \sum_i \left( c_i z_i^2 \right) \tag{A2.3}$$

A and B are two fundamental constants of the Debye Hückel theory and å may be thought of as the mean effective diameter of the ion. Kielland (*2*) tabulated the values of å for 130 ions. The values of å for H⁺ and OH⁻ equal 9 and 3.5 Å respectively. The temperature dependence of A and B will be described later. For simple electrolytes this equation is a very good approximation. For more complex electrolyte mixtures and ionic strength values in the range of I = 0.1 to 0.5 mol/l Davies (*3*) proposed the formula:

$$\log(f_z) = -A z^2 \left[ \frac{\sqrt{I}}{1 + \sqrt{I}} + C I \right] \tag{A2.4}$$

where the value of the empirical parameter C equals 0.2. Later Davies (*3*) re-assessed the accuracy of Eq. (A2.4) and has proposed the revised value of C = 0.3. For a large number of electrolytes this value gives an acceptable fit with experimental data. The use of a higher value, C = 0.4 gives even better results (*4*) for some electrolytes. Other equations to calculate the activity coefficient as well as some further information on the described equations can be found elsewhere (*5,6*).

The constants A and B are temperature dependent according to Eqs. (A2.5) and (A2.6).

$$A = \frac{\log(e) 2^{1/2} e F^2}{8 \pi (\varepsilon \varepsilon_0 R T)^{3/2}} = \frac{0.0244 e F^2}{(\varepsilon \varepsilon_0 R T)^{3/2}} \tag{A2.5}$$

$$B = \frac{2^{1/2} F^2}{(\varepsilon \varepsilon_0 R T)^{1/2}} \tag{A2.6}$$

where: $e = 1.602 \times 10^{-19}$ C, F = 96486.7 C/mol, $\varepsilon_0 = 8.85419 \times 10^{-12}$ F/m and R = 8.3143 J/(mol K).

Apart from the direct effect of T, the temperature also affects $\varepsilon$. Several equations are proposed to describe this dependence (7). Wyman and Ingalls (8) derived the relation:

$$\varepsilon = 78.54\left[1 - 0.00460(T - 298.15) + 0.0000088(T - 298.15)^2\right] \qquad (A2.7)$$

where T is in K.

## References

(1)  Debye, P.; Hückel, E. *Physik. Z.* **1923**, *24*, 305
(2)  Kielland, J. *J. Amer. Chem. Soc.* **1937**, *59*, 1675
(3)  Davies, C.W. *J,Chem. Soc.* **1938**, 2039
(4)  Nancollas, G.H. Electrochemistry. Proc. 1st Aust. Conf. Electrochem. London. Pergamon. 1964
(5)  Nancollas, G.H. *Interactions in electrolyte solutions*; Elsevier Publishing Company: Amsterdam, 1966.
(6)  Bates, R.G. *Determination of pH, Theory and practice*; John Wiley & Sons: New York, 1964.
(7)  Franks, F. *Water a comprehensive treatise*; Plenum Press. New York, 1972.
(8)  Wyman, J.; Ingalls, E.N. *J. Amer. Chem. Soc.* **1938**, *60*, 1182

## Appendix III: Calculation of the pK$_w$

In acid/base titrations the water equilibrium is of crucial importance: while titrating, the water molecules of the aqueous phase dissociate to form protons and hydroxyl ions.

$$H_2O \overset{K_w}{\rightleftarrows} H^+(aq) + OH^-(aq) \tag{A3.1}$$

Under ordinary conditions, the water equilibrium is almost completely on the side of the water molecules. At 24°C and atmospheric pressure the value of the ionic product $K_w = [H^+][OH^-] = 10^{-14.0000}$ and thus pK$_w$ equals 14.0000. The ionic product is defined as:

$$K_w \equiv c_H \times c_{OH} \quad \text{or as} \quad K_w \equiv m_H \times m_{OH} \tag{A3.2}$$

where $c_H$ and $c_{OH}$ is the concentration in mol/l and $m_H$ and $m_{OH}$ that in mol/kg, so that $K_w$ is expressed either as mol$^2$/l$^2$ or as mol$^2$/kg$^2$. These two definitions are only equal when the density $\rho_o$ equals 1000 kg/m$^3$. Further a dimensionless quantity pK$_w^{\cdot}$ has been defined as $K_w/(\text{mol}^2/l^2)$ respectively $K_w/(\text{mol}^2/\text{kg}^2)$.

pK$_w$ is temperature dependent and several equations are available to calculate pK$_w$ (T). Apart from the direct effect of T on $K_w$, the temperature also affects $\rho$. Again several equations are available to calculate the extended pK$_w$ (T, $\rho$). Holzapfel (1) (1969) obtained the following relation for the ionic product pK$_w$ (T) as a function of temperature.

$$pK_w(\rho_0, T) = -(3108/T) - 3.55 \tag{A3.3}$$

where: T in K, $K_w$ in mol$^2$/l$^2$ and $\rho_0$ = 1 kg/dm$^3$. The extended formula, as a function of temperature and density is given by:

$$pK_w(\rho, T) = 2[7.2 + 2.5(\rho/\rho_0)]\log(\rho/\rho_0) + pK_w(\rho_0, T) \tag{A3.4}$$

where: T in K, $K_w$ in mol$^2$/l$^2$ and $\rho_o$ = 1 kg/dm$^3$. The value for $\rho$ is obtained by Eq. (A3.7).

Later Marshall and Franck (2) (1981) have described an improved equation for the ion product of water, based on the reciprocal absolute temperature.

$$pK_w^{\cdot}(\rho_0, T) = A + \frac{B}{T} + \frac{C}{T^2} + \frac{D}{T^3} \tag{A3.5}$$

where: T in K, pK$_w^{\cdot}$ = $K_w$/mol$^2$/kg$^2$, $\rho_o$ = 1 kg/dm$^3$ and the constants have the following values.

$$A = -4.098$$
$$B = -3245.2 \text{ K}$$
$$C = 2.2362E5 \text{ K}^2$$
$$D = -3.984E7 \text{ K}^3$$

(note that the pK$_w^{\cdot}$ described by Marshall and Franck is dimensionless).

The extended equation based on the density and the reciprocal absolute temperature of Marshall and Franck is:

$$pK_w^* (\rho, T) = pK_w^* (\rho_0, T) + k \log(\rho^*) \tag{A3.6}$$

where: $k = (E + F/T + G/T^2)$, $T$ in K, $pK_w^* = K_w/(mol^2\ kg^2)$, $\rho^* = \rho/(kg/dm^3)$, $\rho$ is obtained by Eq. (A3.7) and the additional constants have the following values.

$$E = 13.957$$
$$F = -1261.3\ K$$
$$G = 8.5641E5\ K^2$$

The density of water ($H_2O$) in the range of 0-150°C (273 - 423 K) is given in Eq. (A3.7) as suggested by Kell (3-5):

$$\rho = \frac{a_0 + a_1 t + a_2 t^2 + a_3 t^3 + a_4 t^4 + a_5 t^5}{1 + b\,t} \tag{A3.7}$$

where:
$$a_0 = 999.8396$$
$$a_1 = 18.224944$$
$$10^3\,a_2 = -7.922210$$
$$10^6\,a_3 = -55.44846$$
$$10^9\,a_4 = 149.7562$$
$$10^{12}\,a_5 = -393.2952$$
$$10^3\,b = 18.159725$$
$$t = (T - 273.15),\ T\ \text{in K and}\ \rho\ \text{in kg m}^{-3}.$$

### References

(1) Holzapfel, W.B. *J. Chem. Phys.* **1969**, *50*, 4424
(2) Marshall, W.L.; Franck, E.U. *J. Phys. Chem. Ref. Data* **1981**, *10(2)*, 295
(3) Kell, G.S. *J. Chem. Eng. Data* **1967**, *12*, 66
(4) Gibson, M.R. *Engineer* **1967**, *224*, 417
(5) Franks, F. *Water a comprehensive treatise*; Plenum Press. New York, 1972.

# Summary

The impact of toxic chemicals (like metal ions) on the environment is a phenomenon that has been recognised as a mayor problem over the last decades. The speciation of these chemicals determines whether or not a contaminated site has to be regarded as dangerous. The fate of the contaminants depends on the environment and on the local conditions (pH, electrolyte composition and composition of the natural system). For example: contaminants can leach into the groundwater and become a threat for the drinking water supply, they can have an adverse effect on the organisms living in or on the soil or the chemicals can be stored in the soil without direct adverse effects. The binding capacity of the environment is thus of great importance for predicting the mobility and the bio-availability of metal ions in the natural environment. To make a sound risk assessment of contaminated sites and to support decision makers with information on the need of recovery a specific site, knowledge of the interactions between the different components in the system is inevitable and has to be established.

To approximate the metal ion binding to the soil system, the composition of the soil has to be studied and the different components have to be characterised. Furthermore the proton and metal ion binding to the different components have to be measured, and the effects of the interactions between the different soil components have to be investigated. Once this is done we may be able to predict the speciation of the contaminating metal ions in polluted soils, based on the above described aspects, and make a statement about the risks associated with the contaminated sites.

Soil usually consists of a mixture of organic and inorganic constituents. The inorganic fraction contains silica ($SiO_2$), metal(hydr)oxides of iron, aluminium, and manganese, clay minerals, and may contain calcium carbonate. Clay minerals exhibit a "constant" negative charge, whereas the metal oxides and the organic fraction have a pH dependent charge. For metal(hydr)oxides this variable charge depends on the structure of the material, for humic substances a range of surface groups (carboxylic and phenolic type of groups) with different pK values can be observed. In this investigation we used a "model soil" consisting of a metal(hydr)oxide and a humic acid. Within this system, the metal ions can either bind to the mineral surface, which is presented by hematite particles, and to the organic fraction, a purified commercially available humic acid (PAHA).

A main aspect of studying metal ion binding to model systems is the relation between the metal ion binding in the model system and that in the natural system. Model systems are of most relevance if one can extrapolate directly the obtained results to the much more complicated natural systems. The possible application of laboratory experiments to estimate the speciation of metal ions in natural systems is improved by the experiments described in this thesis. The relative importance of the interaction between metal oxide and humic material on the metal ion binding in the environment depends strongly on the type of environment. So far some results have been obtained in predicting metal ion binding for systems where the above mentioned

interaction is expected to be a second order effect. However, in numerous environmental systems some of the binding sites of the organic soil fraction may be masked or neutralised by the interaction with the metal oxide surfaces or other mineral components of the soil matrix. In my study, the effects of these interactions between the different soil components on the proton and cadmium binding to both the organic and the mineral species have been investigated in detail.

Summarising, the main goal of this study was to establish qualitative, and where possible, quantitative models that can be used to predict the metal ion speciation in the natural environment by doing laboratory experiments with a model soil. To achieve this goal we studied the proton and metal ion binding to the single components of our model soil as well as to some PAHA/ hematite complexes. To be able to investigate the effect of the adsorption of PAHA onto hematite on the metal ion binding, also these interactions were extensively investigated. The latter experiments were compared with theoretical calculations based on the Self Consistent Field theory for polyelectrolyte adsorption.

In general Humic substances are described as a mixture of naturally occurring, polydisperse, heterogeneous polyelectrolytes. Humic acids are predominantly negatively charged due to the abundance of carboxylic and phenolic type of groups. Due to the hydration of the charged groups and the electrostatic repulsion between these charges the humic acids can be described as having an extended conformation that adjusts itself to changes in the environmental conditions. A change in pH and salt concentration resulting in a reduction or increase of the electrostatic repulsion will lead to a more tightly or respectively more loosely coiled configuration.

"The" structure of humic acid does not exist, therefore the structure and the geometry of the molecules always have to be approximated. To study the adsorption of these natural polyelectrolytes and the conformation of the adsorbed molecules and that of the molecules in solution a model would be appropriate. Often cited models are those described by Ghosh and Schnitzer and Cameron et al. Based on the structural features proposed by these authors, humic acids molecules are often described as fairly flexible polyelectrolytes. Following this description it seems sensible to compare the properties of humic substances with the properties of simple polyelectrolytes as is done throughout this thesis.

The humic acid used in this study reflects many characteristics normally found for humic substances and it may be classified as a soil and/ or peat humic acid. The results obtained for the proton and cadmium binding to the humic acid as a function of pH and salt concentration show the following trends: increasing the salt concentration decreases the binding of cations to the humic acid by reducing the electrostatic attraction. Decreasing the pH increases the proton adsorption but decreases the metal ion adsorption due to the decreased electrostatic attraction and due to an increased competition for binding sites.

For the interpretation of the proton and cadmium adsorption isotherms the NICA-Donnan model was applied. The Donnan model is based on the polyelectrolyte properties of the humic matter and accounts for the electrostatic interactions within the humic acid domains. The Donnan volumes are obtained independently by measuring

the hydrodynamic volumes of PAHA at the conditions at which the isotherms are measured. The Donnan volume can be obtained directly at high (0.1 M) salt concentration by viscosity measurements. At low salt concentrations (0.001 M) the measured gel volumes are to small too satisfy the Donnan model. This can be corrected by adjusting the volumes using the Debye length. The measured Donnan volumes correspond with a humic acid molecule that is much larger than its dry volume. This type of behaviour can be compared with the random coil model, commonly used for simple polyelectrolytes. The observed trends in the hydrodynamic volume of the humic acid molecules can be explained by electrostatic effects. With increasing electrostatic repulsion the hydrodynamic radius of the humic acid molecules increases. With increasing ionic strength the charge is shielded and consequently the hydrodynamic radius of the PAHA molecules decreases.

The proton and cadmium binding to the hematite particles show comparable trends upon pH changes as was observed for PAHA, however, some significant differences have to be mentioned. Whereas the humics are negatively charged over the entire pH range studied, the hematite particles are predominantly positively charged. Hematite is strongly positive at low pH, and becomes less positive until the p.z.c. (p.z.c. of hematite equals 8.9) is reached, where the surface is electrically neutral. The adsorption of cadmium ions at pH 4 and 6 occurs against the electrostatic repulsion between the positively charged cadmium ions and the hematite surface. Cadmium ions can, at pH values far below the p.z.c., only adsorb onto the bare hematite due to strong specific interactions. As a consequence the cadmium adsorption at pH 4 is hardly measurable, whereas at pH values around the p.z.c. the adsorption is increased by several orders of magnitude. This in contrast to the humic where the pH dependence of the cadmium adsorption is only small.

The next step in the evaluation of the effects of the interactions between the different components on the metal ion binding was to study the interactions between the humic and the hematite particles. Adsorption isotherms were measured as a function of pH, salt concentration and cadmium concentration. The adsorption of the humic material to the oxide increases with decreasing pH and increasing salt concentration. This is mainly due to charge differences between the negatively charged humic material and positively charged hematite. It was concluded that both coulombic and specific interactions were essential to describe the observed dependencies of the humic acid adsorption. Due to the specific adsorption energy superequivalent adsorption occurs.

Studying the adsorption of PAHA onto hematite again the humic acid molecules were assumed to behave as fairly flexible polyelectrolyte molecules that were able to adjust their conformation upon adsorption. The conformation of the adsorbed layer as well as the adsorbed amount was described using a description that was developed for polyelectrolyte adsorption. Within this model the adsorption of chain molecules is described in terms of "trains" and "loops and tails". At high pH and low salt concentration the PAHA molecules are adsorbed relatively flat on the surface, which was described by a relatively large fraction of "trains". At low pH and high salt concentration a large fraction of the adsorbed PAHA is not in direct contact with the surface. Due to this a significant amount of adsorbed polyelectrolyte can be described

as adsorbed in "loops and tails", which results in a high adsorbed amount. These pH dependencies were also reflected in the layer thickness of the adsorbed PAHA as was measured by Dynamic Light Scattering. Because of the excess negative charge associated with the adsorbed humic acid segments extending from the surface, superequivalent adsorption gives rise to an electrostatic barrier. The developed electrostatic barrier reduces further adsorption, and causes also very long equilibrium times.

The effects of polydispersity on the shape of the adsorption isotherms and on the adsorption/ desorption hysteresis were studied theoretically. From experiments on humic acid/ fulvic acid mixtures it could be concluded that in general the higher molecular weight fraction of the humics adsorbs preferentially onto hematite and causes the gradual increase of the measured adsorbed amount that was observed with increasing humic acid equilibrium concentrations. It was shown that the adsorption/ desorption hysteresis upon dilution could be ascribed to the adsorption fractionation and is not an indication of irreversible adsorption.

Proton adsorption to mixtures of PAHA and hematite, as a function of the overall PAHA concentration, was compared with the proton adsorption to the single components. The proton binding to the humic acid/ hematite complex is influenced by the interactions between both components, and the proton adsorption isotherm is not a simple summation of the proton isotherms to the humic and the hematite separately. Both hematite and humic acid molecules have a variable charge that is affected by mutual interactions between these particles. At low pH values the proton binding to the mixed system was lower compared to the direct sum, whereas at high pH values it was higher. These effects were explained by two additional processes; (1) a decreased proton adsorption to the humic acid and (2) an increased proton adsorption to the hematite particles. Which of the two processes dominates the overall proton adsorption depends on the charge of the interacting particles. Due to the adsorption of the negatively charged humic to the mainly positively charged hematite the electrostatic potential in the vicinity of the hematite surface is changed considerably. The component that influences the potential decay most significantly determines which process dominates. If due to the presence of PAHA a negative potential is developed close to the surface, protons will accumulate in the vicinity of the surface sites resulting in an increased surface charge. If the potential is positive, the dissociation of the adsorbed humic is promoted strongly in the surface region.

An estimate of the differences in proton charge caused by these interactions is obtained by comparison of the proton charge of the individual samples and their complexes. From this comparison it can be concluded that in the adsorbed state some of the carboxylate groups of the humic acid are bound to protonated surface sites of hematite. These groups are less available for further proton binding. In contrast to this an increased proton adsorption on the oxide surface is deducted. The negative potential field of the adsorbed humic acid layer promotes protonation of the hematite surface. The specific adsorption of humic acid to the hematite surface has as additional effect a shift of the p.z.c. of the hematite surface to a higher pH value and an increase of the surface charge of the hematite particles over the entire pH range. Even at moderate coverage with humic acid, the shift of the p.z.c. is of the order of one pH unit,

and therefore quite significant. The screening of the surface by adsorbed PAHA increases the effectiveness of the hematite in binding cations at a given pH value.

The effects observed for cadmium binding to the complex can be ascribed to similar processes as was done for the proton binding. The increased binding to the positively charged surface is the result of a lowering of the positive potential due to the negative adsorbed charge associated with the humic acid. This lowering of the positive surface potential will enhance the binding of cadmium to the reactive sites of the oxide surface. The humic acid adsorption can even overcompensate the positive charge of the oxide. The negative potential for the humic acid molecules not in direct contact with the oxide surface (loops and tails) is equal or less negative than for the free humic acid molecules under the same conditions leading to a measured lowering of the PAHA metal ion affinity as was expected based on the proposed model.

Next to these experiments some model calculations were done to increase our understanding of the complex system. The model calculations were performed with the self consistent field lattice theory for the adsorption of weak polyelectrolytes onto a surface with a variable charge. This theory is an extension of the lattice theory for polymer adsorption originally developed by Scheutjens and Fleer. The lattice in this model serves as discrete sites onto which polymer units, ions and solvent can take positions. The lattice sites in each layer, parallel to the surface, are indistinguishable so that a mean-field approximation should be applied.

The electrostatic double layer was described using a multi-Stern-layer model and the degree of dissociation of the chargeable polyelectrolyte segments was allowed to vary with the distance from the surface. The decay of the electrostatic potential as a function of the distance to the surface and the volume fraction profiles of the polyelectrolyte molecules was calculated numerically as a function of pH, ionic strength and segment-solvent/ segment-surface interaction parameters. Based on these quantities the adsorbed amount, the charge associated with the surface and the adsorbed polyelectrolyte were calculated. Furthermore the importance of different interaction mechanisms; pure electrosorption, specific binding and hydrophobic binding was evaluated.

The incorporation of a variable surface charge within the self consistent field calculations was shown to have a major effect on the description of the interactions. It was shown that both components are able to titrate each other ("internal" titration). Depending on the conditions the charge associated with the adsorbed polyelectrolyte molecules compensates or even overcompensates the surface charge. The electrostatic potential developed around the different components affects the overall electrostatic potential profile which vice versa influences the degree of dissociation of the single components. The segment type that is most important for the developed potential profile determines the degree of dissociation of the other segments. At low pH the surface charge is dominant and consequently the polyelectrolyte segments will mainly be affected via increased dissociation, whereas at high pH mainly the surface sites are affected resulting in an increase of surface charge. Based on these calculations it was possible to approximate the shape of the extra induced charge on the oxide surface in a qualitative way. Using this we could estimate the proton adsorption to the separate components in the PAHA/ hematite complexes.

189

The calculated effects of pH and salt concentration on the conformation of the adsorbed polyelectrolyte were in line with the above described experiments. With decreasing salt concentration and at low pH the surface charge/ polyelectrolyte charge is screened to a lesser extent, the adsorption is increased and the charge adjustment is even more profound. Due to these differences in the degree of dissociation of both components the following trends were observed. At high pH, low salt concentration and high adsorption energy the polyelectrolyte molecules are adsorbed relatively flat on the surface which can be described by a large fraction of train segments. The few segments of the molecule that are not in direct contact with the surface protrude relatively far into the solution due to lateral repulsion effects. Consequently the adsorbed layer formed is very dilute. At low pH and high salt concentration the adsorbed polyelectrolyte layer can be described by a large fraction of adsorbed segments in loops and tails. Due to the high fraction of adsorbed segments in loops the adsorbed amount per surface area is relatively high. The relatively small decrease of the hydrodynamic layer thickness with increasing pH as compared to that of the adsorbed amount is caused by the relatively pronounced reduction in loop segments. The length of the tails decreases only slightly. These observations compared well with the pH dependence of the measured layer thickness as compared to the measured adsorbed amount.

Considering the discussed mechanism controlling the speciation of metal ions in a ternary system, some conclusions can be drawn considering the speciation in the natural environment. It has been discussed that especially at low pH values binding sites are withdrawn from the system, which is attributed to the carboxylate groups of the adsorbed humic acid, whereas at high pH values an increased proton adsorption is observed. Based on the binding characteristics of the metal ions to the single components we may predict the overall adsorption in a qualitative way. The adsorption of metal ions that bind strongly to the organic soil fraction and are only slightly attracted by the oxides will be decreased due to the interactions between the different soil components. In contrast, for species that bind strongly to the mineral particles the adsorption will be increased.

Based on these considerations we can estimate the metal ion binding to a natural, complicated system if we know the binding characteristics of the single components, the composition and the conditions of the system. If the conditions are such that most metal ions bind to the mineral we may expect an increased metal ion adsorption as compared to the laboratory experiments with the single components. A good estimate for this increase can be obtained from the metal ion adsorption isotherm of the surface at about 1 pH unit above the pH of the actual system. If the conditions are such that most metal ions will bind to the organic fraction a decreased metal ion adsorption as compared to the laboratory experiments with the single components may be expected.

In conclusion; by combining laboratory experiments with model calculations further insight has been obtained into the binding of metal ions to mixtures of interacting components. Further it has been shown how this knowledge can be extrapolated to natural systems.

# Samenvatting

De laatste decennia is men er zich steeds meer van bewust geworden dat de vervuiling van de bodem, bijvoorbeeld met zware metalen zoals cadmium, een bedreiging kan vormen voor de huidige samenleving en komende generaties. Steeds vaker blijkt het nodig om gebieden die vervuild zijn door industriële processen en/ of afvallozingen te regenereren. Het spreekt voor zich dat de kosten die met deze schoonmaak verbonden zijn hoog kunnen oplopen. Omdat helaas niet alle vervuilde gronden kunnen worden behandeld, hoofdzakelijk op financiële gronden, zal er een keuze gemaakt moeten worden tussen gebieden met een hoge dan wel een lage prioriteit. Om deze prioriteitsvolgorde vast te kunnen stellen is het van belang dat de risico's, die met de verschillende vervuilde gebieden verbonden zijn, bekend zijn.

Om de risico's van verschillende gebieden tegen elkaar te kunnen afwegen is het van belang te weten hoe de vervuiling in de bodem is opgeslagen. Zo kunnen metaalionen "mobiel" aanwezig zijn; dat wil zeggen dat ze bijvoorbeeld met het regenwater kunnen uitspoelen waardoor ze in het grondwater terecht kunnen komen. Het spreekt voor zich dat het laatste een bedreiging is voor onze drinkwatervoorziening. Ook kunnen ze via de wortels van planten worden opgenomen en vormen ze een bedreiging voor levende organismen die in en op de vervuilde bodem leven. Daarnaast kunnen de zware metaalionen ook zodanig gebonden zijn aan de vaste bestanddelen van de bodem dat ze niet direct beschikbaar zijn, waardoor de chemicaliën als het ware worden opgeslagen en geen direct gevaar opleveren zolang de bindingscapaciteit van de bodem niet wordt overschreden. Het mag dan ook duidelijk zijn dat inzicht in de bindingscapaciteit van het natuurlijk milieu van groot belang is om de verspreiding en de biologische beschikbaarheid van zware metalen te voorspellen.

Om over de verspreiding en de bio-beschikbaarheid van zware metalen een uitspraak te kunnen doen is het van belang dat de compositie van het vervuilde gebied volledig bekend is; de verschillende componenten moeten gekarakteriseerd zijn; de binding van protonen en metaalionen aan deze componenten moet worden gemeten en de interacties en de gevolgen van deze interacties op de metaalbinding moeten worden onderzocht. Slechts wanneer al deze gegevens bekend zijn kunnen we een precieze uitspraak doen over de risico's die aan een bepaalde vervuiling verbonden zijn.

De bodem is een gecompliceerd systeem waarin de volgende componenten voorkomen: organisch materiaal, silicaten ($SiO_2$), metaal(hydr)oxyden van ijzer, aluminium, en mangaan, kleideeltjes en soms kalkdeeltjes. Omdat zo'n natuurlijk systeem te ingewikkeld is om de verschillende interacties te bestuderen hebben we, voor het onderzoek dat in dit proefschrift is beschreven, een modelsysteem gebruikt. Het gebruikte modelsysteem bestaat uit een ijzeroxyde, het hematiet dat aan sommige bodems de kenmerkende rode kleur verleent, en een humuszuur.

Beide componenten hebben een lading die afhankelijk is van de pH van de omgeving waarin ze voorkomen. Hematiet heeft een positieve oppervlakte lading bij pH waarden die in de natuur gebruikelijk zijn (pH < 8), is ongeladen bij pH 9 en negatief geladen bij hogere pH waarden. Humuszuur is bij alle pH waarden die in dit proefschrift worden bestudeerd negatief geladen. Humuszuur is een van de verteringsproducten die zijn ontstaan uit plantaardig en dierlijk afval. Het is heterogeen en polydispers. De belangrijkste reactieve groepen die in humuszuur voorkomen zijn carboxyl- en fenolgroepen. De pH waarbij deze groepen dissociëren hangt af van de aard van de groep en van de omgeving waarin deze groep zich bevindt.

Het doel van het onderzoek dat in dit proefschrift is beschreven was een kwalitatief en, daar waar mogelijk, een kwantitatief model te ontwikkelen dat de metaalionspeciatie in een natuurlijk systeem kan voorspellen, uitgaande van experimenten die in een laboratorium zijn uitgevoerd met modelsystemen. Hiertoe hebben we de proton- en metaalionbinding aan de losse componenten bestudeerd evenals de binding van deze kationen aan enkele humuszuur/ hematiet mengsels. Alvorens laatstgenoemde experimenten uit te voeren hebben we de adsorptie van humuszuur op hematiet bestudeerd. De mate van adsorptie en de conformatie van de geadsorbeerde laag hebben we proberen te begrijpen door de humuszuurmolekulen te beschouwen als eenvoudige lineaire polyelektrolietmolekulen. Hierbij zijn wij ons er van bewust dat humuszuur in werkelijkheid geen eenvoudig lineair polyelektroliet is, maar we nemen aan dat de hoofdeffecten die optreden bij eenvoudig lineaire polyelektroliet ook optreden bij humuszuur. Naast experimentele gegevens worden in dit proefschrift ook berekeningen gepresenteerd. De berekeningen zijn gebaseerd op de zelf-consistente-veldtheorie voor polyelektrolietadsorptie (SCF theorie) die gebaseerd is op de SCF theorie voor polymeeradsorptie zoals die is ontwikkeld door Scheutjens en Fleer.

In hoofdstuk 2 wordt de zelf-consistente-veldtheorie besproken en wordt in deze modelberekeningen een variabel geladen wand geïntroduceerd. In deze theorie worden alle segmenten (water, zout ionen en polyelektrolietsegmenten) die zich in het systeem bevinden in een rooster geplaatst. Een polyelektrolietmolekuul is opgebouwd uit verschillende segmenten met mogelijkerwijs afzonderlijke eigenschappen. Het rooster wordt verdeeld in een aantal parallelle lagen. In laag 0 worden vervolgens segmenten geplaatst die het oxyde-oppervlak modelleren. Alle andere segmenten kunnen zich vervolgens verdelen over de overgebleven roosterplekken. Hierbij zoekt het systeem naar de toestand met een minimale vrije energie. Het doel van deze berekeningen is om de volumefractieprofielen van de verschillende segmenten te bepalen. Deze volumefractieprofielen geven aan welke segmenten zich ophopen in de buurt van het oppervlak en welke in de oplossing zullen blijven. Met deze volumefractieprofielen en de eigenschappen die horen bij de verschillende segmenten kunnen vervolgens een aantal karakteristieke eigenschappen van het systeem bepaald worden. Zoals bijvoorbeeld geadsorbeerde hoeveelheden en laagdikten, maar ook de mate van dissociatie van een bepaald type segment in een bepaalde laag. Hierdoor is het mogelijk om het titratiegedrag van de afzonderlijke deeltjes, die met elkaar een interactie zijn aangegaan, uit te rekenen. Verder is het mogelijk om het optreden van adsorptiefractionatie te onderzoeken. Geadsorbeerde hoeveelheden, laagdikten en de

uitwisseling van kleine molekulen door grotere molekulen zijn ook experimenteel te bepalen, maar het titratiegedrag van de afzonderlijke deeltjes kan slechts bepaald worden als bepaalde vooronderstellingen worden gemaakt. Door de SCF berekeningen te vergelijken met de experimenten kunnen we iets leren over het belang van verschillende adsorptiemechanismen (b.v. specifieke, elektrostatische en hydrofobe interacties) en kunnen we achterhalen of de gemaakte vooronderstellingen redelijk waren.

In hoofdstuk 3 is het gebruikte humuszuur gekarakteriseerd met behulp van verschillende analytische methoden en is aangetoond dat PAHA beschouwd kan worden als een typisch bodem humuszuur.

In hoofdstuk 4 is de proton- en cadmiumbinding aan PAHA beschreven. Met behulp van het Donnan model zijn de elektrostatische interacties verdisconteerd en werd een zoutsterkte onafhankelijke "Master Curve" verkregen. Hierbij werd gebruik gemaakt van viscositeitsmetingen om de Donnan volumina te bepalen. De gemeten Donnan volumina gaven een realistisch beeld van de grootte van een humuszuurdomein en op grond hiervan werd geconcludeerd dat humuszuur beschreven kan worden als een flexibel polyelektroliet dat binnen zijn domeingrenzen vooral uit water bestaat en slechts voor een kleine deel uit vaste stof. Uitgaande van deze "Master Curve" werd vervolgens de intrinsieke affiniteitsdistributie bepaald die de chemische heterogeniteit van humuszuur weergeeft. De gemeten proton- en cadmiumisothermen aan PAHA zijn vervolgens gemodelleerd met behulp van het NICA-Donnan model. De proton- en cadmiumbinding aan hematiet werden kort beschreven in respectievelijk hoofdstuk 5 en hoofdstuk 8.

In hoofdstuk 5 en 6 werden de verschillende aspecten betreffende de interacties tussen PAHA en hematiet onderzocht. Zowel de adsorptie isothermen, gemeten bij verschillende pH waarden en zout en/ of cadmium concentraties, laagdikten als de uitwisseling van kleine door grotere molekulen werd besproken. Uit deze experimenten kwam naar voren dat de geadsorbeerde hoeveelheden relatief hoog waren, evenals de geadsorbeerde laagdikten. Dit werd toegeschreven aan de conformatie van het geadsorbeerde materiaal ofwel, in de terminologie van de polyelektroliet adsorptie theorie, door het voorkomen van grote "lussen" en lange "staarten". De experimenteel verkregen resultaten kwamen overeen met de trends zoals die volgden uit de bovengenoemde SCF berekeningen.

Gebaseerd op de bevindingen in deze hoofdstukken, gecombineerd met de gemeten protonadsorptie-isothermen aan het PAHA/ hematiet complex en verdere SCF-berekeningen werd in hoofdstuk 7 het volgende kwalitatieve model voorgesteld.

Modelbeschrijving:

De binding van protonen en metaalionen aan het complex van humuszuur en een metaal(hydr)oxyde is vergeleken met de proton- en metaalionbinding aan de losse componenten. Hierbij hebben we waargenomen dat er een verschil is tussen de werkelijk gemeten proton- en metaalionadsorptie aan het complex en de berekende som van de adsorptie aan de losse componenten. Dit verschil kan worden veroorzaakt door 2 processen: (1) de werkelijk gemeten adsorptie kan toenemen omdat er meer

ionen adsorberen aan het metaal(hydr)oxyde wanneer dit in contact is met geadsorbeerd humuszuur en (2) de werkelijk gemeten adsorptie kan afnemen omdat er minder ionen adsorberen aan de humuszuur moleculen die in contact zijn met het oxyde-oppervlak.

Zoals hierboven beschreven is, zijn de hematiet deeltjes bij pH waarden lager dan pH 9 positief geladen. Hierdoor moeten de metaalionen, die een constante positieve lading hebben, wanneer ze aan hematiet adsorberen de elektrostatische afstoting overwinnen. Dit is slechts mogelijk wanneer de metaalionen in sterke mate specifiek adsorberen aan het hematiet oppervlak. Beide aspecten zorgen er voor dat de metaalionbinding aan het hematiet oppervlak bij lage pH (pH 4) erg laag is omdat de specifieke adsorptie-energie de sterke repulsie niet of nauwelijks kan compenseren. Des te dichter de pH bij het ladingsnulpunt (pH 9) van het oppervlak komt, hoe meer metaalionen zullen adsorberen. Door het wegvallen van de elektrostatische repulsie neemt de adsorptie zelfs in enkele ordes van grootte toe. Dit laatste in tegenstelling tot de metaalionbinding aan het humuszuur waar de pH afhankelijkheid van de metaalionadsorptie veel geringer is omdat de potentiaal verschillen op humuszuur veel kleiner zijn dan bij oxyden.

De mate van adsorptie van humuszuur aan hematiet wordt bepaald door zowel specifieke als elektrostatische interacties en neemt toe met toenemende pH en toenemende zoutsterkte. Omdat beide componenten een variabele lading hebben die zich zal aanpassen aan de lokale omstandigheden, kan men verwachten dat beide componenten na het adsorptieproces een andere lading zullen hebben dan de initiële lading, voordat de deeltjes met elkaar in contact kwamen. Doordat er naast elektrostatische aantrekking ook een specifieke adsorptie-energie is kan de lading van het geadsorbeerde humuszuur de lading van de hematietdeeltjes overcompenseren, zelfs wanneer in acht is genomen dat beide deeltjes hun lading aanpassen.

Doordat de ladingen die geassocieerd zijn met het geadsorbeerde humuszuur zich ophopen in de nabijheid van het hematietoppervlak verandert het potentiaalprofiel rondom de hematietdeeltjes. Tevens verandert vanzelfsprekend ook het potentiaalveld dat door het geadsorbeerde humuszuur wordt ervaren. Door de wederzijdse invloed ondervindt het oppervlak een minder positieve of zelfs negatieve potentiaal en het humuszuur een minder negatieve of zelf positieve potentiaal dicht bij het oppervlak. Deze wederzijdse be•nvloeding heeft tot gevolg dat een aantal van de mogelijke bindingsplaatsen van het humuszuur worden weggenomen door het oxyde-oppervlak en daardoor minder beschikbaar zijn voor metaalbinding. Daartegenover zullen de positieve metaalionen het oxyde-oppervlak makkelijker kunnen naderen omdat de elektrostatische repulsie is verminderd. Omdat de specifieke adsorptie-energie onveranderd blijft zal dit een hogere metaalionadsorptie tot gevolg hebben.

Welke van de twee processen nu de metaalion binding aan het humuszuur/ hematiet complex domineert hangt af van de affiniteit van het metaalion voor de losse componenten. Een metaalion dat hoofdzakelijk bindt aan het oxyde-oppervlak zal meer worden geadsorbeerd aan het complex dan aan de losse componenten. Terwijl een metaalion dat hoofdzakelijk adsorbeert aan het humuszuur minder zal worden geadsorbeerd aan het complex.

Het ontwikkelde model werd in hoofdstuk 8 getoetst aan experimentele cadmium-adsorptiemetingen aan het PAHA/ hematiet complex en literatuur gegevens van koperbinding aan een vergelijkbaar complex. Hierbij is gebleken dat het opgestelde model, ondanks de in eerste instantie tegenstrijdige resultaten, in staat was om de gemeten cadmium- en koperadsorpties te beschrijven en de achterliggende mechanismen te begrijpen. Ook kan het verschillende adsorptiegedrag van cadmium- en koperionen aan het humuszuur/ hematiet (respectievelijk goetiet) complex verklaard worden. Koperionen binden hoofdzakelijk aan humuszuur en de adsorptie aan het complex is over een groot pH gebied minder dan aan de losse componenten. Daartegenover neemt de adsorptie van cadmiumionen, welke ten opzichte van koperionen sterk aan het oxyde-oppervlak binden, over een groot pH gebied toe.

Concluderend kunnen wij stellen dat een beter inzicht is verkregen in de mechanismen die van belang zijn voor de adsorptie van metaalionen aan complexen van verschillende, elkaar beïnvloedende componenten. Dit inzicht is verkregen door laboratorium experimenten aan een modelsysteem te combineren met model-berekeningen. Verder is aangegeven dat het opgestelde model gebruikt kan worden om metaalbinding in onze natuurlijke omgeving te beschrijven en is een eerste aanzet is gegeven om de metaalbinding aan gecompliceerde systemen kwalitatief te voorspellen op grond van eenvoudige experimenten aan eenvoudige modelsystemen. Uit het gedane onderzoek zijn de kwalitatieve aspecten naar voren gekomen die bij metaalbinding aan humuszuur/ oxyden complexen belangrijk zijn. In de toekomst kan dit begrip gebruikt worden voor het opstellen van theoretische modellen waarmee de nu nog kwalitatieve voorspellingen worden gekwantificeerd.

## Curriculum Vitae

Arnoldus Wilhelmus Petrus Vermeer (roepnaam Ronald) is op 4 augustus 1965 te Oss geboren. Na het doorlopen van MAVO, HAVO en VWO te Oss begon hij in 1986 met een studie Scheikunde aan de Katholieke Universiteit Nijmegen. In augustus 1991 rondde hij deze studie af met als afstudeervakken Anorganische Chemie (bijvak) en Vaste Stof Chemie (hoofdvak). Vanaf oktober 1991 was hij, in het kader van het EU project STEP, voor vier jaar werkzaam als assistent in opleiding bij de vakgroep Fysische en Kolloïdchemie, in samenwerking met de vakgroep Bodemkunde en Plantevoeding van de Landbouwuniversiteit Wageningen. Tijdens deze periode deed hij onderzoek naar de binding van metaalionen aan verschillende bodembestanddelen, en met name naar de invloed van de interacties tussen deze bodembestanddelen op de metaalbinding. In 1996 rondde hij het onderzoek af met het schrijven van dit proefschrift.

## Dankwoord

Het zal iedereen duidelijk zijn dat het afronden van dit promotieonderzoek niet alleen rust op mijn werkzaamheden van de afgelopen vier jaar. Het was een lange maar leerzame weg die hiertoe geleid heeft, waarbij iedere stap zijn sporen heeft nagelaten. Toch wil ik beginnen met mijn ouders en Marion te bedanken voor het feit dat ze mij door de jaren heen mijn eigen weg hebben laten zoeken. Speciaal wil ik Marion er voor bedanken dat ze het geduld kon opbrengen op momenten dat ik wat meer tijd nodig had voor mijn boekje.

De docenten van de Den Bongerd MAVO hebben mij altijd gesteund in mijn plan om naar de Universiteit te gaan en hebben mij hun aandacht gegeven toen ik dat nog nodig had. Op de Vincent van Gogh HAVO kregen wij als leerlingen veel vrijheid en werden we daar waar mogelijk aangemoedigd om zelfstandig te werken, hetgeen mij enorm heeft gestimuleerd. Door tijdens mijn studie scheikunde veel tijd met mijn vrienden door te brengen heb ik altijd het besef kunnen houden dat er meer is dan wetenschap alleen. Tijdens mijn hoofdvakstage bij de vakgroep Vaste Stof Chemie heb ik voor het eerst ondervonden hoe leuk wetenschaplijk onderzoek is, wat dan ook de voornaamste reden was om na mijn studie een promotieonderzoek aan te nemen.

Ik wil van hieruit al mijn afdelingsgenoten bedanken voor de plezierige sfeer die altijd op FYSKO heerste en waar ik me dan ook al snel thuis voelde. Enkele wil ik hier met name noemen. Als eerste wil ik het ondersteunend personeel bedanken omdat ze altijd klaar stonden als er iets van zolder moest worden gehaald, een onderdeel voor de opstelling gemaakt moest worden en voor de hulp bij sommige experimenten. Zonder jullie inbreng had ik nooit zoveel experimenten kunnen uitvoeren. Verder natuurlijk mijn kamergenoten; Martin, Katinka en Jacomien, met wie ik al die tijd de huisdieren, knuffels en ongenuanceerde opmerkingen heb gedeeld (tenslotte als je niet ...). Dick en Joanne, die ik beide bij hun afstudeervak heb mogen begeleiden en Jenny, onze Australische gast, ik denk dat jullie zelf jullie inbreng wel in dit boekje terug kunnen vinden. Dat er naast wetenschap ook nog andere activiteiten plaatsvonden vanuit de afdeling getuigt wel van het feit dat we bij FYSKO niet alleen collega's waren. Met veel plezier denk ik terug aan de wandelweekenden, het volleyballen (inclusief trainingskamp) het jaarlijkse voetballen, klimmen, kanoen en, niet te vergeten, het (hard)lopen. Het risico van namen noemen is dat je mensen vergeet, maar toch volgen er hier enkele: Marcel, Henry, Paulo, Jeannette, Marcel, Ben, Monique, Arie, Luc, Martin, Eveline, ... bedankt.

Natuurlijk werd er ook gewerkt en les gegeven. Frans, ondanks onze meningsverschillen over het onderwijsprogramma was het geven van onderwijs, mede dankzij de vele discussies toch iets waar ik me zeer bij betrokken voelde. Dat er nog lang een frisse wind door het "propedeuse"onderwijs mag blijven waaien.

Dan rest mij nu nog de mensen te bedanken die direct bij het onderzoek betrokken zijn geweest. Frans, bedankt voor je hulp bij de berekeningen, zonder jou zou dit proefschrift er heel anders hebben uitgezien. En natuurlijk ook enkele mensen van

198

buiten de afdeling; Marc, David, Chris, Peter, Erwin, ... Verder wil ik mijn beide begeleiders, Willem en Luuk, bedanken voor de vele opbouwende kritiek die ze op mijn schrijfsels hebben gegeven tijdens het ter schrift stellen van het voorliggende proefschrift. Luuk, al waren we het soms niet met elkaar eens, wat tot verhitte en chaotische discussies kon leiden, jou scherpe kijk op de materie heeft zeker bijgedragen tot het tot stand komen van dit onderzoek.

Als laatste wil ik de hoop uitspreken dat na mijn promotie alles op de afdeling nog even in beweging zal blijven.

En toen ...